Catalytic Performances of NiMo/Zr-SBA-15 Catalysts for the Hydrotreating of Bitumen Derived Heavy Gas Oil

A Thesis submitted to the College of Graduate Studies and Research

in Partial Fulfillment of the Requirements for the

Degree of Master of Science

in the Department of Chemical Engineering

University of Saskatchewan

Saskatoon

By

Piyali Biswas

COPYRIGHT

ABSTRACT

Gas-oil obtained from bitumen contains a significant amount of impurities, which are difficult to remove using a conventional alumina supported hydrotreating catalyst. Innumerable studies have been carried out to develop a highly effective hydrotreating catalyst, and among all utilizing more advanced support is considered as a better alternative. Recently, SBA-15, which is an ordered mesoporous silica support, has received importance as a catalyst support because of its excellent textural properties. However, SBA-15 lacks surface acidity and provides very low metal-support interaction. By modifying SBA-15 with zirconia, an optimum level of surface acidity and Si-Mo interaction can be achieved. Also, by doping zirconia with SBA-15, the textural properties of zirconia can be improved. Hence, a synergistic effect can be obtained while incorporating zirconia onto SBA-15 and the resulting material Zr-SBA-15 can be used as an effective support for hydrotreating catalyst. In the present study, Zr-SBA-15 supports were prepared by the post synthesis and the direct synthesis method with different zirconia loading. Zr-SBA-15 supported NiMo catalysts were prepared by incipient wetness impregnation technique. Catalysts and supports were characterized by small angle X-ray scattering (SAXS), nitrogen adsorption/desorption (BET), powder X-ray diffraction (XRD), transmission electron spectroscopy (TEM), scanning electron microscopy (SEM), and Raman spectroscopy methods. Characterization of support confirmed that the zirconia was successfully incorporated in a mesoporous SBA-15 structure without significantly changing the textural properties of SBA-15. The performance of the Zr-SBA-15 supported NiMo catalysts was evaluated based on hydrodesulfurization and hydrodenitrogenation activities exhibited during hydrotreating

of heavy gas oil derived from Athabasca bitumen at industrial operating condition (temperature 375-395 °C, pressure 8.9 MPa, LHSV 1.0 hr^{-1} and gas/oil ratio 600 $Nm^{3/}m^3$). The comparison of catalytic activities showed that the NiMo catalysts supported on Zr-SBA-15, prepared by direct and post synthesis method exhibited higher hydrotreating activity compared to SBA-15 supported catalyst. NiMo catalyst supported on Zr-SBA-15 with 23 wt% of ZrO_2 loading, prepared by post synthesis method showed the highest activity among all the catalysts.

After determining the best support, the optimum catalyst metal loadings on the Zr-SBA-15 support was found to be 17 wt% of Mo and 3.4 wt% of Ni. This catalyst also showed higher activity in mass basis for the hydrotreating of heavy gas oil compared to that of commercial hydrotreating catalyst.

A kinetic study was performed on the optimum NiMo/Zr-SBA-15 catalyst to predict its HDS and HDN activities while varying the parameters of temperature, liquid hourly space velocity (LHSV), pressure and gas-to-oil ratio. Rate expressions were developed using Power Law and Langmuir-Hinshelwood model to predict the behavior of both the HDS and HDN reactions. Power law models were best fit with reaction orders of 1.8 and 1.3, and activation energies of 115 kJ/mol and 121 kJ/mol, for HDS and HDN reactions, respectively. The activation energies calculated using Langmuir-Hinshelwood model considering H_2S inhibition were found to be 122 kJ/mol and 138 kJ/mol, for HDS and HDN reactions, respectively.

ACKNOWLEDGEMENT

I would first like to thank my supervisors, Dr. Ajay Dalai and Dr. John Adjaye, for their valuable guidance and supervision throughout the initiating, planning, executing and concluding my research work. I greatly appreciate the effort made by them to review and provide recommendations to my written materials. I would also like to thank the other two members of my MSc. supervisory committee, Dr. Richard Evitts and Dr. Jafar Soltan, for their contributions to my graduate studies.

Secondly, I would also like to thank Mr. Richard Blondin, Mr. Dragan Cekic, and Heli Eunike for their assistance in the laboratory work that contributed to my project. My thanks also go to the Natural Sciences and Engineering Research Council of Canada and Syncrude Canada Limited for their much-appreciated financial assistance. I also greatly appreciate the work done by the Saskatchewan Structural Science Center and Geology Department of University of Saskatchewan, University of New Brunswick, and the University of Western Ontario for their assistance in the catalyst characterizations.

Lastly, I would like to express my gratitude to all the professors, post-doctorate fellows, and graduate students that have contributed to my graduate study at the University of Saskatchewan. Most of all, my heartfelt thanks to my mother, father, sister and brother for their unconditional love and constant encouragements. Also, I would like to extend my thanks to my husband Prabhu N., for supporting me in both personal and professional life. Finally, I thank God Almighty for his blessings.

TABLE OF CONTENTS

COPYRIGHT i

ABSTRACT ii

ACKNOWLEDGEMENT iv

TABLE OF CONTENTS v

LIST OF TABLES xi

LIST OF FIGURES xiii

NOMENCLATURE xviii

CHAPTER 1. INTRODUCTION 1

1.1 Research Background 1

1.2 Knowledge Gaps 5

1.3 Hypotheses 6

1.4 Research Objectives 6

CHAPTER 2. LITERATURE REVIEW 8

2.1 World Energy Consumption 8

2.2 Characteristics of Petroleum and Gas Oil 9

2.2.1 Definition of Bitumen, Heavy Oil and Heavy Gas Oil 9

2.2.2 Syncrude Upgrading Process 12

2.2.3 Chemical Compounds Present in Petroleum 14

2.2.4 Reactivity of Sulfur and Nitrogen Compounds 16

2.3 Characteristics of Hydroteating Process 18

2.3.1 Definition of Hydrotreating Process 18

2.3.2 Hydrotreating Process Description 20

2.3.3 Purposes of Hydrotreating 22

2.3.4 Hydrotreated Diesel Specification 23

2.3.5 Challenges of Hydrotreating Processes 24
2.3.6 Chemical Reactions of Hydrotreating 28
2.3.7 Reaction Mechanism of HDS and HDN 30
2.3.8 Factors Affecting Hydrotreating Processes 34
2.3.9 Ways to Improve Hydrotreating Process 38
2.4 Hydrotreating Catalyst 39
2.4.1 Conventional Hydrotreating Catalyst 39
2.4.2 Hydrotreating Catalyst Design and Improvement 41
2.4.3 Structure of Hydrotreating Catalysts 43
2.4.4 HDS Reaction Mechanism by Metal-Sulfide Catalysts 46
2.4.5 Promoters 47
2.4.6 Support Materials 48
2.4.7 Progress on Improvement of Hydrotreating Catalyst Support 51
2.4.8 Desired Properties of HDT Catalyst Support 53
2.4.9 Deactivation 58
2.4.10 Objectives of Catalyst Characterization 62
2.5 Selection of Zr-SBA-15 Support for Hydrotreating of Gas Oil 63
2.5.1 SBA-15 Support 63
2.5.2 ZrO_2 Incorporation into SBA-15 Framework 64
2.5.3 Synergistic effect of SBA-15 and ZrO_2 65
2.6 SBA-15 as Hydrotreating Catalyst Support 68
2.6.1 Characteristics of Mesoporous SBA-15 68
2.6.2 Synthesis Methods of SBA-15 69
2.6.3 Pore Diameter Control of SBA-15 71
2.6.4 Application of SBA-15 Support in Hydrotreating 75
2.7 Zr-SBA-15 as Hydrotreating Catalyst Support 76
2.7.1 Characteristics of Zr-SBA-15 76
2.7.2 Synthesis Methods of Zr-SBA-15 77
2.7.3 Application of Zr-SBA-15 Support in Hydrotreating 84

2.8 Kinetic Modeling of HDS and HDN 85

2.8.1 Purpose of Kinetic Modeling 85

2.8.2 Kinetic Models for HDS and HDN 86

2.8.3 Power Law Model 87

2.8.4 Langmuir-Hinshelwood Model 91

2.8.5 Reactor Performance 95

2.8.6 Effect of Mass Transfer 96

CHAPTER 3. EXPERIMENTAL METHOD 99

3.1 SBA-15 Support Preparation 99

3.2 Zr-SBA-15 Support Preparation 101

3.2.1 Direct Synthesis Method 101

3.2.2 Post Synthesis Method 101

3.3 NiMo/SBA-15 and NiMo/Zr-SBA-15 Catalyst Preparation 103

3.4 Support and Catalyst Characterization Technique 104

3.4.1 Small Angle X-ray Scattering (SAXS) 104

3.4.2 N_2 Adsorption/Desorption 104

3.4.3 Elemental Analysis 105

3.4.4 Transmission Electron Microscopy (TEM) 105

3.4.5 Scanning Electron Microscopy (SEM) 105

3.4.6 Fourier Transform Infrared Spectroscopy (FTIR) 105

3.4.7 Pyridine Adsorbed Fourier Transform Infrared Spectroscopy (Py-IR) 106

3.4.8 X-ray Diffraction (XRD) 106

3.4.9 Raman Spectroscopy 106

3.4.10 UV vis Diffuse Reflectance Spetroscopy 107

3.5 Hydrotreating Experimental Set-up and Activity Test 107

3.5.1 Hydrotreating Reactor Set-up 107

3.5.2 Preparation for Hydrotreating Reaction 107

3.5.3 Catalyst Performance Test 110

3.6 Hydrotreated Product Analysis 111

3.6.1 S and N Conversion 111

3.6.2 Boiling Point Distribution 111

CHAPTER 4. HYDROTREATING OF GAS OIL OVER NiMo/Zr-SBA-15 CATALYSTS 112

4.1 Characterization of Supports 112

4.1.1 Small-Angle X-ray Scattering (SAXS) 112

4.1.2 N_2 Adsorption/Desorption and Chemical Compositions 114

4.1.3 Transmission Electron Microscopy (TEM) 117

4.1.4 Scanning Electron Microscopy (SEM) 119

4.1.5 Fourier Transform Infrared Spectroscopy (FTIR) 119

4.1.6 Pyridine Adsorbed Fourier Transform Infrared Spectroscopy (Py-IR) 122

4.1.7 Powder X-ray Diffraction (XRD) 123

4.2 Characterization of catalysts 125

4.2.1 Small-Angle X-ray Scattering (SAXS) 125

4.2.2 N_2 Adsorption/Desorption and Chemical Compositions 126

4.2.3 Transmission Electron Microscopy (TEM) 129

4.2.4 Powder X-ray Diffraction (XRD) 129

4.2.5 Raman Spectroscopy 131

4.2.6 UV-DRS Spectroscopy 133

4.3 Catalytic Activity Performance Based on HDS and HDN 135

CHAPTER 5. METAL LOADING OPTIMIZATION FOR NiMo/Zr-SBA-15 CATALYSTS 141

5.1 Characterization of Supports 141

5.1.1 Small-Angle X-ray Scattering (SAXS) 141

5.1.2 N_2 Adsorption/Desorption and Chemical Compositions 142

5.1.3 Transmission Electron Microscopy (TEM) 144

5.1.4 Scanning Electron Microscopy (SEM) 145

5.2 Characterizations of Catalysts 146

5.2.1 Small-Angle X-ray Scattering (SAXS) 146

5.2.2 N_2 Adsorption/Desorption and Chemical Compositions 147

5.2.3 Transmission Electron Microscopy (TEM) 148

5.2.4 Pyridine Adsorbed Fourier Transform Infrared Spectroscopy (Py-IR) 150

5.2.5 Powder X-ray Diffraction (XRD) 151

5.2.6 Raman Spectroscopy 152

5.2.7 UV-DRS Spectroscopy 153

5.2.8 High Resolution Transmission Electron Microscopy (HRTEM) 154

5.3 Catalytic Activity Performance Based on HDS and HDN 156

CHAPTER 6. KINETIC STUDY OF HDS AND HDN 161

6.1 Effect of Reaction Condition on HDS/HDN over Optimized Catalyst 161

6.1.1 Effect of Temperature 161

6.1.2 Effect of LHSV 164

6.1.3 Effect of Pressure 166

6.1.4 Effect of Hydrogen Gas/Oil Ratio 168

6.2 Kinetic Study of HDS/HDN for the Optimum NiMo/Zr-SBA-15 Catalyst 172

6.2.1 Evaluation of Hydrodynamic Parameters 173

6.2.2 Mass Transfer Resistances for the HDS and HDN 174

6.2.3 Hydrodesulfurization and Hydrodenitrogenation Rate kinetics 178

6.2.4 Power Law Model 178

6.2.5 Langmuir-Hinshelwood Model 180

6.3 Stability Study for the Optimum NiMo/Zr-SBA-15 Catalyst 186

6.4 Characterization of Spent Catalysts 188

CHAPTER 7. CONCLUSIONS AND RECOMMENDATIONS 189

7.1 Conclusions 189

7.2 Recommendations 191

CHAPTER 8. LIST OF REFERENCES 193

APPENDICES

Appendix A	Calculation of Molar Product Concentration of N/S and Reaction Rates of HDN/HDS	210
Appendix B	Calculation of Product Concentration for HDS and HDN Conversion Obtained from Kinetic Study	211
Appendix C	Evaluation of External Mass Transfer Resistance for HDS and HDN Reactions	213
Appendix D	Evaluation of the Internal Mass Transfer Resistances for the HDS and HDN Reactions	221
Appendix E	Permissions to Use Figures from Literatures	232

LIST OF TABLES

Table 2.1	Characteristics of conventional crude oil, bitumen, and heavy oil	12
Table 2.2	Elemental analysis of petroleum and Athabasca bitumen	12
Table 2.3	Hydrodesulfurization reactivity of various sulfur substituted molecules	16
Table 2.4	Diesel specifications for Europe and USA	24
Table 2.5	Target of product sulfur, required increase in catalyst activity and temperature	27
Table 2.6	Operating conditions for hydrotreating processes	37
Table 2.7	Typical composition of catalyst used for hydrotreating process	40
Table 2.8	Physical characteristics of the hydrotreating catalysts	40
Table 2.9	Role of promoters in the hydrotreating catalyst	48
Table 2.10	Disadvantaged of γ-Al_2O_3 support for hydrotreating	50
Table 2.11	Typical methods for catalyst characterization	63
Table 2.12	Properties of SBA-15, ZrO_2 and Zr-SBA-15 supports	67
Table 2.13	Pore size control of mesoporous SBA-15 structure	74
Table 2.14	Application of SBA-15 support in hydrotreating	75
Table 2.15	Application of Zr-SBA-15 support in hydrotreating	85
Table 2.16	Basic kinetic information derived from Power law for the hydrotreating of real feed	90
Table 2.17	Langmuir-Hinshelwood models for HDS and HDN	92
Table 2.18	Kinetic parameters derived from Langmuir-Hinshelwood model for the hydrotreating of real feed	94
Table 2.19	Parameters for calculating the hydrodynamic parameters	96
Table 3.1	Naming of the supports and catalysts prepared for the project	103
Table 3.2	Characteristics of heavy gas oil derived from Athabasca bitumen	110

Table 4.1	Textural characteristics and chemical compositions of support materials	115
Table 4.2	Textural characteristics and chemical compositions of catalyst materials	127
Table 5.1	Textural characteristics and chemical compositions of support materials	143
Table 5.2	Textural characteristics and chemical compositions of catalysts materials	147
Table 6.1	Effect of temperature, pressure, LHSV and H_2/gas oil ratio on sulfur and nitrogen conversion of HGO with optimized catalyst	170
Table 6.2	Hydrodynamic parameter evaluation for plug flow, wall effect, wetting and back-mixing	173
Table 6.3	Values derived from Power law model for the HDS and HDN of heavy gas oil over optimized catalyst	180
Table 6.4	Values derived from Independent Langmuir-Hinshelwood model for the HDS and HDN of heavy gas oil over optimized catalyst	181
Table 6.5	Values derived from Co-dependent Langmuir-Hinshelwood model for the HDS and HDN of heavy gas oil over optimized catalyst	182
Table 6.6	Values derived from Langmuir-Hinshelwood model with H_2S inhibition for the HDS and HDN of heavy gas oil over optimized catalyst	183
Table 6.7	BET characterization of fresh and spent catalysts	188

LIST OF FIGURES

Figure 2.1	World energy consumption	9
Figure 2.2	Syncrude upgrading process	13
Figure 2.3	Structure of sulfur and nitrogen compounds present in petroleum	15
Figure 2.4	Reactivity of various organic sulfur compounds in HDS versus their ring sizes and positions of alkyl substitutions on the ring	17
Figure 2.5	Relative reactivity of nitrogen compounds	18
Figure 2.6	Application of hydrotreating in a modern refinery	19
Figure 2.7	Process scheme for heavy hydrotreating of gas oil	21
Figure 2.8	Sulfur content in diesel fuel	26
Figure 2.9	NOx emission standard for diesel engine	26
Figure 2.10	Examples of hydrodesulfurization reactions	29
Figure 2.11	Examples of hydrodenitrogenation reactions	29
Figure 2.12	Hydrodesulfurization pathways of DBT	31
Figure 2.13	Hydrodesulfurization pathways of 4, 6-DMDBT	31
Figure 2.14	HDN reaction network of quinoline	33
Figure 2.15	HDN reaction network of pyridine	33
Figure 2.16	Factors affecting hydrotreating process	34
Figure 2.17	Structure of sulfide hydrotreating catalyst	39
Figure 2.18	Triangular concept of catalyst design	41
Figure 2.19	Different phases present in a typical alumina-supported catalyst	45
Figure 2.20	Distinction between rim and edge sites for stacked and unstacked MoS_2 particles	46
Figure 2.21	HDS mechanism of thiophene by metal-sulfide catalyst	47
Figure 2.22	Diffusion and catalytic reaction of sulfur compounds through the catalyst pores	55

Figure 2.23	Effect of pore diameter and surface area on catalytic functionality	55
Figure 2.24	Hydrotreating catalyst deactivation profile	61
Figure 2.25	Major type of catalyst deactivation for hydrotreating catalysts due to a) poison b) deposits c) sintering d) mechanical failure e) evaporation	61
Figure 2.26	DBT conversion over different NiMo catalysts	66
Figure 2.27	4, 6-DMDBT conversion over different NiMo catalysts	66
Figure 2.28	Structure of SBA-15	68
Figure 2.29	Synthesis strategy of mesoporous SBA-15	70
Figure 2.30	Synthesis strategy of Zr-SBA-15 preparation by chemical grafting method	83
Figure 2.31	Heterogeneous catalytic reaction in porous catalyst	97
Figure 3.1	Schematic for the SBA-15 preparation in laboratory	100
Figure 3.2	Schematic for the Zr-SBA-15 preparation by post synthesis method in laboratory	102
Figure 3.3	Schematic of the experimental set-up for hydrotreating reaction	108
Figure 3.4	Catalyst bed for trickle bed reactor	109
Figure 4.1	Small-angle X-ray scattering (SAXS) pattern of SBA-15 and Zr-SBA-15 (Post) (a); Zr-SBA-15 (Direct) (b) supports.	113
Figure 4.2	EDX pattern of Zr-SBA-15 (Post 23) support	115
Figure 4.3	Nitrogen adsorption-desorption isotherm of SBA-15 and Zr-SBA-15 (Post) (a); Zr-SBA-15 (Direct) (b) supports	116
Figure 4.4	Transmission electron microscopy images of SBA-15 front view (a), side view (b); Zr-SBA-15 (Post 23) front view (c), side view (d); Zr-SBA-15 (Direct 20) (e) front view, side view (f); Zr-SBA-15 (direct 40) (g) front view, side view (h) supports	117
Figure 4.5	Scanning electron microscopy images of SBA-15 of 10 μm (a), 1 μm (b); Zr-SBA-15 (Post 23) of 10 μm (c), 1μm (d); Zr-SBA-15 (Direct 20) 10 μm (e), 1 μm (f) supports	120
Figure 4.6	FT-IR spectra comparison for SBA-15 and Zr-SBA-15 (Direct) (a);	121

SBA-15 and Zr-SBA-15 (Post) (b) supports

Figure 4.7 FT-IR spectra of pyridine adsorbed species on SBA-15, Zr-SBA-15 (Direct) and Zr-SBA-15 (Post) supports 123

Figure 4.8 Powder X-ray pattern of SBA-15, Zr-SBA-15 (Direct) and Zr-SBA-15 (Post) supports 124

Figure 4.9 Small-angle X-ray scattering pattern of NiMo catalysts supported on SBA-15, Zr-SBA-15 (Direct) and Zr-SBA-15 (Post) supports 125

Figure 4.10 EDX pattern of NiMo/Zr-SBA-15 (Post 23) catalyst 127

Figure 4.11 Nitrogen adsorption-desorption isotherm of NiMo catalyst supported on SBA-15 and Zr-SBA-15 (Post) (a); Zr-SBA-15 (Direct) (b) 128

Figure 4.12 Transmission electron microscopy images of NiMo catalyst supported on SBA-15 front view (a); side view (b); Zr-SBA-15 (Post 23) front view (c), side view (d); Zr-SBA-15 (Direct 20) front view (e), side view (f) supports 130

Figure 4.13 Powder X-ray diffraction pattern of NiMo catalysts supported on SBA-15, Zr-SBA-15 (Direct) and Zr-SBA-15 (Post) supports. 131

Figure 4.14 Raman spectra comparison for NiMo catalyst supported on SBA-15 and Zr-SBA-15 (Direct) (a); supported on SBA-15 and Zr-SBA-15 (Post) (b) support 132

Figure 4.15 UV-DRS Spectra of NiMo/SBA-15 catalysts supported on SBA-15, Zr-SBA-15 (Post 16) and Zr-SBA-15 (Post 23) supports, absorption band due to Mo(a); Ni (b) 134

Figure 4.16 Effect of time on stream on the stability of the NiMo/Zr-SBA-15 catalyst during hydrotreating of gas oil. P=8.9 MPa, LHSV = 1 h^{-1}, T = 370 °C, H_2/HC ratio 600 Nm^3/m^3 137

Figure 4.17 The hydrodesulfurization and hydrodenitrogenation activity (volume basis) study of NiMo catalysts supported on SBA-15. Zr-SBA-15 (Post) and Zr-SBA-15 (Direct); T = 375/385/395 °C, P=8.9 MPa, LHSV = 1 h^{-1}, H_2/HC ratio 600 Nm^3/m^3. HDS (a); HDN (b) 138

Figure 4.18 The hydrotreating activity (weight basis) comparison of NiMo/Zr-SBA-15 (Post 23) and commercial catalyst; T = 375/385/395 °C, P=8.9 MPa, LHSV = 1 h^{-1}, H_2/HC ratio 600 Nm^3/m^3. HDS (a); HDN (b) 139

Figure 4.19	The simulated distillation of HGO feed and the product obtained by hydrotreating of HGO over NiMo/Zr-SBA-15 (Post 23) catalyst	140
Figure 5.1	Small-angle X-ray scattering pattern of SBA-15 and Zr-SBA-15 (Post 23) support	142
Figure 5.2	Nitrogen adsorption-desorption isotherm of SBA-15 and Zr-SBA-15 (Post 23) supports	143
Figure 5.3	Transmission electron microscopy images of SBA-15 front view (a), side view (b); Zr-SBA-15 (Post 23) front view (c), Zr-SBA-15 (Post 23) (d) support	144
Figure 5.4	Scanning electron microscopy images of SBA-15 of 10 μm (a),1 μm (b); Zr-SBA-15 (Post 23) of 10 μm (c), 1μm (d) support	145
Figure 5.5	Small-angle X-ray scattering pattern of NiMo catalysts supported on SBA-15, Zr-SBA-15 (Direct) and Zr-SBA-15 (Post) support	146
Figure 5.6	Nitrogen adsorption-desorption isotherm of NiMo/SBA-15 and NiMo/Zr-SBA-15 catalysts with varying metal loading	148
Figure 5.7	Transmission electron microscopy images of NiMo/SBA-15 (a); NiMo/Zr-SBA-15 (Mo 12); NiMo/Zr-SBA-15 (Mo 17); NiMo/Zr-SBA-15 (Mo 22) catalysts	149
Figure 5.8	FT-IR spectra of pyridine adsorbed species on NiMo/SBA-15 and NiMo/Zr-SBA-15 catalyst with varying metal loading	151
Figure 5.9	Powder X-ray diffraction pattern of NiMo/SBA-15 and NiMo/Zr-SBA-15 catalysts with varying metal loading	152
Figure 5.10	Raman spectra comparison for NiMo/SBA-15 and NiMo/Zr-SBA-15 catalysts with varying metal loading	153
Figure 5.11	UV-DRS comparison for NiMo/Zr-SBA-15 catalyst with varying metal loading	154
Figure 5.12	HRTEM micrographs of sulfided NiMo/SBA-15 (a), NiMo/Zr-SBA-15 (Mo 12) (b), NiMo/Zr-SBA-15 (Mo 17) (c), NiMo/Zr-SBA-15 (Mo 22) (d) catalysts	155
Figure 5.13	The hydrodesulfurization and hydrodenitrogenation activity (volume basis) study NiMo/SBA-15 and NiMo/Zr-SBA-15 catalysts with varying metal loading; T = 375/385/395 °C, P=8.9 MPa, LHSV = 1 h^{-1}, H_2/HC ratio 600 Nm^3/m^3. HDS (a); HDN (b)	157

Figure 5.14	The hydrotreating activity (weight basis) comparison of NiMo/Zr-SBA-15 (Mo 17) and commercial catalyst; T = 375/385/395 °C, P=8.9 MPa, LHSV = 1 h^{-1}, H_2/HC ratio 600 Nm^3/m^3. HDS (a); HDN (b)	158
Figure 5.15	The hydrotreating activity (volume basis) comparison of NiMo/Zr-SBA-15 (Mo 17) and commercial catalyst; T = 375/385/395 °C, P=8.9 MPa, LHSV = 1 h^{-1}, H_2/HC ratio 600 Nm^3/m^3. HDS (a); HDN (b)	159
Figure 5.16	The simulated distillation comparison of HGO feed and product ontained by hydrotearting of HGO over optimzed NiMo/Zr-SBA-15 (Mo 17) catalyst	160
Figure 6.1	Effect of temperature on the conversion of sulfur and nitrogen present in heavy gas oil at pressure 8.9 MPa, hydrogen/gas oil ratio 600 Nm^3/m^3	163
Figure 6.2	Effect of LHSV on the conversion of sulfur and nitrogen present in heavy gas oil at pressure 8.9 MPa, hydrogen/gas oil ratio 600 Nm^3/m^3	165
Figure 6.3	Effect of pressure on the conversion of sulfur and nitrogen present in heavy gas oil at temperature 385 °C, LHSV 1 hr^{-1} and hydrogen/gas oil ratio 600 Nm^3/m^3	167
Figure 6.4	Effect of hydrogen/gas oil ratio on the conversion of sulfur and nitrogen present in heavy gas oil at temperature 385 °C, Pressure 8.9 MPa and LHSV 1 hr^{-1}	169
Figure 6.5	Arrhenius plot for HDS and HDN derived from Langmuir-Hinshelwood model with H_2S inhibition HDS (a), HDN (b)	184
Figure 6.6	Arrhenius plot for HDS and HDN derived from Langmuir-Hinshelwood model with H_2S inhibition for adsorption equilibrium constant for H_2S (a), sulfur (b) and nitrogen (c)	185
Figure 6.7	Long term stability study of optimized catalyst exhibited during hydrotreating of heavy gas oil	187

NOMENCLATURE

α	proportionality constant relating system pressure to H_2 pressure
β_{HDS}	isothermality ratio for the catalyst pellet in a HDS reaction
β_{HDN}	isothermality ratio for the catalyst pellet in a HDN reaction
γ_P	tortuosity of the catalyst pellets, dimensionless
$\Delta \rho_T$	temperature density correlation, lbs/ft^3
$\Delta \rho_P$	pressure density correlation, lbs/ft^3
$\Delta H_{R,HDN}$	heat of the hydrodenitrogenation reaction kJ/mol
$\Delta H_{R,HDS}$	heat of the hydrodesulfurization reaction kJ/mol
ε	catalyst bed porosity, dimensionless
ε_P	porosity of the catalyst pellets, dimensionless
η	effectiveness factor
$[\eta_O]_N$	effectiveness factor at the inlet of the hydrodenitrogenation reaction
$[\eta_P]_S$	effectiveness factor at the inlet of the hydrodesulphurization reaction
$[\eta_O]_N$	effectiveness factor at the outlet of the hydrodenitrogenation reaction
$[\eta_P]_S$	effectiveness factor at the outlet of the hydrodesulphurization reaction
Φ	thiele modulus
$[\Phi_O]_N$	thiele modulus at the inlet of the hydrodenitrogenation reaction
$[\Phi_O]_S$	thiele modulus at the inlet of the hydrodesulphurization reaction
$[\Phi_P]_N$	thiele modulus at the outlet of the hydrodenitrogenation reaction
$[\Phi_P]_S$	thiele modulus at the inlet of the hydrodesulphurization reaction
μ_L	viscosity of HGO at the operating temperature, g/(s·cm)
$\rho_{15.6}$	density of HGO at 15.6 °C, g/mL
ρ_L	density of HGO at operating condition, g/mL

ρ_T	density of HGO at the operating conditions, g/mL
a_L	interfacial surface area over unit volume of a catalyst, cm^{-1}
a_S	liquid/solid interfacial surface area, cm^{-1}
λ_N	adsorption energy for all nitrogen heteroatoms within gas oil, J/mol
λ_S	adsorption energy for all sulfur heteroatoms within gas oil, J/mol
°API	American Petroleum Institute gravity of petroleum liquids, dimensionless
A	surface area of catalysts and catalyst supports found from BET analysis, m^2/g
A_{HDN}	Arrhenius constant for the hydrodenitrogenation reaction rate, $s^{-1}\cdot(mol/L)^{(1-v)}$
A_{HDS}	Arrhenius constant for the hydrodesulfurization reaction rate, $s^{-1}\cdot(mol/L)^{(1-n)}$
Al	aluminum
Al_2O_3	aluminium oxide
ATM	atmospheric
B	boron
BET	Brunauer-Emmett-Teller method
BT	benzothiophene
BTU	British thermal unit
C_A	concentration of species *A*, mol/L
C_i	concentration of species *i*, mol/L
C_N	concentration of all nitrogen heteroatoms within gas oil, mol/L
Co	cobalt
C_S	concentration of all sulfur heteroatoms within gas oil, mol/L
d	average pore diameter of catalysts and catalyst supports, nm
DBT	dibenzothiophene
DDS	direct desulfurization

DM	demineralized water
DMDBT	dimethyl dibenzothiophene
DRU	diluents recovery unit
E_A	activation energy for the hydrotreating reaction of species 'A', J/mol
EDX	energy dispersive X-ray spectroscopy
E_{HDN}	activation energy for the hydrodenitrogenation reaction, J/mol
E_{HDS}	activation energy for the hydrodesulfurization reaction, J/mol
FBP	final boiling point
FCC	fluid catalytic cracking unit
FID	flame ionization detector
F	fluorine
FTIR	Fourier transform infrared spectroscopy
G/O	ratio of volumetric flow rates between hydrogen gas and gas oil
HC	hydrocarbon
HDA	hydrodearomatization
HDM	hydrodemetallization
HDN	hydrodenitrogenation
HDS	hydrodesulfurization
HGO	heavy gas oil
H_{H2}	Henry's constant for hydrogen in HGO, $MPa \cdot m^3/mol$
HMS	hexagonal mesoporous silica
HRTEM	high resolution transmission electron microscopy
HYD	hydrogenation

IBP	initial boiling point
ICP-MS	inductively coupled plasma mass spectroscopy
IWI	incipient wetness impregnation
k_A	apparent rate constant for species 'A', $(mol/L)^{(1-n)}.s^{-1}$
k_{HDN}	apparent rate constant of hydrodenitrogenation, $(mol/L)^{(1-n)}.s^{-1}$
k_{HDS}	apparent rate constant of hydrodesulfurization, $(mol/L)^{(1-n)}.s^{-1}$
K_A	adsorption equilibrium constant for component A, L/mol
K_{AA}	adsorption equilibrium constant for ammonia
K_{H2S}	adsorption equilibrium constant for hydrogen sulfide, MPa^{-1}
KIT-6	Korean Institute of Technology – 6
K_i	adsorption equilibrium constant for *i* species within gas oil, L/mol
K_N	adsorption equilibrium constant for nitrogen heteroatoms within gas oil, L/mol
K_S	adsorption equilibrium constant for sulfur heteroatoms within gas oil, L/mol
K_{SA}	adsorption equilibrium constant for decahydroquinoline
K_Y	adsorption equilibrium constant for aromatic amines
L_A	liquid mass flow over cross-sectional area, $g/(s \cdot cm^2)$
LGO	light gas oil
LHSV	liquid hourly space velocity, s^{-1}
LPG	liquefied petroleum gas
m	reaction order constant, dimensionless
M_{AVE}	average molecular weight of HGO, g/mol
MCM-41	Mobil Composition of Matter no. 41

MCM-48	Mobil Composition of Matter no. 48
Me	methyl
Mo	molybdenum
MoO_3	molybdenum trioxide
MPa	megapascal
n	reaction order constant, dimensionless
Ni	nickel
NiO	nickel oxide
nm	nanometer
NMR	nuclear magnetic resonance
NOx	nitrogen oxides
OMS	ordered mesoporous silica
P	phosphorus
P_{123}	poly (ethylene oxide)$_{20}$-poly (propylene oxide)$_{70}$-poly(ethylene oxide)$_{20}$ ($EO_{20}PO_{70}EO_{20}$)
PEO	poly (ethylene oxide)
PPO	poly (propylene oxode)
P_{H2}	partial pressure of hydrogen gas, Pa
P_{H2S}	partial pressure of hydrogen sulfide, Pa
r_A	reaction rate of species *A*, mol/(L·s)
r_{HDN}	rate of the overall hydrodenitrogenation reaction, mol/(L·s)
r_{HDS}	rate of the overall hydrodesulfurization reaction, mol/(L·s)
R	universal gas constant, J/(mol-K)
R^2	coefficient of regression for the reaction models, dimensionless

R^2_A	adjusted coefficient of regression for the reaction models, dimensionless
S	sulfur
SAXS	small-angle X-ray scattering
SBA-15	santa Barbara amorpous-15
S_{BET}	surface area found from BET analysis, m^2/g
SCO	synthetic crude oil
SEM	scanning electron microscopy
SG	specific gravity, dimensionless
SOx	sulfur oxides
STEM	scanning tunneling electronic microscopy
T_b	average boiling point of HGO, K
TEOS	tetraethyl orthosilicate
TGA	thermogravimetric analysis
Ti	titanium
TiO_2	titanium oxide
TIPB	triisopropyl benzene
TMB	trimethyl benzene
T_S	pellet surface temperature, K
TEM	transmission electron microscopy
TEOS	tetra ethyl ortho silicate
UV-DRS	ultra violet diffuse reflection spectroscopy
v_C	critical specific molar volume of HGO, mL/mol
v_{Cm}	critical specific mass volume, mL/g

v_i	molar volume of sulphur/nitrogen under standard conditions, mL/mol
v_L	molar volume of HGO under standard conditions, mL/mol
v_N	hydrogen molar volume at standard conditions, L/mol
V_b	hydrogen molar volume at the normal boiling point, mL/mol
V_C	volume of loaded catalyst, mL
VDU	vacuum distillation unit
VGO	vacuum gas oil
V_P	total pore volume found for catalysts and catalyst supports, cm^3/g
x_{HDN}	stoichiometric ratio of H_2 consumption for nitrogen removal, dimensionless
x_{HDS}	stoichiometric ratio of H_2 consumption for sulphur removal, dimensionless
XRD	X-ray diffraction
Zr	zirconium
ZrO_2	zirconium oxide

CHAPTER 1
INTRODUCTION

1.1 Research Background

The annual demand for high value petroleum products, specifically liquid fuels (gasoline and diesel) are increasing annually for most countries in the world (Speight, 2006). On the other hand, conventional lighter crude oil is depleting at an alarming rate across the world (Lee et al., 2007). Due to continuing depletion of lighter crude oil and advancement of oil sand technology, growing tendency to convert lower grade heavy feedstock, particularly heavy oil and bitumen to liquid product is increasing (Ancheyta and Speight, 2007; Domínguez-Crespo et al., 2008). In this regard, synthetic crude derived from oil sands are receiving importance as an alternative source of liquid fuels, which can meet the present and anticipated demand of conventional petroleum (Bej et al., 2001a; Bej et al., 2001b; Speight, 1984). However, oil sand (Athabasca) derived bitumen contains high levels of impurities (such as sulfur and nitrogen), which consequently reduce the quality of liquid products such as heavy gas oil (Bej et al., 2001b; Ding et al., 2007). Furthermore, environmental emission regulations introduce more stringent emission standards to reduce the level of impurities from the diesel fuel (Song and Ma, 2003). Hence, removal of impurities from heavy gas oil has become imperative to meet the more stringent fuel specifications imposed by government and meet the diesel product specification in terms of cetane number, density, aromatic content, boiling point. Hydrotreating, basically a means of removal of nitrogen, sulfur, oxygen, from gas oil, is employed in petroleum industry to improve the product quality without significant changes of the boiling range and molecular weight distribution of gas oil (Botchwey et al., 2006; Speight, 2006).

γ-Al_2O_3 supported NiMo/W and CoMo/W catalysts are used for hydrotreating of gas oil (Bej et al., 2004; Breysse et al., 2008; Speight, 2006). However, gas oil obtained from the processing of tar sands contains very high levels of impurities (sulfur ~ 4 wt % and nitrogen ~ 0.32 wt %), which are difficult to remove using conventional NiMo/γ-Al_2O_3 and CoMo/γ-Al_2O_3 catalysts (Ferdous et al., 2006a; Ferdous et al., 2007). Also, hydrotreating of such lower quality feed stock with the conventional catalysts needs more severe operating conditions (temperature, pressure), resulting in accelerated catalyst deactivation (Ancheyta et al., 2002a; Matsushita et al., 2004). Therefore, development of more advanced hydrotreating catalysts, which are more durable, possess higher activity and have better stability against the severe operating conditions than the conventional hydrotreating catalysts, is essential to process the heavy gas oil while meeting the new stringent fuel specifications (Ancheyta et al., 2002a; Maity et al., 2000).

Innumerable studies have been carried out to develop highly effective hydrotreating catalysts. Different approaches, such as using new supports (such as ZrO_2, TiO_2, MCM-41, and SBA-15), active phases (such as noble metals), promoters (chiral compounds), and additives (such as boron or fluorine) have been explored (Breysse et al., 2003a; Delmon, 1993; Dhar et al., 2003; Eswaramoorthi et al., 2008), and among the various strategies, utilization of more advanced support is considered as a better alternative (Grange and Vanhaeren, 1997; Maity et al., 2000). Catalyst supports play an important role in improving the property of a catalyst in terms of activity, selectivity, and stability, by manipulating its surface properties (Grange and Vanhaeren, 1997). By means of an adequate support designing it is possible to increase the activity of a hydrotreating catalyst significantly. The following properties are desirable for the development of good hydrotreating catalyst

supports: adequate textural properties, high activity and selectivity, appropriate acidity, and optimal metal-support interaction (Afanasiev et al., 1999; Bej et al., 2004; Furimsky, 2007; Hinnemann et al., 2005).

For the hydrotreating of heavy feeds, good textural properties are considered to be the most important criterion that any hydrotreating catalyst support must possess (Afanasiev et al., 1999). Adequate textural properties, namely high specific surface area and well-ordered uniform pore structure, of the catalyst support facilitate the dispersion of the active component on the catalyst support, allow diffusion of larger size molecules and increase the catalyst resistance to deactivation (Ancheyta and Speight, 2007). In this regard, mesoporous materials (such as, MCM-41, MCM-48, HMS, KIT-6, and SBA-15), which have excellent textural properties have been explored as hydrotreating catalyst supports (Huang et al., 2008a; Kostova et al., 2001; Sampieri et al., 2005; Soni et al., 2010). Among all mesoporous materials, SBA-15, which consists of large ordered and defined hexagonal cylindrical channels, received significant attention because of its excellent textural properties, higher hydrothermal stability, and higher hydrotreating activity for refractory compounds (Chen et al., 2004; Fulvio et al., 2005; Rayo et al., 2009). Moreover, in a hydrodesulfurization reaction, the SBA-15 supported catalysts show superior activity compared to γ-Al_2O_3 supported catalyst prepared in a similar way (Dhar et al., 2005).

Although SBA-15 possesses excellent textural properties and exhibits superior activity compared to γ-Al_2O_3 support, it has some limitations including the following: i) pure SBA-15 materials lack acidic sites (Rayo et al., 2009), ii) interaction between silica and Mo is very weak (Gutiérrez et al., 2006a), and iii) it provides inhomogeneous and poor dispersion of a sulfided active phase (Hensen et al., 2001).

To introduce surface acidity and improve catalytic activity of mesoporous SBA-15, various heteroatoms and their oxides (such as, Al, Zr, Ti and Al_2O_3, ZrO_2, TiO_2) have been incorporated into the SBA-15 framework (Gutiérrez et al., 2006a; Klimova et al., 2009; Rayo et al., 2009). Among different heteroatoms and their oxides, zirconia (ZrO_2) has attracted much interest due to higher intrinsic hydrodesulfurization activity in comparison with other metal oxides (Gutiérrez et al., 2009; Ji et al., 2004; Jia et al., 2005). However, the major disadvantage associated with pure zirconia supports is low surface area and porosity, which represent a limitation in its application as hydrotreating catalyst support (Gutiérrez et al., 2006a; Gutiérrez et al., 2007; Jia et al., 2005). In order to overcome limitations associated with both SBA-15 and ZrO_2, incorporation of ZrO_2 into the SBA-15 frameworks has been proven to be a better alternative (Gutiérrez et al., 2009). ZrO_2 incorporation in SBA-15 (Zr-SBA-15) resulted in improving the textural property and surface acidity of the support materials (Gutiérrez et al., 2008; Hensen et al., 2001; Rayo et al., 2009). Hence, a synergistic effect can be obtained while incorporating ZrO_2 onto SBA-15 and the resulting support can be used for hydrotreating catalyst improvement. According to literature, the Zr-SBA-15 supported NiMo catalysts show higher catalytic activity compared to the γ-Al_2O_3 and SBA-15 supported NiMo catalyst for hydrodesulfurization of refractory sulfur compounds (Gutiérrez et al., 2008).

Incorporation of Zr species in SBA-15 can be done by the direct synthesis or the post synthesis methods (Wu et al., 2004). In the direct synthesis method, Zr species incorporation into SBA-15 framework is accomplished during hydrothermal synthesis of SBA-15 materials (Chen et al., 2004). In the post synthesis method, Zr-SBA-15 is synthesized by a two stage

process. In the first stage, well-ordered SBA-15 is synthesized, and, in the second stage, Zr species is impregnated into the SBA-15 structure (Gutiérrez et al., 2006a).

In this thesis, the changes in structural and textural properties due to the incorporation of Zr species (Zr and ZrO_2) in SBA-15 framework by both direct and post synthesis methods are compared and the effects of resulting changes on the hydrotreating activity of supported NiMo catalysts over heavy gas oil feedstock derived from Athabasca bitumen are reported. The activity of the NiMo/Zr-SBA-15 catalyst is compared with the commercial NiMo catalyst supported on γ-Al_2O_3.

1.2 Knowledge Gaps

After a comprehensive review of research articles focusing on formulation and application of hydrotreating catalyst, it has been found that following key areas have not been explored:

- Till now hydrotreating activity study of zirconia doped SBA-15 supported NiMo catalyst is limited to model compounds only with a short run length. However, the activity of the Zr-SBA-15 supported catalysts towards the real feedstock containing various refractory and heavy compounds may not be the same as model compounds and this has not been studied.
- Also, till now Zr-SBA-15 supports with a pore diameter of less than 8 nm have been prepared by the post synthesis methods and tested for the hydrodesulfurization activity. However, Zr-SBA-15 supports with larger pore diameter (> 10 nm) have not been explored for hydrotreating activity using real feedstocks.

- Furthermore, no study has been conducted to investigate the effect of different Zr-SBA-15 support preparation methods (direct synthesis and post synthesis) towards catalytic activity using real feedstocks.
- Also, it is essential to evaluate the kinetics and catalyst stability of such new catalyst before considering for industrial applications. This has not been done earlier using Zr-SBA-15 supported NiMo catalyst.

1.3 Hypotheses

Based on the literature review, the following hypothesis has been considered for this research work:

- Larger pore diameter (> 10 nm) support, prepared by the post synthesis method, will improve the hydrodesulfurization and hydrodenitrogenation activity of NiMo/Zr-SBA-15 catalysts by transporting bulky sulfur and nitrogen molecules into the catalyst pores.
- Incorporation of Zr species into SBA-15 framework will increase the hydrotreating activity of the NiMo/Zr-SBA-15 catalyst for Heavy Gas Oil.
- Hydrotreating catalysts supported on large pore sized Zr-SBA-15 supports will be resistant to catalyst deactivation, which occurs due to coke and metal deposition in the catalyst pores. Larger pore diameter will prolong the on-stream catalyst life.

1.4 Research Objectives

The main objective of this proposed research is to synthesize, characterize and study the hydrodesulfurization (HDS) and hydrodenitrogenation (HDN) activities of NiMo catalyst supported on Zr-SBA-15 material utilizing heavy gas oil (HGO) feed derived from Athabasca bitumen. In order to achieve this objective the work was divided into three phases as followings:

Phase I: Hydrotreating of gas oil over NiMo/Zr-SBA-15 catalysts

The changes in structural and textural properties due to the incorporation of Zr species in SBA-15 material by both direct and post synthesis methods were compared and the effects of the resulting changes on the hydrotreating activity of supported NiMo catalysts over heavy gas oil feedstock derived from Athabasca bitumen were studied. The best method of Zr-SBA-15 support preparation was determined by analyzing the extent of HDS and HDN conversion over NiMo/Zr-SBA-15 catalysts. Furthermore, the activity of the NiMo/Zr-SBA-15 catalyst was compared with the NiMo catalyst supported on SBA-15 and γ-Al_2O_3.

Phase II: Metal loading optimization for NiMo/Zr-SBA-15 catalysts

After determination of the effective Zr-SBA-15 support material for the hydrotreating NiMo catalyst from phase I, variation of metal loading (Ni and Mo) was carried out to find out the optimum metal (Mo and Ni) loading over Zr-SBA-15 support. In this process, molybdenum loading was varied from 12 to 22 wt% whereas the Mo/Ni ratio was kept constant value of 5. Catalytic activities of these catalysts were evaluated based on extent of HDS and HDN activity exhibited during the hydrotreating of heavy gas oil.

Phase III: Kinetic study of HDS and HDN

After determination of the optimized catalyst from the phase-II, the performance of the optimized catalyst was tested under various process conditions. The effect of reaction conditions, such as temperature, pressure, and LHSV and H_2 gas/oil ratio on HDS and HDN over best catalyst was performed. To estimate the kinetic parameters for various reaction conditions and predict the reaction kinetics, kinetic models were developed based on Power Law and Langmuir-Hinshelwood kinetic expressions. Finally, in order to check the long term stability of the optimum catalyst, a long term deactivation study was carried out for the optimum catalyst.

CHAPTER 2
LITERATURE REVIEW

This chapter describes the literature review related to this research work. In section 2.1, world energy consumption is described. Characteristics of petroleum and gas oil, hydrotreating process and hydrotreating catalysts are described in section 2.2, 2.3 and 2.4 respectively. In section 2.5, selection of Zr-SBA-15 supports for hydrotreating of gas oil is described. SBA-15 and Zr-SBA-15 as hydrotreating catalyst supports are described in section 2.6 and 2.7 respectively. Finally, in section 2.8 kinetic modeling of HDS/HDN is described.

2.1 World Energy Consumption

World energy consumption is expected to increase significantly due to rapid economic growth occurring in developing countries. Presently, petroleum, coal and natural gas govern the supply of heat, electrical energy and fuels in energy systems worldwide. These fossil energy cover approximately 90 per cent of primary energy consumption worldwide (petroleum 40 per cent, coal 27 per cent, natural gas 23 per cent) (Ancheyta and Speight, 2007). Energy statistics from the International Energy Agency (IEA) represent the energy consumption of the principal fuel from 1970 to 2025 (shown in Figure 2.1) (International Energy Outlook, 2004). From the figure it is evident that fossil fuels, including oil, coal, and natural gas will remain the dominant sources of energy. Among the conventional fuels, natural gas and oil consumption will increase more rapidly compared to others. Oil consumption will rise continuously, due to increasing demand in the transportation sector. However, due to continuous depletion of conventional oil, over next few decades the world's energy sector encounters challenges, which includes, growing oil scarcity, achieving energy security, combating environmental degradation and meeting the growing needs of the

developing world (Dorian et al., 2006). In order to meet the global energy demand and mitigate the problems related to the depletion of conventional oil, growing tendency to oil production from non-conventional sources are increasing. In this context, synthetic crude oil, extracted from tar sand, has been recognized as a viable option for producing a significant percent of the worlds' oil (Bej et al., 2001b). Western Canada has a large source of oil sands, which is used for bitumen production. Currently, bitumen is used for the production of synthetic crude oil (Yui, 2008).

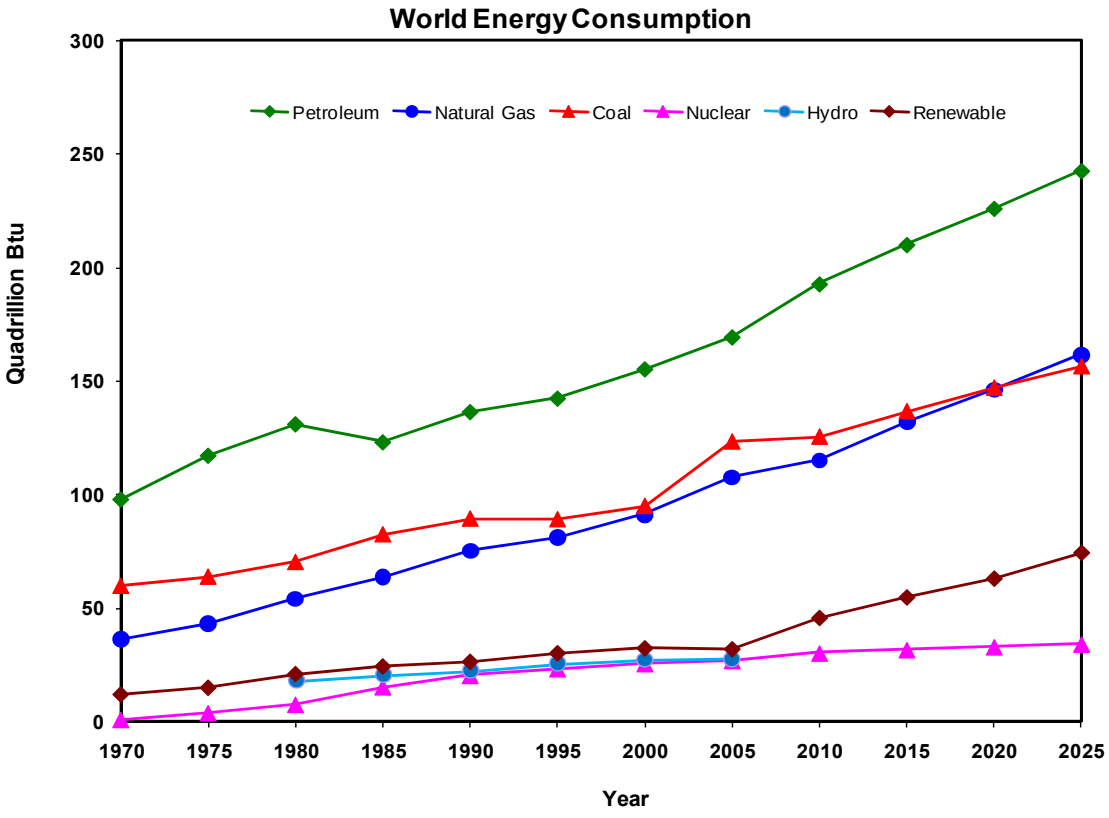

Figure 2.1: World energy consumption (International Energy Outlook, 2004).

2.2 Characteristics of Petroleum and Gas Oil

2.2.1 Definition of Bitumen, Heavy Oil and Heavy Gas Oil

Petroleum or crude are the world's major sources of energy, which is used extensively as the sources of liquid fuels (Ancheyta and Speight, 2007). In some places synthetic crude

oils (heavy oil derived tar sands) are also considered as the viable sources of liquid fuel (Lee et al., 2007). Currently, fuel, transportation and petrochemical industries greatly rely on the petroleum and synthetic crude oil based feedstocks and this reliance is projected to be increased continuously for several decades (Lee et al., 2007). "Petroleum", "bitumen" and "heavy oil" are usually defined by their physical properties as shown in Table 2.1.

Petroleum or crude oil is a naturally occurring, flammable liquid composed of mixtures of hydrocarbons of various molecular weights and other compounds containing small amounts of oxygen, sulfur, nitrogen, vanadium, nickel and chromium (Ancheyta and Speight, 2007; Gray, 1994) The physical characteristics of petroleum vary widely whereas their chemical compositions are relatively uniform (Gray, 1994). The elemental compositions of petroleum and Athabasca bitumen are shown in Table 2.2.

Oil sands (also referred as tar sands and bituminous sands) are a naturally occurring sand deposit that containing about 10-12% bitumen, 4-6% water and 80-85% sand and clay (Yui, 2008). Oil sand derived synthetic crude contains large amounts of middle distillate compared to the conventional crude (Yui, 2008). It contains about 44% gas oil and 56% vacuum bottoms.

Bitumen is the term often referred to as native asphalt and extra heavy oil, is the mixture of hydrocarbons of natural or pyrogenous origin or combination of both (Krishnan and Rajagopal, 2003; Speight, 2006). Bitumen basically includes a wide variety of reddish brown to black materials of semisolid, viscous to brittle character, which are soluble in carbon disulfide (Ancheyta and Speight, 2007; Gary and Handwerk, 2001). Tar sand (or Athabasca) bitumen is a highly viscous hydrocarbonaceous material that consists of carbon and hydrogen with smaller amount of nitrogen, sulfur, oxygen, aromatics, carbon residue,

asphaltenes and metals (Lee et al., 2007; Speight, 2006). In Canadian Athabasca tar sand the anticipated deposited bitumen is 1.7 trillion barrels, which is considered to be a potential source of energy (Ancheyta and Speight, 2007; Lee et al., 2007).

Heavy Oil is a type of petroleum that is different from conventional petroleum, which requires thermal simulation of recovery from subsurface reservoir (Speight, 1999). The term heavy oil is usually is based on °API gravity or viscosity of petroleum or crude oil. Heavy oil is a type of petroleum that has an API gravity of less than 20 degree and sulfur content higher than 2 wt% (Speight, 1999). Heavy oil is characterized by followings: high viscosity, low API gravity, high specific gravity, low hydrogen to carbon ratio, high carbon residues, and high content of asphaltenes, heavy metal, sulfur and nitrogen (Ancheyta and Speight, 2007).

Heavy gas oil (HGO) is a distillate product of petroleum. This cut could be a heavy side stream of atmospheric distillation unit or it could be a distillate cut from a vacuum distillation unit. HGO cut range depends upon the types of crude. HGO obtained from Kuwait crude has boiling range 321-365 °C. HGO obtained from Arabian heavy crude has boiling range 345-565 °C (David and Pujadó, 2006). Boiling range of HGO derived from Athabasca bitumen is 343-525 °C (Yui, 2008). HGO obtained from refinery atmospheric distillation units has a boiling range 315-425 °C (Gray, 1994; Speight, 1999). Heavy gas oil obtained from atmospheric distillation units is routed to heating oil blending pool, gas oil pool or fuel oil pool (David and Pujadó, 2006). Heavy gas oil obtained by vacuum distillation of crude oil is used as catalytic cracker feedstock (Ancheyta and Speight, 2007).

Table 2.1: Characteristics of conventional crude oil, bitumen and heavy oil (Gray, 1994; Lee et al., 2007).

Material	API Gravity	Density, g/cm^3	Viscosity, mPa.s
Conventional Crude Oil	25-37	-	10
Bitumen	<10	>1.00	> 10^5
Heavy Oil	20-10	0.934-1.0	10^2-10^5

Table 2.2: Elemental analysis of petroleum and Athabasca bitumen (Gray, 1994; Speight, 1999).

Element	Percent by weight	
	Petroleum	Athabasca Bitumen
Carbon	83-87	83.1
Hydrogen	10-14	10.3
Sulfur	0.05-6.0	4.9
Nitrogen	0.1-2.0	0.4
Oxygen	0.05 -1.5	1.3
Metals	<0.1	>0.1

2.2.2 Syncrude Upgrading Process

Syncrude Canada Ltd. operates surface mining oil sands, a bitumen extraction plant, and an upgrading facility that process bitumen and produce Synthetic Crude Oil (SCO) from the Athabasca oil sands deposit (Yui, 2008). In Figure 2.2 the Syncrude upgrading process is shown in block diagram. Through upgrading process, Syncrude converts bitumen into high value, light, low sulphur Syncrude Crude Oil. Two upgrading processes are employed for this upgrading process: primary upgrading and secondary upgrading.

In the primary upgrading, the diluted bitumen from the Extraction and Froth Treatment Plant is sent to the Diluent Recovery Unit (DRU), where water is removed and naphtha is recovered. The dry bitumen is then fed to the Vacuum Distillation Unit (VDU), LC-Finer

Hydrocracking and Coker unit. In the VDU, LGO and HGO are distilled off and sent to the hydrotreater unit. The remaining bitumen is sent to the LC-Finer hydrocracking and coker unit, where bitumen is cracked. In the LC-Finer umit, LGO and HGO are produced via a catalytic process in the presence of hydrogen. LGO and HGO are then sent to the hydrotreater unit and the remaining bitumen is sent to the Coker unit. In the Coker unit Naphtha, LGO, HGO, and coke are produced. Naphtha, LGO and HGO are sent to the hydrotreater unit for further treatment. In the secondary upgrading stage, sulfur, nitrogen and aromatics are removed from naphtha, LGO and HGO. The treated liquid products are then blended together to form Syncrude Crude Oil (SCO) and sent to a downstream refinery (Yui, 2008).

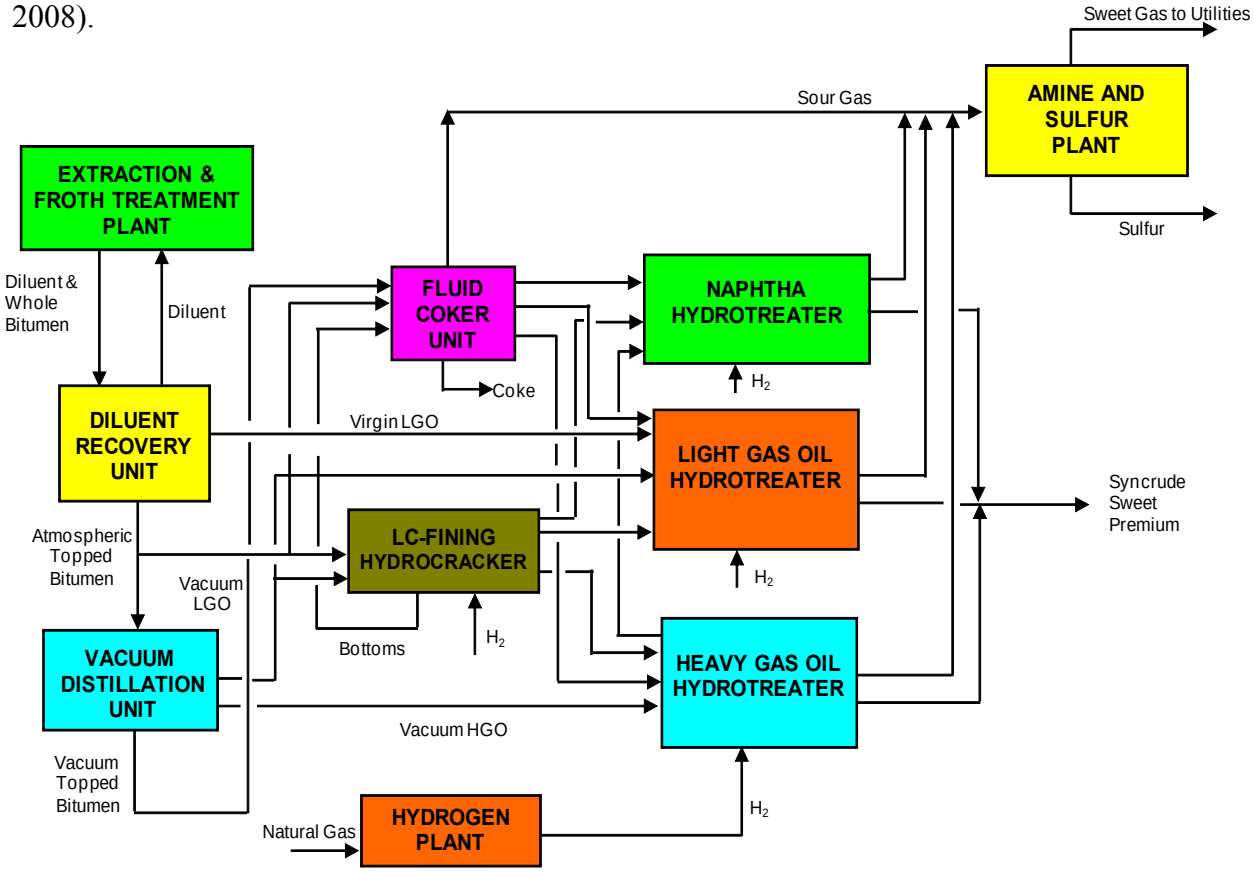

Figure 2.2: Syncrude upgrading process (Yui, 2008).

2.2.3 Chemical Compounds Present in Petroleum

Petroleum contains predominantly hydrocarbons, moderately heteroatoms (nitrogen, sulfur, and oxygen) and a minor extent of metallic constituents. Among the heteroatoms constituents, sulfur and nitrogen are most abundant impurities in petroleum. A wide variety of sulfur and nitrogen compounds are present in petroleum. In general, sulfur content in petroleum varies from 0.1 to 5 wt% depending upon their origin. The most abundant heterocyclic sulfur compounds identified in petroleum includes sulfides, thiophenes, benzothiophenes, dibenzothiophenes, and naphthobenzothiophenes (Song and Ma, 2003; Speight, 1999). The distribution of various sulfur compounds in crude oil variation depends upon the origin of crude oil. In Figure 2.3, the structure of some of the sulfur compounds which are present in crude oil are shown.

The nitrogen content in petroleum varies from 0.1 wt% to 1 wt%. The heterocyclic nitrogen compounds in crude oil fractions are higher molecular weight quinoline derivatives, pyridine derivatives, benzoquinoline derivatives, amides, indole derivatives, and carbazole derivatives (Speight, 1999). The heterocyclic nitrogen compounds in gas oil are present in the form of basic and non-basic aromatic compounds (Ferdous et al., 2006a). Basic nitrogen compounds are mostly six membered pyridine groups. Non-basic nitrogen compounds are usually five membered pyrrole groups. Typical heterocyclic nitrogen compounds present in petroleum are shown in Figure 2.3.

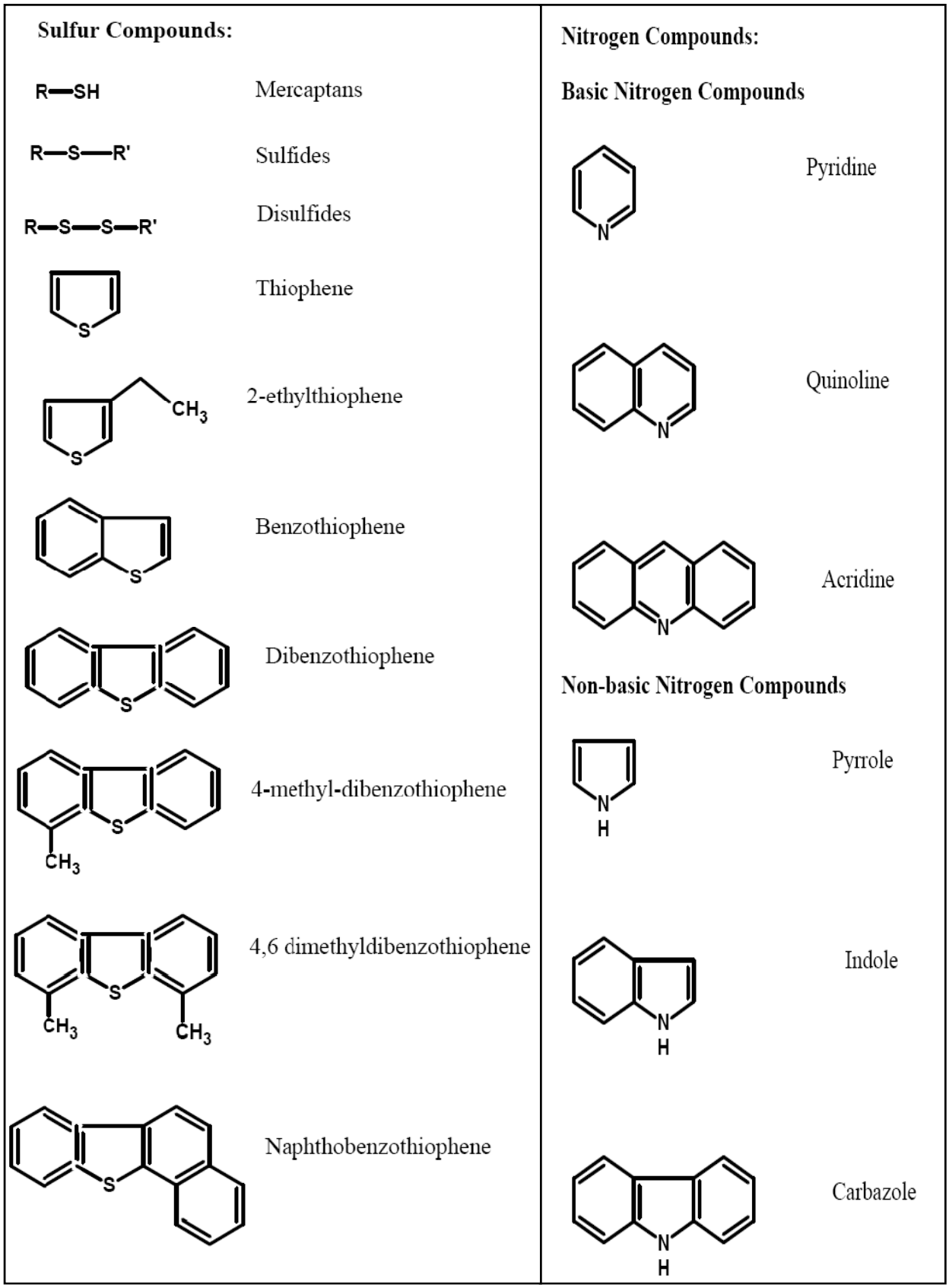

Figure 2.3: Structure of sulfur and nitrogen compounds present in petroleum (Topsøe et al., 1996).

2.2.4 Reactivity of Sulfur and Nitrogen Compounds

Hydrodesulfurization reactivity depends on structure and molecular size of the sulfur containing compounds. A reactivity ranking for the sulfur compounds in HDS reaction is presented in Table 2.3 (Speight, 1999). Desulfurization reactivity is related to the location of the substituent groups. Substituent groups located far from the sulfur atom do not affect the HDS activity (Kabe et al., 1998). However, substituent groups which are located at the adjacent of sulfur atom, retard the HDS rates. For refractory compounds, inhibition of C-S bond cleavage or adsorption of substrates greatly affected by steric hindrance of substituents. In the diesel oil fraction, the most refractive is compound is higher molecular weight dibenzothiophene, which has side chains at the adjacent to the sulfur atom. Sterically hindered compounds, such as 4, 6 –dimethyl dibenzothiophene and 4,-methyl dibenzothiophene are reported to be less reactive than unsubstituted dibenzothiophene (Knudsen et al., 1999). In Figure 2.4, the type and size of sulfur molecules and their reactivity are presented.

Table 2.3: Hydrodesulfurization reactivity of various sulfur substituted molecules (Speight, 1999).

Compound Type	**Relative Activity**
Thiophene	2,5-dimethyl < 2-methyl < no substituent < 3-methyl
Benzothiophene	3-methyl < 2-methyl = no substituent 3,7 – dimethyl < 3-methyl = 2-methyl = 7-methyl < no substituent
Dibenzothiophene	4,6-dimethyl < 4-methyl < no substituent < 3,7-dimethyl < 2,8 – dimethyl

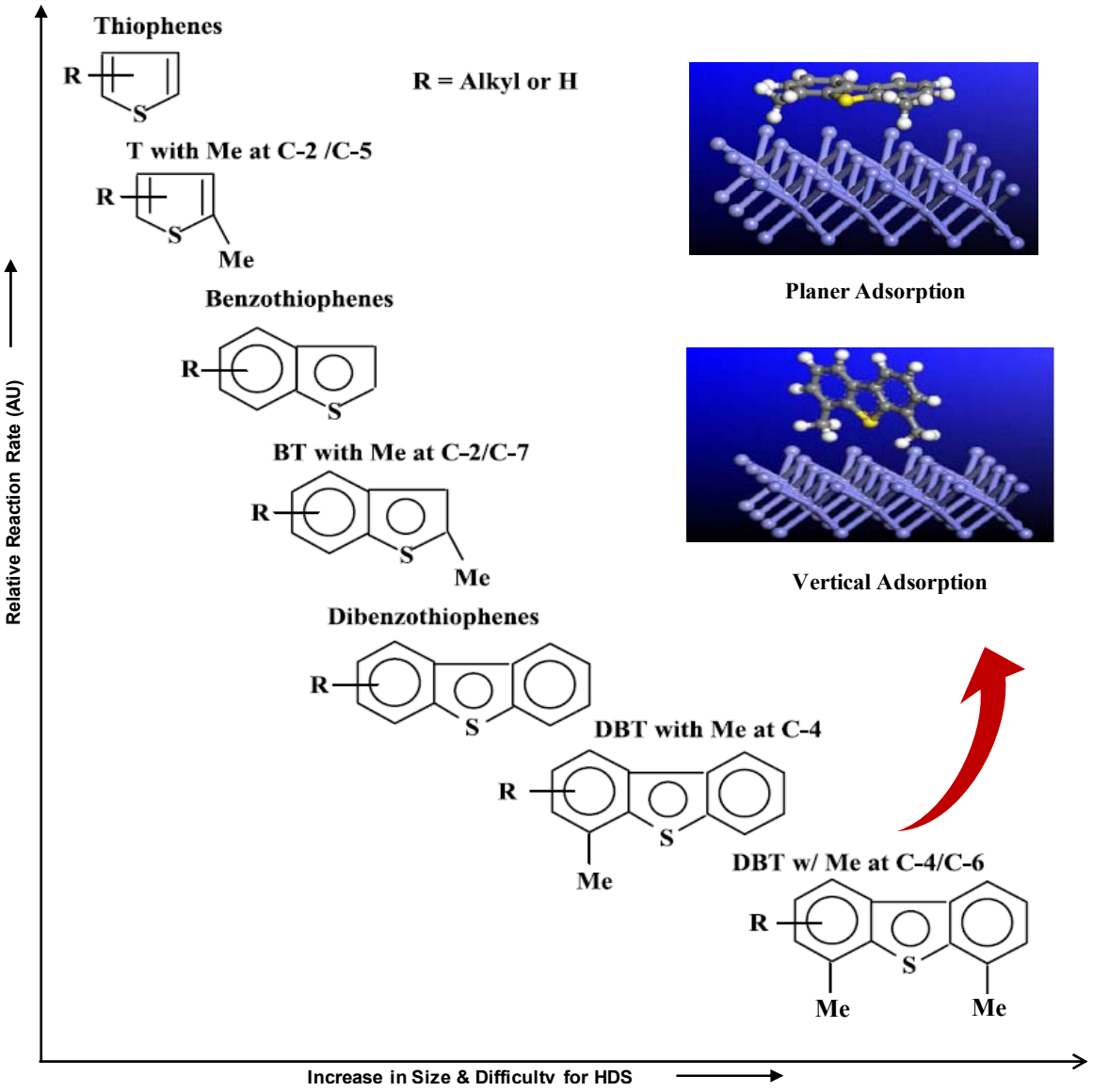

Figure 2.4: Reactivity of various organic sulfur compounds in HDS versus their ring sizes and positions of alkyl substitutions on the ring (Hong et al., 2006; Song, 2003).

Hydrodenitrogenation of heterocyclic nitrogen compounds are initially proceed through the hydrogenation of nitrogen ring and then the subsequent C-N hydrogenolysis. Basic and non-basic nitrogen compounds have different electronic configurations. Five-member nitrogen heteroatomic groups do not readily interact with the acid due to presence of the extra pair of electron in nitrogen (Bej et al., 2001b). On the other hand, six-membered

nitrogen heteroatoms interact with the acid due to presence of unshared pair of electrons. The order of decreasing reactivity for hydrogenation of nitrogen ring compounds is shown in Figure 2.5.

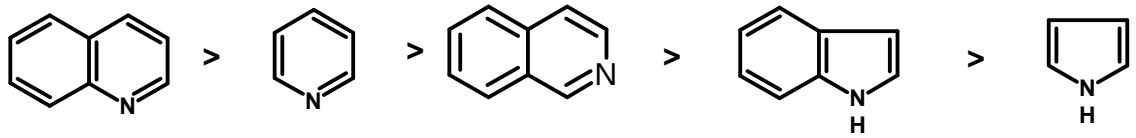

Figure 2.5: Relative reactivity of nitrogen compounds (Schulz et al., 1986).

2.3 Characteristics of Hydroteating Process

2.3.1 Definition of Hydrotreating Process

Hydrotreating or catalytic hydrogen treating is an important catalytic process that removes objectionable materials from petroleum fractions and/or stabilizes petroleum products by selectively reacting them with hydrogen over a catalyst without changing the boiling range of the feed (Ancheyta and Speight, 2007; Gary and Handwerk, 2001). Removal of objectionable elements includes heteroatoms, such as nitrogen, oxygen, sulfur, halides, nickel and vanadium. Stabilization of products includes saturation of olefins, diolefins and aromatics (Speight, 1999). When the purpose of the hydrotreating process is to remove sulfur from the petroleum fraction it is called as hydrodesulfurization (HDS). When the purpose of the hydrotreating process is to remove nitrogen, it is called as hydrodenitrogenation (HDN). Similarly, the removal of oxygen and metals from the feed by means of hydrotreating process is called as hydrodeoxygenation (HDO) and hydrodemetallization (HDM). In a modern refinery the application of hydrotreating depends upon the desired distribution of different products and their compositional requirements. Starting from lighter material such as naphtha to heavier distillates such as jet fuel to heavy vacuum gas oil are treated in the hydrotreating

unit to meet the environmental regulation or to use as feedstock for other units (Gary and Handwerk, 2001). Hydrotreating process is also used for upgrading the quality of atmospheric residues. Application of hydrotreating in a modern refinery is shown in Figure 2.6. However, depending upon the type of crude, local product demand and desired product slate there will be a variation in the final process schemes.

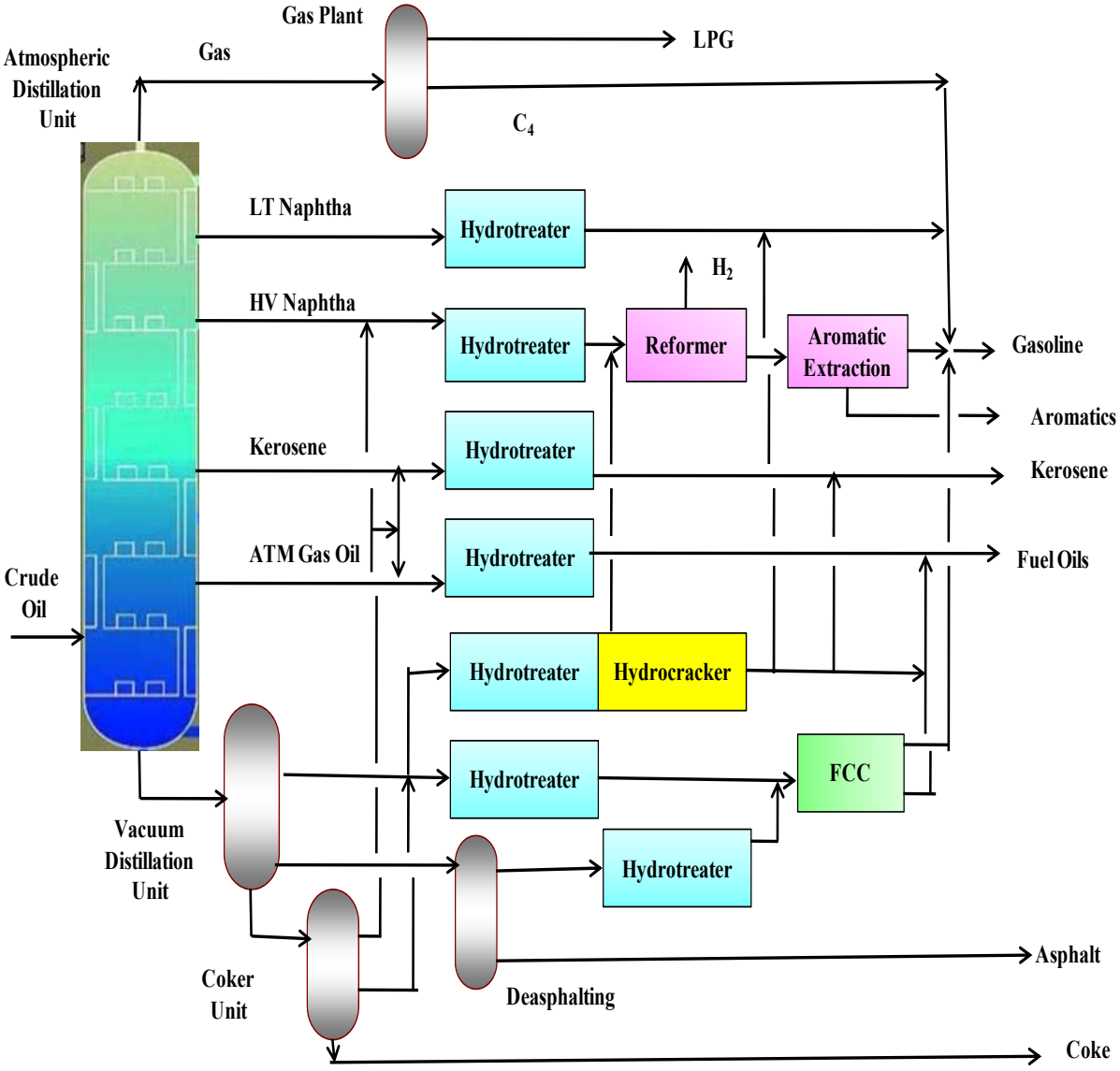

Figure 2.6: Application of hydrotreating in a modern refinery (Mochida and Choi, 2004).

2.3.2 Hydrotreating Process Description

Although the hydrotreating process has several different applications (e.g. desulfurization, olefin saturation, denitrification etc.) practically all units have the same flow scheme as shown in Figure 2.7 (David and Pujadó, 2006). In the process description, the gas oil hydrotreating unit is divided into three main process sections as mentioned below-reaction section, separation section and fractionation section.

Reaction Section: The feed arrives to the unit and is received by a feed surge drum. Compressed hydrogen gas coming from the make-up gas compressor, is joined with the recycle gas and mixed with the pumped feed. The feed and hydrogen mixture is sent to the preheating section before sending to the furnace. Feed and recycle gas is heated together in the reactor charge heater to obtain desired reactor inlet temperature. The reactor feed is then sent to down-flow trickle bed hydrotreating reactor. Hydrotreated reactor effluent is sent for cooling, which is accomplished in the reactor feed/effluent exchanger and sent to the separation section.

Vapor/liquid Separation: High and Low temperature separator separates liquid and vapors from the reactor effluent. A High Temperature (HT) separator is used after the feed/effluent exchanger to separate the liquid and vapor before sending the liquid product to the main fractionator. The overhead vapor from the HT separator continues to air cooled into a Low Temperature (LT) separator. Purge gas is removed from the top of the LT separator and the bottom liquid is sent to the main fractionation section.

Fractionation Section: The purpose of the fractionation section is to separate the reactor effluent into the desired products. Fractionator column, diesel stripper and naphtha stripper are employed to accomplish this. A stripper column is provided to strip lighter materials from the LT and HT separator bottoms. The liquid products from the separators are preheated in the fractionator pre-heater before sending it to the fractionator. Stripping steam is used to

remove lighter material from the products. The overhead product of the fractionator is sent to the naphtha stripper to obtain naphtha products. The bottom of the fractionators is basically heavy product, and is sent for further treatment. The fractionator side cut is sent to the diesel stripper to remove any water and H_2S before sending to diesel storage as the final diesel product.

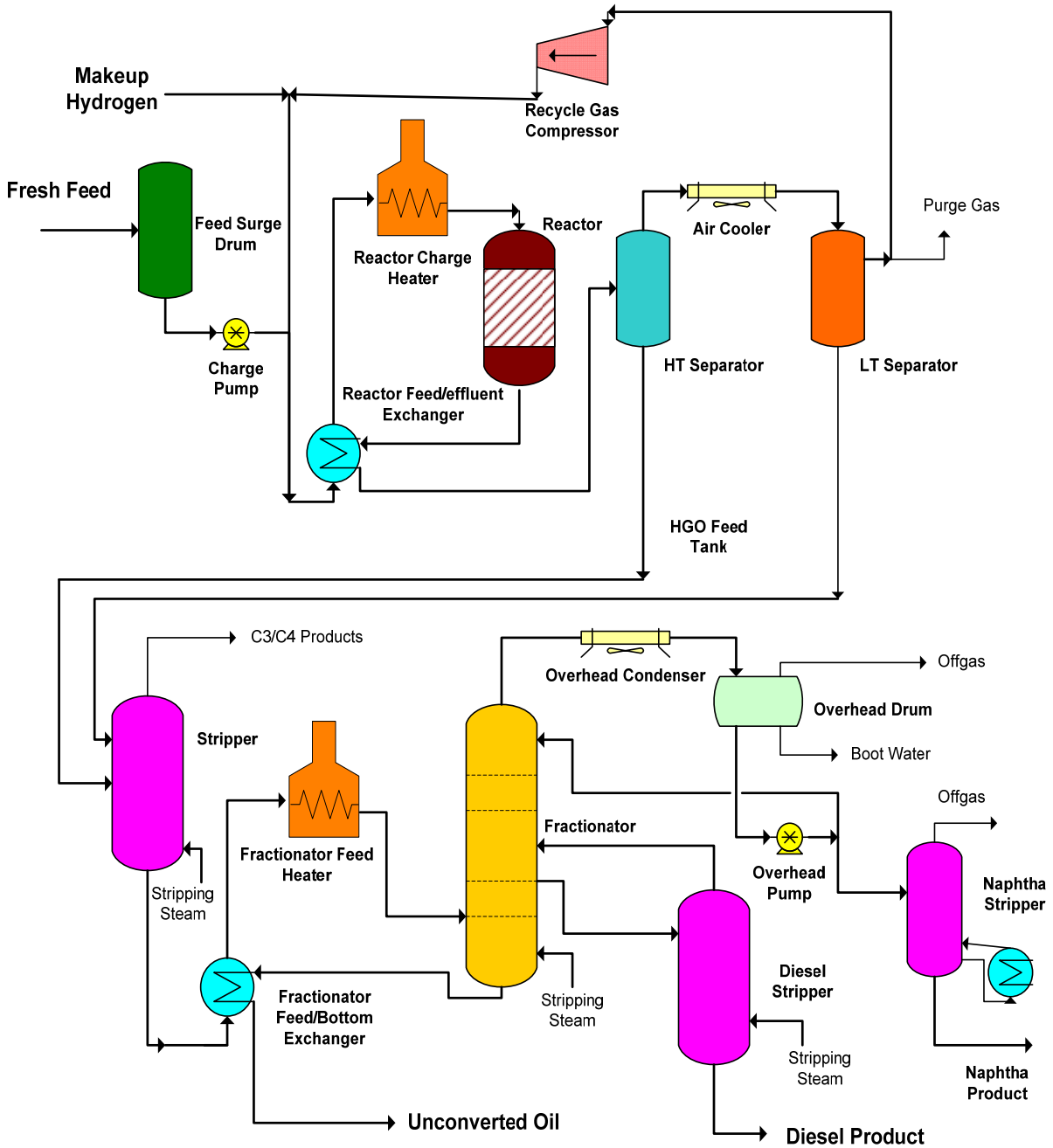

Figure 2.7: Process scheme for hydrotreating of gas oil (David and Pujadó, 2006).

2.3.3 Purposes of Hydrotreating

Hydrotreating process is applied for various process streams depending upon the desired product specification of the final products. Hydrotreating for gas oil stream is done to remove heteroatoms from the gas oil. The elimination of heteroatoms from heavy gas oil is required for the following reasons:

- **Abatement of SO_X and NO_X emission**: The major emission from diesel engines constitute of SO_x and NO_x. Control of these emissions is targeted by improving the fuel specification and engine performance. Environmental emission regulations introduce more stringent national emission standards to maintain SO_x and NO_x emissions below regulatory levels (Song and Ma, 2003). Hence, sulfur and nitrogen removal from gas oil has become imperative in order to meet the more stringent fuel specifications imposed by government.
- **Improvement of diesel fuel properties:** Diesel product specification needs to be met in terms of cetane number, aromatic content, density, and boiling point, which can be achieved by hydrotreating process (Furimsky, 2007).
- **Protection of catalyst:** Hydrotreating processes helps to protect the catalysts used in downstream units (such as fluid catalytic cracking and hydrocracking) of the refining process (Grange and Vanhaeren, 1997).
- **Fuel stability:** Hydrotreating processes increases the stability of the final diesel fuel during storage (Rahimi et al., 1998).
- **Reduction of equipment corrosion:** High level of sulfur in feedstock can cause corrosion in the refinery process equipments (Speight, 1999). Hydrotreating processes reduces the corrosion during refining and handling of various refinery streams.

2.3.4 Hydrotreated Diesel Specification

The major emissions from diesel engines constitute of SO_X, particulates, CO, NOx and HC. Hydrotreating process technology is applied to improve the diesel fuel specification and control the emissions from diesel engine. The following key properties of diesel fuel have been identified which are considered to have major impact on emission and needs to be improved by hydrotreating process (Gray, 1994; Satterfield, 1991; Speight, 1999).

- **Sulfur:** Sulfur present in the crude oils and essential to remove to an acceptable level during refining process since it promotes corrosion. Sulfur in diesel fuel has a direct relationship on SOx emission from the exhaust. The H_2SO_4 formed in the exhaust stream due to emission of "S" compounds causes increased formation of particulate matter in the exhaust. Also, sulfur reduces the efficiency of catalytic converters.

- **Cetane Number:** Cetane number (CN) is a measure of the ignition properties and combustion of the diesel fuel. Cetane number influences the length of the time from the start of fuel injection to the start of combustion in diesel engines. Higher cetane values results in better combustion and lower emissions. Cetane (n-hexadecane), has cetane number a 100 and it ignites very easily. It is related to the aromatic content of the fuel. The cetane number is important for the quality measurement of diesel fuel, as a higher cetane number reduces the ignition delay, provides smoother combustion and lower combustion noise.

- **Density:** Diesel is made up of a mixture of complex hydrocarbons of various densities and molecular weights. Hence, the density of diesel is related to other parameters, such as cetane number, aromatic content, viscosity and distillation. Variation of fuel density can result in variation in the energy content of fuel, ignition temperature and NOx emission.

- **Viscosity:** Viscosity is the measure of fuels' resistance to flow. High viscosity fuel can reduces the flow rate of the fuel, which results in insufficient flow rate and reduces the performance of the diesel fuel pump. Low viscosity may result in leakage of fuel from pumping system. Hence the viscosity range of diesel needs to be maintained.

- **Aromatics:** Aromatics and polyaromatics are the key factors for particulate formation. Polyaromatics also have an effect on ignition temperature. The formation of NOx is related to ignition temperature.

- **95% boiling point:** The volatility of the diesel is measured by the distillation curve. For diesel T95 distillation is very important as this provides the information about the proportion of heavier components. The presence of heavier components in diesel results in incomplete combustion. Hence, reduction of end point is required to decrease the quantity of unburned HC and the level of particulate emitted. This also improves viscosity and cold flow properties of diesel. The diesel specifications for Europe and USA are presented in Table 2.4.

Table 2.4: Diesel specifications for Europe and USA (Topsøe et al., 1996).

	Europe	**USA**
Year	2005	2005
Density , kg/m^3 , max	825	876
S, ppmw, max	50	500 (15 from 2006)
Cetane no	58	40
Aromatics , vol%	-	10
Poly aromatics, wt% , max	1	2
Boiling range , IBP-FBP, °C	180-340	180-365
Viscosity@40 °C, mm^2/s	2.0-4.5	1.9-4.1

2.3.5 Challenges of Hydrotreating Processes

An innumerable number of articles have been published regarding the difficulties associated with hydrotreating of gas oil. Presently, societal needs for the high quality valuable liquid fuels, especially diesel and gasoline, are increasing. In order to meet these

requirements, refineries are facing challenges to product high quality diesel product due to following reasons (Babich and Moulijn, 2003).

- **Degradation of quality of crude oil:** The depletion of the reserves of the conventional petroleum has created an interest in the conversion of the heavier feedstock, such as Athabasca bitumen (Speight, 1999). Processing of heavier feedstock causes the quality degradation of gas oil. Currently, it is difficult to achieve the required level of conversion of heavier feedstock with the Ni (Co) Mo/γ-Al_2O_3 catalysts, which have been widely used for hydroprocessing of conventional feeds (Bej et al., 2001a).

- **Presence of refractory sulfur compounds in gas oil:** The most refractive sulfur compounds are higher molecular weight compounds that contain side chains with sulfur atoms. Refractory molecules, 4-methyl-DBT (4-MDBT) and 4, 6-dimethyl-DBT (4, 6-DMDBT) are key sulfur compounds in the gas oil fraction and they are difficult to desulfurize. However, in order to achieve desired level of HDS and targeted product sulfur level of 15 ppm, it is essential to desulfurize these refractory molecules (Furimsky, 2007).

- **Presence of high level of nitrogen:** Bitumen derived gas oil contains a high level of nitrogen (0.30 wt %) compared to other crude such as Kuwait crude oil derived gas oil (0.13wt %) (Bej et al., 2001a; Ferdous et al., 2006b). In order to obtain a desirable conversion of hydrotreating reactions a high level of hydrodenitrogenation is essential (Furimsky and Massoth, 2005). In addition, during hydrotreating process, nitrogen compounds are more strongly adsorbed on catalytic sites than the refractory compounds. Strong adsorption of nitrogen compounds adversely affect the hydrogen activation process and hinder the adsorption of refractory compounds on the catalyst surface resulting in lower hydrotreating activity (Furimsky and Massoth, 2005).

- **Stringent environmental regulation:** Stringent environmental regulation creates major technical challenges. In Canada, diesel fuel specification for off-road engines is set at 500 ppm untill 31st May 2010 and 15 ppm from 31st May 2010 onwards (Environmental Canada). The limit of sulfur in on-road diesel fuels set by government from 1990 to 2015 is shown in Figure 2.8. Also, the NOx emission level standard over the period of 20 years for on-road diesel engines is shown in Figure 2.9. Hence, the projected changes in the final diesel fuel specification require modification of process parameters or replacing current catalysts with more active catalysts.

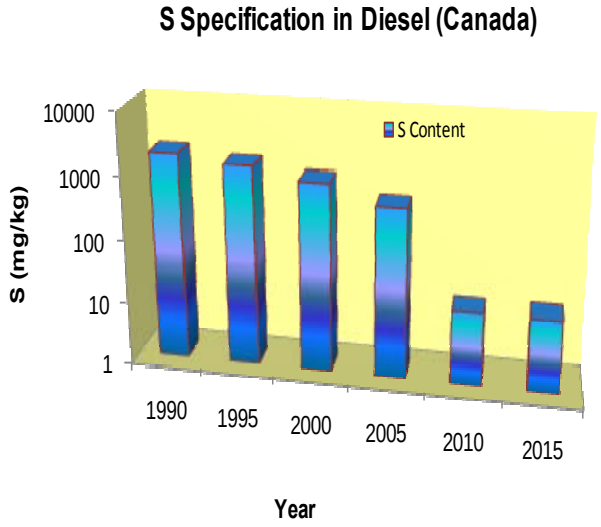

Figure 2.8: Sulfur content in diesel fuel (Environmental Canada)

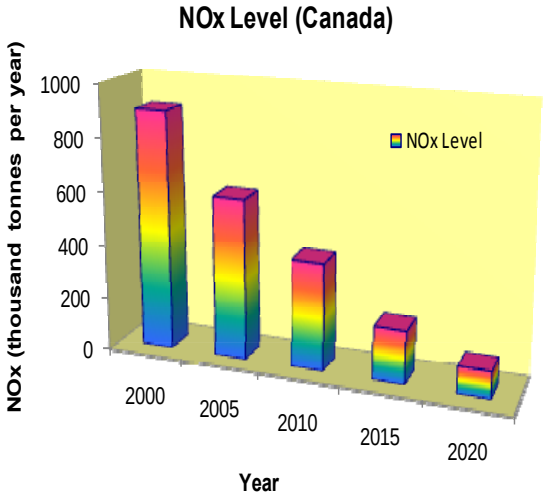

Figure 2.9: NOx emission standard for diesel engine (Environmental Canada)

- **Process, reactor and catalyst improvement:** The ultra-low sulfur diesel (ULSD) production target necessitates major modification in the refinery process, including changing of process conditions, reactor configuration and catalyst. Hydrotreating efficiency can be increased by employing advanced reactors (e.g. multiple bed reactors), new reactor internals and catalyst. In refinery, conventional HDS process is employed to improve the desulfurization process. However, several other processes, such as transformation of sulfur compounds by catalytic distillation etc, have been proposed, which may prove very

promising for producing ULSD (Babich and Moulijn, 2003). Deep desulfurization also can be obtained by increasing the severity of HDS process conditions. Required increase in catalyst activity (for typical Co-Mo catalyst) and temperature to achieve different reduction in sulfur content of diesel product is shown in Table 2.5. However, improving of hydrotreating process, reactor and catalyst involve significant economic constraints.

- **Product demand:** Due to advancement of oil sand technology, supply of the heavy crude oil is increasing to meet the energy demand. In order to satisfy the changing pattern of the liquid fuel demand and processing of heavier oil, considerable investment in the improvement of refinery hydrotreating processes will be necessary. Challenges lies to utilize the heavy crude oil profitably for the production of liquid fuel.

- **Economic requirement:** In the refinery, hydrotreating process technology and catalyst have significant economic importance. Economic efficiency of the hydrotreating process depends upon the process technology being employed. In order to obtain the deep desulfurization several process technologies such as, UniPure aromatic sulfur reduction technology and SulphCo desulfurization technology have been suggested (Babich and Moulijn, 2003). But, further progressive research is required to develop the more economically favorable technology for the hydrotreating process.

Table 2.5: Target of product sulfur, required increase in catalyst activity and temperature (Knudsen et al., 1999).

Product Sulfur (ppm)	Required Increase in Catalyst Activity(%)	Required Increase in Temperature (°C)
500	100	0
350	130	+7
200	190	+17
100	300	+29
50	420	+38

2.3.6 Chemical Reactions of Hydrotreating

A wide range of competitive reactions can occur during hydrotreating process. The desirable reactions, which correspond to the purpose of the hydrotreating process, are:

- Hydrodesulfurization (elimination of sulfur)
- Hydrodenitrogenation (elimination of nitrogen)
- Demetallization (elimination of metal)
- Saturation of olefins and diolefins
- Hydrogenation of aromatic compounds

The undesirable reactions, which cause loss of valuable components of the feedstock and reduce the activity of catalyst, are:

- Hydrocracking: Hydrocracking is an undesirable reaction, which consume hydrogen and reduces product yields.

- Coking: Coking occurs due to adsorption of heavy molecules on the acidic sites of the catalyst and form coke. Coking is responsible for the catalyst activity reduction.

Desirable Hydrotreating Reactions:

Hydrodesulfurization Reactions: In this process sulfur compounds, present in the feedstock such as mercaptants, sulfides, and disulfides reacts with hydrogen and get converted into corresponding saturated or aromatic compounds. These reactions are exothermic and lead to formation of hydrogen sulfides. Examples of hydrodesulfurization reactions are shown in Figure 2.10 (David and Pujadó, 2006).

Hydrodenitrogenation Reactions: In this process nitrogen compounds present in the feedstock such as amine and pyridine reacts with hydrogen and gets converted into corresponding saturated or aromatic compounds. These reactions are exothermic and lead to

formation of ammonia. The examples of hydrodenitrogenation reactions are shown in Figure 2.11 (David and Pujadó, 2006).

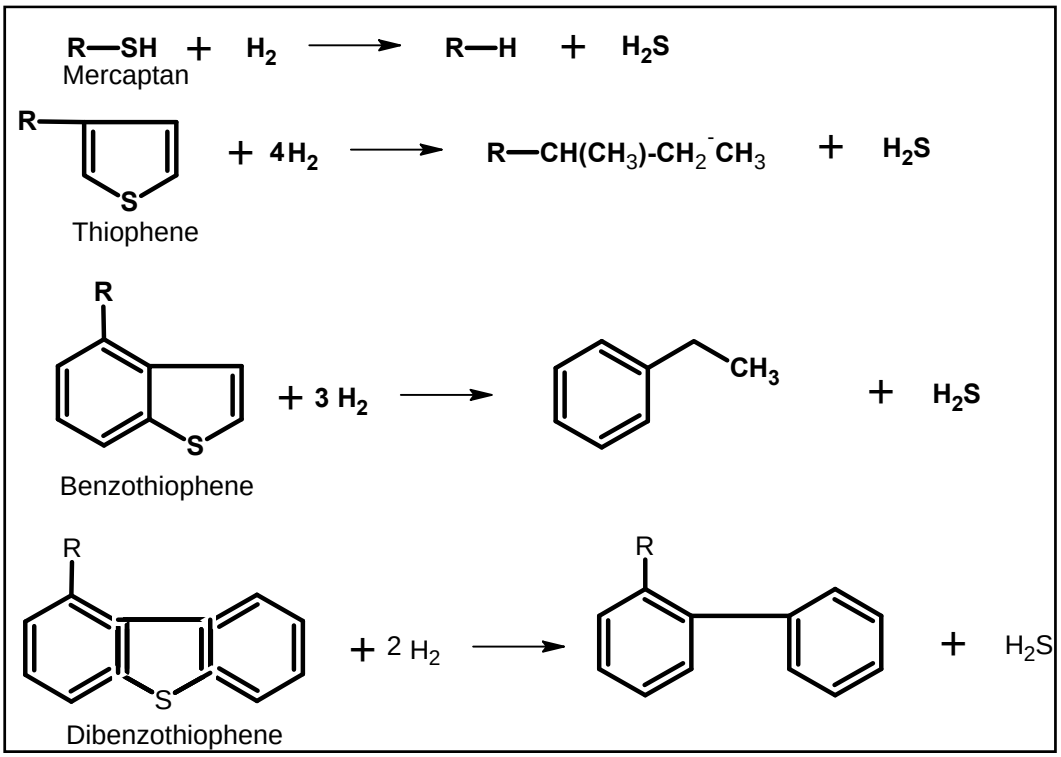

Figure 2.10: Examples of hydrodesulfurization reactions (David and Pujadó, 2006).

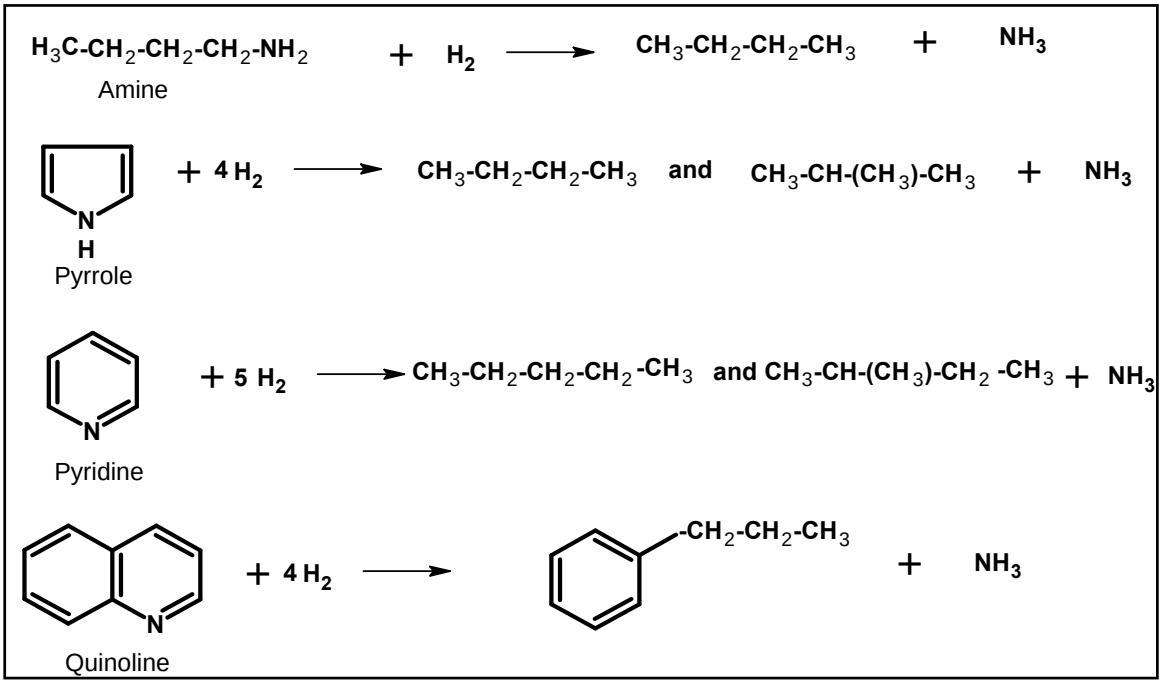

Figure 2.11: Examples of Hydrodenitrogenation reactions (David and Pujadó, 2006).

2.3.7 Reaction Mechanism of HDS and HDN

A) Hydrodesulfurization: Hydrodesulfurization involves removal of sulfur from gas oil feedstock (Ancheyta and Speight, 2007). Adsorption of the organosulfur compounds occur through both coordination of the sulfur atom and through their aromatic rings (Girgis and Gates, 1991). It is acknowledged that during hydrodesulfurization, sulfur removal may occur via two possible paths - i) direct desulfurization (DDS) by direct hydrogenolysis of C-S bond and ii) hydrogenation (HYD) by hydrogenation of aromatic rings (Prins et al., 2006). Benzothiophenes and dibenzothiophenes are major contributors in gas oil; hence desulfurization pathways for dibenzothiophene and 4, 6-dimethyldibenzothiophene can serve as a good example of industrial HDS process. The proposed reaction pathways for desulfurization of dibenzothiophene and 4, 6-dimethyldibenzothiophene is explained in following sections:

Dibenzothiophene reaction pathways: The HDS of DBT occurred through two parallel reactions: i) direct desulfurization (DDS) and ii) hydrogenation (HYD). Biphenyl (BP) type compounds are produced via the DDS pathway. On the other hand, cyclohexylbenzene (CHB) and dicyclohexyl (DCH) are produced via the HYD route after DBT is partially hydrogenated to the intermediates, such as tetra hydro-DBT (TH-DBT) (Liu and Ng, 2010). The detail reaction pathways are shown in Figure 2.12.

4, 6-Dimethyldibenzothiophene reaction pathways: HDS of 4, 6-DMDBT goes through two reaction pathways: i) direct desulfurization (DDS) and ii) hydrogenation (HYD). In the direct desulfurization (DDS) 3, 3'-dimethylbiphenyl is produced. In the hydrogenation (HYD) reaction pathway, first hydrogenation of 4,6-DMDBT yields 4,6-dimethyl-tetrahydro-DBT (4,6-DM-TH-DBT), and 4,6-dimethyl-hexahydro-DBT (4,6-DMHH-DBT) and then desulfurization produces 3,3'-dimethylcyclohexylbenzene (3,3'-DMCHB) (Speight, 1999). The detail reaction pathways are shown in Figure 2.13.

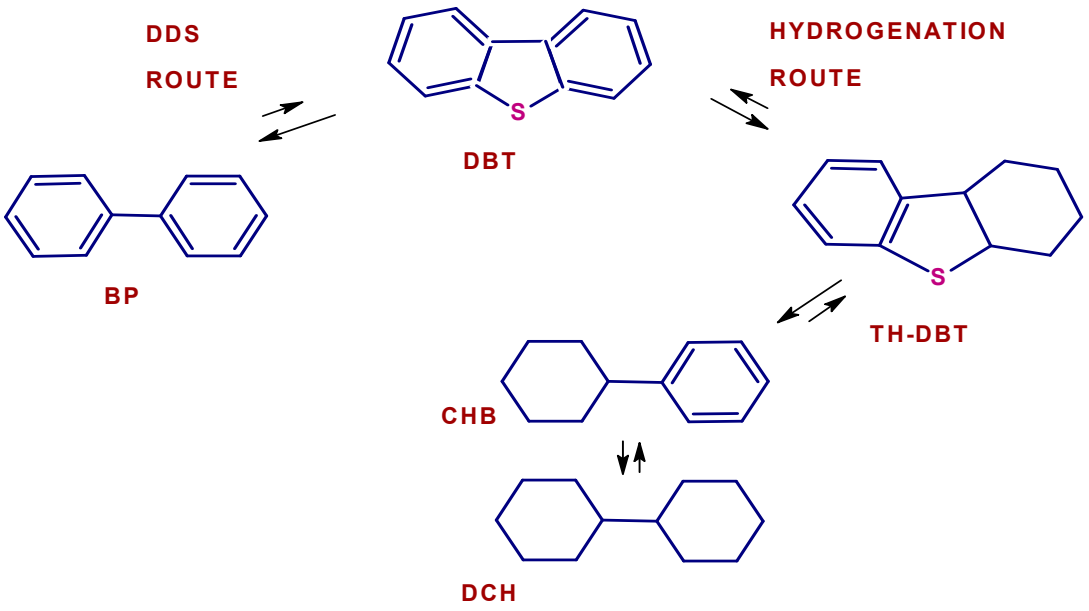

Figure 2.12: Hydrodesulfurization pathways of DBT (Liu and Ng, 2010).

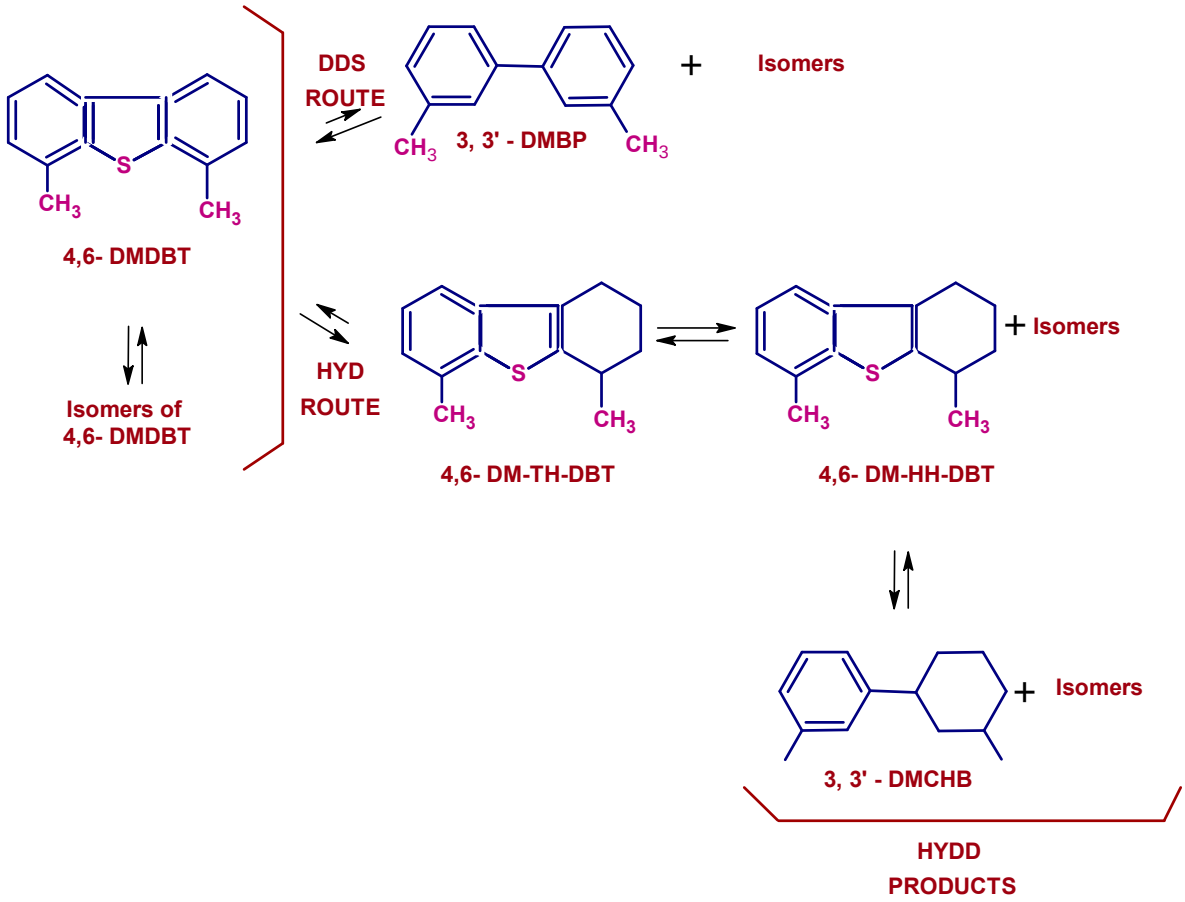

Figure 2.13: Hydrodesulfurization pathways of 4, 6-DMDBT (Liu and Ng, 2010).

B) Hydrodenitrogenation: Hydrodenitrogenation involves removal of nitrogen from nitrogen containing compounds present in gas oil feedstock (Ancheyta and Speight, 2007). Nitrogen removal from heterocyclic organo-nitrogen compounds proceed initially through hydrogenation of the ring containing the nitrogen atom followed by the hydrogenolysis of the carbon-nitrogen bond (Lu et al., 2007). Major pathways involved in the hydrodenitrogenation are: i) hydrogenation of nitrogen ring ii) cleavage of C-N bond and formation of amine intermediates and c) hydrogenolysis of hydrocarbon (Furimsky and Massoth, 2005). Quinoline and pyridine, heterocyclic nitrogen compounds, are identified in middle distillates in significant concentration. Also, quinoline and pyridine contain both a heterocyclic ring and benzene ring. Hence, reaction pathways of quinoline and pyridine HDN are good example of those involved in industrial HDN process (Lu et al., 2007). In the following section hydrodenitrogenation of quinoline and pyridine are described:

Quinoline reaction pathways: The mechanism of quinoline HDN reaction consists of three steps: i) hydrogenation of quinoline, PY-TH (1, 2, 3, 4 -propyl tetrahydro) quinoline and BZ-TH (5,6,7,8-tetrahydro) quinoline, ii) hydrogenolysis of O-propylaniline and decahydroquinoline and iii) cracking of n-propylbenzene and n-propyl cyclohexane (Lu et al., 2007). A reaction pathway for quinoline is shown in Figure 2.14.

Pyridine reaction pathways: The mechanism of pyridine HDN reaction consists of two steps: i) hydrogenation of pyridine to intermediate piperdine and ii) sequential hydrogenolysis of C-N bond to form n-pentylamine and C_5 hydrocarbon. A reaction pathway for quinoline is shown in Figure 2.15.

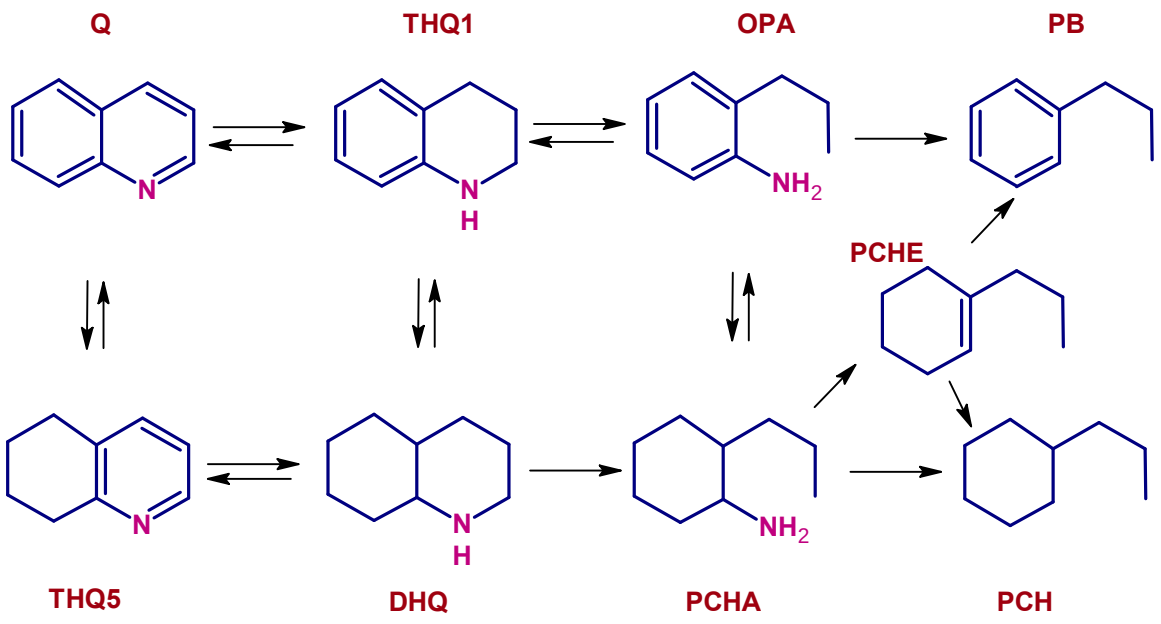

Figure 2.14: HDN reaction network of quinoline. Q, quinoline; THQ5,5,6,7,8-tetrahydroquinoline; DHQ, decahydroquinoline; THQ1, 1,2,3,4-tetrahydroquinoline; OPA, *ortho*-propylaniline; PCHA, 2-propylcyclohexylamine; PCHE, propylcyclohexene; PCH, propylcyclohexane; PB, propylbenzene. Reaction network for quinoline HDN proposed by (Lu et al., 2007)

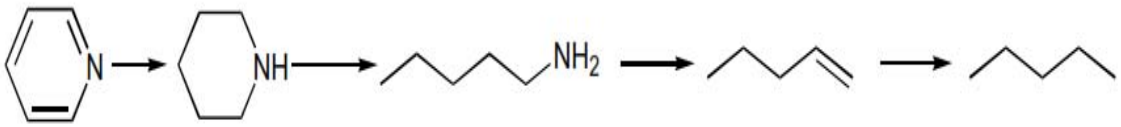

Figure 2.15: HDN reaction network of pyridine (Ancheyta and Speight, 2007).

2.3.8 Factors Affecting Hydrotreating Processes

Hydrotreating process depends on followings parameters as shown in Figure 2.16.

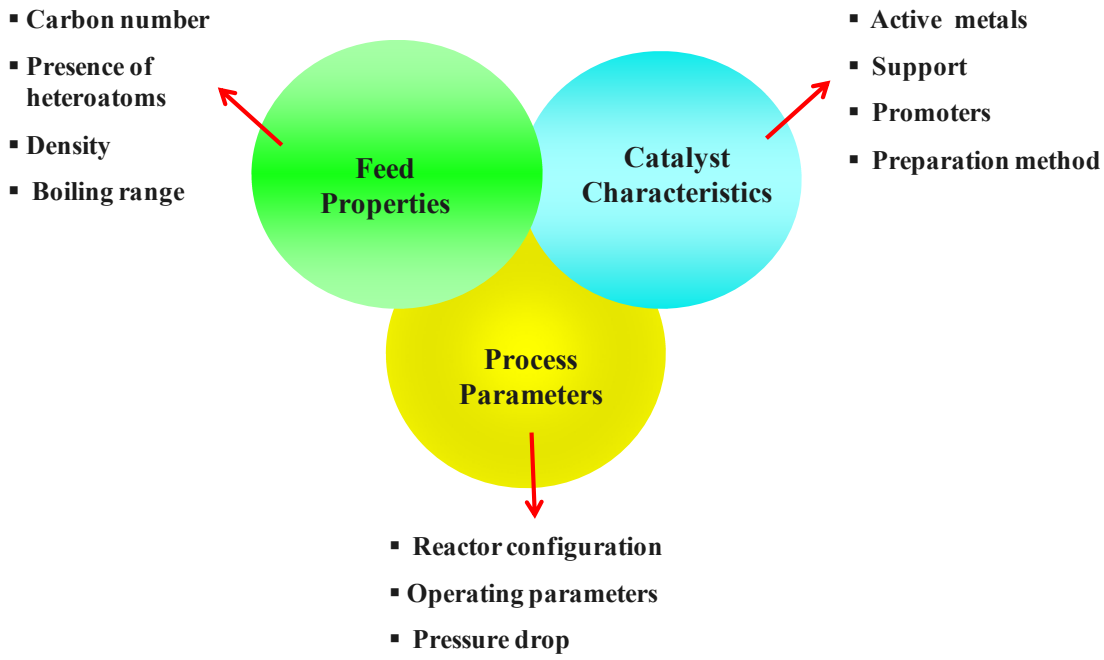

Figure 2.16: Factors affecting hydrotreating process (Speight, 1999).

1) Feed Properties: The degree of complexity of hydrotreating process depends on feedstock properties (amount of complex compounds and higher boiling constituents) (Ancheyta and Speight, 2007). Feedstock complexity depends upon carbon number, density, boiling point range and presence of various model compounds and heteroatoms. Physical and chemical compositions of a feedstock determine the choice of processing schemes, hydrogen consumption and nature of the products. An increase in end point of feed will make sulfur and nitrogen removal more difficult. Also, high boiling fractions contain more metal, which accelerate catalyst deactivation.

2) Process Parameters: Process parameters includes reactor configuration, reaction kinetics, operating variables (Temperature, Pressure, LHSV, H_2/HC ratio) (Speight, 1999).

Hydrotreating process parameters are adjusted depending on the feed quality, type and amount of heteroatom present and desired product slate.

- Reactor Configuration: Reactors used for hydrotreating of heavy feeds are different from the lighter feed being used for the hydrotreating. Depending upon the types of feed, commercial hydrotreating reactors are divided into: fixed bed, moving bed, and ebullated bed. The fixed bed reactors are in general used for the lighter feed such as naphtha and middle distillates. Moving bed and ebullated bed reactors are used for hydroprocessing of difficult feed, such as vacuum residua (Ancheyta and Speight, 2007). The fixed-bed reactor is commonly used industrially in hydrotreating process since they are easy and simple to operate. In this reactor, feed enters from the top, trickle down through the fixed catalyst bed and product leaves from the bottom of the reactor. For naphtha processing, fixed bed reactor are convenient, as the undesirable impurities such as sulfur compounds are easy to remove by this reactor. However, to obtain deep desulfurization of gas oil, which contains difficult refractory sulfur (such as 4,6-DMDBT), nitrogen and aromatics molecules, it is difficult to product ultra low sulfur diesel using simple fixed bed reactor. In this case, multibed system with different catalysts has been suggested as better option. In this reactor hydrogen is introduced between the catalyst bed to control the reaction temperature.

- Operating Conditions: By careful monitoring of process variables of hydrotreating unit the desired product quality can be obtained. The operating conditions of the hydrotreating process are determined by the type of feed being processed, degree of desulfurization (or denitrogenation), product specification, such as cetane improvement or extent of aromatic saturation. The following operating parameters are important for the hydrotreating process:

hydrogen partial pressure, reactor temperature, liquid hourly space velocity, H_2/HC ratio, other parameters such as H_2/H_2S ratio.

i) Hydrogen partial pressure: This is one of the key parameters for the hydrotreatment process. Hydrogen partial pressure varies based on degree of sulfur, nitrogen or aromatic removal. Reduction of operating pressure below the design level will have effect on activity of catalyst and will accelerate catalyst deactivation. An increase in hydrogen pressure results in increasing the hydrotreatment reaction and decreasing the coke deposits on the catalysts. Adequate pressure needs to be kept to obtain desired product yield. The operating pressure depends upon the type feed stock needs to be processed. In case of aromatic saturation or improvement of cetane number the pressure needs to be increased. Typical pressure range for the hydrotreating process is shown in the Table 2.6.

ii) Reactor temperature: Diesel hydrotreating is an exothermic process, where the heat is generated. The catalyst bed temperature generally increases over the time. Increasing reactor temperature will accelerate coke formation and reduce the length of the operating cycle. An average temperature needs to be maintained to allow efficient hydrotreatment and a long catalyst life. In order to obtain maximum conversion and control the reaction temperature, catalyst beds are divided into two or three beds by injecting quench gas between the beds. The required reactor temperature for the hydrotreating process depends upon the feed rate and quality (David and Pujadó, 2006). Aromatic saturation is favored by low temperature. For the diesel hydrotreatment in industrial hydrotreating reactor, the average bed temperature varies from 340 °C at the start of run (SOR) condition to 410 °C to end-of-run (EOR).

iii) Liquid hourly space velocity: Liquid hourly space velocity is defined as :

LHSV = [Volumetric flow rate of feed (m^3/h)/Catalyst Volume (m^3)] ($time^{-1}$)

LHSV is basically inverse to the residence time. Hence, lower the value of LHSV is the higher the reaction rate. Increasing the space-velocity requires higher reactor temperature to achieve the desired conversion level, which results in faster catalyst deactivation rate. In case of diesel desulfurization, LHSV are maintained 1-2.5 h^{-1} for the pilot plant and 2.5 h^{-1} for the commercial plant (Ancheyta and Speight, 2007).

iv) Hydrogen/gas oil ratio: Hydrogen gas flow rate for the hydrotreating is governed by the economic consideration. Increasing the partial pressure improves the hydrotreating process and reduces the catalyst deactivation (Ancheyta and Speight, 2007). However, above certain gas rate, the change in hydrotreating process is not very significant. In general hydrogen recycle stream is used to maintain the higher H_2/oil ratio and hydrogen partial pressure. Operating conditions for the hydrotreating processes are shown in the Table 2.6.

Table 2.6: Operating conditions for hydrotreating processes (David and Pujadó, 2006; Gray, 1994).

Feedstock	**Naphtha**	**Kerosene**	**Gas Oil**	**Vacuum Gas Oil**	**Residue**
Boiling Range (°C)	70-180	160-240	230-350	350-550	>550
Operating Temperature (°C)	260-300	300-340	320-350	360-380	360-380
Operating Pressure (MPa)	0.5-1.0	1.5-3.0	1.5-4.0	4.0-7.0	12.0-16.0
LHSV (hr^{-1})	4-10	2-4	1-3	1-2	0.15-0.3
H_2/HC Ratio (std m^3/m^3)	36-48	36-48	36-48	36-48	12-24

3) Catalyst Characteristics: Catalyst activity depends upon specific surface area, surface morphology, and mechanical strength. The hydrotreating catalysts consist of metals in an

oxide state. The active form (sulfide state) is obtained by sulfiding the catalyst either prior to use or with the feed during processing. The hydrotreating process is greatly influenced by the type of catalyst. Selection of catalyst is done based on the feed characteristic and required level of the product specification. Recently, in order to achieve deep desulfurization and denitrogenation several methods are employed to develop better hydrotreating catalyst compared to the commercial one.

2.3.9 Ways to Improve Hydrotreating Process

There are many ways to attain the desired level of heteroatom (sulfur, nitrogen) removal from more difficult molecules. Some of the most currently popular suggested and proven methods are (Ancheyta and Speight, 2007):

- Replacing current catalyst with more active catalyst
- Higher operating temperature
- End point adjustment of the feed
- Higher purity hydrogen make-up or increased hydrogen partial pressure
- Adding additional reactor volume (one or more reactors)
- H_2S removal from the recycle gas
- Improving the feed distribution to the trickle-bed (conventional) reactor

Among all the method, replacing current catalyst with more active catalyst is suggested and proven to be more promising. There has been a growing interest to develop catalyst that can perform deep desulfurization and hydrodenitrogenation. Catalysts are considered to have significant role to solve the problem of conversion of heavy oil into more valuable lighter oil.

2.4 Hydrotreating Catalyst

2.4.1 Conventional Hydrotreating Catalyst

Hydrotreating catalysts contain active components (molybdenum or tungsten) and promoters (cobalt or nickel), which are uniformly dispersed over a support (alumina, silica, silica-alumina) (Speight, 1999). The structure of commercial sulfided catalyst is shown in Figure 2.17. Cobalt acts as a promoter for sulfided Mo/γ-Al_2O_3 in hydrodesulfurization (HDS), whereas nickel is favored in hydrodenitrogenation (HDN) (Speight, 1999). The commercial hydrotreating catalysts consisting of varying amount of active component and promoters, depending upon the intended application of hydrotreating process. Gamma alumina (γ -Al_2O_3) is usually used as hydrotreating catalyst support (David and Pujadó, 2006; Speight, 1999). Occasionally, hydrotreating catalysts contain P, B, F, or Cl, (modifier), which may influence both the catalytic and mechanical properties of the catalyst (Speight, 1999). Hydrotreating catalysts are active in the sulfide form (Speight, 1999). Typical composition for the hydrotreating catalyst is shown in the Table 2.7.

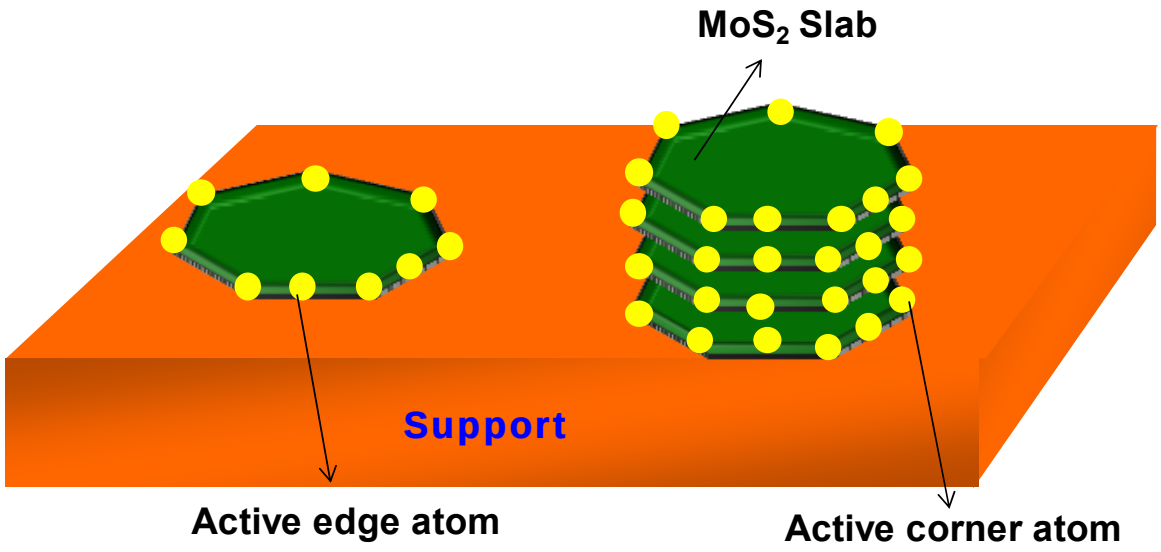

Figure 2.17: Structure of sulfided hydrotreating catalyst (Topsøe et al., 1996).

Table 2.7: Typical composition of catalyst used for hydrotreating process (Speight, 1999).

Components	HDS	HDN
Mo (as MoO_3)	12 wt%	25 wt%
Ni or Co (As NiO or CoO)	3 wt%	5 wt%
H_3PO_3	-	1 wt%
Al_2O_3	Remainder	Remainder

Physical characteristic of catalyst varies, depending on the desired applications. The physical characteristics of common hydrotreating catalysts are shown in Table 2.8 (David and Pujadó, 2006).

Table 2.8: Physical characteristics of the hydrotreating catalys (David and Pujadó, 2006).

Characteristics	Values
Surface area	>150 m^2/g
Pore Volume	0.6-1.0 ml/g
Average pore radius	30 -100 Å
Average length	3.2 – 9.5 mm

CoMo catalysts are useful for hydrodesulfurization reaction. However some extent of hydrodenitrogenation and hydrodemetallization can be obtained (David and Pujadó, 2006). CoMo based catalyst has very low hydrogenation and denitrogenation activity. It has been reported that the CoMo catalyst exhibits higher desulfurization activity at the lower operating pressure (<4 MPa). NiMo catalyst is useful for the hydrogenation and hydrodenitrogenation reactions. Also, hydrodemetallization can be obtained by this catalyst. Advantages of NiMo catalyst is that, for the treatment of wide variety feed this catalyst can be used (David and Pujadó, 2006). Furthermore, NiMo catalyst exhibits good olefins saturation due to its higher hydrogenation activity. At high pressure, NiMo catalyst shows good performance. In

hydrotreating process NiW catalyst is used for the application of higher hydrogenation reaction (Speight, 1999). This catalyst is good for the saturation of one of the double bond in diolefins (David and Pujadó, 2006).

2.4.2 Hydrotreating Catalyst Design and Improvement

Hydrotreating Catalyst Design: Catalyst design is the careful optimization of physical, chemical, mechanical and catalytic properties, which can be described by the catalyst design triangle concept (shown in Figure 2.18) (Richardson, 1989). A good catalyst possesses high activity and selectivity. A high activity allows relatively small reactor volumes, short reaction times, and operation under mild condition. A good catalyst should maintain its activity and selectivity over a period of time. Catalyst activity can be increased by increasing the porosity and surface area. However, the surface area decreases with the increase of catalyst porosity. Also, strength of catalyst decreases as porosity increases.

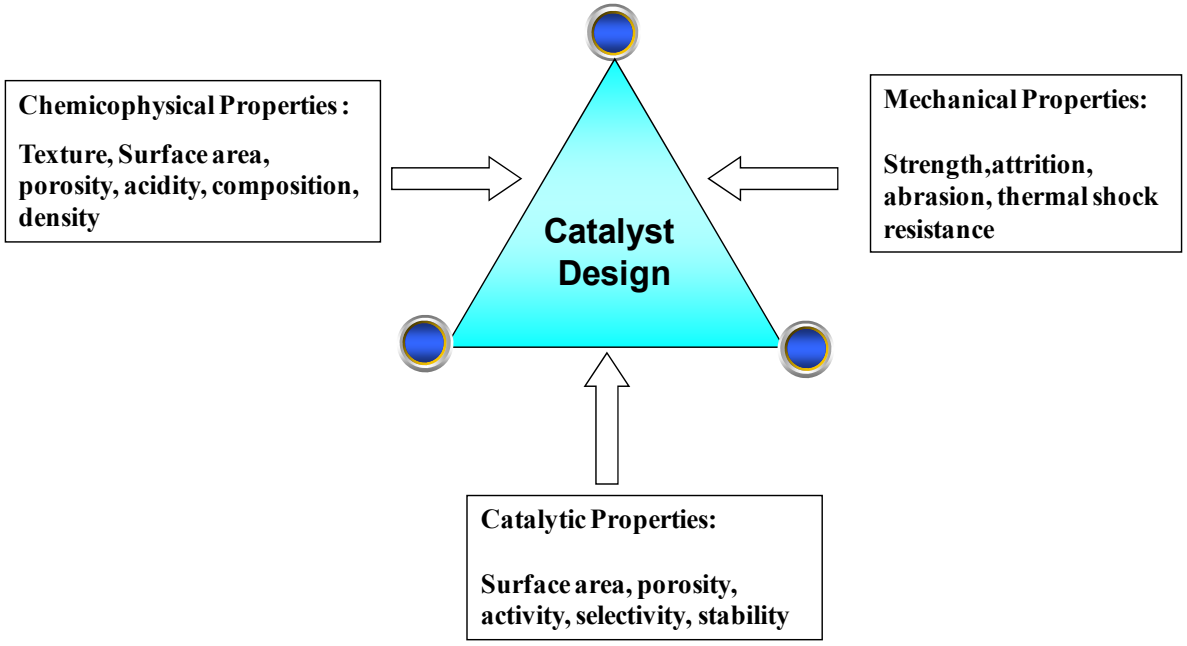

Figure 2.18: Triangular concept of catalyst design (Richardson, 1989).

Improvement of Hydrotreating Catalysts: In order to improve activity of hydrotreating catalyst, several research works have been carried out. In order to develop more advanced HDT catalysts following main areas are explored (Babich and Moulijn, 2003; Breysse et al., 2003a; Eswaramoorthi et al., 2008):

- Active Metals: Hydrotreating catalyst are the sulfides of Group VI A (Mo, W) promoted by sulfides of metals of group VIII (Ni, Co). Various pairs of sulfides are available with different activity for various conversions. Hence, it is imperative to select a well-defined association of sulfides depending on the feed characteristics and desired product slate. Chemical composition of the catalyst also plays an important role in determining overall activity of the catalyst. In order to develop highly active catalyst, increasing the amount of active metals or changing of active metal (using noble metals such as Pt, Pd, Ru etc) have been explored by several researchers.

- Structure of Support: Choice of support used for hydrotreating and characteristics of support determines activity and selectivity for catalyst. Modification or change of supports (type, texture, and chirality) is performed to enhance the catalytic activity of hydrotreating catalysts. Support formulations are optimized to obtain desired product slate. Acidity of the catalyst is imparted by the support. Acid strength and acid site distribution is imperative for optimum activity and selectivity of the hydrotreating catalyst. Some of the acidic supports have been explored in order to enhance the catalyst activity.

- Preparation Routes: Preparation parameters such as i) impregnation method, ii) metal loading, iii) activation procedure and iv) calcination temperature strongly affect the activity of the catalyst. Different catalyst preparation routes (such as sol-gel method, multiple impregnations) have been investigated in order to improve the HDT catalyst activity.

- Additives: Changes in catalyst structure and activity can be achieved by adding a third element to hydrotreating catalyst. In order to improve the acidity and activity several additives such as phosphorous, boron, zinc, alkali dopant and fluorine have been tested.

- Promoters: New promoters in terms of organic, inorganic and chiral compounds have been also tested for the improvement of catalyst.

2.4.3 Structure of Hydrotreating Catalysts

Molybdenum (Mo) and Tungsten (W) are effectively used as catalyst active components for the hydroprocessing of various petroleum fractions and synthetic crudes. Commercial hydrotreating catalyst comprise of active components (Mo or W), which are promoted by Co or Ni and dispersed on high surface area support (Lauritsen et al., 2007). Hydrotreating catalysts are active only in their sulfide forms, such as molybdenum sulfide (MoS_2) or tungsten sulfide (WS_2). For the hydrotreating catalyst ($NiMo/Al_2O_3$ or $CoMo/Al_2O_3$) the structure and dispersion on the active phase changes during the catalyst life cycle (Eijsbouts, 1997).

Various catalyst models are presented in the literature about the structural information of sulfide Co-Mo or NiMo phases, the function and location of Co or Ni for the hydrotreating catalysts (Eijsbouts, 1997; Lauritsen et al., 2007; Topsoe and Clausen, 1984). These models are:

- the "monolayer model" (Schuit and Gates, 1973), where molybdenum species are proposed to be bonded to the surface of alumina by forming a monolayer;

- the "intercalation models" (Voorhoeve, 1971), where MoS_2 slab (WS_2) is proposed to be consisting of plane of Mo (W) atoms sandwitched between two hexagonal closed-packed of sulfur atom and Co is considered to interact into the layer structure of MoS_2;

- the “contact synergy model” (Delmon, 1979), where the promoting effect of Co is proposed to be due to contact between Co_9S_8 and MoS_2 phases;

- the “remote control model” (Vissers et al., 1987), where H_2 is dissociatively adsorbed on Co sulphide and subsequently transferred to the MoS_2 surface, where it reacts with the adsorbed sulfur containing molecules (Topsoe and Clausen, 1984);

- the “Co-Mo-S model” (Topsoe and Clausen, 1984), where the Co-Mo-S phase is proposed to be MoS_2 structure and the location of promoters are supposed to be at the edge plane of MoS_2;

- the “rim-edge model” (Daage and Chianelli, 1994), where morphology of the MoS_2 or WS_2 structure is assumed to affect the reaction pathways selectivity (direct desulfurization and hydrogenation) of overall hydrodesulfurization reaction.

Among all models, the “Co-Mo-S model” and “rim-edge model” are the most widely accepted models for the structure of the hydrotreating catalyst (Topsoe and Clausen, 1984). According to the “Co-Mo-S model”, the catalyst is proposed to be consist of MoS_2 crystallites supported on the alumina surface and promoted by Co or Ni atoms at the edge plane of MoS_2 (Delgado, 2002). The Co-Mo-S structure is not a single phase, but it is basically a bulk phase with a fixed overall Co: Mo: S stoichiometry (Delgado, 2002). The structure is described as a family with varying Co concentration ranging from pure MoS_2 to full coverage of MoS_2 by Co. In Co-Mo-S, Co is present in three different phases as shown in Figure 2.19 (Lauritsen et al., 2007) i) the catalytically active Co-Mo-S phase, which has MoS_2-like structure decorated by Co, ii) a thermodynamically stable Co_9S_8 and iii) Co dissolved in the Al_2O_3 structure. Among three phases, Co-Mo-S structure is associated with

appreciable catalytic activity, and this characteristic is applicable for other related catalysts structure, such as Ni-Mo-S, Co-W-S, and Ni-W-S (Delgado, 2002).

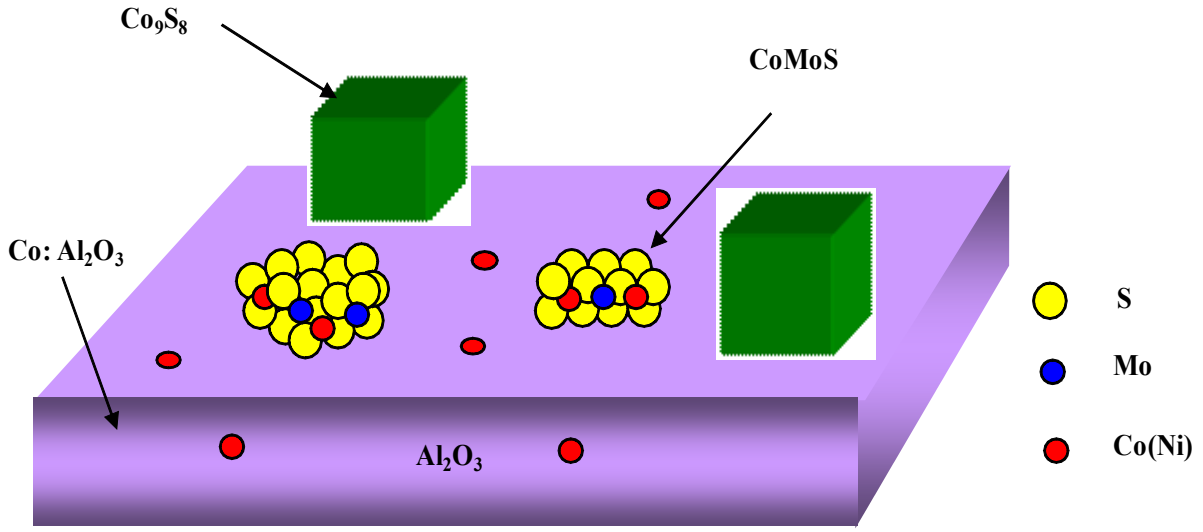

Figutre 2.19: Different phases present in a typical alumina-supported catalyst (Lauritsen et al., 2007)

Depending on the type of support, preparation and activation parameters, metal loading, presence of additives, both single and multiple Co-Mo-S structure (Delgado, 2002; Eijsbouts, 1997) are proposed. The type I phases, i.e. $CoMoS_2$ type-I, consists of highly dispersed monolayer MoS_2 particles interacting with the support via Mo-O-Al bond and supposed to be incompletely sulfided, i.e. have lower S coordination of Mo and Co (Ni) (Eijsbouts, 1997; Hensen et al., 2001; Joshi et al., 2008). The type II, i.e. $CoMoS_2$ II consists of lower dispersed MoS_2 particles of higher stacking degree and proposed to be fully sulfided, i.e. have higher S coordination of Mo and Co (Ni). In the type-II structure, MoS_2 particles weakly interact with the support via Van der Waals interactions. Catalytic activity of type-I and type-II phases depends upon the reactants. For thiophene hydrodesulfurization, CoMoS type-II phases are reported to be more active than the type-I phases (Topsoe and Clausen, 1984). However, for the dibenzothiophene HDS in trickle flow, CoMoS type-I

reported to be more active than the CoMoS type-II phase. The activity difference for thiophene and DBT HDS reaction is attributed to the difference in HDS mechanism for both the cases.

In the "Rim-edge" model, the catalyst particles are assumed as a stack of several discs as shown in Figure 2.20 (Daage and Chianelli, 1994). The top and bottom disc are described as "rim site" and the disc located in between the top and bottom disc are described as "edge site". According to this model, sulfur hydrogenolysis (C-S bond breaking) takes places both rim and edge sites, whereas, DBT hydrogenation takes place on the rim site only. The proportions of of rim site are very high in Al_2O_3 supported catalyst.

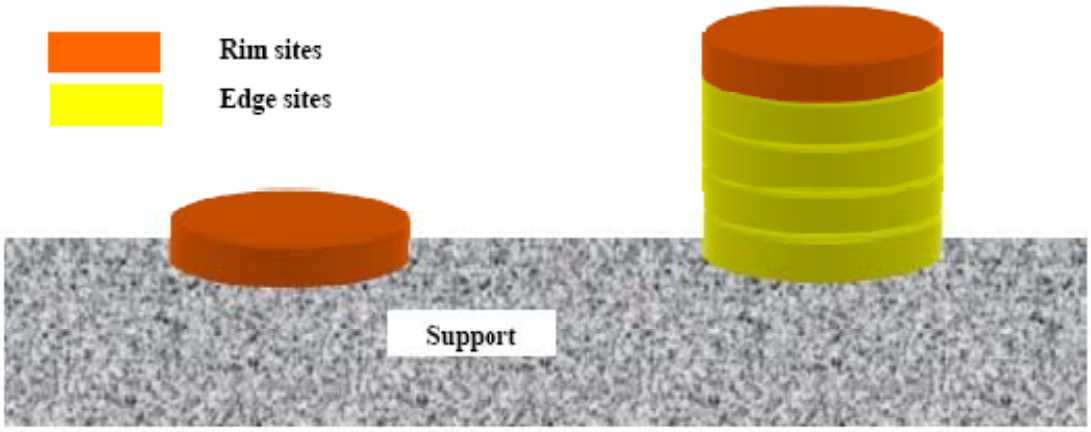

Figure 2.20: Distinction between rim and edge sites for stacked and unstacked MoS_2 particles (Berhault et al., 2008).

2.4.4 HDS Reaction Mechanism by Metal-Sulfide Catalysts

Hydrodesulfurization of sulfur molecules on metal sulfide catalysts is described by the concept of "vacancy" (Delgado, 2002; Gray, 1994). Vacancies in the catalyst are generated due to reaction of hydrogen with surface sulfide group. Thermodynamically unstable vacant sites then tend to regain the stability by forming metal bonded sulfide group. Hence, sulfur extrusion from organosulfur compounds takes place by C-S bond cleavage and the extruded

sulfur fills the vacant sites of the metal-sulfide catalyst. The catalytic site is regenerated by removing sulfur by hydrogen. Catalytic cycle for hydrodesulfurization of a sulfur-containing molecule by a sulfur vacancy on MoS_2 is shown in Figure 2.21.

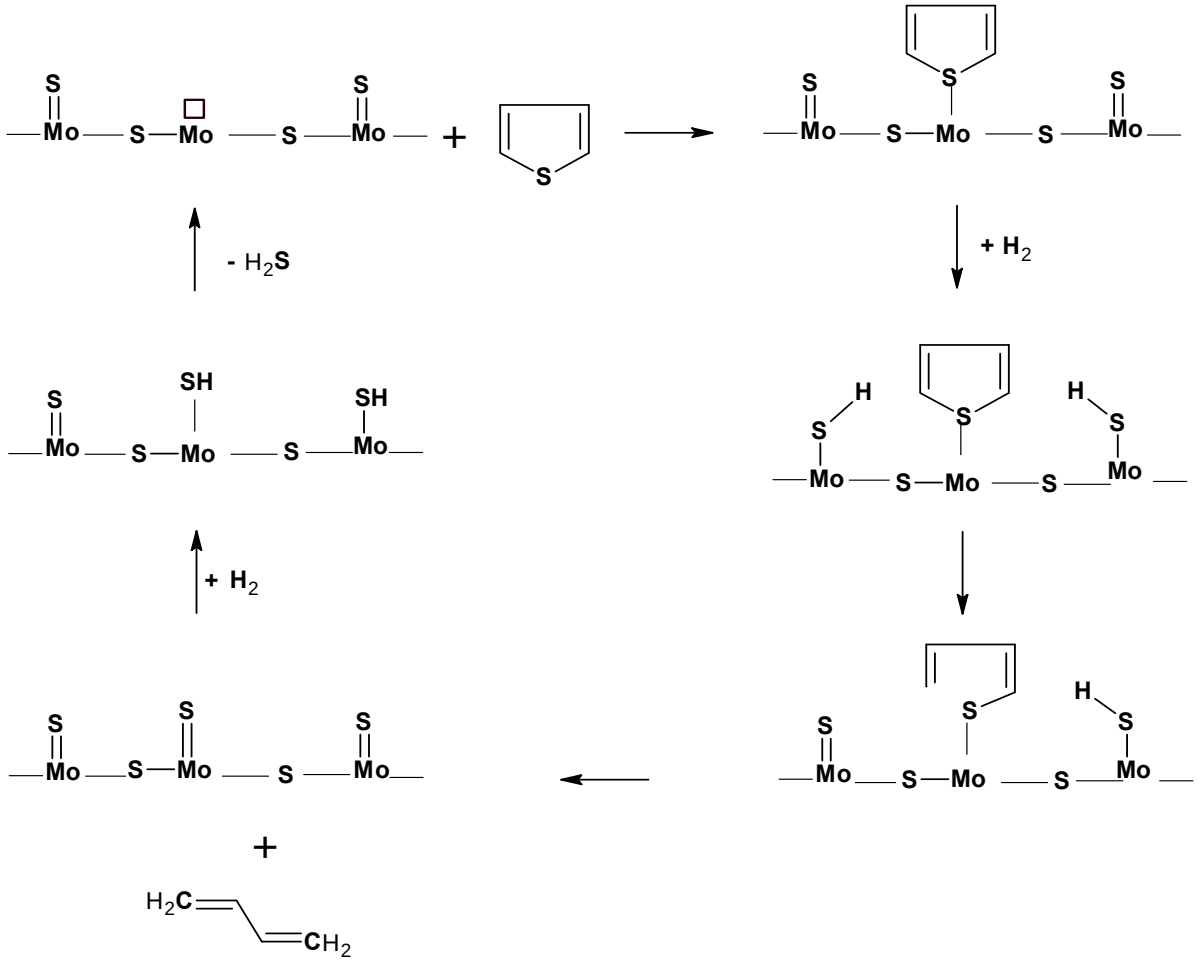

Figure 2.21: HDS mechanism of thiophene by metal-sulfide catalyst (Mochida and Choi, 2004).

2.4.5 Promoters

Catalytic activity of hydrotreating catalyst can be significantly enhanced by adding promoters. Several models have been suggested in order to describe the promotional effect of hydrotreating catalyst by many authors. The role of Co and Ni promoters in hydrotreating catalysts are shown in the Table 2.9.

Table 2.9: Role of promoters in the hydrotreating catalyst.

Role of Promoters	Mechanism	References
As textural promoters alter the catalyst surface	• formation of Co species in alumina	(Schuit and Gates, 1973)
	• increase in number of Mo sites	(Voorhoeve, 1971)
	• formation of intercalation structure	(Voorhoeve, 1971)
	• formation of pseudo intercalation structure	(De Beer et al., 1974b; Voorhoeve, 1971)
	• formation of CoMoS phase and provide structural stability to MoS_2 crystallites	(Ratnasamy and Sivasanker, 1980)
As a promoter to enhance hydrogen spillover by proving H atom to MoS_2	• contact synergism	(Delmon, 1979; Grange, 1980)
As bonding modifier of active site by influencing adjacent Mo sites	• increase dispersion and stability of active phase	(De Beer et al., 1974a)
	• change in sulfur-sulfur interaction	(Burdett and Chung, 1990)
	• creates sulfur vacancies in Co-Mo-S equilibrium structure	(Moses et al., 2009)
	• increase number of sulfur vacancies	(Topsøe et al., 1981; Voorhoeve, 1971)
	• increase electron density of sulfur	(Chianelli et al., 1984; Harris and Chianelli, 1986)
	• decrease metal-sulfur bond energy	(Nørskov et al., 1992)
	• enhance the mobility of labile sulfur	(Kabe et al., 1993; Kabe et al., 1994; Kabe et al., 1997)
As a producer of a new catalytic site or by acting as catalyst	• to make Co-Mo-S edge suitable for both hydrogenation and C-S scission	(Ledoux et al., 1985; Moses et al., 2009)
	• bind reactants to unreactive portion of catalytic surface	(Kushmerick et al., 2000)
	• transport reactant to active sites on the catalytic surface	(Kushmerick et al., 2000)

2.4.6 Support Materials

Supported catalyst consists of an active phase dispersed on a carrier. The catalytic reaction takes place at the internal surface (pores) of the catalyst. Catalyst support is used with catalytic component for controlling its specific surface area or pore size distribution in a

solid catalyst (Furimsky, 2007; Grange and Vanhaeren, 1997). Catalyst support plays an important role to improve the property of catalyst by manipulating its surface properties, because the nature of the individual sites at the surface is responsible for the activity, selectivity and stability of the catalyst (Grange and Vanhaeren, 1997). The hydrotreating catalyst support affects the activity and selectivity of hydrotreating catalyst (Hagen, 2006). Nature of support is of great importance to the design of hydrotreating catalyst. By means of an adequate support design it is possible to increase the HDS and HDN functionality of hydrotreating catalysts significantly. Role of hydrotreating catalyst supports are:

- Anchoring and stabilization of active component on catalyst support (Hagen, 2006)
- Improvement of dispersion of the active phases by formation of high dispersed particles (Satterfield, 1991)
- Improvement of textural property (such as surface area, pore diameter) of catalyst (Hagen, 2006)
- Modification of the reducibility of oxide precursor through change of the interaction between the active phase and support (Grange and Vanhaeren, 1997)
- Increase the useable promoter (Co/Ni) content of the catalyst by decreasing the concentration of spinel phase (Grange and Vanhaeren, 1997)
- Reduce the catalyst deactivation resulting from coking and pore mouth plugging (Furimsky, 2007; Satterfield, 1991)

Conventional Hydrotreating Catalyst Support: Conventional commercial hydrotreating catalysts are composed of a sulfide active phase, molybdenum sulfide (or tungsten sulfide) promoted by cobalt or nickel and usually supported on alumina. γ-alumina is widely used as support for hydrotreating catalyst because of following reasons (Satterfield, 1991):

- Outstanding textural properties, such as surface area, pore diameter and pore volume
- Good mechanical properties, including attrition resistance, hardness, compressive strength
- Provide high dispersion of active metal components
- Relatively low cost
- Ability to regenerate catalytic activities after intensive use under hydrotreating condition

Recently, due to increase interest of deep desulfurization of heavier feed stock, the conventional γ-alumina support is becoming inadequate to obtain the desired level of hydrotreating. In the Table 2.10 the disadvantages associated with γ- Al_2O_3 is presented.

Table 2.10: Disadvantages of γ-Al_2O_3 support for hydrotreating.

Properties	Disadvantages of γ-Al_2O_3	Remarks
Textural Properties	• Broad pore size distribution (Furimsky, 2007) • Pore dia. 5-15 nm (Chorkendorff and Niemantsverdriet, 2003) • Surface area 50-300 m^2/g	• Diffusional limitation of large reactant molecules into the catalyst pore • Deactivation rate by coke and metal deposits is higher
Activity of NiMo/ γ- Al_2O_3	• DBT conversion - 81% (Klimova et al., 2009) • 4,6-DMDBT conversion - 61% (Gutiérrez et al., 2006a) [condition: batch reactor, 300 °C,7.3 MPa, 8h]	• Require higher activity for HDS of refractory compounds
Acidity	• Higher acidity required for hydrotreating 4,6-DMDBT (Bej et al., 2001b)	• Require more acidity for HDS of refractory compounds
Metal-Support Interaction	• Strong chemical interaction between γ-Al_2O_3 and transition metal oxides	• It's difficult to obtain complete sulfidation of supported metal oxides. Very high metal support interaction not desirable for HDT (Eswaramoorthi et al., 2008)

2.4.7 Progress on Improvement of Hydrotreating Catalyst Support

Extensive works have been carried out in the research realms regarding the development of new supports for hydrotreating catalysts. Due to necessity to develop advanced hydrotreating catalyst with enhanced properties several supports have been explored. It is acknowledged that the activity of support can be improved by enhancing the textural properties, metal-support interaction and acidic or basic properties. In this regards, following progresses are made to improve the hydrotreating catalyst support:

A) Textural Properties of Support: Over the years significant efforts have been made to improve the textural properties of hydrotreating catalyst support. It has been acknowledged that the TiO_2 and ZrO_2 supported MoS_2 catalyst exhibits three to five times higher desulfurization and hydrogenation activities than Al_2O_3 supported MoS_2 catalyst (Breysse et al., 2003b). However, the very low surface areas of these materials limit their application as catalyst support. Various methods have been explored in order to improve the specific surface area. By improving preparation method, relatively higher specific surface area and larger pore diameter for both ZrO_2 and TiO_2 supports can be obtained. For example, by changing the preparation method, the specific surface area of ZrO_2 was improved from 100 m^2/g to 300 m^2/g (Breysse et al., 2003b). Also, in order to improve specific surface area combination of mixed oxides are studied as catalyst support.

B) Oxide Support: Oxide supports such as silica and silica-alumina have been studied as hydrotreating catalyst support. Further, this study has been expanded to other oxides as well. Unconventional oxides such as TiO_2 and ZrO_2 have been used as treatment of heavy oils and hydrocracking of bituminous coal and these oxides are appear to be promising for the hydrotreating process. Also, the combinations of two mixed oxides supports such as TiO_2-

ZrO_2, TiO_2-Al_2O_3, SiO_2-ZrO_2 and SiO_2-TiO_2 have been tested as hydrotreating catalyst. The combination of two oxides observed to be more effective as HDT catalyst supports (Breysse et al., 2003b). For example, ZrO_2 –TiO_2 mixed oxide with specific surface area 254 m^2/g was studied as catalyst support and proved to be promising for the HDS reaction (Maity et al., 2001).

C) Acidic and Basic Support: For the deep desulfurization of heavy feed, acidic supports have received importance in several studies. In this context, acidic zeolite or silica-alumina, alumina-zeolite supports have been studied as hydrotreating catalyst support. It is reported that zeolite-supported catalysts are more active in HDS than alumina counterparts due to better dispersion of molybdenum in the zeolitic material (Bataille et al., 2001).

Basic supports has attracted significant attention as catalyst support, since basicity increases (high and stable) dispersion of Mo species on support and inhibits coking (Klicpera and Zdražil, 2002). For example, for the hydrotreating of thiophene, Co (Ni) promoted basic MgO supported catalyst has been proven as 1.5 – 2.3 times more active as γ-Al_2O_3 supported catalyst. Zirconium oxide (zirconia) posses both acidic and basic properties and can be used as effective support material for hydrotreating catalyst (Chuah et al., 1996).

D) Carbon: Carbon supported transition metal sulfide exhibits higher activity in HDS and HDN compared to γ-Al_2O_3 supported counterpart (Pawelec et al 2001). Advantages of using carbon as supports are: carbon facilitate sulfidation of metal oxides, provide large specific surface area with control volume, reduce coking propensity and easy metal recovery (Breysse et al., 2003b). CoMo catalyst supported on carbon is proven to be more active than γ-Al_2O_3. Also, natural clay and pillared clays getting more attentions due to high specific surface area, mechanical and thermal stability and acidic properties (Breysse et al., 2003b).

E) Ordered Mesoporous Material: Recently mesoporous materials, specifically various mesoporous silicas, MCM-41, MCM-48, HMS, FSM-16, KIT-1, and SBA-15 have received great attention in the field of catalysis due to their remarkable features. Ordered mesoporous material was first developed by scientists of Mobil Corporation in 1992. MCM-41 consists of highly ordered hexagonal array with unidimensional pores (Taguchi and Schüth, 2005). The most important features of ordered mesoporous oxide are their exceptionally high surface area. The narrow and uniform pore size of mesoporous materials with extremely high surface area can be utilized as potential support for the development of novel solid catalysts. Due to their high specific surface area and good thermal stability, ordered mesoporous oxides have been used as supports for metals, and metal oxides for certain catalysts. In many reported studies it is observed that mesoporous materials have a comparable and superior performance compared to conventional microporous zeolites or amorphous silica–alumina catalysts (Taguchi and Schüth, 2005).

2.4.8 Desired Properties of HDT Catalyst Support

A) Textural Property: Good textural properties, namely a high specific surface area, a well-ordered porous structure, and narrow pore size distribution are considered to be the most important criterion that any catalyst support should fulfill (Ancheyta and Speight, 2007; Furimsky, 2007). The activity of the HDS and HDN depends on the pore diameter of the catalyst for some of the reactions taking place inside catalyst pores during hydrotreating (Ancheyta and Speight, 2007). Diffusion of bulky reactants, such as DBT (molecular size 0.8 nm) and 4, 6-DMDBT (molecular size 0.9 nm), into the catalyst pores significantly affects the activity of the catalyst having smaller pore size (Jayne et al., 2005). Diffusion and catalytic reaction of different sizes of sulfur molecules are shown in the Figure 2.22.

Thiophene, smaller sulfur molecules, can easily diffuse through the catalyst and converted to the saturated compounds. However, the bigger molecules, such 4,6-DMDBT, cannot enter to the catalyst pores, resulting in no desulfurization reaction due to restriction in the diffusion through the catalyst pores. Therefore, in case of heavy feeds, to convert heavy molecules into smaller molecules and to remove objectionable species (such as sulfur, nitrogen), catalyst with wide range of pores is essential. Moreover, adequate porosity is required to increase the catalyst life since the catalyst life reduces due to coking and pore mouth plugging (Furimsky, 2007).

However, increasing in catalyst porosity leads to a reduction in surface area, and consequently a decrease in specific activity. Hence, a balance between porosity and surface area needs to be maintained in order to obtain optimum textural property of the catalyst. The ranges of surface area and pore diameter suitable for hydrotreating processes are shown in Figure 2.23 (Ancheyta and Speight, 2007).

Mesoporous (pore radius of 20–500 Å) material (such as, MCM-41, MCM-48, HMS, FSM-16, KIT-1, and SBA-15) may serve as excellent support for hydrotreating catalyst since it provides good diffusion rates of bulky reactants, good surface area and resistance to deactivation (Taguchi and Schüth, 2005).

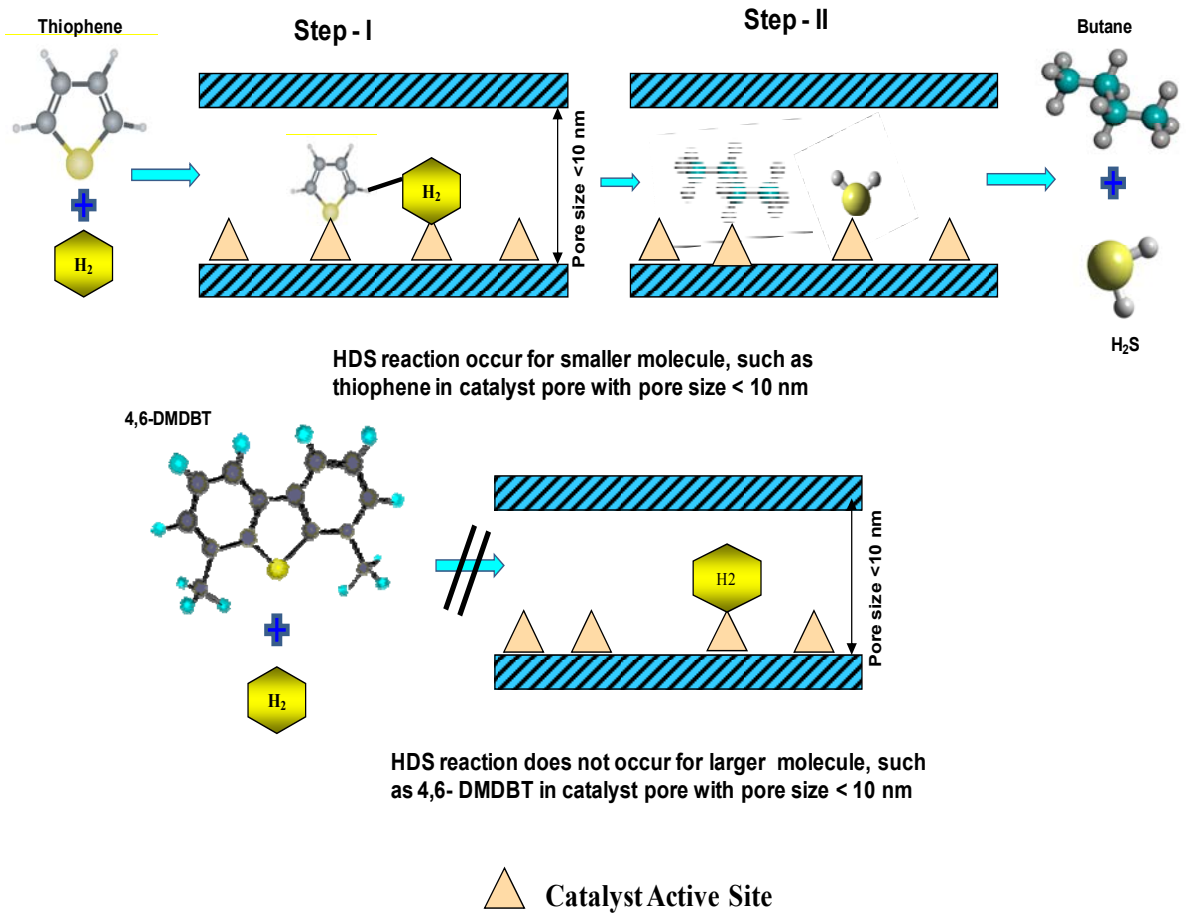

Figure 2.22: Diffusion and catalytic reaction of sulfur compounds through the catalyst pores.

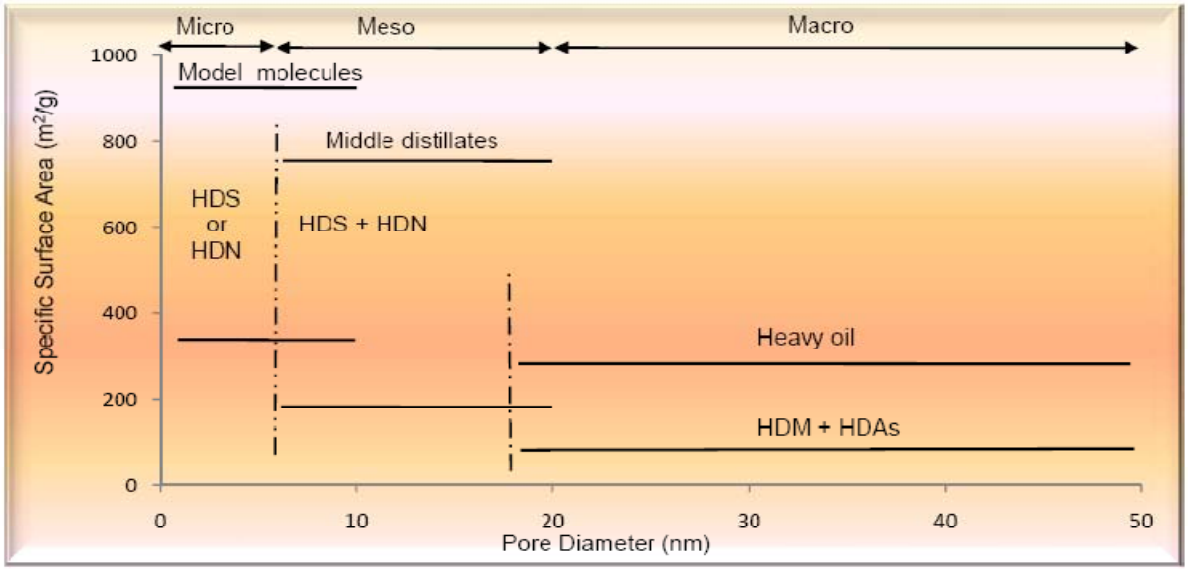

Figure 2.23: Effect of pore diameter and surface area on catalytic functionality (Ancheyta and Speight, 2007).

B) Activity and Selectivity: Other important parameters for catalyst formulation are activity and selectivity. High activity of the catalyst results in fast reaction rates and short reaction time. High selectivity of catalyst facilitates maximum yield while eliminating undesirable reactions (Chorkendorff and Niemantsverdriet, 2003). The new catalyst should possess a high activity and high selectivity for middle distillate (Furimsky, 2007). Supports play an important role in changing both activity and selectivity of the catalyst towards HDS and HDN reactions (Klimova et al., 2009). SBA-15 supported catalyst shows superior catalytic activity compared to γ-Al_2O_3 supported catalyst for the HDS of thiophene (Dhar et al., 2005). Also, metal oxide (TiO_2, ZrO_2, Al_2O_3) supported catalysts have been explored as support for hydrotreating catalyst. It is reported that for hydrodesulfurization reactions, ZrO_2 supported MoS_2 catalysts are three times more active than alumina supported ones with an equivalent Mo loading/nm^2 (Breysse et al., 2003).

C) Acidity: In hydrotreating process, removal of refractory dialkyl dibenzothiophenes [4, 6-dimethyl dibenzothiophene (4, 6-DMDBT)] is essential in order to reduce the sulfur content from diesel fuel (Bej et al., 2004). Conversion of 4, 6-dimethyldibenzothiophene (4, 6-DMDBT) into a more reactive compound, can be achieved either through isomerization, dealkylation and C-C bond scission (Rayo et al., 2009). The increase in acidity in support helps to enhance the isomerization, dealkylation and C-C bond scission of the alkyl groups present in 4, 6-DMDBT (Bej et al., 2004). However, increases in acidity may lead to undesirable cracking reactions. Hence, an appropriate tuning of the support acidity is imperative for achieving desirable HDS activity of refractory compounds. Improvement in the catalytic performance of the HDT catalyst can be achieved by using supports, which can provide optimal level of surface acidity as well as excellent well-ordered porous structure. In

this context, heteroatom (such as Zr, Ti, Al) modified SBA-15 materials have been investigated by several researchers (Klimova et al., 2009; Rayo et al., 2009).

D) Metal Support Interaction: Supported metal catalysts consist of small metal particles dispersed on the surface of a support material (Furimsky, 2007). Apart from increasing surface area, the role of the support is to control the course of a catalytic reaction by allowing specific interaction of the support with the active phase. Due to recent emphasis on the production of ultralow sulfur diesel (ULSD), special attention has been dedicated to the development of improved catalysts and to the understanding of metal-support interactions to produce catalysts with desired activity (Joshi et al., 2008). Catalytic properties depend on the nature of the metal-support interactions (Hinnemann et al., 2005). It is acknowledged that Co-Mo-S/Ni-Mo-S phase is responsible for the most important part of the catalytic activity (Eijsbouts, 1997). Co-Mo-S/Ni–Mo–S structures may be classified as either Type I or II on the basis of metal-support interaction (Hinnemann et al., 2005). In type I, presence of some Mo-O-Ms linkages between the MoS_2 and the support metal (Ms) is formed (Joshi et al., 2008). Strong linkage between MoS_2 and Ms is responsible for the low catalytic activity for γ-Al_2O_3 supported hydrotreating catalyst (Hinnemann et al., 2005). On the other hand, Type II structure is considered as highly active catalyst for the hydrotreating process due to absence of such linkage (Topsøe, 2007).

Very weak metal-support interaction results in inhomogeneous dispersion of MoS_2 phase, which adversely affect the catalytic activity. In SBA-15 supported catalyst, low and inhomogeneous dispersion of the MoS_2 phase is attributed to the very weak interactions between silica and molybdenum sulfide (Hensen et al., 2001). An optimal level of metal-support interaction is essential to obtain the desired catalytic activity. Since ZrO_2 provide

relatively stronger metal–support interaction, hence, incorporation zirconia into SBA-15 framework improves the metal-support interaction final catalyst (Gutiérrez et al., 2008). The rank order of the supports representing Type-I (strong interaction) tendency is SiO_2 < Al_2O_3 < ZrO_2 (Joshi et al., 2008).

2.4.9 Deactivation

Deactivation is a physical or chemical process, which decreases the activity of a catalyst (Furimsky and Massoth, 1999). Catalyst deactivation, also refer to as ageing, is basically the decrease in catalytic activity with time. Hydrotreating reaction takes place on the active sites of the catalyst. Deactivation of hydrotreating catalyst occurs due to the loss of active sites due to following reasons.

A) Catalyst Poisoning: Catalyst poisoning is defined as loss of catalytic activity by impurities due to formation of strong adsorptive bond with the catalyst surface (Hagen, 2006). During hydrotreating process, catalyst poisoning occurs due to presence of strongly adsorbed species, such as, nitrogen-compounds, coke molecules, metal deposits, which occupy an active site (Mo vacancy or Co or Ni sites) of the catalyst (Furimsky and Massoth, 1999).

A poison can be reversible or irreversible depending on the nature of feed and reaction conditions (Furimsky and Massoth, 1999). In reversible or temporary poisons, the catalyst activity can be restored by removing the poison from the feed. In irreversible or permanent poisoning, the bonding between the impurities and the active sites are so strong that the poison cannot be desorbed. For the hydroprocessing, the nitrogen containing compounds are the main source of catalyst poison due to their strong adsorption nature on the catalyst sites (Furimsky and Massoth, 1999). Other poisons are H_2S, Pb, Hg, S and P.

B) Deactivation by Deposits: Catalyst deactivation occurs by external impurities (metals coming with feed) or reaction bi-products (coke), which block the pore mouth or filling up the pore volume of the catalyst (Furimsky and Massoth, 1999; Moulijn et al., 2001). Catalyst activity loss by coke and metal deposition depends upon the feed properties, catalyst properties and hydrotreating process condition (Furimsky and Massoth, 1999). Deactivation by coke and metals are simultaneous. Coke deposition is rapid at the initial stage of hydrotreating until it reaches to the steady-state. On the other hand metal deposition follows the linear deposition patter with time.

In hydroprocessing, polymeric compounds, especially coke, are formed from the side reactions. Aromatic and olefinic hydrocarbons, sourced from the feed stream or formed as intermediate product in the hydrotreating process, are the precursor for the coking process (Hagen, 2001). Coking process takes places at high temperature by dehydrogenating polymers to carbon. During hydrotreating, the metals present in the feed stream causes the catalyst deactivation. Heavy oils derived from the tar sand contains vanadium, nickel, titania, iron and small amount some other metal, which deposits on the catalyst pores and reduces the catalyst activity. Deactivation by metal is an irreversible process. In the Figure 2.24, the typical catalytic activity loss of hydrotreating catalyst over the time-on-stream is shown. Catalyst deactivation profile is divided into three phase. In phase I, rapid decline of catalyst activity, occurs due to linear increase in metal deposits and saturation of coke deposits. In phase II, slow deactivation of catalyst, observed due to continuous deposition of metal. Phase III, accelerated and complete deactivation of the catalyst, due to pore plugging.

C) Sintering: Sintering (thermal degradation) of catalyst occurs due to 1) loss of catalytic surface area due to crystallite growth in catalytic phase 2) loss of support area due to collapse of support materials 3) transformation of catalytic phases to non-catalytic phases 4) catalyst damage due to thermal shock (Furimsky and Massoth, 1999; Moulijn et al., 2001) . Sintering takes place at very high temperature. Main parameters affecting the rates of sintering are temperature, atmosphere, metal type, metal dispersion, promoters, impurities, support surface area, texture, and porosity etc.

D) Mechanical Deformation: Mechanical breaking or failure of catalyst is occur due to high pressure in several different forms 1) crushing of granular or pellet due to load 2) attrition, the size reduction and break up of catalyst granules or pellet to produce fines 3) erosion of catalyst particles at high fluid velocity (Furimsky and Massoth, 1999; Moulijn et al., 2001). Commercial catalysts are vulnerable to mechanical failure because of their forms, cylindrical, spherical, and extrudated etc.

E) Evaporation (leaching): Metal loss occurs due to direct vaporization of components at very high temperature (Moulijn et al., 2001). This may result in catalyst activity loss and contamination of product. Evaporation at high temperature may affect the supported metals by 1) reaction of the metals with promoters or carriers (for example, solid state reaction of NiO with Al_2O_3 at high temp to form stable but inactive $NiAlO_4$) 2) segregation of metals or carrier phase and 3) metals and carrier phase transition (γ-Al_2O_3 to α -Al_2O_3).

In Figure 2.25, the major catalyst deactivation for hydrotreating catalyst due to above mentioned reasons are shown.

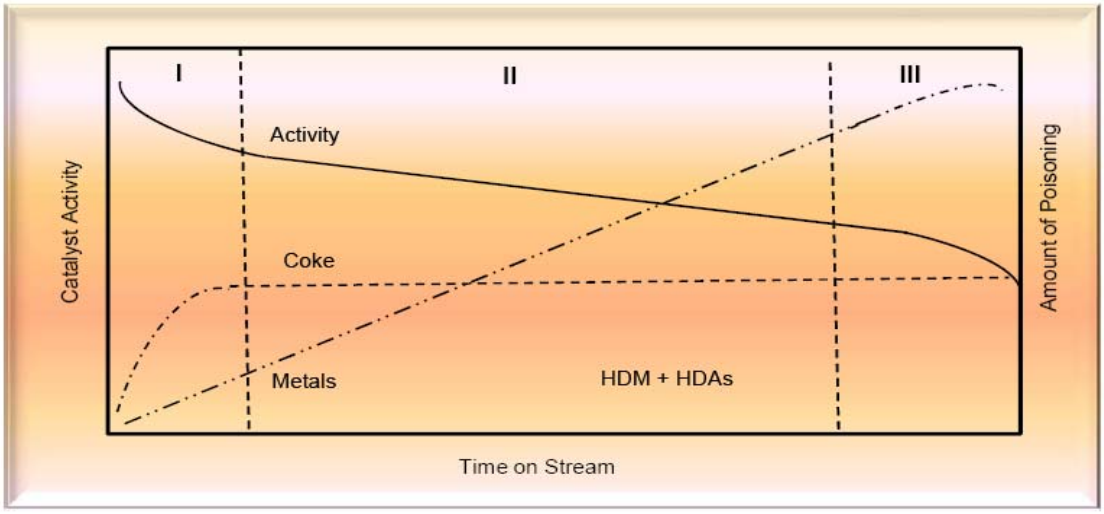

Figure 2.24: Hydrotreating catalyst deactivation profile (Moulijn et al., 2001).

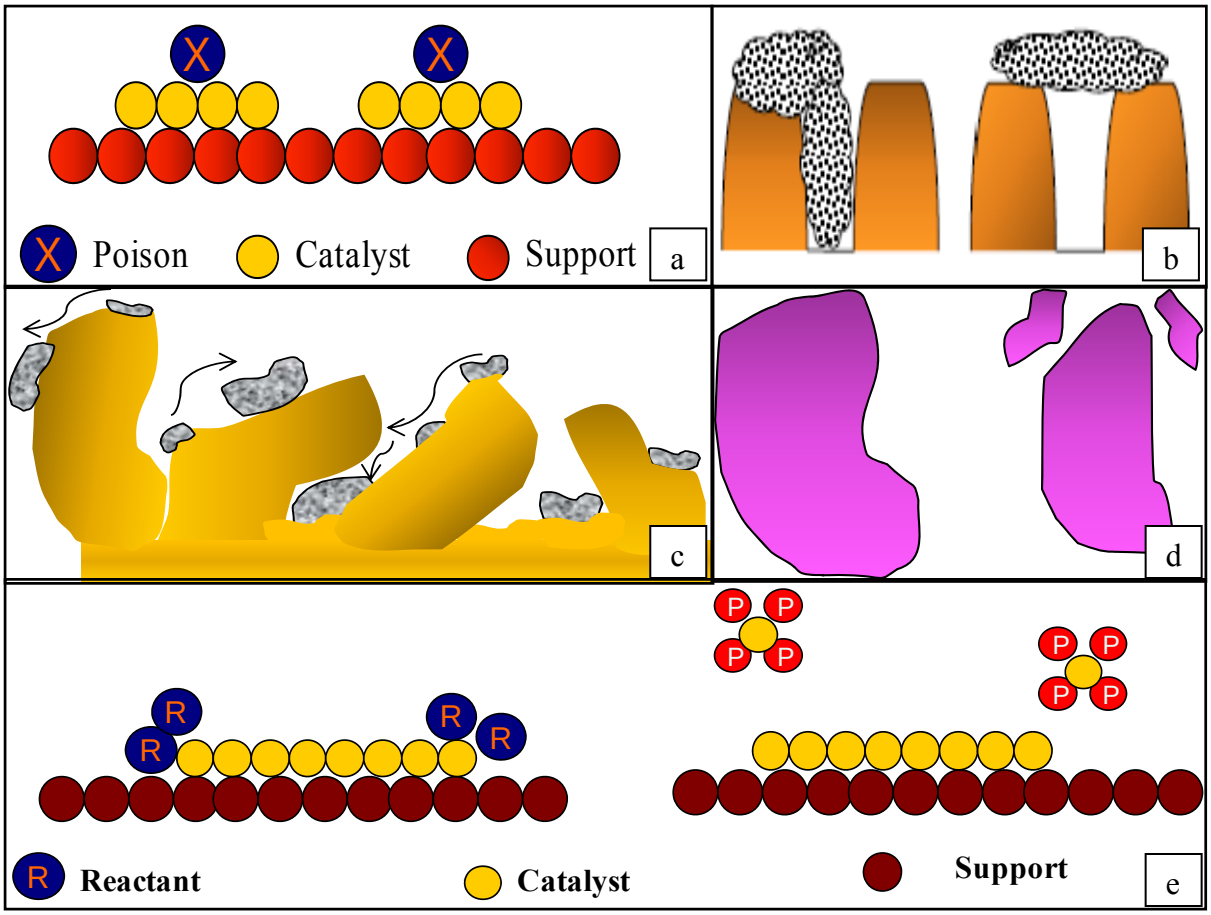

Figure 2.25: Major types of catalyst deactivation for hydrotreating catalysts due to a) poison b) deposits c) sintering d) mechanical failure e) evaporation (Furimsky and Massoth, 1999; Hagen, 2006; Moulijn et al., 2001)

2.4.10 Objectives of Catalyst Characterization

Industrial hydrotreating catalysts are extremely complex materials containing a mixture of multiphase compounds, including active compounds, promoters and additives. An understanding of this complex system is essential for selection of catalysts and for design and development of newer catalyst systems. Catalyst characterization provides valuable guidelines for monitoring the quality of catalyst. Objectives for catalyst characterization are (Satterfield, 1991; Topsøe et al., 1996):

i) Understanding relationship among physical, chemical, and catalytic properties related to the catalyst structure and function. Physical properties involve geometric structure, and morphology from macro scale to micro scale. Chemical properties is referred to elemental composition, structure and properties of individual crystallographic phases present in the catalyst, as well as surface compositions and the nature of properties of functional group present on catalyst surface. Catalytic properties are referred to its activity, i.e. ability to carry out a chemical reaction under specified conditions.

ii) Investigating causes of catalyst deactivation, designing procedures for regeneration and choosing catalyst properties to minimize deactivation.

iii) Determining physical and chemical properties [composition, pore size, surface area, particles size, strength] for purpose of catalyst marketing, reactor design, modeling, and process optimization.

iv) Ensuring quality control in catalyst manufacturing, i.e. monitoring changes of physical and chemical properties of the catalyst during preparation, activation and reaction stage.

Typical method for catalyst characterization is presented in Table 2.11.

Table 2.11: Typical methods for catalyst characterization (Satterfield, 1991; Topsøe et al., 1996).

Properties	Characterization Methods
• Composition and chemical elements	Elemental analysis (ICP-MS),SEM, TEM, X-ray fluorescence, atomic absorption
• Texture of catalyst and support(porosity, specific surface area, pore size distribution), state of dispersion, active agent	BET, Porosimetry, Chemisorption, XRD, SEM,TEM,
• Nature and structure of catalytic chemical species	XRD, NMR,FTIR, Raman, UV-DRS, TGA
• Mechanical Properties	Crushing test in hydraulic press, ultrasonic test

2.5 Selection of Zr-SBA-15 Support for Hydrotreating of Gas Oil

2.5.1 SBA-15 Support

Highly ordered and large pore size mesoporous siliceous materials have attracted significant attention for reactions involving large molecules (Corma, 1997; Zhao et al., 1998a; Zhao et al., 1998b). Among various ordered mesoporous silica (OMS), SBA-15, which is a polymer-templated silica with hexagonally ordered mesopores, became very popular in the application of catalysis, due to their excellent textural properties, high hydrothermal stability and thick pore walls (Fulvio et al., 2005; Zhao et al., 1998a; Zhao et al., 1998b).

Although, SBA-15 possesses excellent textural properties and exhibit superior activity compare to γ-Al_2O_3, but it has some limitation including the followings: i) pure SBA-15 materials lack acidic sites, which is essential for the hydrodesulfurization of refractory compounds (Rayo et al., 2009), ii) interaction between silica and Mo is very weak (Gutiérrez

et al., 2006a), and iii) it provides inhomogeneous and poor dispersion of sulfided active phase (Hensen et al., 2001).

2.5.2 ZrO_2 Incorporation into SBA-15 Framework

To introduce strong surface acidity and improve catalytic activity, various heteroatoms, such as Al, Zr, Ti, have been incorporated into SBA-15 (Rayo et al., 2009). Heteroatoms modified SBA-15 catalyst has been stated as more active for HDS than those supported on pure silica SBA-15 (Klimova et al., 2009). Among various heteroatoms and their oxides, Zr and zirconia (ZrO_2) has attracted much interest in view of their potential applications in heterogeneous catalysis. Already, zirconia has been used as support for hydrotreating catalysts by many research workers and showed promising results in hydrotreating reactions (Maity et al., 2000). Zirconium oxide has drawn great attention as catalyst and catalyst support due to their following characteristics (Gutiérrez et al., 2008; Ji et al., 2004; Maity et al., 2000):

- ZrO_2 has higher intrinsic HDS activity compared to γ –alumina
- ZrO_2 exhibits higher intrinsic HDS activity compared to other metal oxides (TiO_2, MgO)
- ZrO_2 has a high melting point of about 2700°C and is stable even under reducing conditions.
- ZrO_2 has higher thermal stability, extreme hardness, high specific mass of zirconia are the advantages for its use as catalyst support
- ZrO_2 improves reduction and sulfidation of MoO^{+6}
- ZrO_2 supported Ni promoted Mo catalyst shows higher activity in both HYD and HDS

ZrO_2 supported NiMo catalyst is proven to be better for HDS of model compounds and significantly better in the hydrogenation reactions than γ-alumina supported catalyst (Ji et al., 2004). However, specific surface area of ZrO_2 is very small and hence it is not advantageous for the hydrotreating of heavy molecules.

2.5.3 Synergistic effect of SBA-15 and ZrO_2

In order to overcome limitation associated with SBA-15, incorporation of ZrO_2 has been proven as better alternatives in improving its surface acidity, stability and metal support interaction (Dhar et al., 2005; Gutiérrez et al., 2008). Furthermore, mesoporous ordered material having higher specific surface area can provide appropriate textural properties to ZrO_2. Hence, the combination of silica and zirconia, to a certain extent, not only increases the textural properties, but also improves surface acidity, stability and metal-support interaction (Gutiérrez et al., 2008; Rayo et al., 2009). Zr-SBA-15 supported NiMo catalyst shows higher catalytic activity for hydrodesulfurization of refractory sulfur compounds (Gutiérrez et al., 2008). DBT conversion over Zr-SBA-15 is reported higher compared to other metal doped SBA-15 which is evident from Figure 2.26 (Klimova et al., 2009). For supported NiMo catalyst, incorporation of ZrO_2 in SBA-15 increases hydrodesulfurization activity of 4, 6-DMDBT significantly and it is reported to be 50% higher than that of γ-Al_2O_3 supported NiMo catalyst (Gutiérrez et al., 2008). 4,6-DMDBT conversion over NiMo/Zr-SBA-15 catalyst is shown in Figure 2.27. Higher catalytic activity of ZrO_2 incorporated SBA-15 supported catalyst is attributed to better textural property, better active phase-support interaction and improvement of surface acidity. Properties of SBA-15, ZrO_2, and Zr-SBA-15 supports are summarized in Table 2.12.

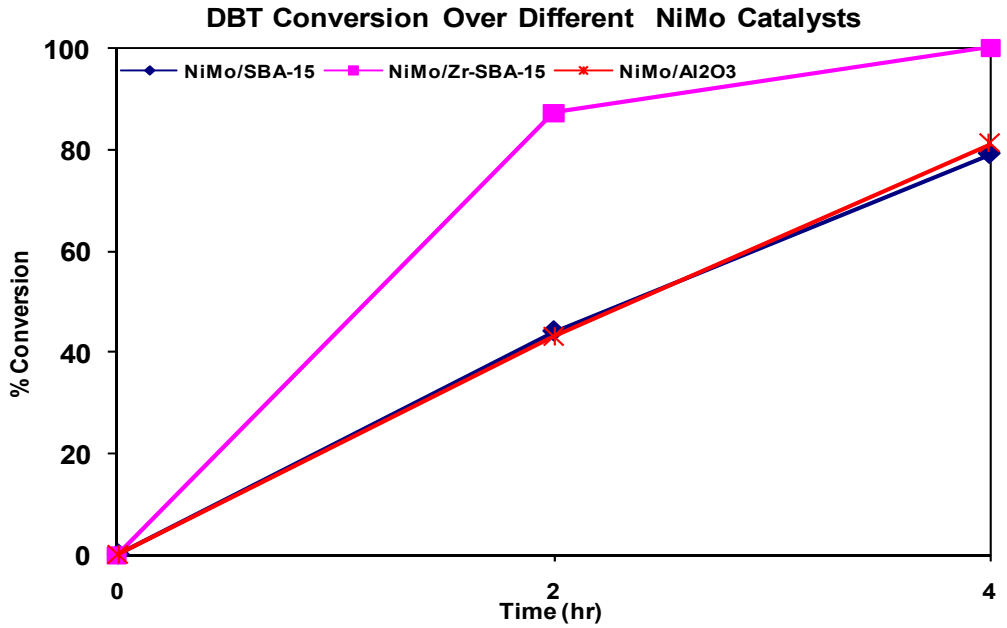

Figure 2.26: DBT conversion over different NiMo catalysts (batch reactor, 300 °C, 7 MPa, 8 hrs) (Klimova et al., 2009).

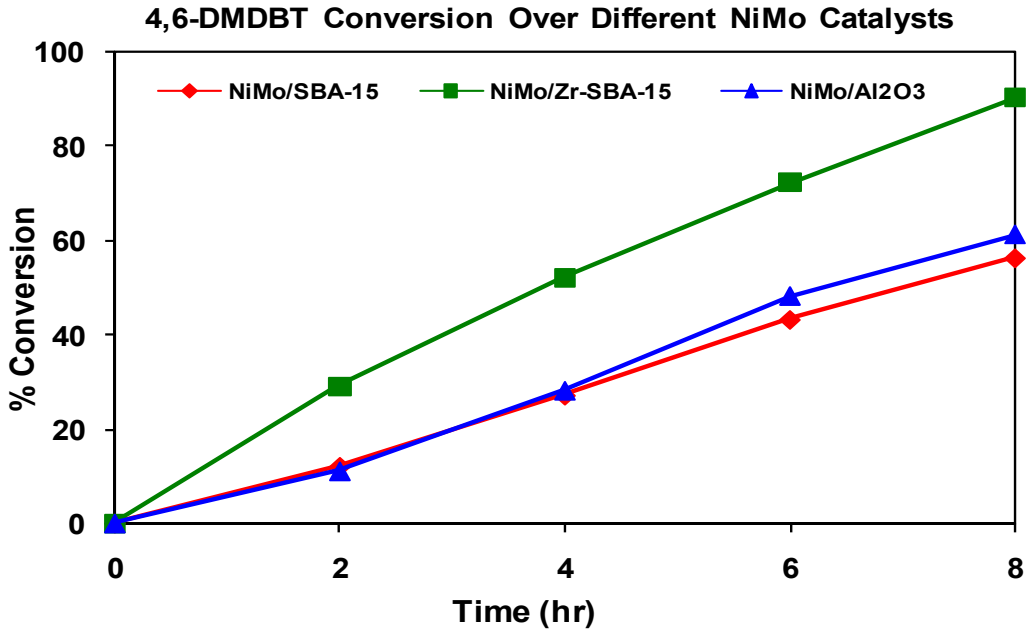

Figure 2.27: 4, 6-DMDBT conversion over different NiMo catalyst (batch Reactor, 300 °C, 7.3 MPa, 8 h) (Gutiérrez et al., 2008).

Table 2.12: Properties of SBA-15, ZrO_2, and Zr-SBA-15 supports.

Desired Properties	SBA-15	ZrO_2	Zr-SBA-15	References
• Textural properties	S_{BET}: 500-1200 m^2/g D_P: 5-30 nm V_P: 0.7-1.5 cc/g	S_{BET} : 100-336 m^2/g D_P: 2-5 nm V_P: 0.025-0.27 cc/g	S_{BET}: 175-860 m^2/g D_P: 3.1-4.0 nm V_P: 0.25-1.06 cc/g	(Breysse et al., 2003; D'Souza et al., 2006; Gutiérrez et al., 2009; Vradman et al., 2003)
• Catalytic activity	Superior to γ-Al_2O_3	Higher intrinsic HDS activity than γ-Al_2O_3	i) DBT conversion ~ 100% ii) 4,6-DMDBT conversion ~ 92% [Batch reactor, 300 °C, 7.3 MPa, 8h]	(Prins et al., 2006; Rayo et al., 2009)
• Acidity	Lacks acidic sites	Provides surface acidity	Provides optimum acidity	(Gutiérrez et al., 2006a; Maity et al., 2000)
• Metal-support interaction	Very weak	Improves metal-supprt interaction	Provides optimum metal-support interaction	(Joshi et al., 2008)

2.6 SBA-15 as Hydrotreating Catalyst Support

Since their discovery in 1992, ordered mesoporous materials (OMS) with high surface area and large, uniform, adjustable pore sizes have attracted widespread attention for their potential application as catalysts in the petrochemical industry (Taguchi and Schüth, 2005; Zhao et al., 1998a; Zhao et al., 1998b). Among the OMS group, SBA-15 became very popular as catalyst support in catalysis application.

2.6.1 Characteristics of Mesoporous SBA-15

SBA-15 (Santa Barbara Amorphous-15) is a mesoporous organosilica, which consists of large, ordered and defined hexagonal cylindrical channels with diameter 5 to 30 nm (Taguchi and Schüth, 2005). SBA-15 is promising as supports for HDS and HDN catalysts because of its attractive textural properties. Structure of SBA-15 is shown in Figure 2.28. The followings are some of the interesting properties of SBA-15 that are utilized for the application in hydrotreating (Kruk and Cao, 2007; Taguchi and Schüth, 2005; Vradman et al., 2003).

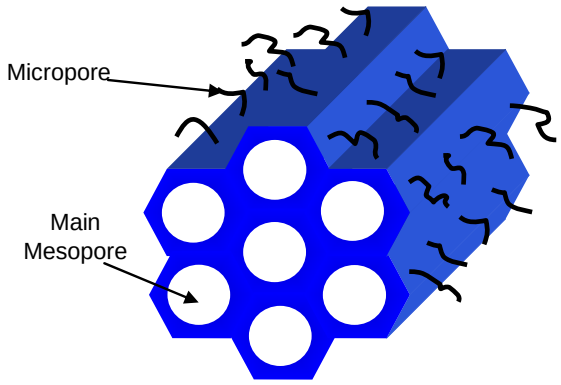

Figure 2.28: Structure of SBA-15

- It has exceptionally high surface area (500 – 1200 m^2/g), which provides high concentration of active sites per mass of materials.
- It has narrow distribution of uniform large pores of about 5-30 nm, which facilitate the diffusion of large molecules.

- It has large pore volumes of ordered mesopores (0.7-1.5 cc/g).
- It has high hydrothermal stability due to thicker wall thickness of 3-6 nm.
- In HDT reaction, it shows superior activity compared to γ-Al_2O_3 prepared in a similar way.
- It improves HDS activity for refractory compounds.
- It can be modified easily to improve the pore diameter.

2.6.2 Synthesis Methods of SBA-15

Steps of SBA-15 preparation by sol-gel method are: hydrogel formation, aging, separation, drying and template removal (Wan and Zhao, 2006; Zhao et al., 1998b). Following materials are used in the synthesis method: triblock copolymer P_{123} as a surfactant template, tetraethyl orthosilicate as silica source, water as solvent, and HCl as catalyst. Additives, such as hexane and NH_4F are added during the synthesis process for the pore size adjustment of SBA-15. The detailed procedure includes following steps:

First, dissolve the P_{123} ($EO_{20}PO_{70}EO_{20}$) in acidic water to obtain a homogeneous solution. In water, the micelle of triblock copolymer form by a hydrophobic PPO core and a hydrophilic PEO shell. In the presence of hydronium ions, PEO shell gets positively charged. When silicate precursors are added into the solution, hydrolysis of silica precursor takes place catalyzed by acid and results in formation of silicate oliomers. Afterwards, electrostatic interaction occurs between silica oligomers and PEO, which results in cooperative assembly and aggregation of silica oligomers. During this stage, microphase separation and continuous condensation of silicate oligomers takes place. Further solidification and reorganization takes place to form mesoporous structure. In order to complete condensation and solidification hydrothermal treatment is carried out. The material is then filtered, washed and dried at room temperature. Finally, mesoporous SBA-15 material is obtained by removing template by calcination method. The synthesis strategy of mesoporous SBA-15 is shown in Figure 2.29.

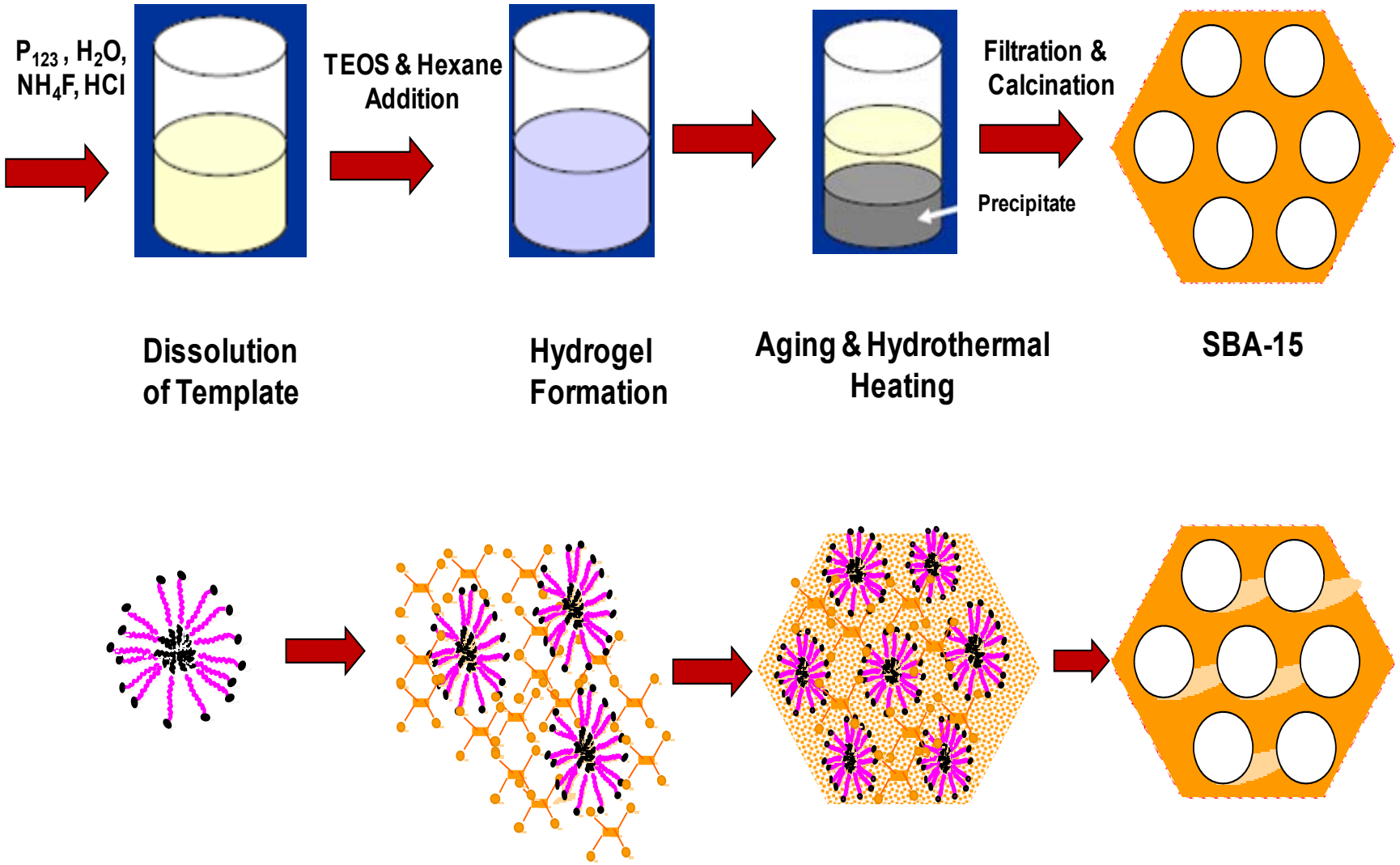

Figure 2.29: Synthesis strategy of mesoporous SBA-15 (Kim et al., 2004; Wan and Zhao, 2006).

2.6.3 Pore Diameter Control of SBA-15

Since the discovery of mesoporous siliceous materials, significant efforts have been made by several researchers to develop ordered mesoporous silica with two-dimensional (2-D) hexagonal structure (p6mm symmetry) that consists of cylindrical pores of 2 to 12 nm or larger (Kruk and Cao, 2007). In the catalysis realm, growing interest to develop large pore size mesoporous material is observed for the catalytic conversion of bulky molecules present in the feedstock. In this regards, several studies have been conducted on pore size control of mesoporous material, which can be effectively used for the industrial catalytic application. The control over pore size of mesoporous materials can be obtained by adjusting volumes of the hydrophobic group in the surfactants (Wan and Zhao, 2006). From various research on synthesis of mesoporous silica molecular sieve material, it has been observed that the mesoporous diameter of mesoporous materials can be adjusted by using followings (Jana et al., 2004): surfactants with different chain length (Corma, 1997; Namba et al., 1998), triblock polymer templates (Zhao et al., 1998b), organic swelling agent 1,3,5-trimethylbenzene (TMB) (Corma, 1997; Lettow et al., 2000), organic swelling agent triisopropylbenzene (TIPB) (Li et al., 2000), alkanes (Blin and Su, 2002; Nagarajan, 1999), amines (Sayari, 1996), and hydrothermal post-synthesis treatment. Among various strategies of pore diameter control of SBA-15, followings are widely reported in the literature:

A) Addition of Swelling Agent: The addition of a swelling agent (micelle expander) is reported to be effective for the pore size control of 2-D hexagonal mesoporous SBA-15 (Zhao et al., 1998a; Zhao et al., 1998b). The advantage of using swelling agent is that by increasing the amount of swelling agent, the pore size of the SBA-15 can be increased proportionally. Different swelling agents are:

i) 1,3,5–Trimethylbenzene (TMB/mesitylene): By adding 1,3,5-trimethylbenzene (TMB or mesitylene) as organic swelling agent, the pore size of hexagonal mesoporous SBA-15 has been expanded from 50 nm to 300 Å successfully (Zhao et al., 1998a; Zhao et al., 1998b). However, a subsequent study confirms that the large amount of TMB (mesitylene) addition results in phase transition from highly ordered cylindrical 2D hexagonal SBA-15 (7-12 nm) structure to mesoporous cellular forms (MCF) (Schmidt-Winkel et al., 2000). Using TMB as swelling agent, the largest obtainable pore diameter with highly ordered 2D hexagonal structure SBA-15 was 12 nm (Lettow et al., 2000). Also, using of organic swelling agent is not desirable since their use involve addition of large volume of organic swelling agent, which needs additional separation process (Corma, 1997).

ii) 1,3,5-Tri isopropylbenzene (TIPB): Using 1,3,5-Tri isopropylbenzene (TIPB) as organic swelling agent, the pore size of hexagonal 2D ordered mesoporous SBA-15 can be expanded upto 140 Å successfully (Cao et al., 2009; Li et al., 2000).

iii) Alcohol additives: Large pore SBA-15 can be synthesized using alcohol additives (butanol, pentanol, hexanol), some instances combine with octane utilizing pluronic F_{127} block polymers ($EO_{106}PO_{70}EO_{106}$) (Feng et al., 2000). However, high mass fraction hydrophilic PEO blocks lead to formation of spherical templates rather than cylindrical ones (Kruk and Cao, 2007; Zhao et al., 1998b).

iv) Alkanes additives: Alkanes (pentane, hexane, heptanes, octane) acts as powerful micelle expanders for the synthesis of mesoporous materials, which has been reported by Blin and Kruk (Blin et al., 2000; Blin and Su, 2002; Kruk and Cao, 2007). In their studies, alkane swelling agent showed low degree of structural ordering and limited

swelling capability for the preparation of 2D hexagonal structure (Jana et al., 2004). However, subsequent studies reported that adding linear alkanes with small amount of NH_4F and maintaining the suitable initial synthesis temperature, large pore highly ordered 2D hexagonal structure could be achievable (Kruk and Cao, 2007).

Details of pore size control of mesoporous SBA-15 is shown in Table 2.13.

B) Hydrothermal Treatment Temperature: The pore size of ordered hexagonal SBA-15 structure can be controlled by varying the reaction temperature from 35 – 140 °C (Zhao et al., 1998a).

C) Hydrothermal Treatment Time: The adjustment of pore size of ordered mesoporous hexagonal SBA-15 material can be achieved by changing the duration of the hydrothermal treatment time from 11 – 72 hours (Zhao et al., 1998a; Zhao et al., 1998b).

Table 2.13: Pore size control of mesoporous SBA-15 structure.

References	Swelling Agent	Block Polymer	Pore Size Obtained (nm)	Structure Obtained	Remarks
(Lettow et al., 2000)	TMB	P_{123} ($EO_{20}PO_{70}EO_{20}$)	6-12	2D hexagonal cylindrical pores	Mesocellular form formation upon increase of TMB
(Zhao et al., 1998a)	TMB	P_{123} ($EO_{20}PO_{70}EO_{20}$)	5-30	Until 12 nm 2D hexagonal cylindrical pores	Large amount of TMB causes change of structure from 2D hexagonal to mesocellular form [Schimdt and winkel, 1999]
(Zhao et al., 1998b)	TMB	P_{123} ($EO_{20}PO_{70}EO_{20}$)	4.6-8.9	2D hexagonal cylindrical pores	Addition of large amount of TMB causes change of structure of SBA-15
(Cao et al., 2009)	TIPB	P_{123} ($EO_{20}PO_{70}EO_{20}$)	10-26	2D hexagonal cylindrical pores	Loss of hexagonal 2D structure beyond pore diameter 26 nm
(Feng et al., 2000)	Alcohol	F_{127} ($EO_{106}PO_{70}EO_{106}$)	up to 19	2D hexagonal pores	Spherical structure obtained
(Lin et al., 2006)	Alcohol	($MA_xEO_yMA_x$)	9	2D hexagonal cylindrical pores	Large-pore 2-D hexagonally ordered structure was obtained using new triblock copolymers as templates.
(Jana et al., 2004)	Alkane	P_{123} ($EO_{20}PO_{70}EO_{20}$)	0.9	2D hexagonal cylindrical pores	Disordered meso-cellular foam formation for the larger pore diameter
(Sun et al., 2005)	Alkane & NH_4F	P_{123} ($EO_{20}PO_{70}EO_{20}$)	15	2D hexagonal cylindrical pores	SBA-15 with good mesoporous structure is obtained
(Kruk and Cao, 2007)	Alkane & NH4F	P_{123} ($EO_{20}PO_{70}EO_{20}$)	12-18	2D hexagonal cylindrical pores	SBA-15 with good mesoporous structure is obtained

Where, ($MA_xEO_yMA_x$) = Poly (methyl acrylate)-poly (ethylene oxide)-poly (methyl acrylate) [x = 33-70]

2.6.4 Application of SBA-15 Support in Hydrotreating

SBA-15 mesoporous materials as catalyst support have been tested for the hydrotreating with various model compounds and real feedstocks. The application of SBA-15 support in the hydrotreating reaction is presented in Table 2.14.

Table 2.14: Application of SBA-15 support in hydrotreating.

References	Catalysts	Feed	Remarks
(Dhar et al., 2005)	Mo/SBA-15, CoMo/SBA-15, NiMo/SBA-15	Thiophene and cyclohexane	SBA-15 supported catalysts showed superior catalytic activity compared to the γ-Al_2O_3 supported catalyst
(Vradman et al., 2003)	NiW/SBA-15	Dibenzothiophene and toluene	SBA-15 supported NiW catalysts showed higher HDS activity compared to the commercial CoMo catalyst
(Sampieri et al., 2005)	Mo/SBA-15	Dibenzothiophene	SBA-15 supported catalysts showed higher catalytic activity compared to the γ-Al_2O_3 supported catalyst
(Rayo et al., 2008)	NiMo/SBA-15	Thiophene	NiMo/SBA-15 catalyst prepared under acidic condition showed higher catalytic activity
(Huang et al., 2008b)	Mo/SBA-15 and CoMo/SBA-15	Dibenzothiophene	CoMo/SBA-15 catalyst showed higher HDS activity compared to γ-Al_2O_3 catalyst
(Soni et al., 2010)	NiMo/SBA-15	Coker Light Gas Oil	NiMo/SBA-15 catalyst showed higher HDS and HDN activity compared to NiMo/ γ-Al_2O_3 catalyst

2.7 Zr-SBA-15 as Hydrotreating Catalyst Support

2.7.1 Characteristics of Zr-SBA-15

Zirconium Oxide (ZrO_2) and zirconium containing compounds have got significant attention as an effective catalyst and an efficient catalytic support for many catalytic reactions (Chuah et al., 1996; Gutiérrez et al., 2009). In particular, growing interest towards the zirconium based materials in catalysis is observed for many years due to following: i) it possess high mechanical, chemical, and thermal stability and ii) it possess both acidic, basic and redox properties, which are advantageous for the hydrotreating process as well (Gutiérrez et al., 2009; Maity et al., 2000):

However, pure zirconia has very unpromising (low) textural properties (specific surface area (100 m^2/g) and porosity 2-3 nm), which limit its possibility in hydrotreating application, where good dispersion of active components over supports, good diffusion of bulky molecules inside catalyst pores and resistance towards deactivation are essential (Gutiérrez et al., 2009). In order to overcome these limitations associated with ZrO_2 and improve its catalytic activity, combination of ZrO_2 with SBA-15 (materials with good textural characteristic), has been received significant attention. By incorporating zirconia onto SBA-15 support promising effect has been observed in Zr-SBA-15 support. Following promising characteristics are reported for Zr-SBA-15 support in the hydrotreating catalyst application:

- excellent textural properties
- homogeneous dispersion of active metal over the support materials
- good metal-support interaction

- presence of surface acidity, which is essential for the desulfurization of refractory compounds.

2.7.2 Synthesis Methods of Zr-SBA-15

Zirconia incorporation into the framework of mesoporous materials can be done by two typical methods, namely direct synthesis and post synthesis.

A) Direct Synthesis Method: In direct synthesis method, zirconia incorporation into SBA-15 framework is accomplished during hydrothermal synthesis of SBA-15 materials. This is a single stage process wherein silica precursor (TEOS) and zirconia precursor ($ZrOCl_2.8H_2O$) are sequentially added to the block copolymer template P_{123} ($EO_{20}PO_{70}EO_{20}$) (pore directing agent) before hydrothermal treatment (Chen et al., 2004)

Advantages of Direct Synthesis:

- Better dispersion of active sites (Szczodrowski et al., 2008).
- More homogeneous distribution of metal produces more stable and dispersed framework (Melero et al., 2005).
- Formation of extra framework can be avoided (Szczodrowski et al., 2008).
- The procedure of heteroatom into mesoporous material by this method is quite simple for the incorporation (Szczodrowski et al., 2009; Wu et al., 2004).
- Decrease of surface area is not significant.
- Chances of partial pore blockage can be avoided.

Disadvantages of Direct Synthesis Method:

- Efficiency of direct synthesis method is low compared to the post synthesis method, since only small amount of heteroatom can be incorporated into SBA-15 (Wu et al., 2004).

- Zirconia incorporation by direct synthesis method becomes difficult, since during synthesis majority of zirconia precursor gets dissolved in the strong acidic medium (Amezcua et al., 2005; Chen et al., 2010).
- Difficult to maintain the pore ordering of mesoporus material upon large amount of zirconia incorporation by direct synthesis method, since zirconia precursor causes the disturbance of self-assembly of surfactant micelles and silicate (Chen et al., 2010; Newalkar et al., 2001).
- Reaction mechanism for the co-condensation method is relatively complex (Szczodrowski et al., 2009) and very difficult to control the heteroatom insertion in SBA-15 framework. Temperature, pH, aging time, precursor nature, reaction mixture composition and reactivity, are very difficult to control by this synthesis method. Hence chances of high heterogeneity and poor reproducibility of the resultant samples.
- Various sizes of ZrO_4^-, formed around the templating structure, cause local distortion of inorganic framework (Szczodrowski et al., 2009).
- Co-condensation reaction is very sensitive to the experimental condition (Szczodrowski et al., 2009). Zr-O-Si bonds become fragile due to presence of strong acidic hydrothermal environment and the significant difference between hydrolysis rate of silicon and metal precursors (Szczodrowski et al., 2009).
- Difficult to obtain larger pore diameter of Zr-SBA-15.

Zr-SBA-15 Preparation by Direct Synthesis Methods:

Several methods are developed for the direct synthesis of Zr-SBA-15.

- Self-generated Acidic Environment (Chen et al., 2004): In this method, Zr-SBA-15 is prepared in the absence of HCl and using $ZrOCl_2.8H_2O$ as zirconium precursor, TEOS

as silica source and amphiphilic triblock copolymer P_{123} ($EO_{20}PO_{70}EO_{20}$) as pore-directing agent. In this method, P_{123}, $ZrOCl_2.8H_2O$ and water mixture is stirred at 35 °C for one day and then allowed hydrothermally reacted at 90 °C for one day. After that the solution is filtered, washed and calcined to obtain Zr-SBA-15 mesoporous material. By this method the loading of zirconia is relatively low (Si/Zr ratio >10).

- Microwave Assisted Synthesis (Du et al., 2009; Newalkar et al., 2001): Using this method Zr-SBA-15 is prepared (up to bulk Si/Zr =20) without changing the textural properties (Newalkar et al., 2001). However, in the subsequent literature the disadvantages of this method have been reported. The mesostructure of Zr-SBA-15 materials decreases significantly upon Zr/Si atomic ratio greater than 5% and structure gets disorganized at a Zr/Si ratio of 10% (Chen et al., 2004). In this method followings are used: $ZrOCl_2.8H_2O$ as zirconium precursor, TEOS as silica source and amphiphilic triblock copolymer P_{123} ($EO_{20}PO_{70}EO_{20}$) as pore-directing agent. In this method, first P_{123} is dissolve in distilled water. The resultant solution is then mixed with HCl and $ZrOCl_2.8H_2O$ to obtain homogeneous solution. Then TEOS is added to the solution and kept for crystallization under microwave-hydrothermal condition. The product is then filtered, washed and calcined.

- "pH" Adjusting Method (Du et al., 2009): Highly ordered hexagonal Zr-SBA-15 with large amount of zirconium (Si/Zr ratio 5.0 to 9.0) can be prepared using urea as pH adjustor. However, in this process aqueous leaching and thermal decomposition of the active components cannot be avoided. In this method, materials are used: $ZrOCl_2.8H_2O$ as zirconium precursor, tetraethyl orthosilicate (TEOS) as silica source, amphiphilic triblock copolymer P_{123} ($EO_{20}PO_{70}EO_{20}$) as pore-directing agent and urea as pH adjustor.

In this method, TEOS is added to HCl containing P_{123} solution. After that, $ZrOCl_2.8H_2O$ and urea is added subsequently to the solution. The solution is then stirred and refluxed until the pH of solution changes from 5 to 6. Then the solution is kept for aging. The final product is then filtered, dried and calcined to obtain Zr-SBA-15.

- Surfactant Templated Method (Salas et al., 2009): Highly ordered Zr-MCM-41 with large amount of zirconium (Si/Zr molar ratio 40 to 5) can be prepared by this method. In this method, materials are used: cetyltrimethylammonium bromide (CTAB) as template, tetraethyl orthosilicate (TEOS) as silica source and zirconium-n-propoxide (70% propanol) as zirconium source. First, solution is prepared by mixing zirconium-n-propoxide with TEOS. Second solution is prepared by adding CTAB, $(NH_4)_2SO_4$ and $NH_3.H_2O$ into hot water. These two solutions were mixed and keep for aging. The final product is then filtered, dried and calcined to obtain Zr-MCM-41 material.

- Two-step Process (Fuxiang et al., 2007): High loading of Zr into SBA-15 (Si/Zr ratio 0.43 to ∞) is obtained by this process. However, the most of the Zr species present in the Zr-SBA-15 materials prepared by this method are crystalline ZrO_2 instead of isolated Zr^{4+} .In this method, hexadecyl trimethyl ammonium bromide (CTAB) and triblock copolymer P_{123} ($EO_{20}PO_{70}EO_{20}$) as template, tetraethyl orthosilicate (TEOS) as silica source and zirconium nitrate ($Zr(NO_3)_4.3H_2O$) as zirconium source. In this method the first sample is prepared by mixing CTAB alcohol with $Zr(NO_3)_4.3H_2O$ and preheating the mixture. The second sample is prepared by adding TEOS into HCl containing $EO_{20}PO_{70}EO_{20}$. These samples are then added, stirred continuously and kept for aging. Finally the product is filtered, dried and calcined to obtain Zr-SBA-15 material.

B) Post Synthesis Method: Zirconia or zirconia isopropoxide can be successfully attached to the walls of mesoporous materials by post synthesis methods (Hagen et al., 1998; Luan et al., 1999). In the post synthesis method, Zr-SBA-15 is synthesized by two stage process. In the first stage, well-ordered SBA-15 is synthesized by conventional sol-gel process by using triblock copolymer P_{123} ($EO_{20}PO_{70}EO_{20}$) as the structure directing agent and TEOS as silica source (Kruk and Cao, 2007). In the second stage, zirconia is impregnated into SBA-15 structure using zirconia precursor (zirconium (IV) propoxide) and calcined SBA-15 (Gutiérrez et al., 2008).

Advantages of Post Synthesis:

- In this method, greater concentration of heteroatom can be loaded effectively on the surface (Luan et al., 1999; Rayo et al., 2009; Wu et al., 2004).
- This method offers deposition of highly dispersed zirconia sites on the SBA-15 surface without changing its texture and structure significantly (Luan et al., 1999).
- Post synthesis grafting method allows the allocation of grafting species (zirconia) on the surface of SBA-15 materials, which are more accessible for the interaction with catalyst active sites (Amezcua et al., 2005; Klimova et al., 2001).
- Characteristics of deposited zirconia species can be fine tuned by changing the preparation methods (chemical grafting or incipient impregnation method) (Amezcua et al., 2005; Klimova et al., 2001; Luan et al., 1999).
- By this method, increase of thermal and hydrothermal stability of mesoporous materials is obtained by increasing the pore wall thickness.
- Post-synthesis grafting method can be carried out under both acidic and basic condition (Wu et al., 2004).

- Larger pore diameter of Zr-SBA-15 can be prepared.

Disadvantages of Post Synthesis:

- Formation of segregated metal oxide on the surface causes partial blockage of the pore (Rayo et al., 2008).
- Reduction of textural properties of the mesoprous framework upon zirconia incorporation, which will cause decrease in catalytic activity (Newalkar et al., 2001; Wu et al., 2004).
- Post synthesis routes for the heteroatom insertion into mesoporous materials are quite complicated and in some routes the synthesis methods needs to be performed in the absence of water and oxygen (Luan et al., 1999; Wu et al., 2004).
- It is difficult to achieve quantitatively incorporation of heteroatom by grafting method, since heteroatom partially leached out during filtration (Wu et al., 2004).
- By post synthesis method, 4-coordinated heteroatom incorporation into SBA-15 not obtainable exclusively. There are some 6-coordinated heteroatom incorporated species are present in the final material (Luan et al., 1999; Wu et al., 2004).

Zr-SBA-15 Preparation by Post Synthesis Methods:

Zirconia incorporation into SBA-15 mesoporous material can be done by following post synthesis methods:

- Chemical Grafting (CG) (Klimova et al., 2001): In this method, zirconium (IV) propoxide ($Zr(n\text{-}PrO)_4$ 70 wt% solution in 1-proponal) is used as zirconia precursor and dry ethanol as solvent. In this method, grafting procedure carried out by mixing SBA-15 with ($Zr(n\text{-}PrO)_4$) containing dry ethanol. Excess ethanol is removed from the grafting material by filtrating and washing with ethanol. Finally, Zr-SBA-15 material is obtained

by drying and calcine. The synthesis strategy of Zr-SBA-15 support by chemical grafting method is shown in Figure 2.30.

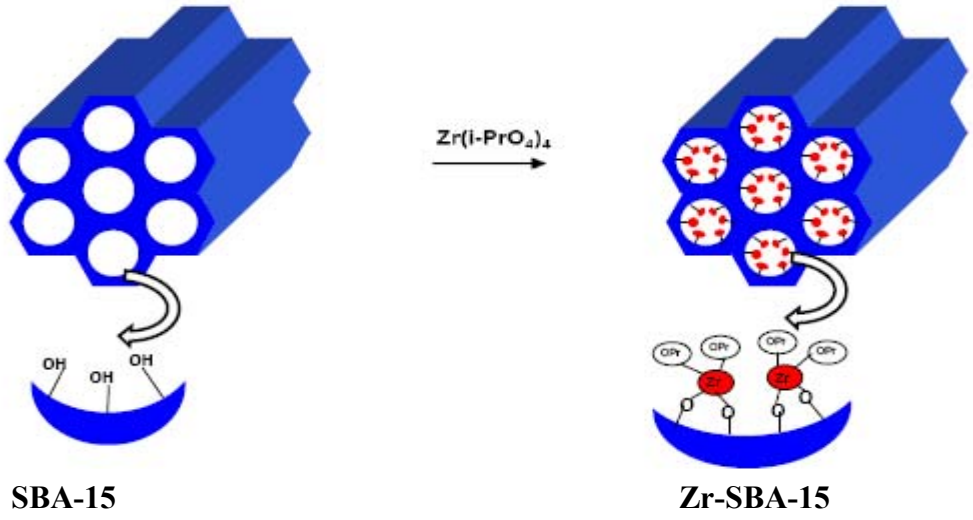

Figure 2.30: Synthesis strategy Zr-SBA-15 preparation by chemical grafting method (Zhang et al., 2010).

- Incipient Wetness Impregnation (IWI) (Klimova et al., 2001): In this method, zirconium (IV) propoxide is used as zirconia precursor and n-propanol is used as solvent. First, SBA-15 is impregnated with n-propanol containing zirconium (IV) propoxide. Then the sample is dried and calcined.

- Vapor Induced Internal Hydrolysis (Cheralathan et al., 2008): Higher loading of zirconia (>30%) can be accomplished without pore blocking. In this process, zirconia precursor is loaded inside the pores of SBA-15 materials by repeated multi-step wet impregnation method. After that the material is hydrolyzed internally by hydrolysis agent, (NH_3/H_2O vapor) at higher temperature. Zirconium hydroxide precipitate on the SBA-15 walls in highly dispersed by internal hydrolysis method. Finally, zirconia coated SBA-15 material is obtained after calcinations.

- Chemical Solution Deposition (CSD) (Landau et al., 2005): Landau and coworkers successfully prepared Zr-SBA-15 (ZrO_2 loading 48-75 wt %) by Chemical Solution Deposition method. In this method materials are used: calcined SBA-15, zirconium (IV) propoxide ($Zr(n\text{-}PrO)_4$ 70wt% in n-propanol) as zirconia source. SBA-15 is impregnated with zirconium (IV) propoxide ($Zr(n\text{-}PrO)_4$) under nitrogen atmosphere. The wet solid obtained after the filtration from excess solution is placed in a n-propanol containing autoclave. The chemical solution deposition is performed at higher temperature. The final Zr-SBA-15 product is then cooled, dried and calcined.
- Internal Hydrolysis (Landau et al., 2005): In this method zirconium (IV) propoxide ($Zr(n\text{-}PrO)_4$) is used as zirconia precursor. The Zr impregnation inside the SBA-15 is carried by hydrolysis of ($Zr(n\text{-}PrO)_4$). First, SBA-15 is impregnated with zirconium (IV) propoxide ($Zr(n\text{-}PrO)_4$) under nitrogen atmosphere. After separation from excess solution, the solid is hydrolyzed by distilled water in a glass vessel. The solid is separated from water by filtration. Final zirconia impregnated SBA-15 is obtained by dried and calcined the materials.
- "pH Adjusting" Method (Wu et al., 2004): In this method, high content of heteroatom is impregnated in strongly high acidic media. First, the heteroatom source is added into a highly acidic solution (pH<0). When the mesostructure is formed, the pH value of solution is adjusted from strong acid (pH<0) to neutral media (pH=7). Thereafter, hydrothermal treatment is carried out. Finally, material is dried and calcined.

2.7.3 Application of Zr-SBA-15 Support in Hydrotreating

Zr-SBA-15 support has been explored as catalyst for hydrotreating of model compounds. The details are presented in Table 2.15.

Table 2.15: Appication of Zr-SBA-15 support in hydrotreating.

References	Catalysts	Feed	Remarks
(Garg et al., 2008)	Zr-SBA-15 supported Mo, NiMo,CoMo	Thiophene and cyclohexane	Zr-SBA-15 supported CoMo Catalysts highly effective for hydrodesulfurization
(Gutiérrez et al., 2006a; Gutiérrez et al., 2006b)	NiMo/Zr-SBA-15	4,6-dimethyl dibenzothiophene	NiMo/Zr-SBA-15 showed high activity for HDS of 4,6-dimethylbenzene
(Klimova et al., 2009)	NiMo catalyst supported on ZrO_2, TiO_2, Cao, MgO	Dibenzothiophene	ZrO_2 supported catalysts showed higher catalytic activity compared to the other metal oxide supported catalyst
(Rayo et al., 2009)	NiMo catalyst supported on M-SBA-15 (M=Ti,Zr,Al)	Thiophene	Zr-SBA-15 supported NiMo catalyst showed highest activity compared to others.

2.8 Kinetic Modeling of HDS and HDN

2.8.1 Purpose of Kinetic Modeling

The kinetic information is important for the hydrotreating of heavy gas oil since they offer following advantages (Landau, 1997):

- Design of commercial reactors, pilot plant study, improvement of process parameters, and optimization of operating condition.
- Investigation of reaction pathways.
- For the formulation of new catalyst the basic kinetic information such as reaction order, reaction rate constants, activation energy, effectiveness factor calculation and effect of operating conditions on conversion.
- Comparison of the activity of different catalysts.
- Development of kinetic model for the hydrotreating process.

Deep hydrodesulfurization and hydrodenitrogenation of heavy gas oil feedstock necessitates the development of more active catalysts and the modification of existing kinetic of hydrodesulfurization and hydrodenitrogenation models (Van Looij et al., 1998). In this section, the purpose of the kinetic study is to develop kinetic models for hydrotreating activity of NiMo/Zr-SBA-15 catalyst on heavy gas oil feed under industrial condition which will be reliable for the scale-up of pilot plat data.

2.8.2 Kinetic Models for HDS and HDN

Several kinetic models have been documented in the literature for hydrodesulfurization and hydrodenitrogenation of model compounds. Generally, it has been reported that kinetic studies based on model compounds follows first order for the hydrodesulfurization and hydrodenitrogenation reaction (Ancheyta et al., 2002a; Botchwey et al., 2004). However, heavy gas oil is highly complex mixture of hundreds of paraffins, naphthenes, (polycyclic) aromatics, organo-sulfur, and nitrogen compounds hence kinetic data of HGO won't be analogous to the kinetic data based on model compounds (Callejas and Martínez, 1999). Due to complex mixture of the different compounds, it is difficult to express the overall hydrodesulfurization or hydrodenitrogenation reaction kinetics with a single rate expression (Sie, 1999).

Also, several investigations on hydrodesulfurization of model compounds show that the presence of inorganic reactants and products such as hydrogen, hydrogen sulfide, and ammonia can significantly affect the rate of the hydrodesulfurization reaction (Korsten and Hoffmann, 1996). Similar observation was made while using the complex mixture of hydrocarbons Also, hydrodesulfurization reactivity depends on the type of sulphur compounds present in the feed (Ancheyta et al., 2002a). In case of HDN, the complexity

of HDN kinetic results arise predominantly from the competitive adsorption of various reactants, intermediates and products on catalytic sites. Hence, for the heavy gas oil, complex mixture of hydrocarbon, an appropriate kinetic model is imperative in order to generate reliable data and to quantify the effect of various parameters on overall HDS and HDN reaction (Van Looij et al., 1998).

Apart from the feedstock variation, the kinetic parameters, such as reaction order and activation energy changes with the variation of catalyst. The HDS and HDN reaction mechanism and kinetics observed with new catalysts differ from the conventional catalysts. In this context, kinetic models are very useful to evaluate the performance of the new catalyst using real feedstock.

In general, Power Law model and the Langmuir-Hinshelwood model are applied to express the kinetic rate of hydrodesulfurization and hydrodenitrogenation reactions (Ferdous et al., 2006a).

2.8.3 Power Law Model

Power law model is a more comprehensive approach to generate the basic kinetic information, such as reaction order, reaction rate constant, activation energy, effect of operating condition on conversion (Marroquín et al., 2005). Due to its simplicity, the power law model is very popular to generate basic kinetic information, such as reaction order, reaction rate constant, activation energy, effect of operating condition on conversion (Ferdous et al., 2006a). Also, it is documented that to represent kinetics of hydrotreating reaction for real feed stock, power law is more useful. The removal of sulfur and nitrogen from HGO are described by following power law model (Ferdous et al., 2006b):

$$-r_A = k_A C_A^n = \frac{dC_A}{dt} \qquad (2.8.1)$$

Where, $-r_A$ = rate of HDS or HDN reaction, k_A = apparent rate constant, C_A = sulfur and nitrogen content, n = reaction order, t = residence time.

The solutions for the above equation are:

$$k_A = LHSV[C_0 - C_P] \qquad for\ n = 0 \qquad (2.8.1, a)$$

$$k_A = LHSV \ln[\frac{C_o}{C_P}] \qquad for\ n = 1 \qquad (2.8.1, b)$$

$$k_A = LHSV(\frac{1}{n-1})(\frac{1}{C_P^{n-1}} - \frac{1}{Co^{n-1}}) \qquad for\ n \neq 0, 1 \qquad (2.8.1, c)$$

Where, k_A = apparent rate constant; LHSV= liquid hourly space velocity; C_o = nitrogen and sulfur in heavy gas oil, C_P = nitrogen and sulfur in hydrotreated product, n = reaction order.The activation energy can be expressed using Arrhenius equation as shown in equation 2.8.2

$$k_A = k_0 e^{(-E/RT)} \qquad (2.8.2)$$

Where k_0 = Arrhenius constant; E = activation energy (kJ/mol); R= gas constant (kJ/mol); T = temperature (K).

Values of reaction order and activation energy depend on type of feedstock, catalyst, operating condition, and experimental set up. For HDS of gas oil feed, order of reactions is reported between 1- 2.5 (Ferdous et al., 2006b). For HDN of gas oil, order of reactions is reported between 1-2 (Bej et al., 2001a). For HDS and HDN reactions the

power law model is used by researchers extensively (Ferdous et al., 2006b). However, power rate laws are stated as simply an explanation of experimental data and provide insufficient knowledge about the underlying process (Chorkendorff and Niemantsverdriet , 2003).

Basic kinetic information, such as reaction order and activation energy, derived from power law model for the hydrodesulfurization and hydrodenitrogenation of real feed is summarized in Table 2.16.

Table 2.16: Basic kinetic information derived from Power law for the hydrotreating of real feed.

References	Feed	Catalyst	Boiling Range,°C	Order of Reaction		Activation Energy kJ/mol	
				HDS	HDN	HDS	HDN
(Ferdous et al., 2006b)	Heavy Gas Oil	NiMo/γ-Al_2O_3	185-576	1.5	1	87	74
(Bej et al., 2001b)	Heavy Gas Oil	NiMo/γ-Al_2O_3	210-655	2	1.5	28	80
(Yui and Dodge, 2006)	Heavy Gas Oil	NiMo/γ-Al_2O_3	242-566	1.5	1	94	79
(Diaz-Real et al., 1993)	Heavy Gas Oil	NiMo/ zeolite-alumina-silica	345-524	PS 1st	PS 1st	176	208
(Yui and Sanford, 1989)	Heavy Gas Oil	NiMo/γ-Al_2O_3	196-515	1.5	1	138	92
(Mann et al., 1988)	Heavy Gas Oil	NiMo/zeolite-alumina-silica	345-524	1.5	2	87	105
(Botchwey et al., 2004)	Heavy Gas Oil	NiMo/γ-Al_2O_3	210-600	PS 1st	PS 1st	122	96
(Marin et al., 2002)	LCO+SRGO	NiMo/faujasite modified γ-Al_2O_3	209-369	PS 1.5	PS 1st	77.8	51.4
(Ancheyta et al., 2002a)	Middle distillate blend	NiMo/γ-Al_2O_3	156-344	1.5-2.0	-	58-175	-
(Mapiour et al., 2010a)	HGO	NiMo/γ-Al_2O_3	258-592	2.0	1.5	101	79

Where, PS = Pseudo

2.8.4 Langmuir-Hinshelwood Model

Langmuir-Hinshelwood Model is based on following assumptions (Satterfield, 1991):

1. The adsorbed species are adsorbed onto definite points of the catalyst surface.
2. Each active site can accommodate only one adsorbed species.
3. Reaction takes place among the adsorbed species on the catalyst active sites.
4. Desorption of products from the active sites into the bulk solution.

Real HGO feed contains complex mixtures of nitrogen and sulfur. During hydrotreating reaction, heterocyclic molecules and hydrogen molecules are adsorbed on the different types of catalyst sites. Adsorption of different species on the catalyst active sites inhibits the reaction rate (Girgis and Gates, 1991). Nitrogen compounds are considered as strong inhibitors of HDS and other reactions because of their preferential adsorption on catalytic sites (Furimsky and Massoth, 2005). Also, hydrogen sulfide tends to inhibit the adsorption of nitrogen and other sulfur molecules during hydrotreating. The system with strong adsorption characteristics of reactants and products, Langmuir-Hinshelwood model is useful to account for adsorption strengths of reactants, generated hydrogen sulfide, the nature of chemisorptive bond between sulfur compounds and active sites. Following are the rate equation for the hydrodesulfurization and hydrodenitrogenation reactions derived by authors based on Langmuir-Hinshelwood model (Table 2.17):

Table 2.17: Langmuir-Hinshelwood models for HDS and HDN.

References	Feed	Catalyst	HDS or HDN Model
(Van Hasselt et al., 1999)	DBT	Co(Ni)Mo/ Al_2O_3	$r_A = \frac{k_r \cdot C_{DBT}^{\ 2} \cdot C_{H2}}{\left[1 + K\ C_{H2S}\right]}$
(Tsamatsoulis and Papayannakos, 1998)	VGO	Co(Ni)Mo/ Al_2O_3	$r_{HDS} = \frac{k_{HDS} \cdot P_{H2}\ \cdot C_S^{\ 2.3}}{\left[1 + K_{H2S} P_{H2S}\right]}$
(Satterfield and Yang, 1984)	Quinoline	$NiMo/Al_2O_3$	$-r_{ij} = \frac{k_{ij} \cdot K_i \cdot C_i}{\left[K_{AA} C_{AA} + K_{SA} C_{SA} + K_Y C_Y\right]}$
(Rodríguez and Ancheyta, 2004)	VGO	$NiMo/Al_2O_3$	$r_{HDS} = k_{HDS} \frac{(C^{S}_{S})(C^{S}_{H2})^{0.45}}{(1 + K^{S}_{H2} C^{S}_{H2S})^2}$
(Knudsen et al., 1999)	Diesel	Co(Ni)Mo/ Al_2O_3	$\frac{-dC_s}{dt} = \frac{k \cdot C_S^{\ n} \cdot P_{H2}^{\ \infty}}{(1 + K_{H2S} P_{H2S})} + \frac{k \cdot C_S^{\ m} \cdot P_{H2}^{\ \beta}}{(1 + K_F C_F)}$
(Botchwey et al., 2006)	HGO	$NiMo/Al_2O_3$	$-r_i = \frac{k_i K_i K_{H2} P_{H2} C_i}{1 + K_i C_i + K_{H2} P_{H2} + K_{H2S} P_{H2S}}$
(Broderick and Gates, 1981)	DBT	$CoMo/Al_2O_3$	$r = \frac{k \cdot C_{DBT}\ \cdot C_{H2}}{(1 + K_{DBT} \cdot C_{DBT} + K_{H2S} \cdot C_{H2S})^2 \cdot (1 + K_{H2} \cdot C_{H2})}$

Considering inhibition effect of hydrogen sulfide, nitrogen, sulfur compounds, the kinetic expression for HDS and HDN of heavy gas oil can be expressed by following equations:

A) Langmuir-Hinshelwood Model I:

Considering reaction occur on separate active sites:

$$\boxed{-r_{HDS} = \frac{k_{HDS} \cdot K_S \cdot C_S^{\ n}}{\left[1 + K_S \cdot C_S\right]}} \quad (2.8.3) \qquad \boxed{-r_{HDN} = \frac{k_{HDN} \cdot K_N \cdot C_N^{\ m}}{\left[1 + K_N \cdot C_N\right]}} \quad (2.8.4)$$

B) Langmuir-Hinshelwood Model II:

Considering the reaction occur on same active site:

$$-r_{HDS} = \frac{k_{HDS} \cdot K_S \cdot C_S^{\,n}}{\left[1 + K_S \cdot C_S + K_N \cdot C_N\right]} \qquad (2.8.5)$$

$$-r_{HDN} = \frac{k_{HDN} \cdot K_N \cdot C_N^{\,m}}{\left[1 + K_S \cdot C_S + K_N \cdot C_N\right]} \qquad (2.8.6)$$

C) Langmuir-Hinshelwood Model III:

Considering the inhibition due to H_2S:

$$-r_{HDS} = \frac{k_{HDS} \cdot K_S \cdot C_S^{\,n}}{\left[1 + K_S \cdot C_S + K_{H2S} \cdot P_{H2S}\right]} \qquad (2.8.7)$$

$$-r_{HDN} = \frac{k_{HDN} \cdot K_N \cdot C_N^{\,m}}{\left[1 + K_N \cdot C_N + K_{H2S} \cdot P_{H2S}\right]} \qquad (2.8.8)$$

Where, $-r_{HDS/HDN}$ = rate of HDS or HDN reaction; $k_{HDS/HDN}$ = apparent rate constant for HDS and HDN; K_S, K_N, K_{H2S} = adsorption equilibrium constant of species sulfur, nitrogen and H_2S; $C_{S/N}$ = sulfur or nitrogen content.

The Langmuir-Hinshelwood model is a detailed model for representing the kinetic model for HDS and HDN reactions. The use of this model for real industrial feed is very complicated due to presence of different types of sulfur, nitrogen and aromatic compounds. Also, it is difficult to determine too many coefficients resulted from competitive adsorption effects on the active surface of the catalyst by too many compounds.

Basic kinetic information, such as reaction order and activation energy, derived from Langmuir-Hinshelwood model for the hydrodesulfurization and hydrodenitrogenation of real feed is summarized in Table 2.18.

Table 2.18: Kinetic parameters derived from Langmuir-Hinshelwood model for the hydrotreating of real feed.

References	Feed	Catalyst	Boiling Range,°C	Order of Reaction		Activation Energy kJ/mol	
				HDS	HDN	HDS	HDN
(Ferdous et al., 2006b)	Heavy Gas Oil	NiMo/γ-Al_2O_3	185-576	PS	PS	159	110
(Mapiour et al., 2010b)	Heavy Gas Oil	NiMo/γ-Al_2O_3	258-592	PS	PS	99	69
(Tsamatsoulis and Papayannakos, 1998)	Vacuum Gas Oil	Co(Ni)Mo/γ-Al_2O_3	243-514	2.1-2.3	-	140-143	-
(Botchwey et al., 2004)	Heavy Gas Oil	NiMo/γ-Al_2O_3	210-600	PS	PS	114.2	93.5
(Owusu-Boakye et al., 2006)	Light Gas oil	NiMo/γ-Al_2O_3	170-439	PS	-	55	-

Where, PS = Pseudo

2.8.5 Reactor Performance

Small-scale trickle bed microreactors are widely used for the generation of meaningful data which is can be useful for the studying the new catalyst (Bej et al., 2000). In kinetic study, the basic assumptions of the trickle bed microreactor operation are isothermality and plug flow (Mann et al., 1988). However, the dimension of commercial reactor and catalyst bed length are different from that of the microreator which causes some limitation of trickle bed microreactor. Major problem arises during the catalyst performance evaluation in trickle bed microreactors are: poor wetting of catalyst, wall effects and back mixing of liquid. These problems cause the deviations of performance of the laboratory trickle bed reactor from that of an ideal flow reactor (Mann et al., 1988). Considerable efforts have been made by several authors to address this issues and several recommendation have been made to solve this problem. Diluting catalytic bed with nonporous, inert particles have been suggested by several researchers to avoid deviations from ideal plug flow which is observed in micro scale trickle bed reactor during hydrotreating of real feedstock with commercial size catalysts (Bej et al., 2000; Ramírez et al., 2004). The performance of the trickle bed microreactor is suggested to be improved by eliminating wall effect. For the kinetic studies of hydroprocessing reaction several experiments have been reported by the researchers using catalyst pellets diluted with appropriate inert diluents (Bej et al., 2002). It has been reported that hydrodynamic are controlled by the diluents whereas the kinetics are dictated by the catalyst pellet.

Hydrodynamic evaluation for Plug Flow Reactor:

In order to investigate the reactor hydrodynamic, following calculations are essential to evaluate the hydrodynamic parameters. Important parameters for calculating the hydrodynamic parameters are shown in Table 2.19.

Table 2.19: Parameters for calculating the hydrodynamic parameters.

References	Parameters	Correlations	Remarks
(Gierman, 1988)	Plug flow behavior	$Pe_L > 8n[\ln(\frac{1}{1-X})] = Pe_{L\,\min}$	Deviation from plug flow is ensured if this criteria is satisfied
(Mears, 1971)	Back-mixing	$\frac{L}{dp} > 100$	Back-mixing can be neglected if this criteria is satisfied
(Chu and Ng, 1989)	Wall effect	$\frac{D_b}{dp} > 25$	Wall effect can be discard if this criteria is satisfied
(Gierman, 1988)	Wetting	$W = \frac{\eta_L u_L}{\rho_L dp^2 g} > 5 * 10^{-6}$	Wetting effect can be negligible if this criteria is satisfied

2.8.6 Effect of Mass Transfer

Trickle bed microreactors are used experimentally for the hydrotreating of heavy gas oil feed to generate reliable experimental data, which can be used for design commercial reactors, evaluating activity of new catalyst (Bej et al., 2000). Catalyst active sites are dispersed throughout the internal pore of the catalyst. Hence, in order to maximize the reaction rates on porous catalyst, it is imperative to essential to maximize the accessibility of reactants to the active sites of the catalysts (Fogler, 2006). Following typical steps occur during the heterogeneous catalytic reaction:

1. Film mass transfer of the reactant A from bulk fluid to external catalyst surface
2. Diffusion of reactant species A from pore mouth through the porous structure of catalyst to catalytic surface

3. Adsorption of reactant A into catalyst surface
4. Reaction of A to B on catalytic sites on catalyst surface
5. Desorption of product B molecules from surface
6. Diffusion of product species B from interior of pellet through porous structure to pore mouth
7. Film mass transfer of product B from external surface to the bulk fluid.

Step 1, 2, 6, and 7 are diffusional processes and step 3, 4, and 5 are chemical processes. Any of these steps can be slow, relative to others, controls the overall rate of reaction. In Figure 2.31, the details step for the catalytic reaction in a porous catalyst is shown.

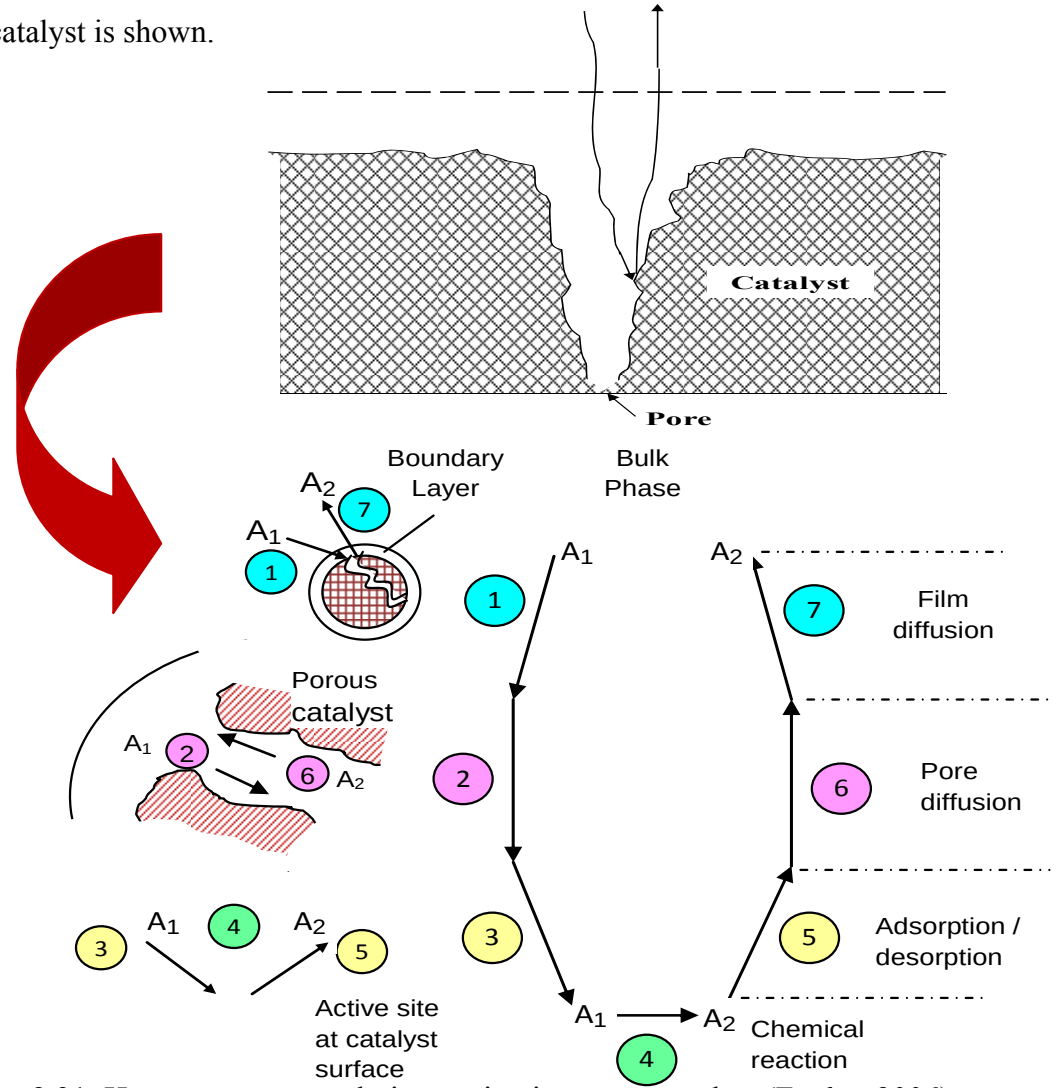

Figure 2.31: Heterogeneous catalytic reaction in porous catalyst (Fogler, 2006).

Depending upon the presence or absence of internal and external mass transfer limitation, the kinetic studies can be performed under three different conditions (Bej et al., 2002):

1) Intrinsic Kinetic model: Intrinsic kinetic study involves detailed mechanistic understanding of all reactions. In order to eliminate both internal and external mass transfer limitation the experiments are conducted using a fine size of catalyst and appropriate condition is considered.

2) Apparent kinetic model: Apparent kinetic study is derived from the overall stoichiometric reaction where the experiments are conducted using commercial size catalyst by eliminating only external mass transfer resistence. This type of kinetic model is generally used by the industrial researcher for the scale-up of the commercial reactors.

3) Extrinsic kinetic model: In this kinetic study, the internal and external mass transfer limitation cannot be eliminated.

CHAPTER 3
EXPERIMENTAL METHOD

This chapter outlines the experimental procedure and reactor set-up for the hydrotreating process. Preparation of SBA-15 support, Zr-SBA-15 support and NiMo/Zr-SBA-15 catalyst are illustrated in section 3.1, 3.2 and 3.3 respectively. Support and catalyst characterization method is described is in section 3.4. In section 3.5, description of catalyst performance test is illustrated.

3.1 SBA-15 Support Preparation

SBA-15 material was synthesized according to the procedure described in literature (Kruk and Cao, 2007). The following chemicals were used in SBA-15 material synthesis: triblock copolymer P_{123} ($EO_{20}PO_{70}EO_{20}$) as structure directing agent, tetraethyl orthosilicate (TEOS) as silica source, hexane (C_6H_{14}) as swelling agent, hydrochloric acid (HCl) as acid media, ammonium fluoride (NH_4F) as frame order enhancer, and water (H_2O) as dissolving media. The molar composition of the synthesis mixture was TEOS: P_{123}: C_6H_{14}: NH_4F: HCl: H_2O = 1: 0.0168: 4.02: 0.0295: 4.42: 186. The triblock copolymer P_{123} and NH_4F were dissolved in the diluted HCl aqueous solution by magnetic stirring at room temperature. TEOS and hexane were added into the solution sequentially, and the mixture was stirred at 15 °C for 24 hrs. Subsequently, the mixture was transferred into a Teflon autoclave bottle and was aged at 130 °C for 48 hrs. The product was filtered, washed by demineralized water and air-dried at room temperature. Finally, calcination of the material was carried out at 550 °C for 5 hrs. Schematic for SBA-15 support preparation in laboratory is shown in Figure 3.1.

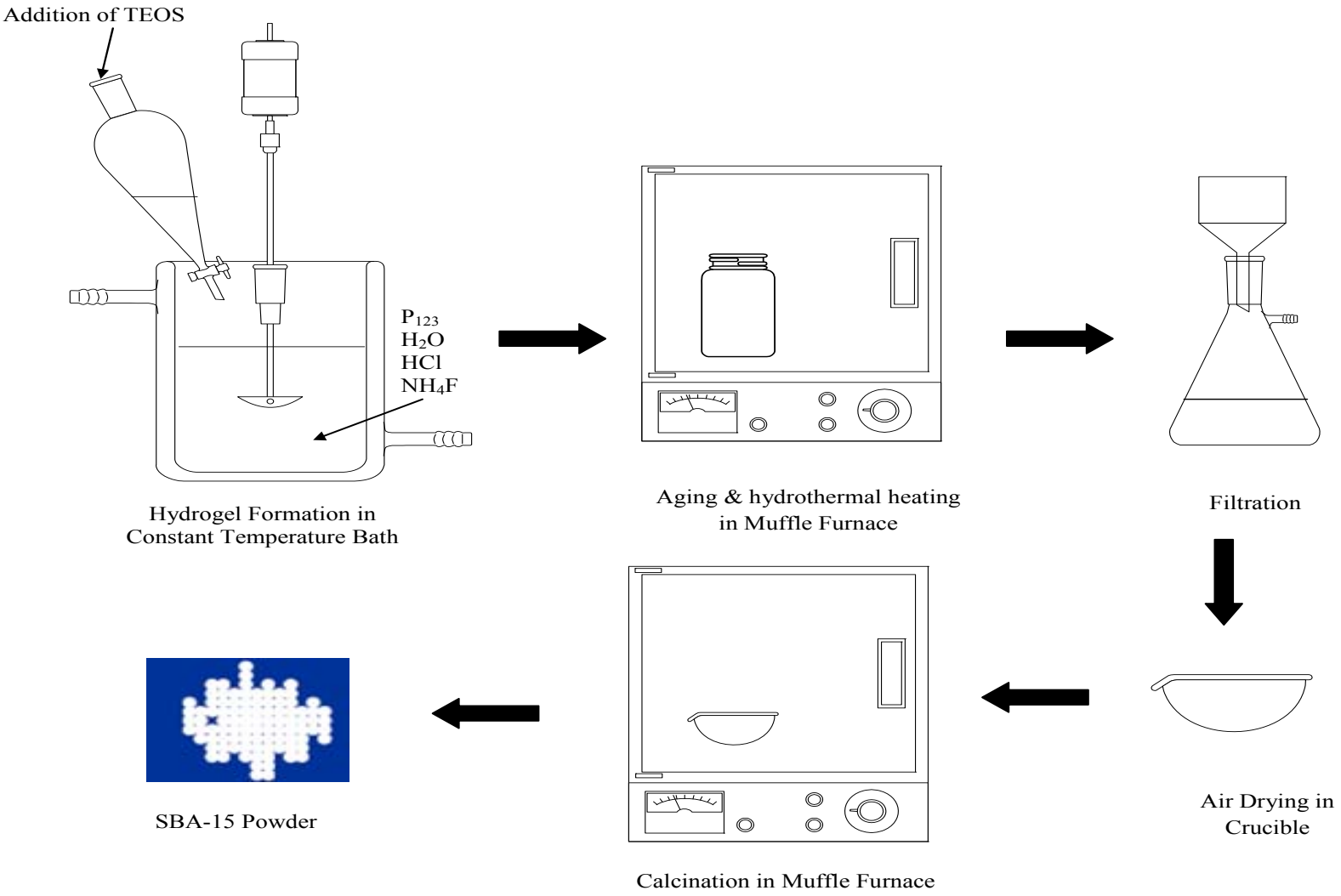

Figure 3.1: Schematic for SBA-15 support preparation in laboratory.

3.2 Zr-SBA-15 Support Preparation

3.2.1 Direct Synthesis Method

Zr-SBA-15 supports were prepared by both direct synthesis and post synthesis methods. In the direct synthesis method, Zr incorporation into the SBA-15 framework was accomplished as per the procedure provided by literature (Chen et al., 2004), using block copolymer template P_{123} ($EO_{20}PO_{70}EO_{20}$) as pore directing agent, tetraethyl orthosilicate (TEOS) as silica precursor, and zirconium oxychloride ($ZrOCl_2.8H_2O$) as zirconia precursor (Chen et al., 2004). In the synthesis condition atomic ratio of the following chemicals was used- P_{123}: Si: Zr: H_2O =0.017: 1.0: (0.05 and 0.025): 220. The mixture was stirred at 35 °C for 24 hrs. Then, the mixture was transferred into a Teflon autoclave bottle and was kept for aging at 130 °C for 48 hrs. The product was filtered and washed with demineralized water and dried at room temperature. Finally, the material was calcined at 550 °C for 5 hrs.

3.2.2 Post Synthesis Method

Zirconia modified support was prepared by the post synthesis (chemical grafting) method as described in previous literature (Gutiérrez et al., 2006a). Zirconium (IV) propoxide [$Zr(n\text{-}PrO)_4$] (70 wt% solution in 1-propanol) was used as the zirconia source and dry ethanol (EtOH 99.999 %) was used as the solvent. Calcined SBA-15 was slurried in the dry ethanol for 8 hours at room temperature. The material was filtered and washed with dry ethanol. The solid was then dried at room temperature for overnight. Finally, the material was calcined at 550 °C for 5 hrs. Schematic for Zr-SBA-15 support preparation by post synthesis method is presented in Figure 3.2.

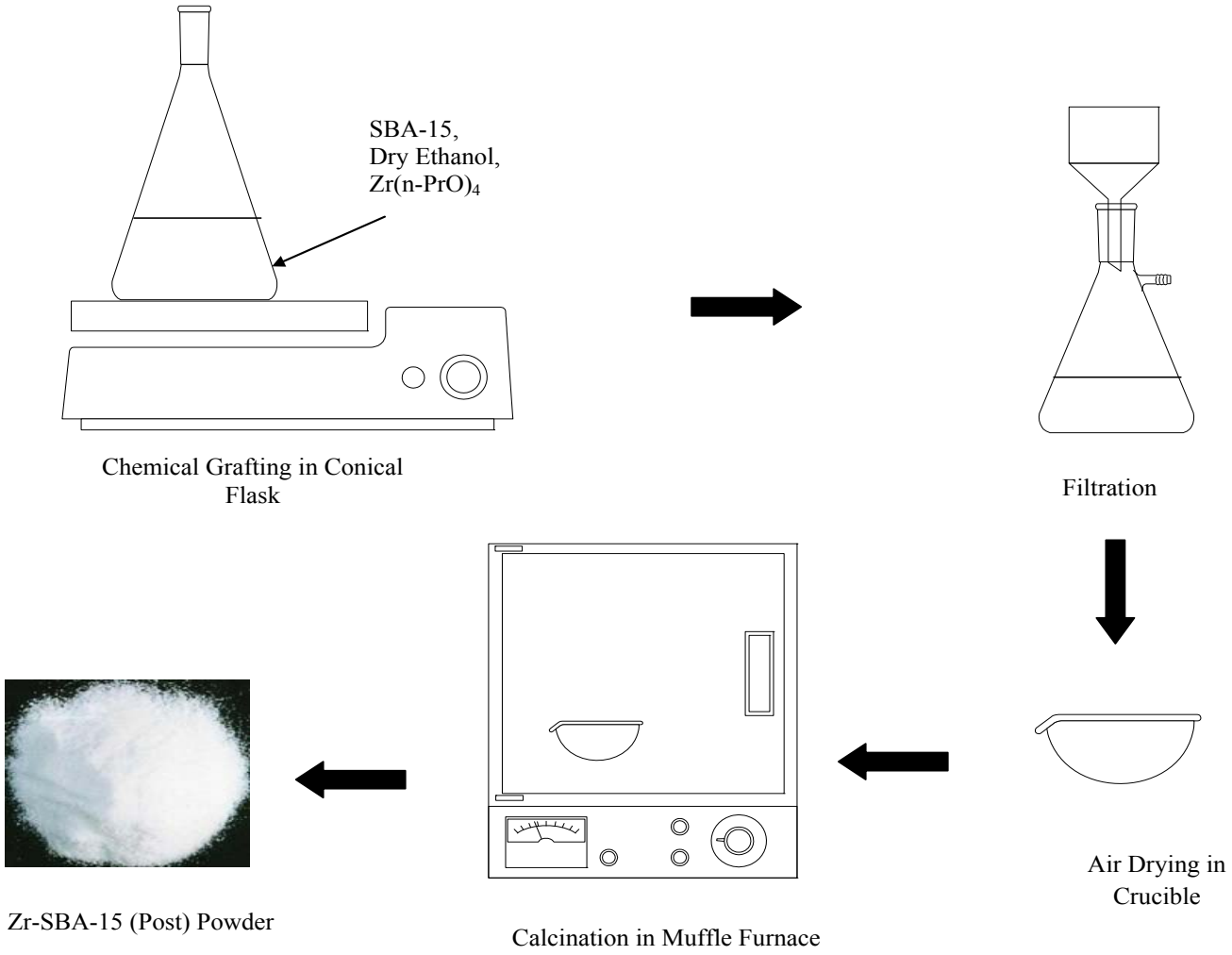

Figure 3.2: Schematic for Zr-SBA-15 support preparation by post synthesis method in laboratory.

3.3 NiMo/SBA-15 and NiMo/Zr-SBA-15 Catalyst Preparation

NiMo catalysts supported on SBA-15 and Zr-SBA-15 were prepared by standard incipient wetness impregnation (IWI) technique. Ammonium heptamolybdate, $(NH_4)_6Mo_7O_{24}.4H_2O$ (Aldrich) was used as the molybdenum source and nickel nitrate, $Ni(NO_3)_2.6H_2O$ (Aldrich) was used as the nickel source. Molybdenum and nickel were impregnated into the calcined SBA-15 and Zr-SBA-15 successively. After each impregnation, the catalysts were dried at 100 °C for 24 hrs and calcined at 500 °C for 4 hrs. The naming of the synthesized supports and catalysts are presented in Table 3.1.

Table 3.1: Naming of the supports and catalysts prepared for the project.

Support	Synthesis Method	Target ZrO_2 (wt %)	Target Si/Zr Ratio	Target Mo	Target Ni
		Phase - I			
SBA-15	-	-	-	-	-
Zr-SBA-15 (Post 16)	Post	16.0	-		
Zr-SBA-15 (Post 23)	Post	23.0	-		
Zr-SBA-15 (Direct 40)	Direct	-	40.0		
Zr-SBA-15 (Direct 20)	Direct	-	20.0		
NiMo/SBA-15	IWI	-	-	12.0	2.4
NiMo/Zr-SBA-15 (Post 16)	IWI	16.0	-	12.0	2.4
NiMo/Zr-SBA-15 (Post 23)	IWI	23.0	-	12.0	2.4
NiMo/Zr-SBA-15 (Direct 40)	IWI	-	40.0	12.0	2.4
NiMo/Zr-SBA-15 (Direct 20)	IWI	-	20.0	12.0	2.4
		Phase - II			
Zr-SBA-15 (Post 23)	Post	23.0	-	-	-
NiMo/Zr-SBA-15 (Mo 12)	IWI	23.0	-	12.0	2.4
NiMo/Zr-SBA-15 (Mo 17)	IWI	23.0	-	17.0	3.4
NiMo/Zr-SBA-15 (Mo 22)	IWI	23.0	-	22.0	4.4
NiMo/Zr-SBA-15 (Optimum)	IWI	23.0	-	17.0	3.4

3.4 Support and Catalyst Characterization Technique

The support and catalyst were characterized by following characterization method as described below:

3.4.1 Small Angle X-ray Scattering (SAXS)

Structural analysis of mesoporous support and catalysts were evaluated by SAXS analysis. A small amount of sample was placed in between two sheets of Mylar film supported by a flat, metal holder with a hole through it (for transmittance). Data were obtained using a still data collection with an exposure time of 300 seconds with a Bruker Smart6000 CCD detector on a 3-circle D8 goniometer. The source was a Rigaku RU200 Cu rotating anode generator fitted with parallel focusing cross-coupled mirrors and a 0.5 mm pinhole collimator.

3.4.2 N_2 Adsorption/Desorption

Brunauer-Emmett-Teller (BET) surface area, pore volume, and pore size measurements of support and catalysts were performed using Micrometrics adsorption equipment (Model ASAP 2000) using liquid N_2 (99.995% pure, obtained from Praxair, Canada). About 0.20 g of sample was used for each analysis. The samples were degassed at 200°C for 2 hrs in a vacuum of 550 Torr to remove moisture from the support and catalyst surface before analysis. The N_2 adsorption and desorption isotherms used in the evaluation of BET surface area (S_{BET}) were obtained at the liquid nitrogen temperature (77 K). The pore volume (V_P) and pore sizes (D_P) were determined using the BJH algorithm (developed by Barrett–Joyner–Halenda, using the Kelvin equation for calculation of pore volume and pore sizes) for adsorption and desorption of nitrogen.

3.4.3 Elemental Analysis

The amount of Si and Zr in the support was determined by SEM-EDX analysis. The EDX spectra were collected using a JEOL 6400 SEM. Quantitative estimation of Zr, Mo, and Ni in the catalysts was performed using inductively coupled plasma - mass spectrometer (ICP-MS). A catalyst sample (0.1 g) was dissolved in concentrated hydrofluoric acid (48-51%) at a temperature of 100-150°C for three days. After cooling, samples were further dissolved in concentrated HNO_3 to ensure the complete dissolution of the metals. The final solution was prepared using 0.2 N HNO_3 and analyzed with a mass spectrometer.

3.4.4 Transmission Electron Microscopy (TEM)

The morphology and structure of support and catalyst were analyzed by TEM. The TEM images were recorded using a 200 keV JEOL 2011 STEM. The sample was sonicated in ethanol for 10 minutes before the analysis.

3.4.5 Scanning Electron Microscopy (SEM)

The morphology of mesoporous supports were examined by the scanning electron microscopy (SEM) instrument. The SEM image of support sample was retrieved in a JOEL 840A SEM instrument.

3.4.6 Fourier Transform Infrared Spectroscopy (FTIR)

The framework vibration of calcined SBA-15 and Zr-SBA-15 materials was examined by FTIR spectroscopy. KBr pellet technique was employed to obtain infrared spectra of the samples at room temperature. The spectra were retrieved in the wave number range of 400-2000 cm^{-1} with a resolution of 4 cm^{-1} by an infrared spectrometer type JASCO FTIR 4100.

3.4.7 Pyridine Adsorbed Fourier Transform Infrared Spectroscopy (Py-IR)

The strength and type of acid site on calcined SBA-15 and Zr-SBA-15 were analyzed by pyridine adsorbed FTIR spectroscopy. 10 mg of sample was placed in IR cell and heated up to 200 °C with a heating rate of 3 °C /min while maintaining the helium flow of 50 ml/min. The sample was cooled to 35 °C and the background spectra of the sample were recorded. The pyridine was introduced along with the helium flow and kept for 30 min. After that, the pyridine flow was stopped, and the adsorbed pyridine from the sample was removed by purging with the helium at 120 °C for 1 hr. Finally, the spectra were retrieved in a Perkin-Elmer (Spectrum –GX) spectrometer for the wavelength of 1400-1600 cm^{-1}.

3.4.8 X-ray Diffraction (XRD)

XRD studies were carried out on the calcined catalyst samples to identify the presence of any crystalline species. Analyses were performed using a Rigaku diffractometer (Rigaku, Tokyo, Japan) with Cu Kα radiation filtered by a graphic monochromator at a setting of 40 kV and 80 mA. The powdered samples were spread on a glass slide with acetone and dried at room temperature. The X-ray diffraction analyses were carried in the scanning angle range of 10 to 80° at a scanning speed of 1°/min.

3.4.9 Raman Spectroscopy

The vibrational characteristic of NiMo/SBA-15 and NiMo/Zr-SBA-15 were analyzed by Raman spectroscopy using a Renishaw Micro-Raman System 2000 spectrometer at the argon laser wavelength of 785 nm.

3.4.10 UV vis Diffuse Reflectance Spetroscopy

The UV-vis-DRS electronic spectra of the catalyst samples were recorded in the wavelength of 270-2500 nm using Cary spectrophotometer equipped with diffuse reflectance attachment. $BaSO_4$ was used as reference.

3.5 Hydrotreating Experimental Set-up and Activity Test

3.5.1 Hydrotreating Reactor Set-up

The schematic of the experimental set-up for the hydrotreating reaction is shown in Figure 3.3. The system consists of a liquid and gas feeding section, a reaction section and a high pressure gas-liquid separation section. The feed section comprises of heavy gas oil (HGO) feed tank, an Eldex syringe feed pump and hydrogen gas source. The reaction section consist of a 304 stainless steel, tubular, micro scale trickle bed reactor (length 240 mm and diameter 10 mm) filled with catalyst (diluted with silicon carbide particles) and a heater with a temperature controller (Eurotherm Controls, model No. 2216e) for controlling the temperature of the catalyst bed. Liquid product and gas phase separation section includes water scrubber, high pressure (HP) separator and H_2S Scrubber. At the downstream of the separation section, hydrotreated liquid product collection vessel is provided. A H_2S scrubber is provided to collect the gaseous product. The reactor section is pressurized by helium gas and the pressure is maintained by adjusting a back-pressure regulator.

3.5.2 Preparation for Hydrotreating Reaction

Reactor loading, reactor pressurizing and catalyst sulfidation were performed prior to the hydrotreating reaction run. After cleaning the reactor thoroughly, the bottom of the

reactor was covered with Swagelok filter and a gasket. Thereafter, catalyst was loaded with the 5 ml catalyst (average size of 1.7 mm), silicon carbide (16, 46 and 60 mesh) and

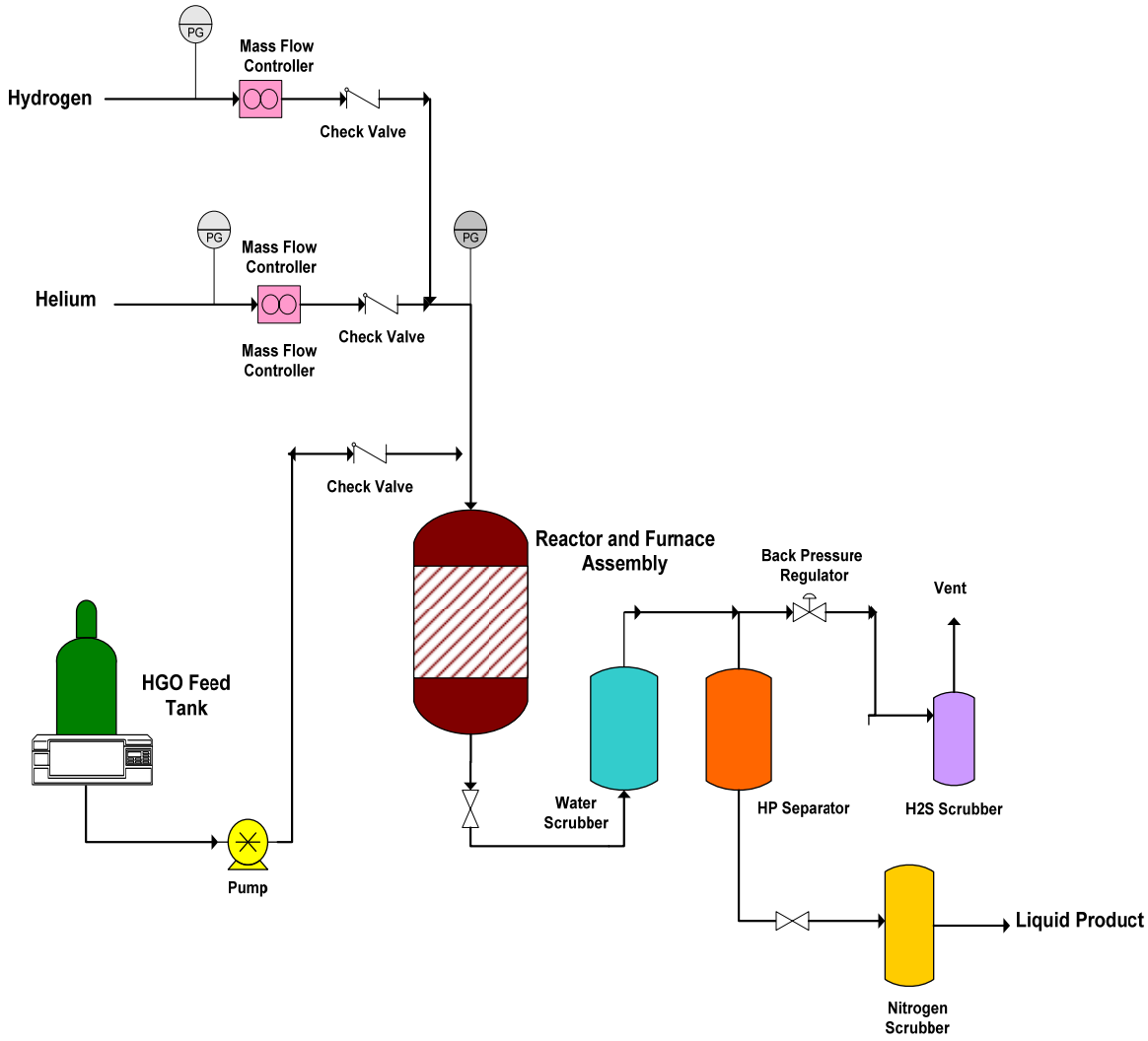

Figure 3.3: Schematic of the experimental set-up for hydrotreating reaction.

glass beads (33 mm diameter) in three sections. Details of reactor loading is shown in Figure 3.4. After the reactor loading the reactor top part was closed by Swagelok gasket.

After reactor loading, the reactor was placed in the reactor system and water scrubber was filled with 50 ml of DM water. Reactor pressure test was performed using helium gas prior to the pressurizing of reator. Reactor was kept pressurized with helium

pressure of 8.9 MPa. After that catalyst sulfidation was carried out using 2.9 vol% butanethiol at 100 °C.

The initial rate of sulfidation was kept at 2.5 ml/min for 2 hours and then the flow was set to 5 ml/hr (LHSV 1 hr^{-1}). Hydrogen flow was introduced at 600 Nm^3/m^3 and helium flow was stopped. The temperature of reactor was raised to 193 °C for 24 hours. After that the temperature was increased to 343 °C and maintained for 24 hours. After sulfidation, the catalyst was precoked (catalyst activity stabilization) by passing heavy gas oil at 5ml/hr rate. Precoking was done at 370 °C, 8.9 MPa, 1 hr^{-1} LHSV, 600 Nm^3/m^3 gas/oil ratio for 5 days.

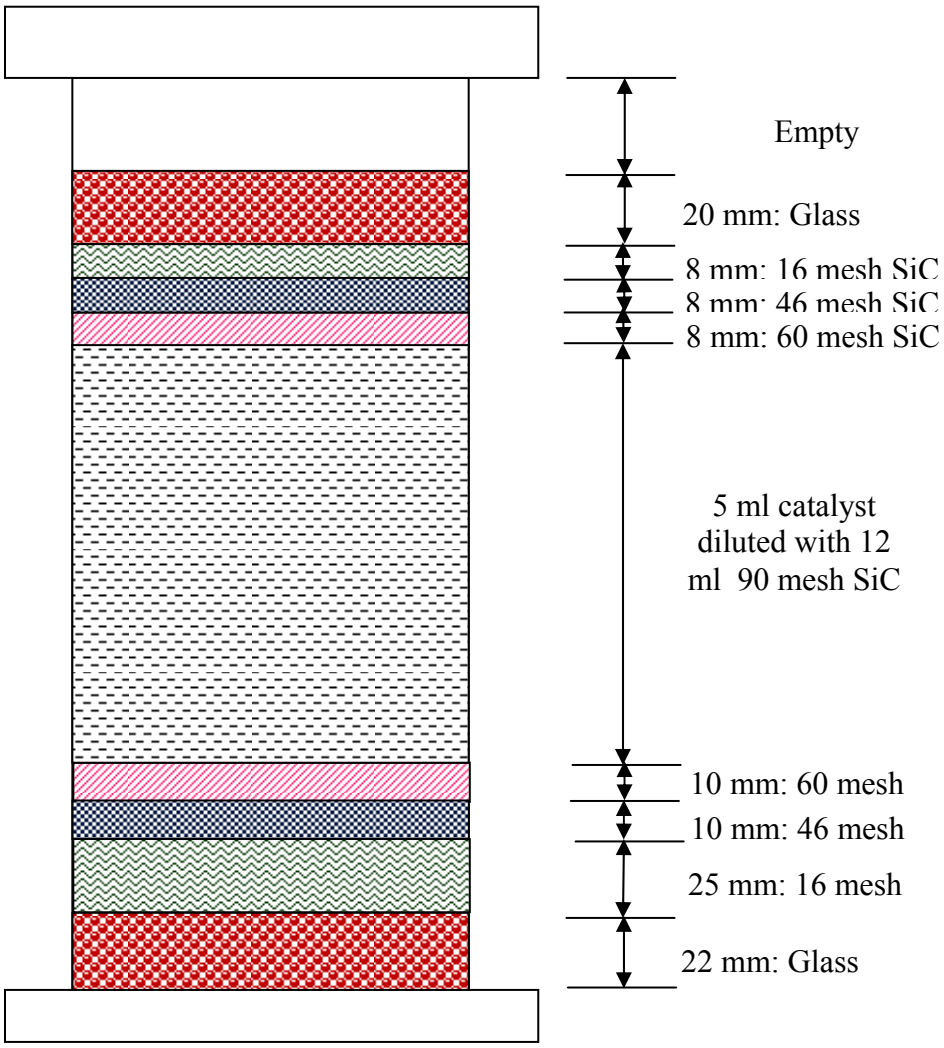

Figure 3.4: Catalyst bed for trickle bed reactor.

3.5.3 Catalyst Performance Test

The performance of all synthesized catalysts for hydrodesulfurization (HDS) and hydrodenitrogenation (HDN) reactions were evaluated in a down-flow concurrent trickle bed microreactor using heavy gas oil (HGO) derived from Athabasca bitumen provided by Syncrude Canada as feedstock. The characteristic of heavy gas oil is presented in Table 3.2. The hydrotreating reactor system consists of a liquid and gas feeding section, a reaction section and a high pressure gas-liquid separation section. The HGO was pumped by metering pump and mixed with the hydrogen gas before entering the reactor.

Table 3.2: Characteristics of heavy gas oil derived from Athabasca bitumen.

HGO Characteristics	
Sulfur (wt%)	3.4424
Nitrogen (wt%)	0.3081
Density (g/ml)	0.98
Simulated Distillation	
IBP (°C)	282
FBP (°C)	648
Boiling Range (°C)	wt%
IBP-310	2
310-350	6
351-400	17.2
401-450	27.2
451-500	26.3
501-600	19.2
600-FBP	2.1

Hydrotreating reaction takes place inside the reactor, and the hydrotreated product was sent to the water scrubber for removing ammonia or ammonium sulfide. Liquid and gas were separated in high pressure gas-liquid separator. The gaseous product is sent to the H_2S scrubber to remove H_2S gas and the hydrotreated liquid product was collected

from the HP separator. The HDS and HDN activity study of the catalyst were performed at three temperatures, namely 375, 385 and 395 °C, while keeping pressure 8.9 MPa, LHSV 1 hr^{-1}, and gas/oil ratio 600 Nm^3/m^3. The transition samples (first sample) were collected after 24 hours of changing process condition. The second and third samples were collected in 12 hours of gap and used for the analysis. The residual gases from the product samples were removed by N_2 stripping. The liquid product was tested for sulfur and nitrogen content using an Antek 9000 NS analyzer.

3.6 Hydrotreated Product Analysis

3.6.1 S and N Conversion

The concentrations of sulfur and nitrogen compounds present in feed and products were determined using an Antek 9000 NS analyzer. The sulfur content was measured using the combustion-fluorescence technique of the ASTM D5463 method. The nitrogen content of the liquid product was determined by the combustion-chemiluminescence technique of the ASTM D4629 method. The instrumental error for both N and S analysis was found to be approximately ±2%, based on analyzing standard solutions of known composition.

3.6.2 Boiling Point Distribution

To determine the boiling point distribution of the liquid feeds and products, a simulated distillation ASTM D6352 method was used. The simulated distillation of the heavy gas oil feed and product liquids was performed using a Varian Model CP 3800 Gas Chromatograph coupled with a Varian CP 8400 Auto sampler. The components boiling range were determined using a flame ionization detector (FID). The boiling fractions were determined by comparing them against a calibration curve.

CHAPTER 4
HYDROTREATING OF GAS OIL OVER NiMo/Zr-SBA-15 CATALYSTS

This chapter describes the results of support and catalyst characterizations obtained for phase-I work. Detailed description of various characterizations methods, such as BET, SAXS, FT-IR, SEM, TEM, XRD, UV-DRS, and Raman spectroscopy, performed on the supports and catalysts are elaborated in this chapter. Also, a comparison of the characteristics of Zr-SBA-15 supports prepared by direct synthesis and post synthesis method is provided in this chapter. Furthermore, the implication of characterization results on catalyst performances for HDS and HDN of HGO are described. Also, evaluation of best method of Zr-SBA-15 support preparation is illustrated in this chapter.

4.1 Characterization of Supports

4.1.1 Small-Angle X-ray Scattering (SAXS)

The small-angle X-ray scattering pattern for parent the SBA-15 shows typical three well-resolved peaks (Figure 4.1a) that are indexable as (100), (110), and (200) reflections associated with 2-D hexagonal symmetry (Kruk and Cao, 2007). From Figure 4.1 it is evident that the Zr-SBA-15 (Post) support prepared by the post synthesis method shows a similar SAXS pattern as parent SBA-15, implying that the hexagonal order is preserved after incorporation of ZrO_2 on the SBA-15 surface. However, intensity for Zr-SBA-15 (Post) decreases upon incorporation of ZrO_2 into the SBA-15 surface, indicating the slight modification of long-range order of pores of SBA-15 that occurs with ZrO_2 loading, which also reported in previous article. The SAXS pattern (Figure 4.1b) for Zr-SBA-15 support prepared by the direct synthesis method with a Si/Zr atomic ratio of 20 and 40 also exhibits three well-resolved peaks, which indicates that the 2-D hexagonal structure of SBA-15 is maintained during the synthesis and calcinations of Zr-SBA-15 (Direct).

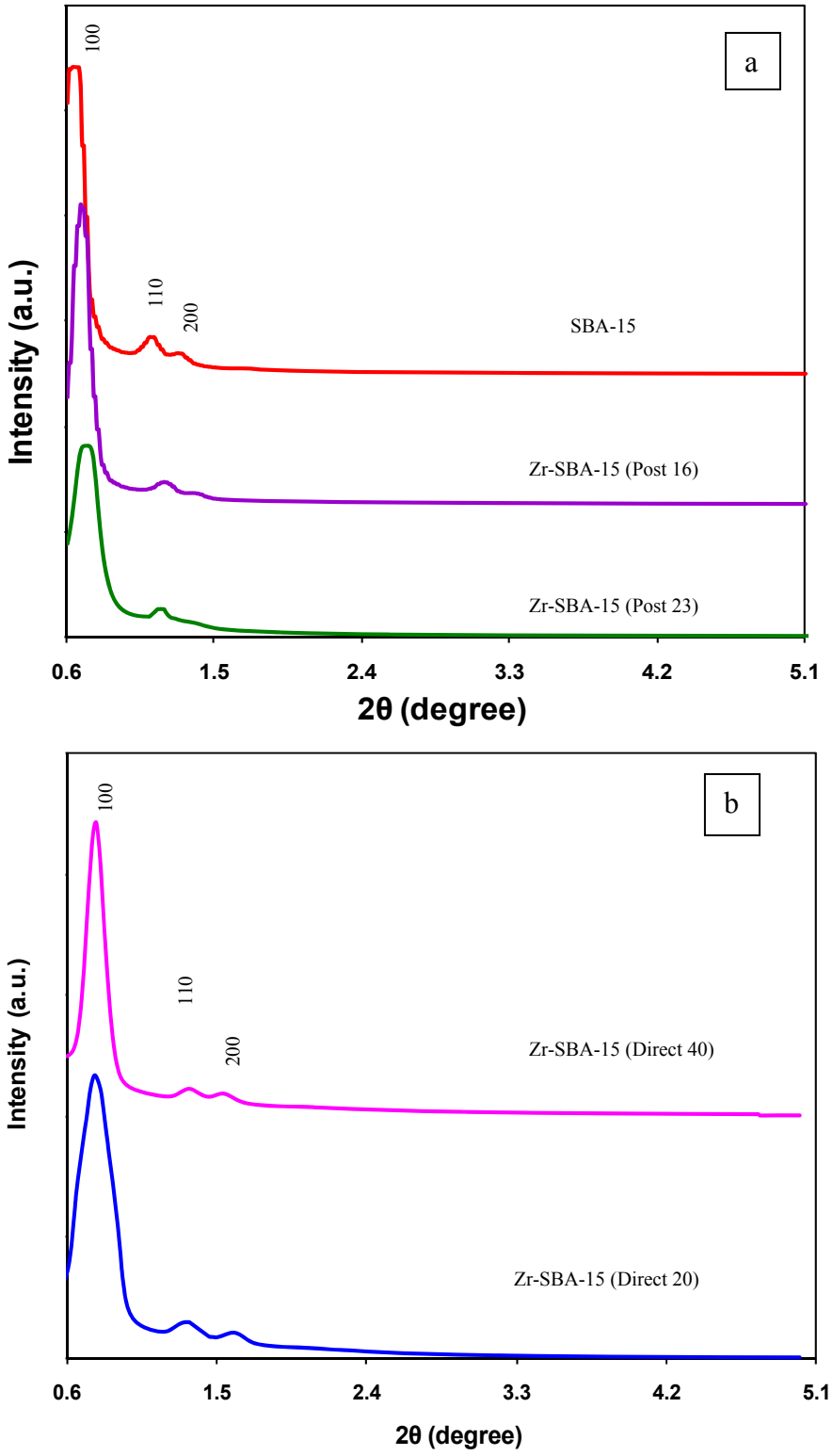

Figure 4.1. Small-angle X-ray scattering (SAXS) pattern of SBA-15 and Zr-SBA-15 (Post) (a); Zr-SBA-15 (Direct) (b) supports.

4.1.2 N_2 Adsorption/Desorption and Chemical Compositions

The textural characteristics and chemical compositions of SBA-15 and Zr-SBA-15 supports are summarized in Table 4.1. Chemical compositions of the support materials are calculated based on ICP-MS and SEM-EDX characterization results. An example of SEM-EDX characterization for the Zr-SBA-15 (Post 23) support is shown in the Figure 4.2. From the result of textural characteristics it is evident that there is a decrease in the surface area and the pore diameter of SBA-15 upon the incorporation of zirconia in the SBA-15 framework by post synthesis method, which is also observed by other researchers (Gutiérrez et al., 2006a). However, no significant surface area and pore volume reduction was observed for the Zr-SBA-15 (Direct) sample prepared by the direct synthesis method. This trend indicates that the Zr species is incorporated in silica framework for the direct synthesis method (Chen et al., 2004). Furthermore, it is observed that the Zr-SBA-15 supports of larger pore diameter can be obtained by the post synthesis method. Figure 4.3 shows the nitrogen adsorption-desorption isotherm for SBA-15, Zr-SBA-15 (Post) and Zr-SBA-15 (Direct) supports. SBA-15, Zr-SBA-15 (Post), and Zr-SBA-15 (Direct) support samples exhibit a type-IV isotherm with a hysteresis loop, which correspond to hexagonal pore system generally reported for mesoporous SBA-15 and Zr-SBA-15 materials (Garg et al., 2008; Gutiérrez et al., 2006a; Kruk and Cao, 2007). It is evident from Figure 4.3a that the height of the hysteresis loop decreases with the increase in ZrO_2 loading on SBA-15 prepared by the post synthesis method, which also reported in previous literature. A similar trend is observed for the Zr-SBA-15 (Direct) support with the increase in Zr loading (Figure 4.3b).

Table 4.1. Textural characteristics and chemical compositions of support materials.

Support	Achieved ZrO_2 (or Zr) Content	Surface Area, S_{BET} (m^2/g)	Pore Volume, V_P (cm^3/g)	Average Pore Dia., D_P (nm)
SBA-15	-	471	1.44	12.2
Zr-SBA-15(Post 16)	ZrO_2 wt% = 16.0	416	1.12	10.8
Zr-SBA-15(Post 23)	ZrO_2 wt% = 23.9	402	1.02	10.1
Zr-SBA-15(Direct 40)	Si/Zr Ratio = 39.7	982	1.36	6.2
Zr-SBA-15(Direct 20)	Si/Zr Ratio = 22.0	790	1.31	6.6

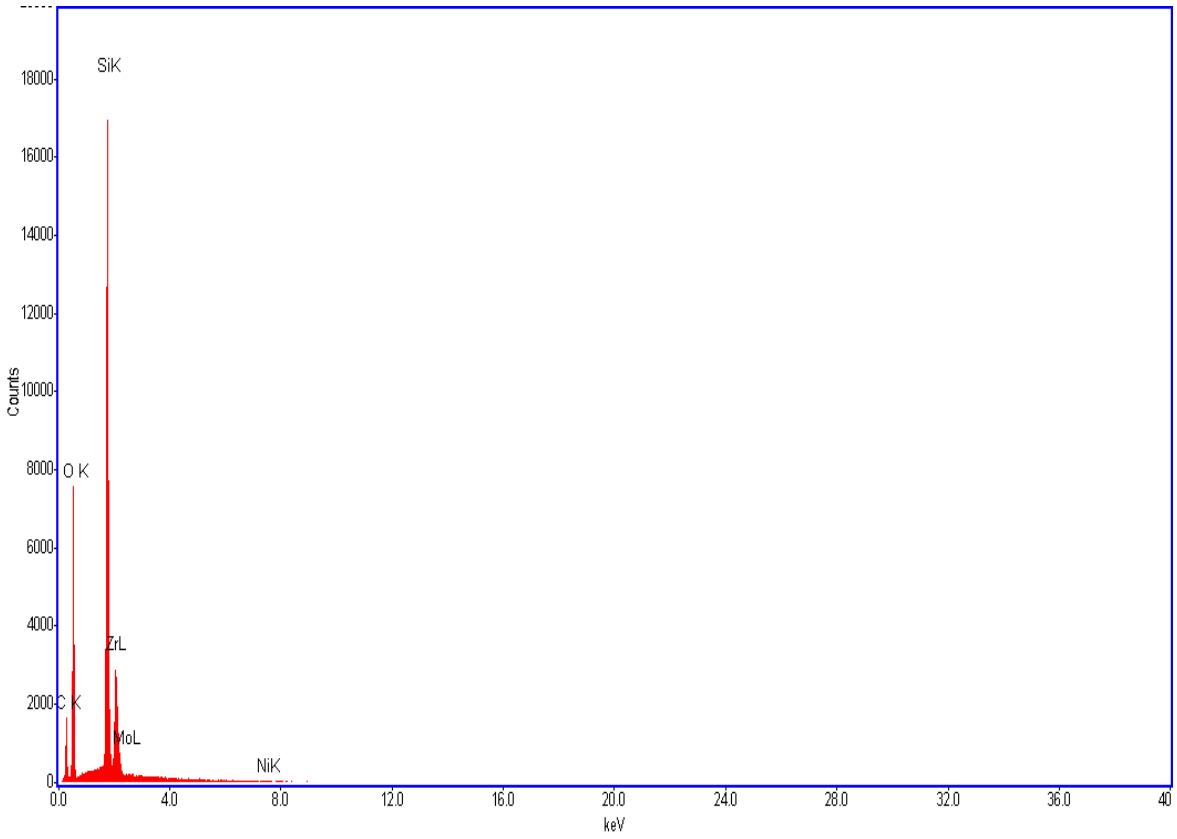

Figure 4.2. EDX pattern of Zr-SBA-15 (Post 23) support.

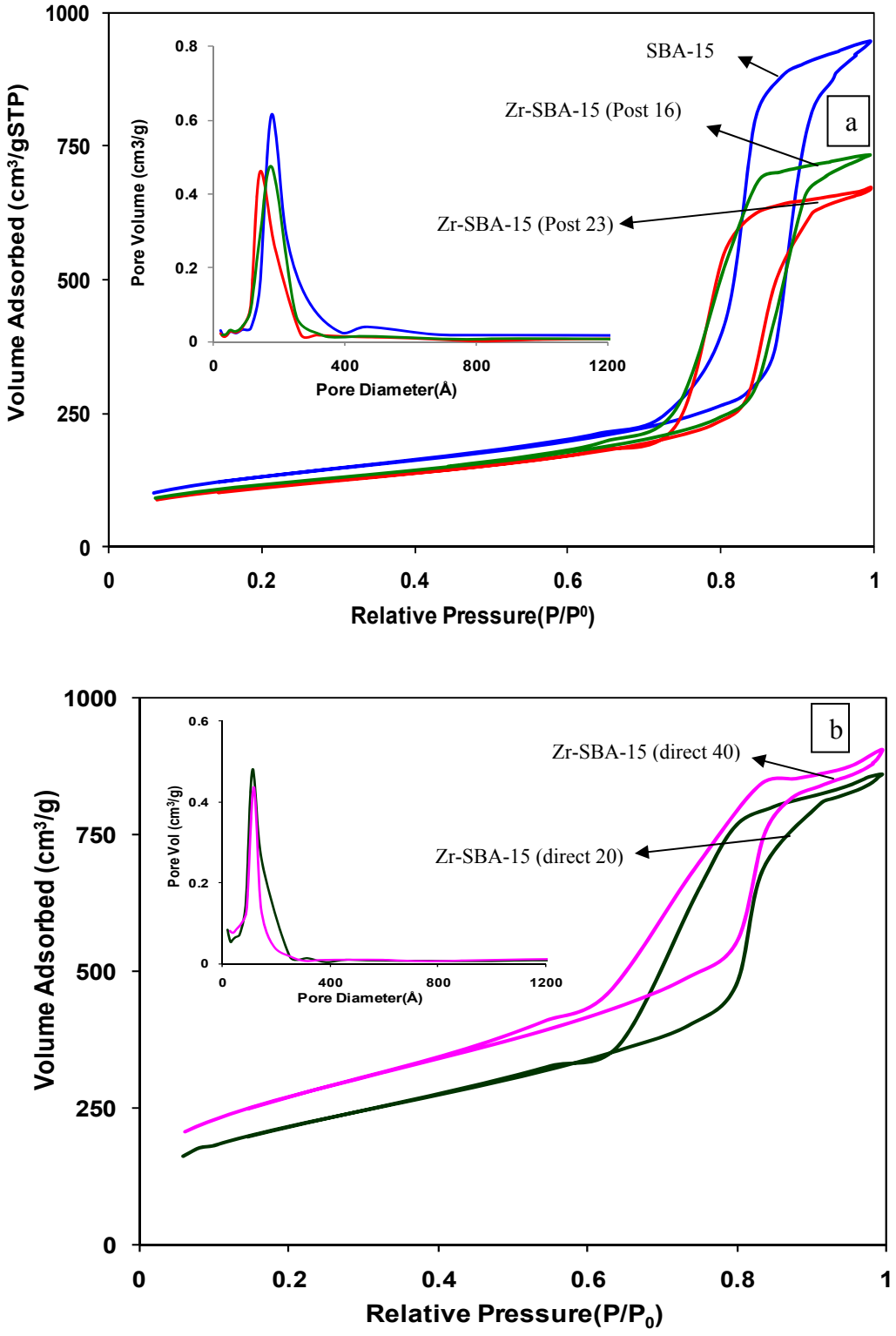

Figure 4.3. Nitrogen adsorption-desorption isotherms of SBA-15 and Zr-SBA-15 (Post) (a); Zr-SBA-15 (Direct) (b) supports.

4.1.3 Transmission Electron Microscopy (TEM)

Further structural features of SBA-15, Zr-SBA-15 (Post), and Zr-SBA-15 (Direct) material are studied by TEM. TEM images of SBA-15 (Figure 4.4a and 4.4 b) confirm that SBA-15 has a highly ordered 2-D hexagonal structure, which is in good agreement with the SAXS analysis. The distance between the two adjacent pore centers is 160 Å and the average pore diameter is about 120 Å. TEM of Zr-SBA-15 (Post 23) containing 23 wt% ZrO_2 is shown in Figure 4.4c and 4.4d. It is observed from the figure that a well-defined hexagonal arrangement of mesopores is intact after ZrO_2 incorporation onto parent SBA-15. Zirconia particles are visible mainly inside the pore structure. TEM images (Figure 4.4e and 4.4f; 4.4g and 4.4h) of Zr-SBA-15 support with a Si/Zr ratio of 20 and 40 prepared by the direct synthesis method also demonstrates the highly well-ordered 2-D hexagonal structure, which is similar to SBA-15.

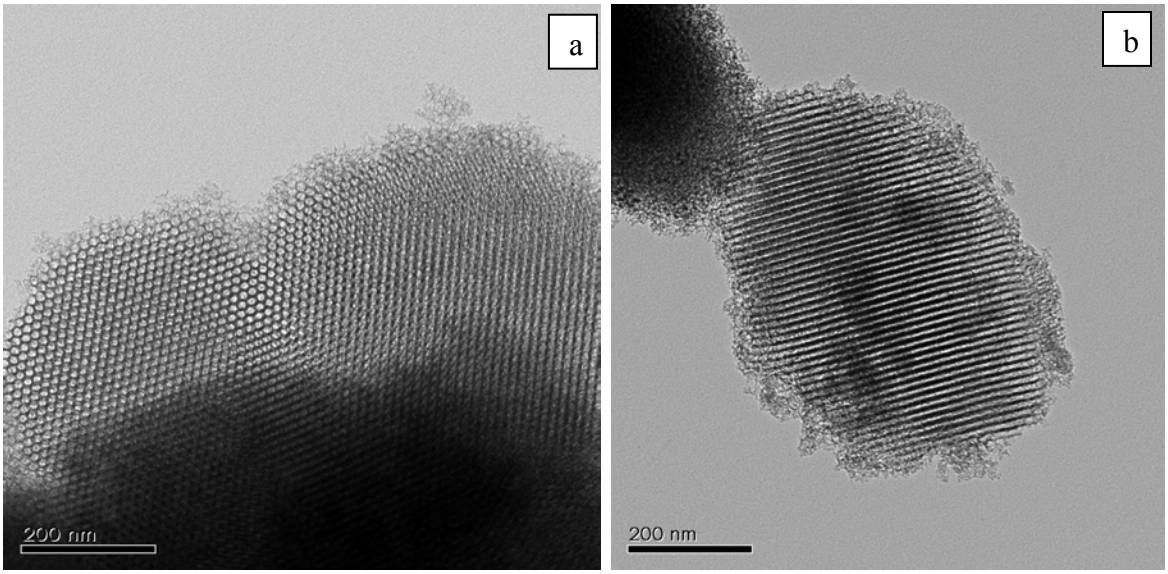

Figure 4.4: Transmission electron microscopy images of SBA-15 front view (a), side view (b); supports (continued in next page).

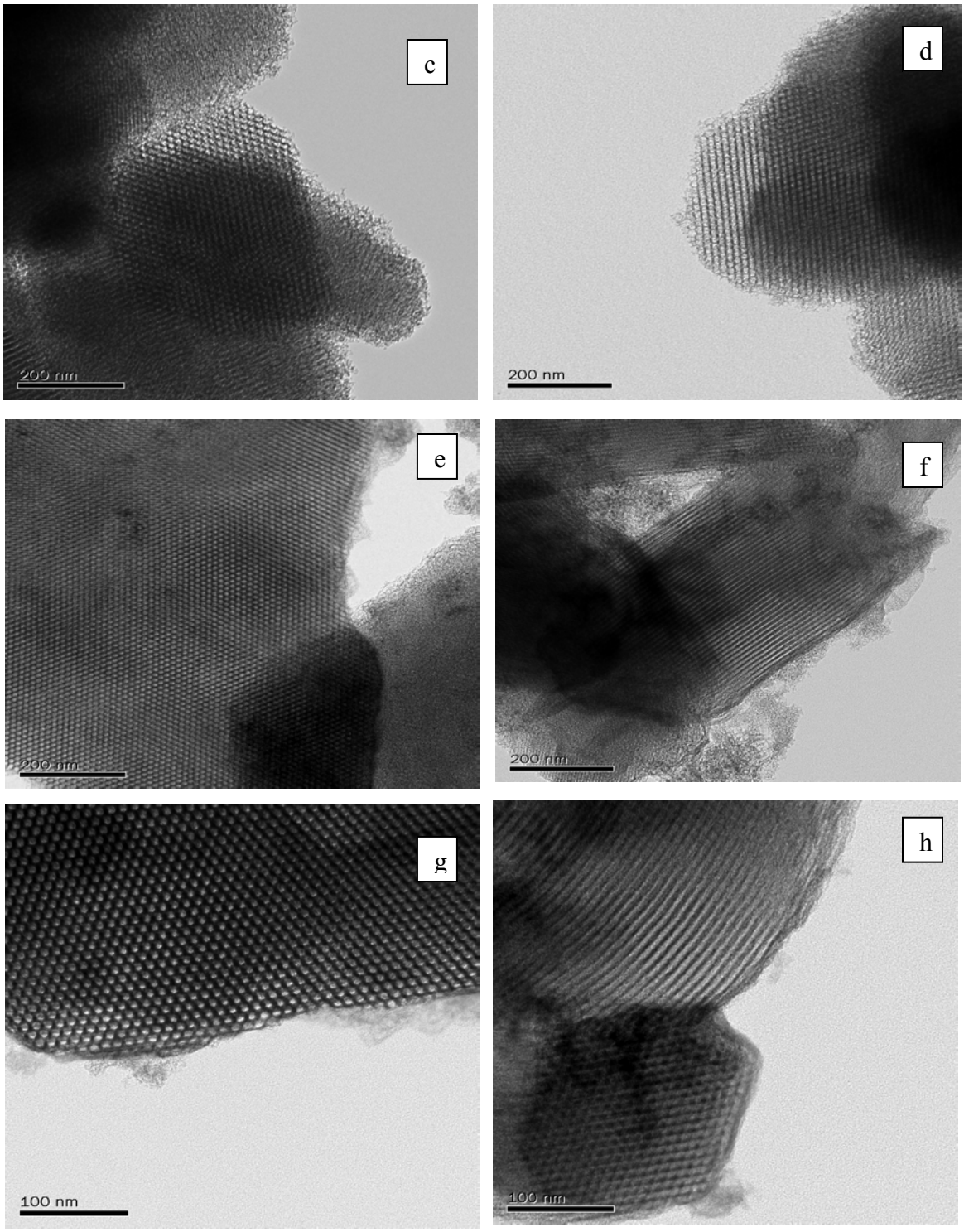

Figure 4.4: Transmission electron microscopy images of Zr-SBA-15 (Post 23) front view (c), side view (d); Zr-SBA-15 (Direct 20) front view (e), side view (f); Zr-SBA-15 (Direct 40) front view (g), side view (h) supports.

4.1.4 Scanning Electron Microscopy (SEM)

The morphology and structure of SBA-15 and Zr-SBA-15 supports are investigated by SEM. SEM micrograph of calcined SBA-15 is shown in Figure 4.5a and 4.5b. The SEM image exhibits fiberlike uniform cylindrical morphology, which is in good agreement with previous articles (Eswaramoorthi et al., 2008; Landau et al., 2005; Liu et al., 2004) . The SEM image of Zr-SBA-15 (Post) prepared by the post synthesis method reveals that the morphology of the sample is preserved after the zirconia impregnation. Zr-SBA-15 support prepared by direct synthesis method also displays the similar fiberlike cylindrical image as observed in parent SBA-15.

4.1.5 Fourier Transform Infrared Spectroscopy (FTIR)

FTIR spectroscopy was utilized to verify the nature of Zr species incorporated into the SBA-15 framework. FTIR spectra of calcined SBA-15, Zr-SBA-15 (Direct), and Zr-SBA-15 (Post) supports are shown in Figure 4.6. All support samples exhibit broad band at 1220-1070 cm^{-1} corresponding to Si-O-Si vibration (Bhaumik et al., 2004). A weaker band observed at 803 cm^{-1} is due to Si-O-Si symmetric stretching, and a strong band identified at 465 cm^{-1} is due to vibration of Si-O-Si (Gómez-Cazalilla et al., 2007). For Zr-SBA-15 (Direct) support the strong band observed at 966 cm^{-1} can be attributed to the Si-O-Zr vibration, which validates the Zr incorporation into SBA-15 framework effectively (Dang et al., 1995; Ferrer et al., 2009). However, in the pure SBA-15, the band at 966 cm^{-1} is absent. For Zr-SBA-15 (Direct) supports, as the Si/Zr ratio decreases, the intensity of the band at 966 cm^{-1} increases (Salas et al., 2009). This can be explained by the fact that with the decrease in the Si/Zr ratio, there is a substitution of silicon ion by zirconium ion in the Zr-SBA-15 framework, which results in an increase in the number of the Zr-O-Si bonds (Salas et al., 2009). Similarly, Zr-SBA-15 (Post) support exhibits the broad band at 1220-1070 cm^{-1}, a moderately strong band at 966 cm^{-1}, a weaker band at 800 cm^{-1} and a strong band at 460 cm^{-1}. The presence of the 966 cm^{-1} band indicates that

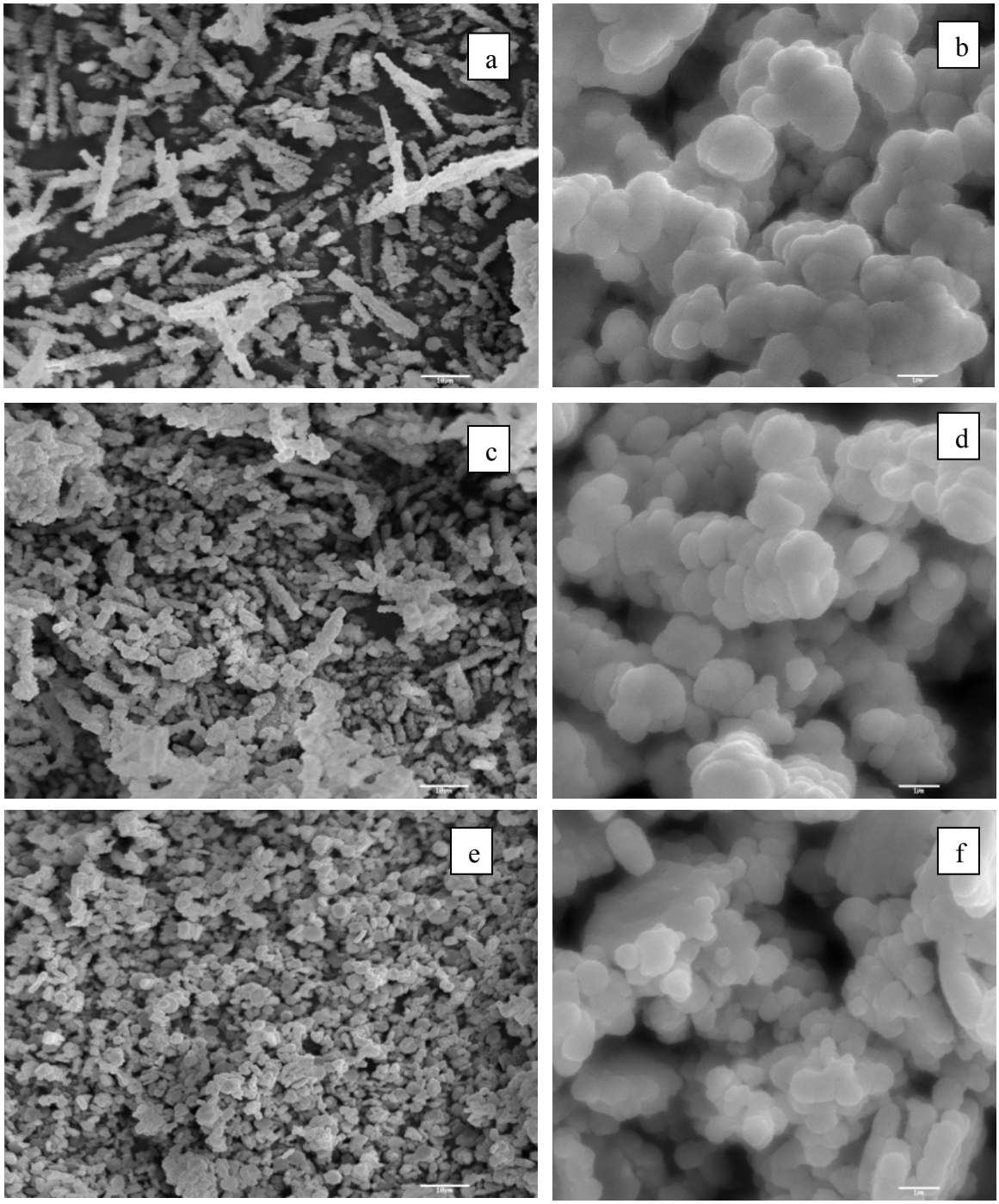

Figure 4.5. Scanning electron microscopy images of SBA-15 of 10 µm (a), 1 µm (b); Zr-SBA-15 (Post 23) of 10 µm (c), 1 µm (d); Zr-SBA-15 (Direct 20) of 10 µm (e), 1 µm (f) supports.

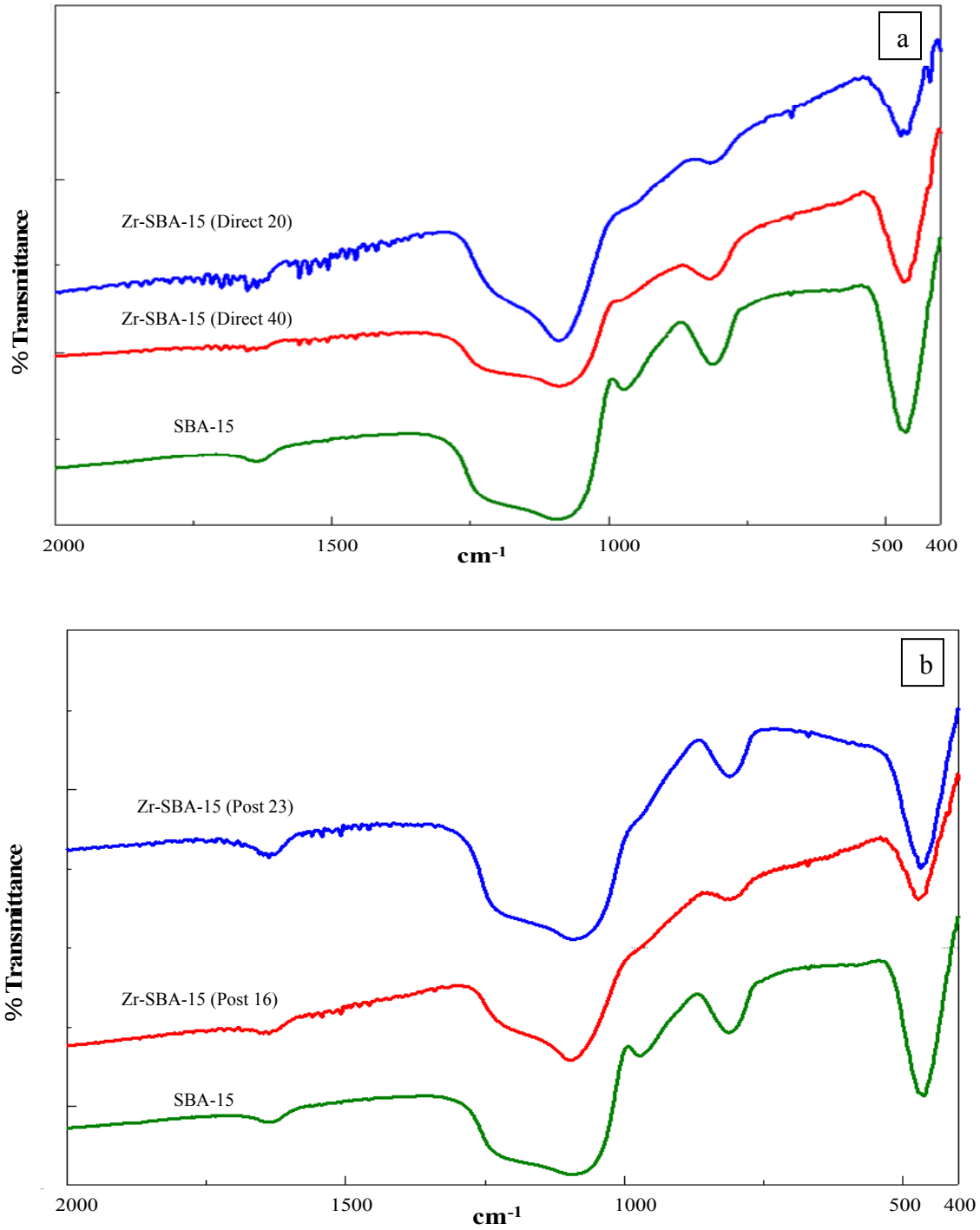

Figure 4.6. FT IR spectra comparison for SBA-15 and Zr-SBA-15 (Direct) (a); SBA-15 and Zr-SBA-15 (Post) (b) supports.

for the Zr-SBA-15 (Post) support there must be a chemical attachment of ZrO_2 to the SBA-15 framework (Dang et al., 1995). There is an increase in intensity of the 966 cm^{-1} band due to the incorporation of higher zirconia by the post synthesis method, indicating the increment of Zr-O-Si linkage due to an increase of ZrO_2 loading on the SBA-15 framework.

4.1.6 Pyridine Adsorbed Fourier Transform Infrared Spectroscopy (Py-IR)

To examine the type of surface acidity of the supports, pyridine adsorption of the support materials was performed. Figure 4.7 shows the FTIR spectra of pyridine adsorption SBA-15 and Zr-SBA-15 (Direct), and Zr-SBA-15 (Post) supports. All support samples show the characteristic bands at 1450 cm^{-1} (strong), 1480 cm^{-1} (strong), 1580 cm^{-1}(weak), and 1609 cm^{-1}(weak), which correspond to the pyridine adsorbed on Lewis acid sites (Chen et al., 2006; Kemdeo et al., 2010; Nava et al., 2007). A band appeared at 1540 cm^{-1}, indicating the creation of the Brønsted acid sites in all Zr-SBA-15 samples. In addition, for all the Zr-SBA-15 samples, bands at 1490 cm^{-1} can be associated with pyridine adsorbed on both Lewis and Brønsted acid sites (Chen et al., 2006). In pure SBA-15 support, the bands corresponding to the Lewis acid sites at 1450 cm^{-1}, 1624 cm^{-1} and 1580 cm^{-1} are observed. However, no band is observed at 1540 cm^{-1} and 1490 cm^{-1}. Hence, it can be concluded that the Brønsted acid sites were generated due to the presence of Zr and ZrO_2 in SBA-15 support during direct synthesis and post synthesis Zr-SBA-15 supports, respectively. For Zr-SBA-15 (Direct) support, the intensity bands for Brønsted acidity increases with increasing Zr content in SBA-15. Similarly, for the Zr-SBA-15 (Post) supports, the intensity of Brønsted acid sites has increased with the increasing of ZrO_2 onto the SBA-15 surface. Hence, the highest Brønsted acidity peak is observed for the Zr-SBA-15 (Post 23) support loaded with 23wt% of zirconia.

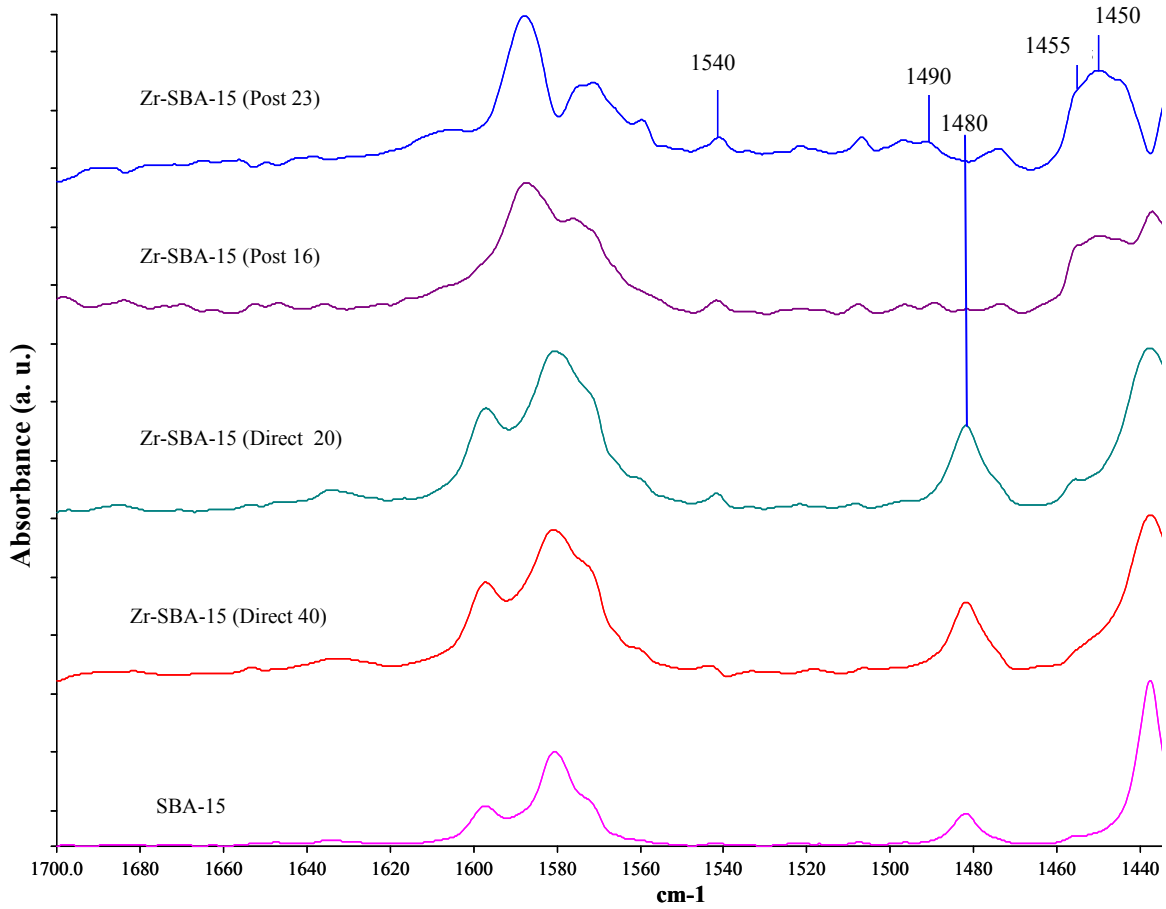

Figure 4.7. FT IR spectra of pyridine adsorbed species on SBA-15, Zr-SBA-15 (Direct) and Zr-SBA-15 (Post) supports.

4.1.7 Powder X-ray Diffraction (XRD)

Powdered XRD analysis was performed to determine the presence of any crystalline phase present in SBA-15 and Zr-SBA-15 support materials. Powder XRD patterns for SBA-15, Zr-SBA-15 (Direct) and Zr-SBA-15 (Post) supports are shown in Figure 4.8. No diffraction was observed in pure SBA-15 material, confirming that, no crystalline phase is present for the pure SBA-15 support material. Similarly, no characterization peak is found for the Zr-SBA-15 (Direct) and Zr-SBA-15 (Post) materials. Absence of any crystalline phase indicates good dispersion of ZrO_2 and Zr species on SBA-15 material.

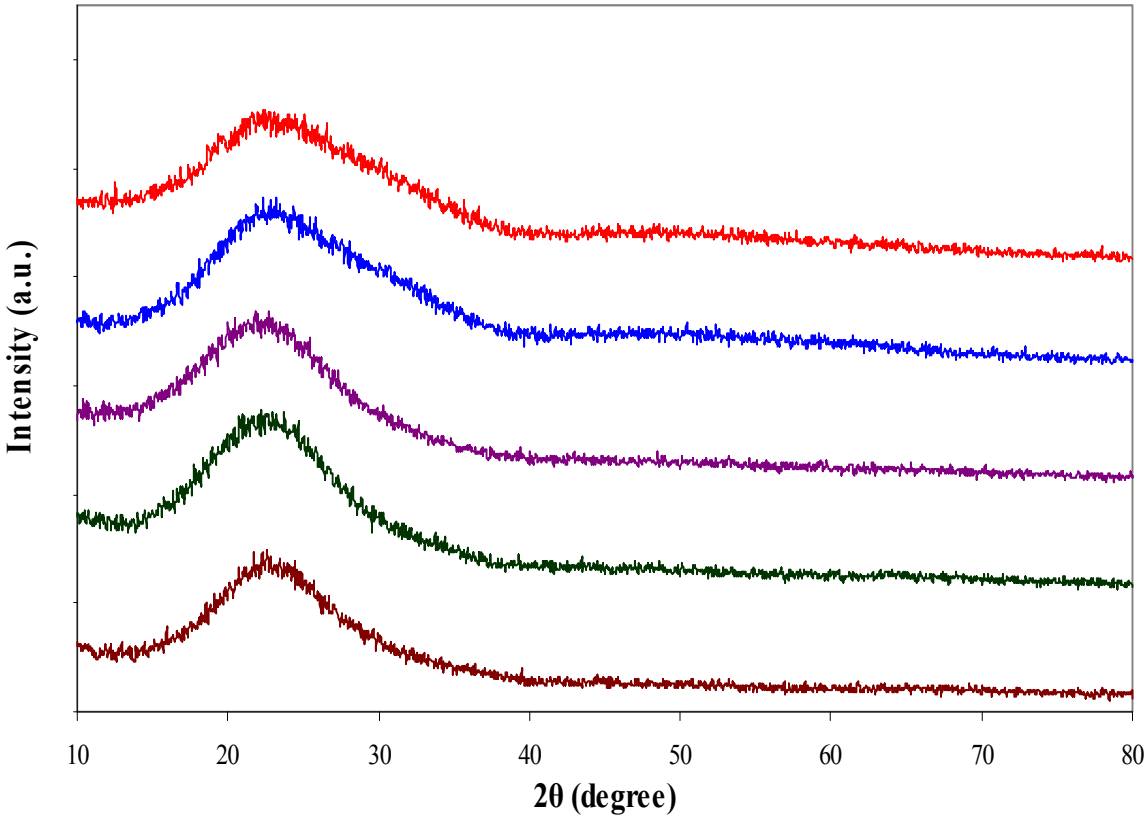

Figure 4.8. Powder XRD pattern of SBA-15; Zr-SBA-15 (Direct 40); Zr-SBA-15 (Direct 20); Zr-SBA-15 (Post 16); Zr-SBA-15 (Post 23) supports.

4.2 Characterization of catalysts

4.2.1 Small-Angle X-ray Scattering (SAXS)

The small-angle X-ray scattering spectra (Figure 4.9) for NiMo catalysts show similar patterns corresponding to that of the support material. These data show that the three characteristic peaks of hexagonal structure (100), (110), and (200) are preserved, which are associated with the well-ordered hexagonal structure. However, a mild reduction of peak intensities is observed in SBA-15, Zr-SBA-15 (Post), and Zr-SBA-15 (Direct) supports due to the addition of metal to the support materials, indicating a mild reduction of hexagonal long-range periodicity of SBA-15 and Zr-SBA-15 support materials upon the metals incorporation.

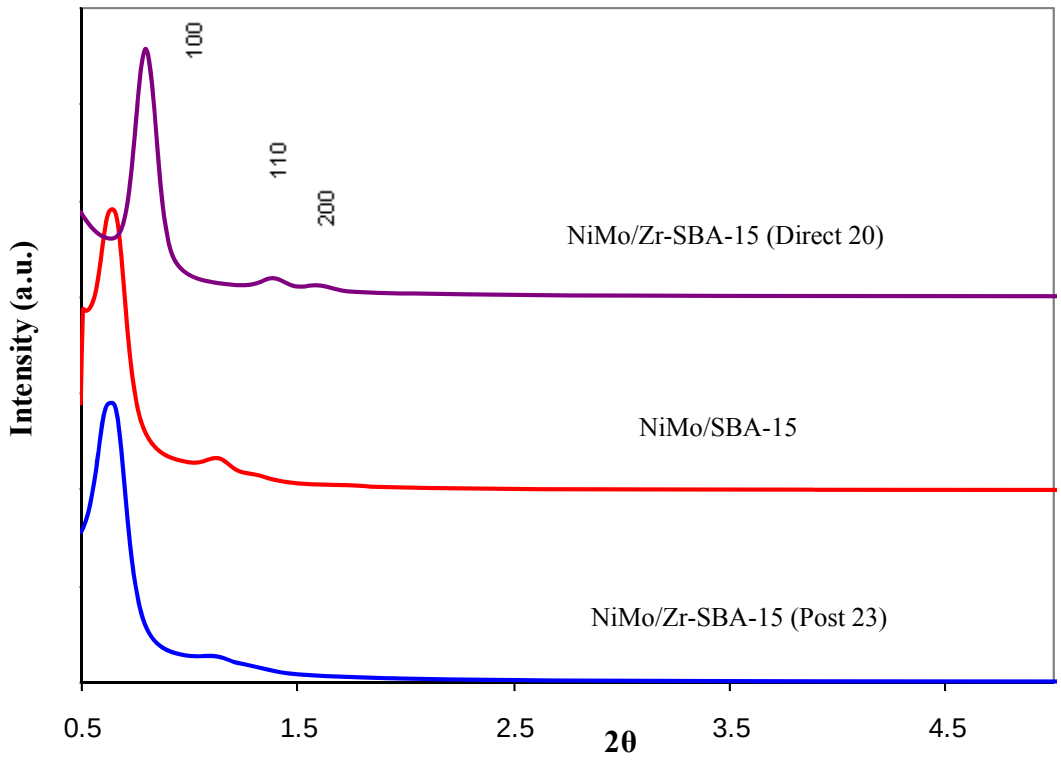

Figure 4.9. Small-angle X-ray scattering pattern of NiMo catalysts supported on SBA-15, Zr-SBA-15 (Direct) and Zr-SBA-15 (Post) supports.

4.2.2 N_2 Adsorption/Desorption and Chemical Compositions

The textural characteristics and chemical compositions of NiMo catalysts supported on SBA-15 and Zr-SBA-15 supports are summarized in Table 4.2. Chemical compositions of the catalysts are calculated based on ICP-MS and SEM-EDX characterization results. Example of SEM-EDX characterization for the NiMo/Zr-SBA-15 (Post 23) catalyst is shown in the Figure 4.10. It is observed that for all catalysts, the achieved Mo and Ni concentration are lower than those of targeted ones. This discrepancy can be attributed to the diffusion limitations of Mo and Ni occurs during catalyst preparation or the inherent nature of these elements to form considerable metal vacancies (Jacobsen et al., 1995; Yu et al., 1998). The results of textural characteristics of the catalysts show that there is a decrease in specific surface area and pore volume for all the catalyst samples due to loading of NiO and MoO_3. Also, metal oxide addition produces a minor decrease in pore diameter, indicating a relatively large pore plugging due to the incorporation of metal oxide. It can be observed that NiMo catalysts supported on Zr-SBA-15 material prepared by the post synthesis method provides larger pore diameter compared to the Zr-SBA-15 support prepared by the direct synthesis method. Figure 4.11 shows the nitrogen adsorption-desorption isotherm for NiMo catalyst supported on pure SBA-15, Zr-SBA-15 (Post) and Zr-SBA-15 (Direct) supports. All catalyst samples exhibit a type-IV isotherms with a hysteresis loop, which indicates that all isotherms preserved the characteristic shape of the SBA-15 and Zr-SBA-15 mesoporous materials, even after metal loading onto SBA-15 and Zr-SBA-15 supports.

Table 4.2: Textural characteristics and chemical compositions of catalysts materials.

Catalyst	Targeted/ Achived Mo Content (wt%)	Targeted/ Achieved Ni Content (wt%)	Surface Area, S_{BET} (m^2/g)	Pore Vol.e, V_P (cm^3/g)	Av. Pore Dia., D_P (nm)
NiMo/SBA-15	12 / 11.4	2.4 / 2.1	333	0.96	11.4
NiMo/Zr-SBA-15(Post 16)	12 / 11.5	2.4 / 2.4	298	0.78	10.7
NiMo/Zr-SBA-15(Post 23)	12 / 10.2	2.4 / 2.1	281	0.71	10.1
NiMo/Zr-SBA-15(Direct 40)	12 / 11.6	2.4 / 2.1	532	0.80	6
NiMo/Zr-SBA-15(Direct 20)	12 / 11.3	2.4 / 2.2	481	0.80	6.6

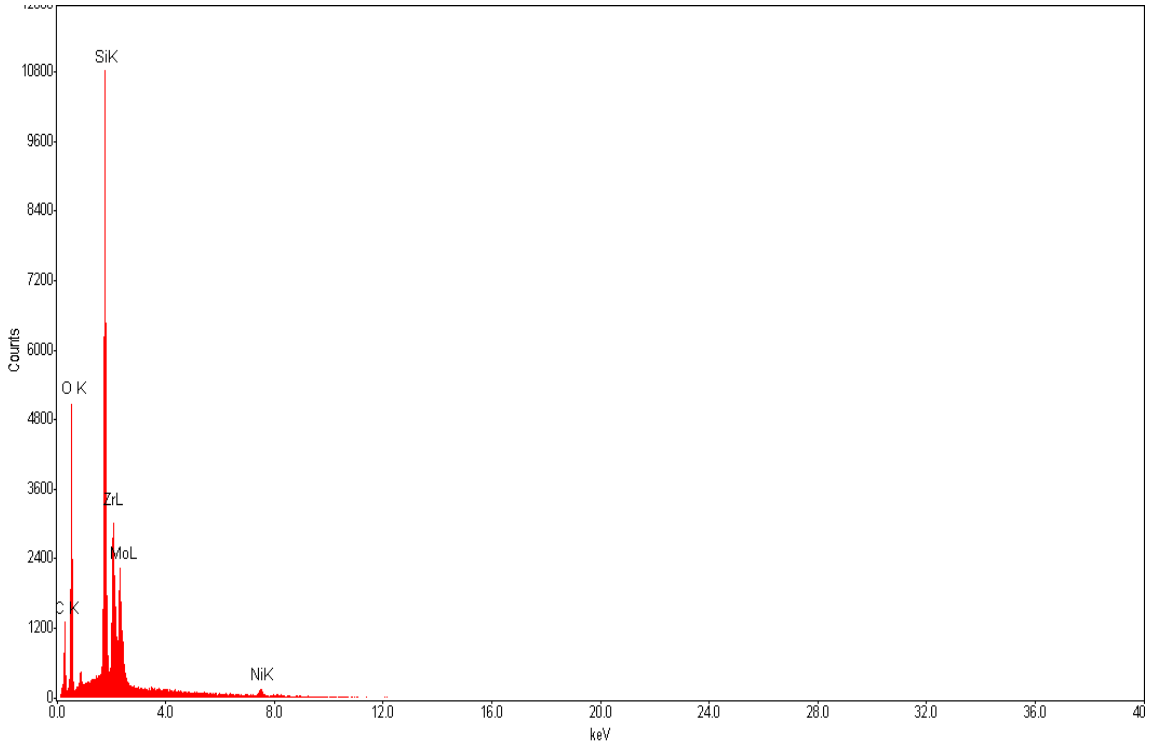

Figure 4.10: EDX pattern for NiMo/Zr-SBA-15 (Post 23) catalyst

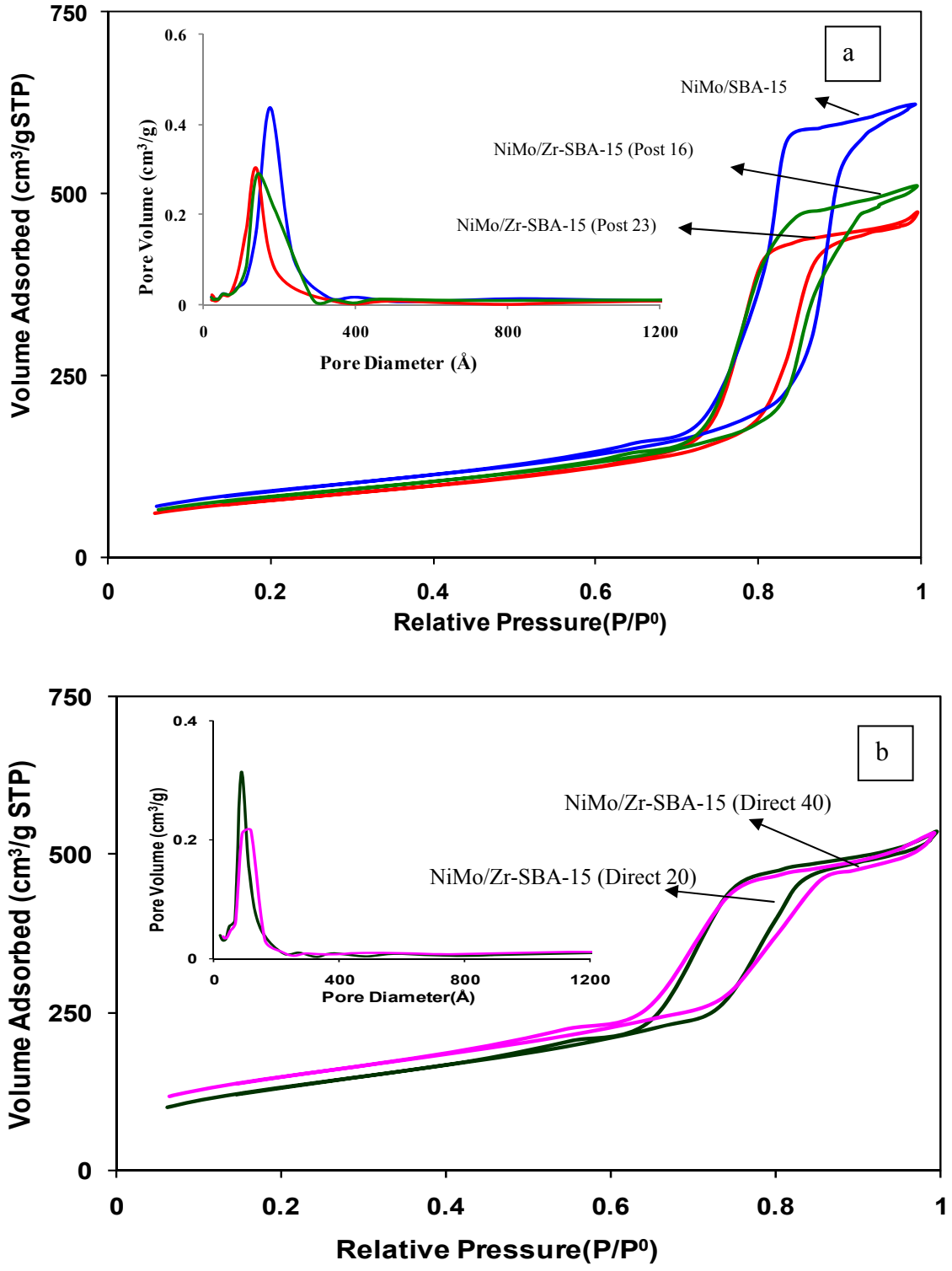

Figure 4.11 Nitrogen adsorption-desorption isotherm of NiMo catalyst supported on SBA-15 and Zr-SBA-15 (Post) (a); Zr-SBA-15 (Direct) (b).

4.2.3 Transmission Electron Microscopy (TEM)

TEM images of NiMo/SBA-15, NiMo/Zr-SBA-15 (Post), and NiMo/Zr-SBA-15 (Direct) catalysts are presented Figure 4.12a/b/c/d/e/f. All catalyst samples display uniform and long-range ordered structure, implying that the structural integrity of support remains intact even after incorporation of metal on SBA-15 and Zr-SBA-15 materials. From the TEM images, hexagonal structures (front view) and cylindrical pores (side view) of the catalysts are observed, which are similar to the corresponding supports materials.

4.2.4 Powder X-ray Diffraction (XRD)

Powdered XRD analysis was performed to determine the presence of any crystalline phases present in the NiMo/SBA-15 and NiMo/Zr-SBA-15 catalysts. Powder XRD patterns for the NiMo catalysts supported on SBA-15, Zr-SBA-15 (Direct), and Zr-SBA-15 (Post) supports are shown in Figure 4.13. Diffraction due to the crystalline MoO_3 phase (JCPDS card 35-609 and JCPDS card 05-0508) (Gutiérrez et al., 2006a; Gutiérrez et al., 2009; Li et al., 2006) is observed for the NiMo catalysts supported on pure SBA-15 and Zr-SBA-15 (Direct) supports. However, XRD reflections of the crystalline MoO_3 phase disappear for the NiMo catalysts supported on Zr-SBA-15 (Post) supports prepared by the post synthesis method. Disappearance of XRD reflection for these catalysts indicates good dispersion of nickel and molybdenum oxide due to an increase in zirconia loading on the pure SBA-15 support. The NiMo catalyst supported on Zr-SBA-15 with 23 wt% ZrO_2 loading shows excellent dispersion of MoO_3 species.

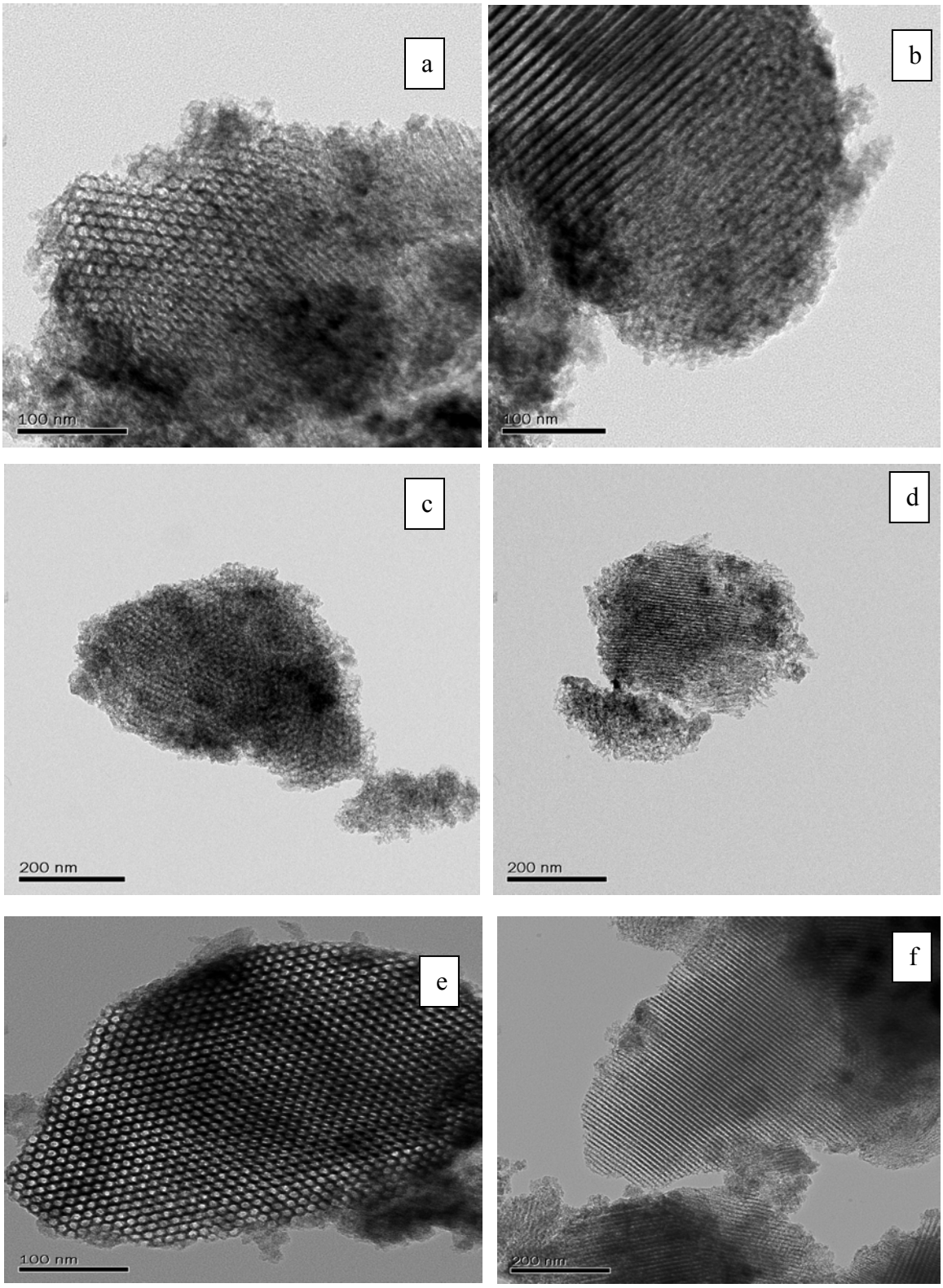

Figure 4.12. Transmission electron microscopy images of NiMo catalyst supported on SBA-15 front view (a), side view (b); Zr-SBA-15 (Post 23) front view (c), side view (d); Zr-SBA-15 (Direct 20) front view (e), side view (f).

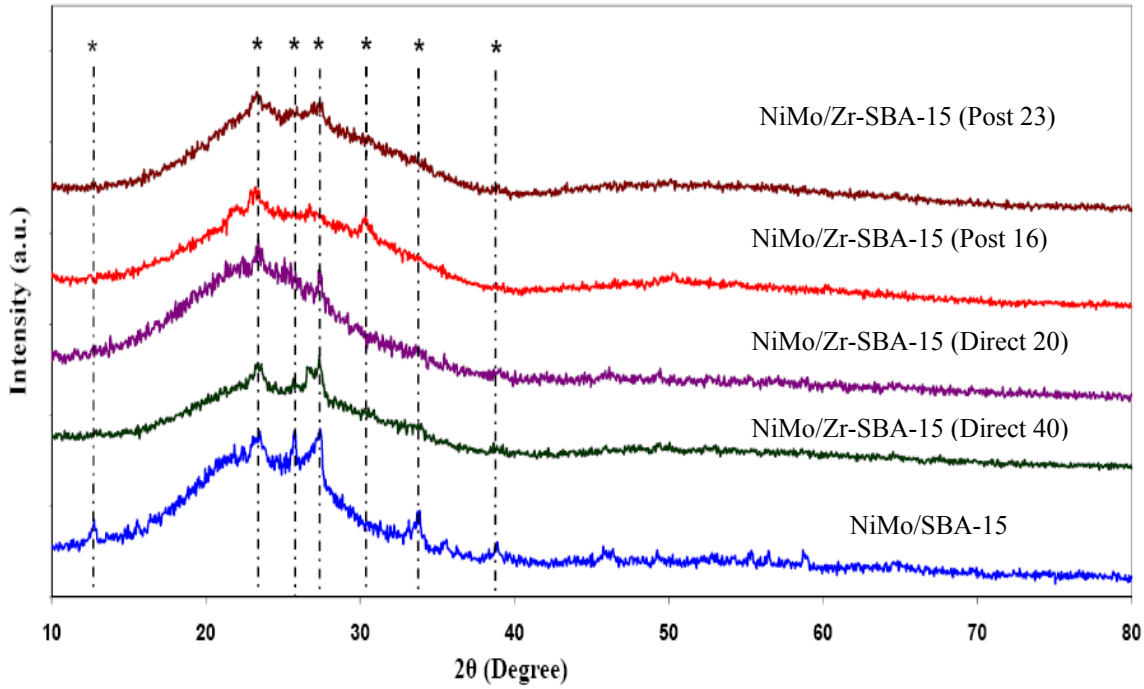

Figure 4.13. Powder X-ray diffraction patterns of NiMo catalysts supported on SBA-15, Zr-SBA-15 (Direct) and Zr-SBA-15 (Post) supports. * represents MoO_3 peaks (JCPDS card 35-609 and JCPDS card 05-0508).

4.2.5 Raman Spectroscopy

To investigate the nature of molybdenum oxide phases present on the Zr-SBA-15 support, Raman spectroscopy was employed. The Raman spectra of SBA-15, Zr-SBA-15 (Direct), and Zr-SBA-15 (Post) supported NiMo catalysts are shown in Figure 4.14. All spectra exhibit Raman bands at 285.5, 335.5, 377, 663, 816.5, 945, and 991 cm^{-1}. The bands at 285.5, 335.5, 663, 816.5 and 991 cm^{-1} are attributed to the crystalline MoO_3 particles (Ferdous et al., 2007; Sigurdson et al., 2008). The bands at 377 and 945 cm^{-1} were assigned to the Mo=O bending vibration (Ferdous et al., 2007; Montesinos-Castellanos and Zepeda, 2008). The intensity band due to MoO_3 particles is strong for the NiMo catalyst supported on pure SBA-15. However, the intensity of these bands decreases with the incorporation of Zr species (Zr or zirconia) in NiMo catalyst. This trend is in agreement with the powder XRD results. Hence, it can be concluded that the

incorporation of the zirconia into the SBA-15 support [Zr-SBA-15 (Post)] increases the interaction of an active component (Mo) with the support material. A similar trend is observed for the NiMo catalyst supported on Zr-SBA-15 (Direct) supports.

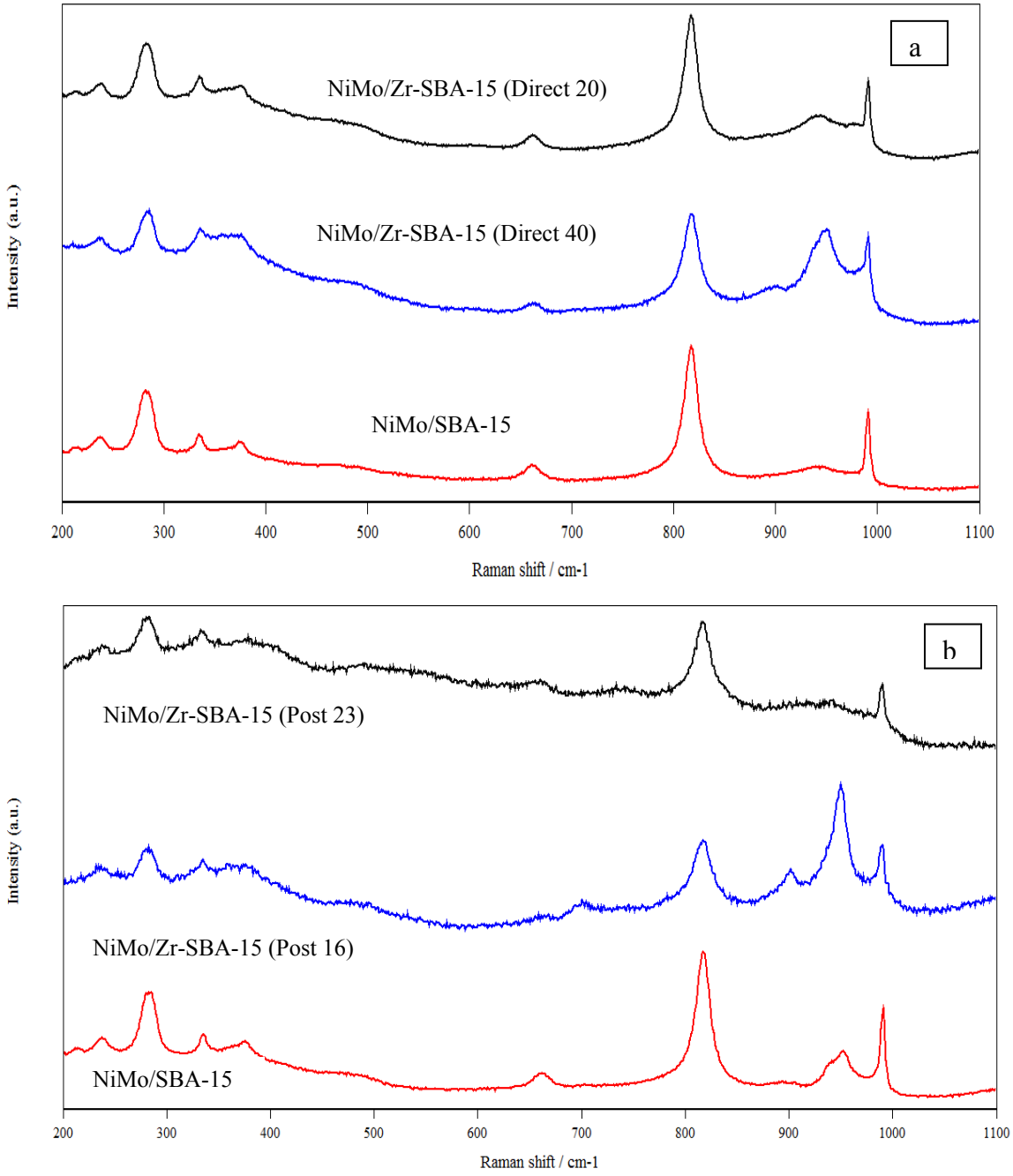

Figure 4.14. Raman spectra comparison for NiMo catalyst supported on SBA-15 and Zr-SBA-15 (Direct) (a); supported on SBA-15 and Zr-SBA-15 (Post) (b) support.

4.2.6 UV-DRS Spectroscopy

UV-DRS spectra of NiMo/Zr-SBA-15 (Post) catalysts were recorded in order to obtain information about the coordination and aggregation state of Mo and Ni oxidic species. DRS spectra corresponding to Mo and Ni species are shown in Figure 4.15 (a) and (b) respectively. The absorption due to ligand-to-metal charge transfer (LMCT) O^{2-} to Mo^{6+} for molybdenum is observed in the range of 270-350 nm (Gutiérrez et al., 2008). The absorption band due to isolated molybdate (tetrahedral) is observed in 270-280 nm range. Whereas, the absorption band due to polymolybdate (octahedral) is observed in 300-320 nm (Gutiérrez et al., 2006a). From the DRS spectra of NiMo catalysts it is evident that mixture of Mo^{6+} species is present in all catalysts samples. However, the proportion of different Mo species changes depends upon the type of support materials. Spectra in the range of 270-280 nm are very intense for the NiMo catalyst supported on SBA-15 material compared to the NiMo catalyst supported on Zr-SBA-15 material. Also, it is observed that the absorption due to octahedral Mo species becomes less intense upon zirconia incorporation onto SBA-15 support. This indicates that zirconia addition to SBA-15 support leads to decrease in the proportion of octahedral Mo species. Hence, it can be concluded that the better dispersion of Mo species takes place in zirconia modified support compared to the SBA-15 support (Gutiérrez et al., 2006a). The DRS spectra corresponding to absorption band in Ni^{2+} is shown in Figure 4.15.b. The presence of octahedral Ni species is observed at 720 nm for all catalysts.

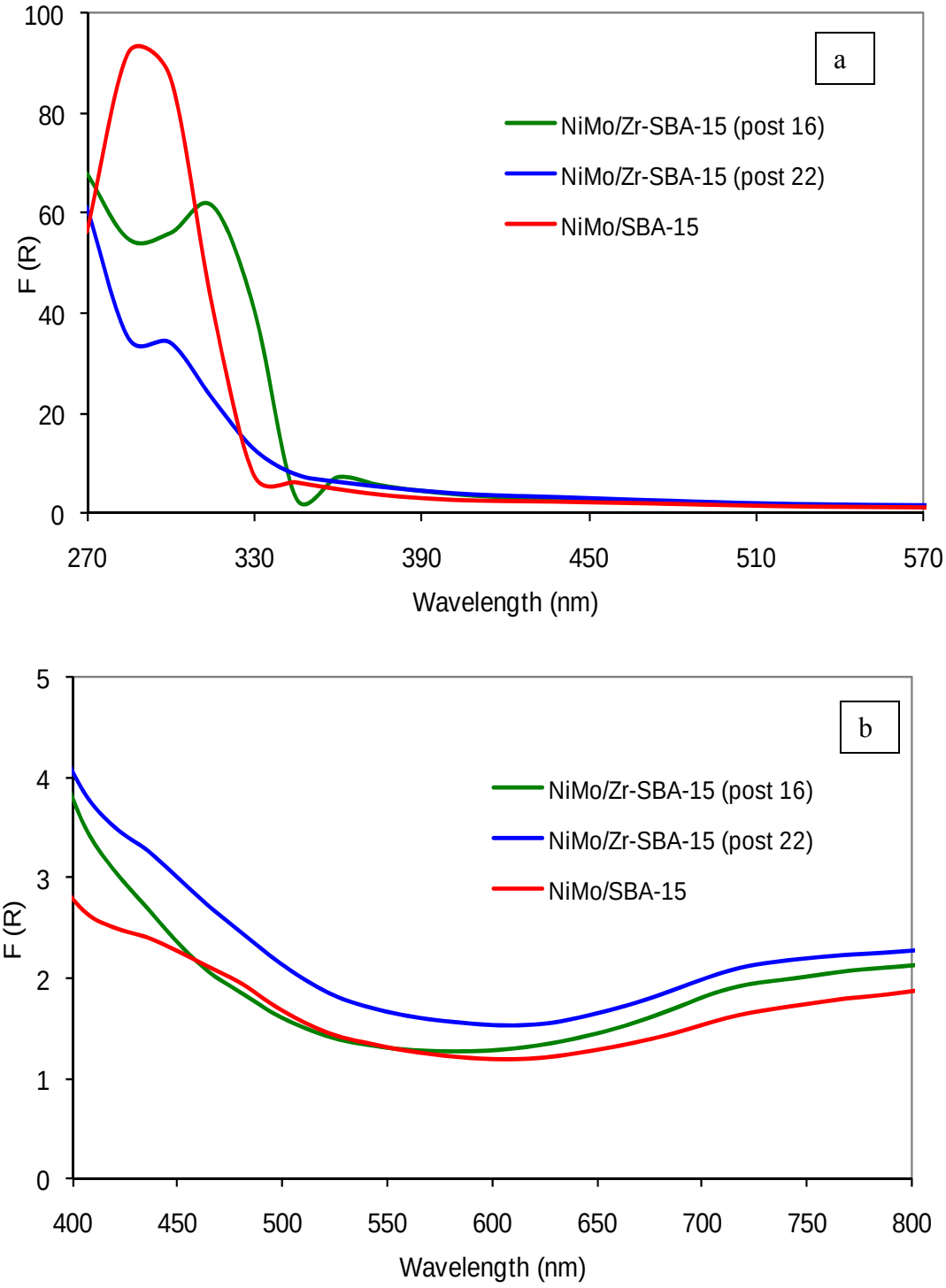

Figure 4.15. UV-DRS spectra of NiMo catalysts supported on SBA-15 and Zr-SBA-15 (Post 16) and Zr-SBA-15 (Post 23) support absorption band due to Mo (a); Ni (b).

4.3 Catalytic Activity Performance Based on HDS and HDN

In the present study, the performance of all catalysts was evaluated based on hydrodesulfurization (HDS) and hydrodenitrogenation (HDN) activities exhibited during hydrotreatment of heavy gas oil (HGO) derived from Athabasca bitumen. In a typical run, 5 ml of catalyst was loaded in the reactor, and sulfidation of catalyst was carried out for 48 hrs. The sulfided catalyst was then precoked (stabilized) using HGO for 5 days (T = 370˚C, P=8.9 MPa, LHSV = 1.0 h^{-1}, gas-to-oil ratio = 600 Nm^3/m^3). From the catalyst stabilization study (Figure 4.16) it was evident that the HDS and HDN activity decrease with time for an initial two days due to the coke deposition on catalyst surface and then level out.

Hydrotreating of gas oil was carried out for three different temperatures, namely 375˚C, 385˚C, and 395˚C. As seen from Figure 4.17, the HDS and HDN activities of NiMo catalysts supported on Zr-SBA-15 are higher than that of the catalysts supported on pure SBA-15. This higher hydrotreating activity of NiMo/Zr-SBA-15 catalysts may be due to the better dispersion of Mo active species (as seen in XRD and UV-DRS data), good metal-support interaction (as seen in Raman spectra), and higher acidity (as observed by FT-IR of pyridine adsorption) compared to those that of the NiMo/SBA-15 catalyst. A similar trend in HDS activity was observed for the hydrotreating of model compounds over NiMo/Zr-SBA-15 catalysts and the NiMo/SBA-15 catalyst (Gutiérrez et al., 2006a; Gutiérrez et al., 2008).

In the case of all Zr-SBA-15 supported catalysts, the NiMo catalyst supported on Zr-SBA-15 (Post) prepared by the post synthesis method shows significantly higher HDS and HDN activities compared to the NiMo/Zr-SBA-15 (Direct) catalysts, prepared by the

direct synthesis method. This can be attributed to the better textural characteristics (higher pore diameter), higher zirconia loading, and higher acidity of NiMo/Zr-SBA-15 (Post) catalysts than that of NiMo/Zr-SBA-15 (Direct) catalysts. It is interesting to note that the hydrotreating activities of NiMo/Zr-SBA-15 (Direct) catalysts are lower, in spite of the higher surface area compared to NiMo/Zr-SBA-15 (Post) catalysts, indicating that the higher pore diameter plays an important role in avoiding excessive pore blockage during the hydrotreating of heavy gas oil feedstock, which contains many refractory sulfur and nitrogen compounds in significant quantities (Bej et al., 2001; Ferdous et al., 2006b).

It can be observed that among NiMo catalysts supported over Zr-SBA-15 (Direct) material, support with a Si/Zr ratio of 20 exhibits higher HDS and HDN activities than that of the support with a Si/Zr ratio of 40. This trend may be attributed to the better structural ordering, better dispersion of Mo species, and higher acidity due to higher Zr content in Zr-SBA-15 (Direct 20) support compared to the Zr-SBA-15 (Direct 40) support. Furthermore, the NiMo catalyst supported on the Zr-SBA-15 support with 23wt% zirconia loading shows higher hydrotreating activity compared to the Zr-SBA-15 support with 16 wt% zirconia loading. An increase in zirconia loading on the SBA-15 structure results in well-dispersed ZrO_2 species and higher acidity on the surface of SBA-15, leading to higher HDS and HDN activities. This trend has been reported by other researchers for HDS of 4,6-DMDBT (Gutiérrez et al., 2006b; Gutiérrez et al., 2008). The results of the comparative study show that the NiMo/Zr-SBA-15 (Post 23) catalyst has maximum HDS and HDN activities compared to all other NiMo/Zr-SBA-15 catalysts as well as the NiMo catalyst supported on SBA-15.

The hydrotreating activity test of the commercial hydrotreating catalyst (NiMo catalyst supported on γ-Al_2O_3) with similar mass loading ($\approx$ 2 gm) was compared with that of the best catalysts from the previous step (i.e., NiMo/Zr-SBA-15 (Post 23)) under similar operating conditions. It can be seen from Figure 4.18 that the HDS and HDN activities of NiMo/Zr-SBA-15(Post 23) are higher than that of the commercial catalyst at all temperatures studied. The superior hydrotreating activity of NiMo/Zr-SBA-15(Post 23) can be attributed to its lower metal support interaction and uniform mesoporous structure compared to the commercial NiMo catalysts supported over γ-Al_2O_3. Also, the simulated distillation comparison of feed and product obtained by hydrotreating of HGO over NiMo/Zr-SBA-15 (Post 23) catalyst is shown in Figure 4.19. From the figure it is evident that the production of lighter cut is obtain due to mild cracking of the HGO. However, from the overall distribution of heavier cut of feed and heavy material, it is clear that the significant hydrocracking has not occurred during the hydrotreating of HGO by NiMo/Zr-SBA-15 (Post 23) catalyst.

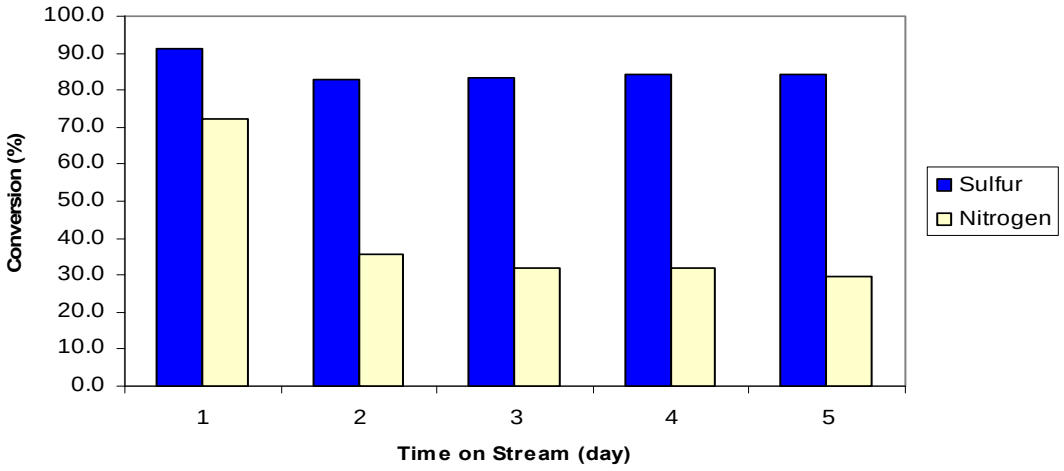

Figure 4.16: Effect of time on stream on the stability of the NiMo/Zr-SBA-15 catalyst during hydrotreating of heavy gas oil. P=8.9 MPa, LHSV=1.0 hr^{-1}, T=370 °C, G/O ratio =600 Nm^3/m^3.

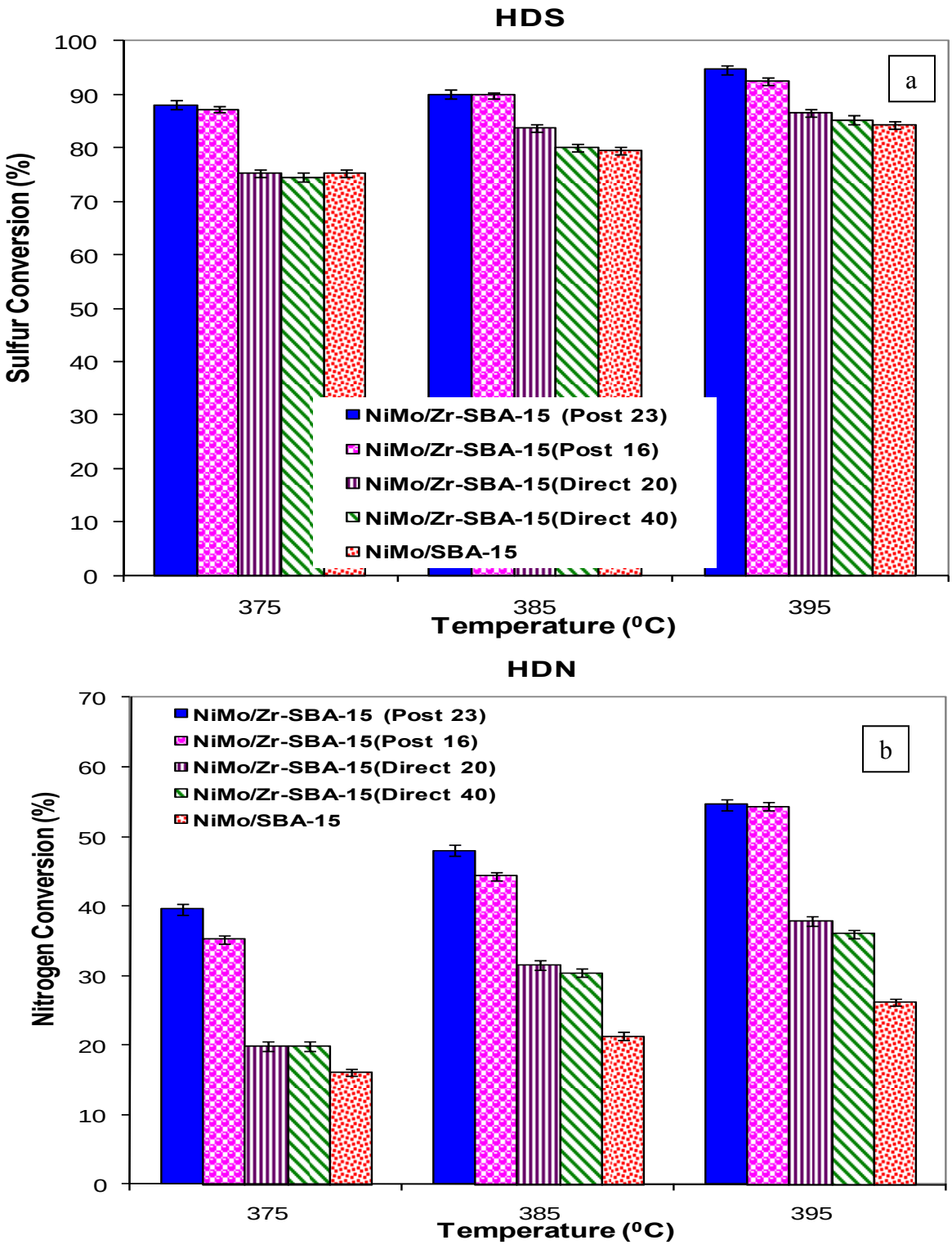

Figure 4.17. The hydrodesulfurization and hydrodenitrogenation activity (volume basis) study of NiMo catalysts supported on SBA-15, Zr-SBA-15 (Post) and Zr-SBA-15 (Direct); T = 375/385/395 °C, P=8.9 MPa, LHSV = 1 h^{-1}, H_2/HC ratio 600 Nm^3/m^3. HDS (a); HDN (b)

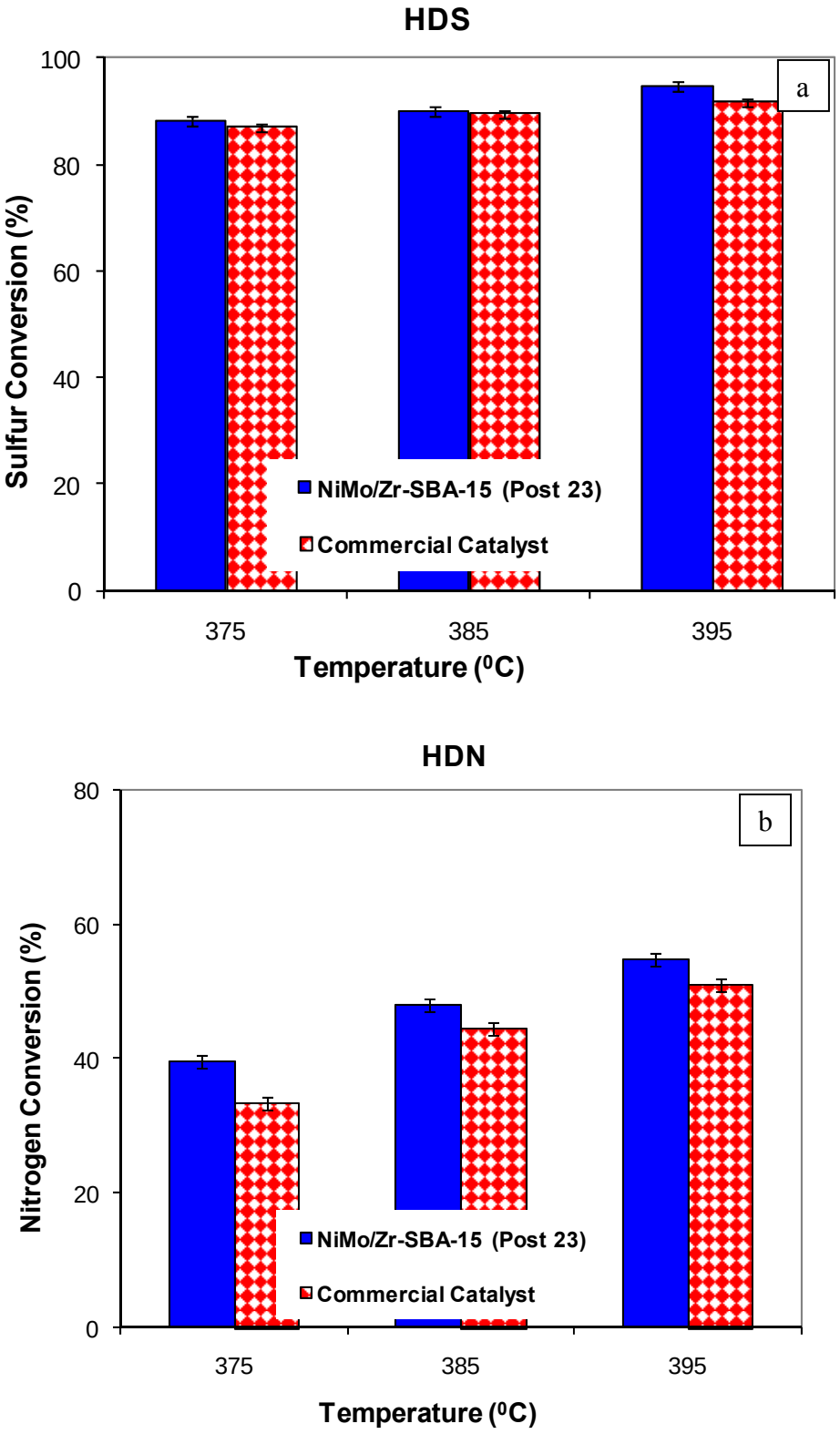

Figure 4.18. The hydrotreating activity (weight basis) comparison of NiMo/Zr-SBA-15 (Post 23) and commercial catalyst; T = 375/385/395 °C, P=8.9 MPa, LHSV = 1 h^{-1}, H_2/HC ratio 600 Nm^3/m^3. HDS (a); HDN (b).

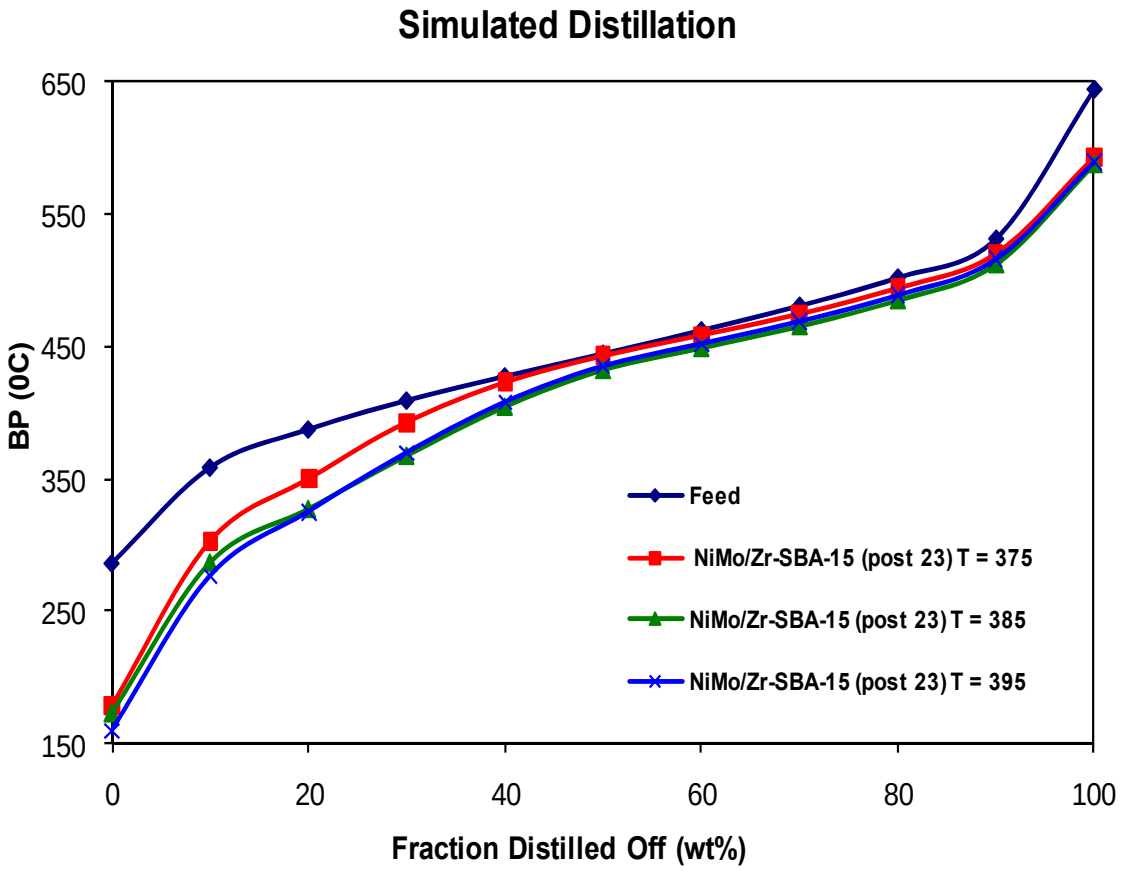

Figure 4.19. The simulated distillation of HGO feed and the product obtained by hydrotreating of HGO over NiMo/Zr-SBA-15 (Post 23) catalyst.

CHAPTER 5
METAL LOADING OPTIMIZATION FOR NiMo/Zr-SBA-15 CATALYSTS

This chapter describes the results of support and catalyst characterizations obtained for phase-II work. Detailed description of various characterizations methods, such as BET, SASX, FT-IR, SEM, TEM, XRD, UV-DRS, Raman etc, performed on supports and catalyst are elaborated in this section. Also, a comparison of catalysts with different metal loading illustrated in this chapter. Furthermore, determination of best catalyst is described based on catalyst characterization results and HDS and HDN activity performances on heavy gas oil.

5.1 Characterization of Supports

5.1.1 Small-Angle X-ray Scattering (SAXS)

The small-angle X-ray scattering (SAXS) pattern of calcined parent SBA-15 and Zr-SBA-15 (Post 23) are shown in Figure 5.1. Both the samples displayed three well-resolved peaks that confirmed well ordered structure for mesoporous materials. These three peaks can be indexable as (100), (110), and (200) reflections associated with 2-D hexagonal symmetry. Furthermore, presence of three peaks for Zr-SBA-15 support confirms that the hexagonal orderliness is preserved even after incorporation of ZrO_2 on SBA-15 surface by post synthesis method. However, intensity for the Zr-SBA-15 support decreases upon incorporation of ZrO_2 into the SBA-15 surface, indicating that slight modification of long range order of pores of SBA-15 occurs with ZrO_2 loading.

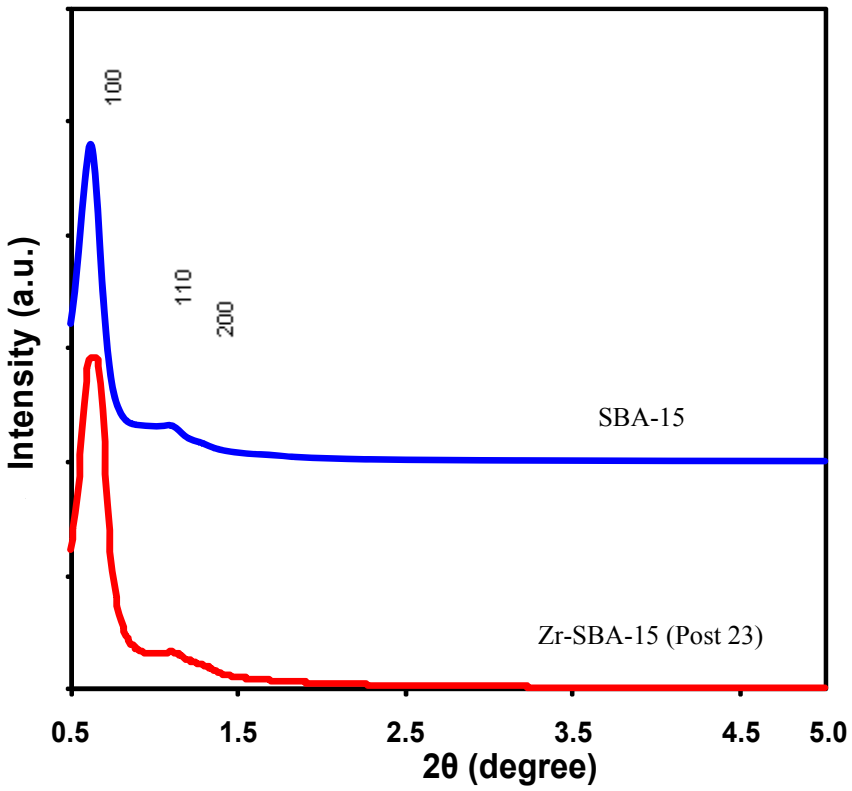

Figure 5.1. Small-angle X-ray scattering pattern of SBA-15 and Zr-SBA-15 (Post 23) supports.

5.1.2 N_2 Adsorption/Desorption and Chemical Compositions

The textural characteristics results and chemical compositions of SBA-15 and Zr-SBA-15 (Post 23) support are summarized in Table 5.1. From the table it is observed that the mesoporous structures of SBA-15 and Zr-SBA-15 support were obtained. There is a decrease in textural properties (surface area and pore diameter) of SBA-15 upon the incorporation of zirconia on the SBA-15 surface. Decrease of textural properties of Zr-SBA-15 (Post 23) may be due to blocking of SBA-15 mesopores by zirconia. Nitrogen adsorption-desorption isotherm for SBA-15 and Zr-SBA-15 supports are presented in Figure 5.2, which shows that these support samples exhibit type-IV hysteresis loop, due

to presence of large pore mesoporous material with narrow pore size distribution (Gutiérrez et al., 2006a; Kruk and Cao, 2007).

Table 5.1: Textural characteristics and chemical compositions of support materials.

Support	Targeted / Achieved ZrO_2 Content (wt%)	Surface Area (m^2/g)	Pore Volume (cm^3/g)	Average Pore Dia., (nm)
SBA-15	-	466	1.44	12.4
Zr-SBA-15(Post 23)	23.0 / 22.7	422	1.11	10.6

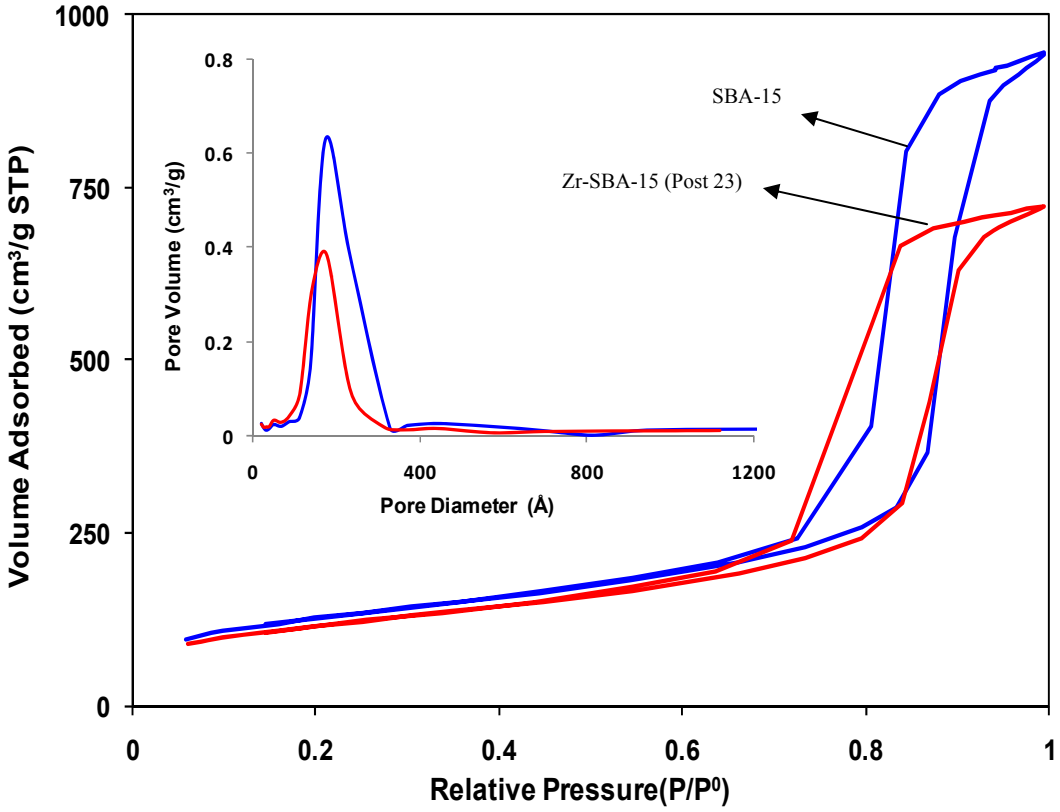

Figure 5.2. Nitrogen adsorption-desorption isotherm of SBA-15 and Zr-SBA-15 (Post 23) supports.

5.1.3 Transmission Electron Microscopy (TEM)

Further structural features of SBA-15 and Zr-SBA-15 (Post 23) material are studied by TEM. The TEM images in Figure 5.3 show the channel-like arrangement of pores for all support samples. Figure of SBA-15 shows the highly ordered 2-D hexagonal pore structure, which is in good agreement with the SAXS analysis (Figure 5.1). The distance between the two adjacent pore centers is 160 Å and the average pore diameter is about 120 Å. TEM of Zr-SBA-15 (Post 23) support also demonstrates well-defined 2-D hexagonal arrangement of mesopores, implying that the mesoporous structure is intact after ZrO_2 incorporation onto parent SBA-15.

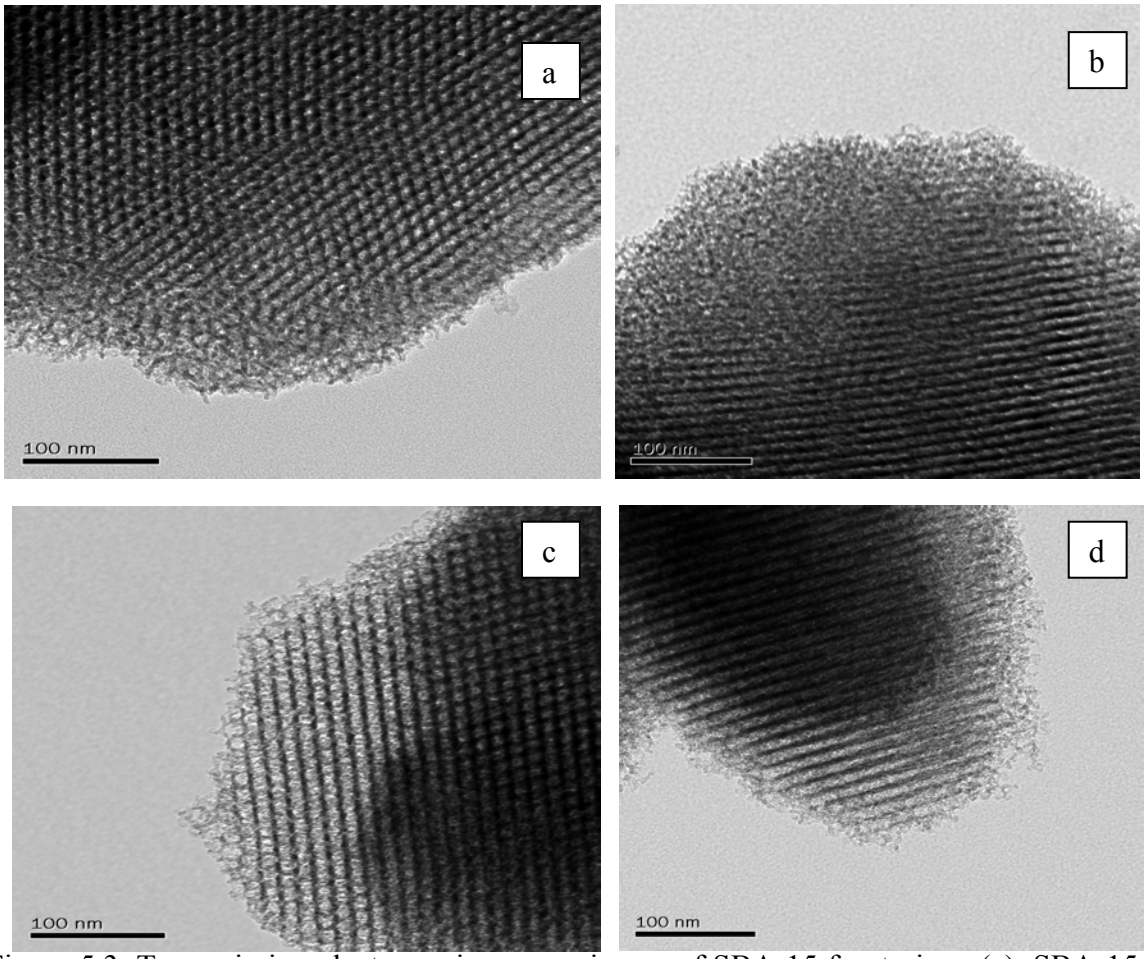

Figure 5.3. Transmission electron microscopy image of SBA-15 front view (a), SBA-15 side view (b); Zr-SBA-15 (Post 23) front view (c), Zr-SBA-15 (Post 23) side view (d).

5.1.4 Scanning Electron Microscopy (SEM)

The morphology and structure of SBA-15 and Zr-SBA-15 (Post 23) supports are investigated by SEM. SEM micrograph of calcined SBA-15 is shown in Figure 5.4a/b. SBA-15 sample exhibits uniform cylindrical form with diameter of 1-3μm and consists of fiber-like packages. The similar morphology of SBA-15 is reported by other researchers (Eswaramoorthi et al., 2008; Landau et al., 2005). SEM image of Zr-SBA-15 (Post 23) support also displays the similar fiber like cylindrical image as observed in parent SBA-15. It can be inferred that the morphology of the sample is preserved after the zirconia impregnation in SBA-15 support.

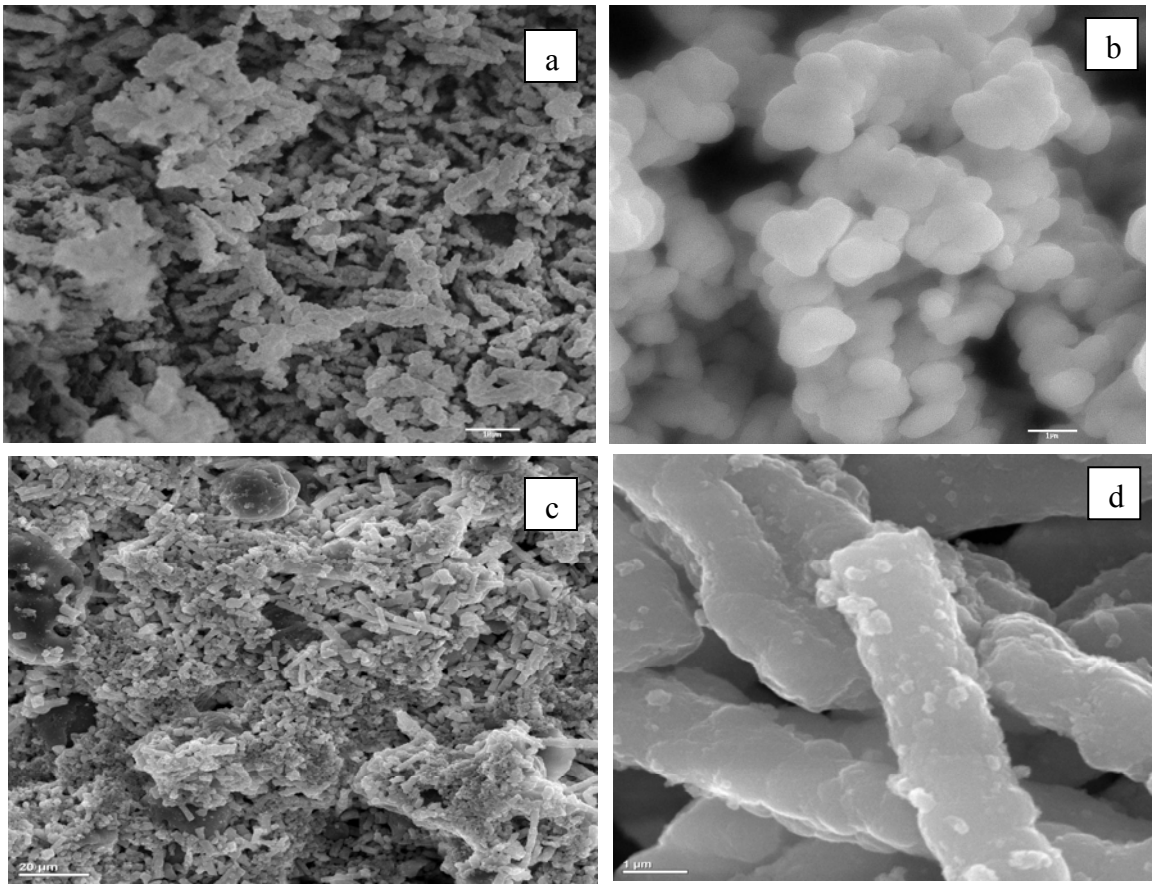

Figure 5.4. Scanning electron microscopy image of SBA-15 of 10 μm (a); SBA-15 of 1 μm (b); Zr-SBA-15 (Post 23) of 10 μm (c); Zr-SBA-15 (Post 23) of 1μm (d)

5.2 Characterizations of Catalysts

5.2.1 Small-Angle X-ray Scattering (SAXS)

The SAXS pattern of NiMo catalysts supported on SBA-15 and Zr-SBA-15 are presented in Figure 5.5. All catalysts samples exhibit well-defined hexagonal structures as represented by typical SAXS pattern of mesoporous material. The SAXS pattern of NiMo catalyst preserves the three characteristic peaks namely (100), (110), and (200), which are associated with the well-order hexagonal structure. However, a mild reduction of peak intensities is observed in SBA-15 and Zr-SBA-15 supports due to addition of metal to the support materials. Reduction of hexagonal long-range periodicity of Zr-SBA-15 support material becomes intense with the higher metal loading onto the Zr-SBA-15 support. Hence, catalyst with 22 wt% of Mo loading shows noticeable reduction in peak.

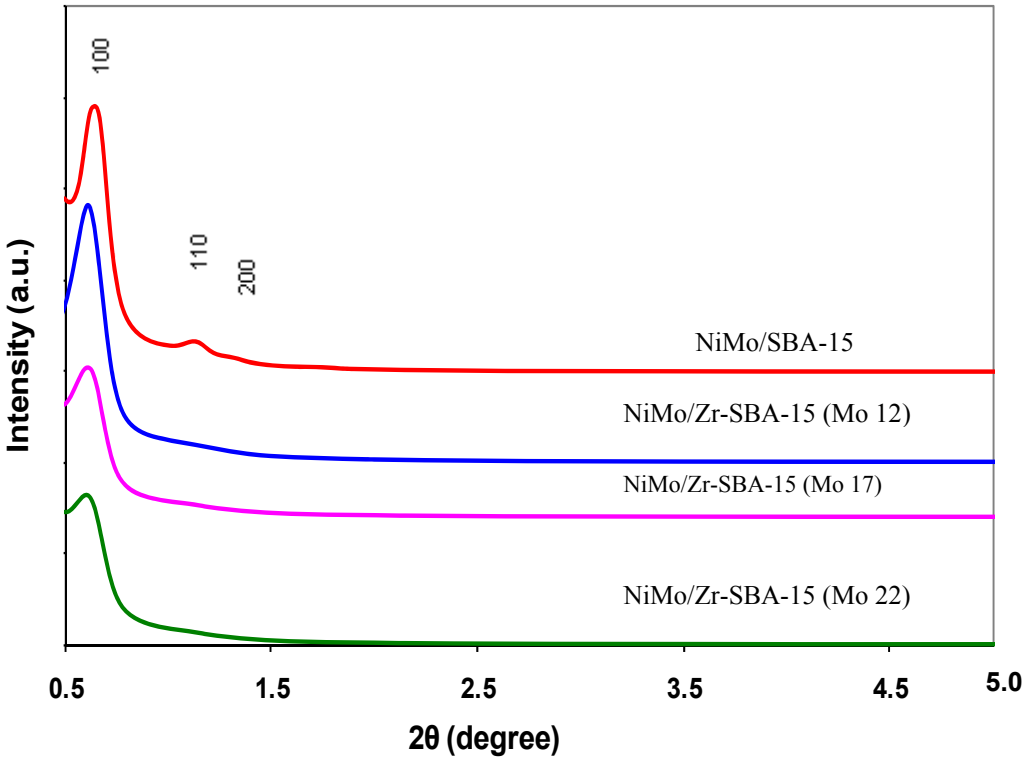

Fig 5.5. Small-angle X-ray scattering pattern of NiMo/SBA-15 and NiMo/Zr-SBA-15 catalysts with varying metal loading.

5.2.2 N_2 Adsorption/Desorption and Chemical Compositions

The textural characteristics and chemical compositions of NiMo catalysts supported on SBA-15 and Zr-SBA-15 (Post 23) supports are summarized in Table 5.2. The results of textural characteristic of catalyst show that there is a decrease in specific surface area, pore volume and pore diameter for all the catalyst samples due to loading of NiO and MoO_3. Decrease in surface area may be contributed to the pore blocking of support materials by impregnated metals. The decrease in surface area as well as pore volume is significant for higher metal loading. Also, metal oxide addition produces minor decrease in pore diameter, indicating metal oxide incorporation inside the pores. Nitrogen adsorption/desorption isotherm for catalysts samples are presented in Figure 5.6. All catalyst samples exhibit type-IV isotherm with hysteresis loop, which is the characteristic for uniform mesoporous materials. These characteristics isotherm indicates that all isotherms maintain the characteristic shape of mesoporous SBA-15 and Zr-SBA-15 materials, even after MoO_3 and NiO loading onto supports. However, the height of the hysteresis loop decreases with increase in metal loading, indicating that the volume of gases adsorbed by mesopores decreases with the metal loading over the support materials. This decrease is significant for the catalyst with 22 wt% of Mo loading.

Table 5.2: Textural characteristics and chemical compositions of catalysts materials.

Catalyst	Targeted / Achived Mo Content (wt%)	Targeted / Achieved Ni Content (wt%)	Surface Area (m^2/g)	Pore Volume (cm^3/g)	Av. Pore Dia., (nm)
NiMo/SBA-15	12 / 11.4	2.4 / 2.1	325	0.98	12.1
NiMo/Zr-SBA-15(Mo 12)	12 / 10.6	2.4 / 2.3	284	0.74	10.4
NiMo/Zr-SBA-15(Mo 17)	17 / 15.6	3.4 / 3.3	221	0.56	10.1
NiMo/Zr-SBA-15(Mo 22)	22 / 19.7	4.4 / 4.4	185	0.45	9.7

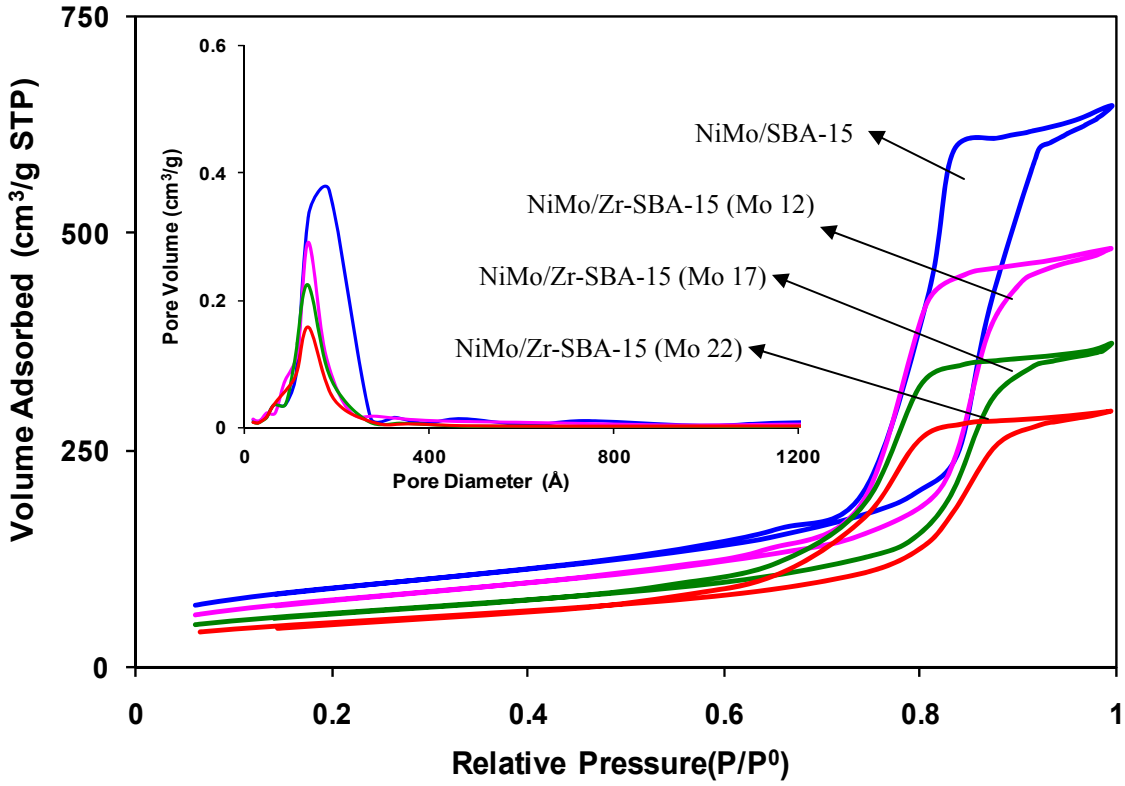

Figure 5.6. Nitrogen adsorption-desorption isotherm of NiMo/SBA-15 and NiMo/Zr-SBA-15 catalysts with varying metal loading.

5.2.3 Transmission Electron Microscopy (TEM)

Further structural features of NiMo catalysts supported on SBA-15 and Zr-SBA-15 material are studied by TEM. The TEM images in Figure 5.7 show the channel-like arrangement of pores for all catalyst samples. Figure of NiMo/SBA-15 shows the well ordered hexagonal pore structure, which is in good agreement with the SAXS analysis. TEM of NiMo catalysts supported on Zr-SBA-15 supports also demonstrate well-defined 2-D hexagonal arrangement of mesopores, implying that the mesoporous structure is intact after metal incorporation onto parent SBA-15 and Zr-SBA-15 (Post 23) supports.

However, there is a decrease of hexagonal structure due to increase of metal loading, which is significant for the catalyst with 22 wt% of Mo loading.

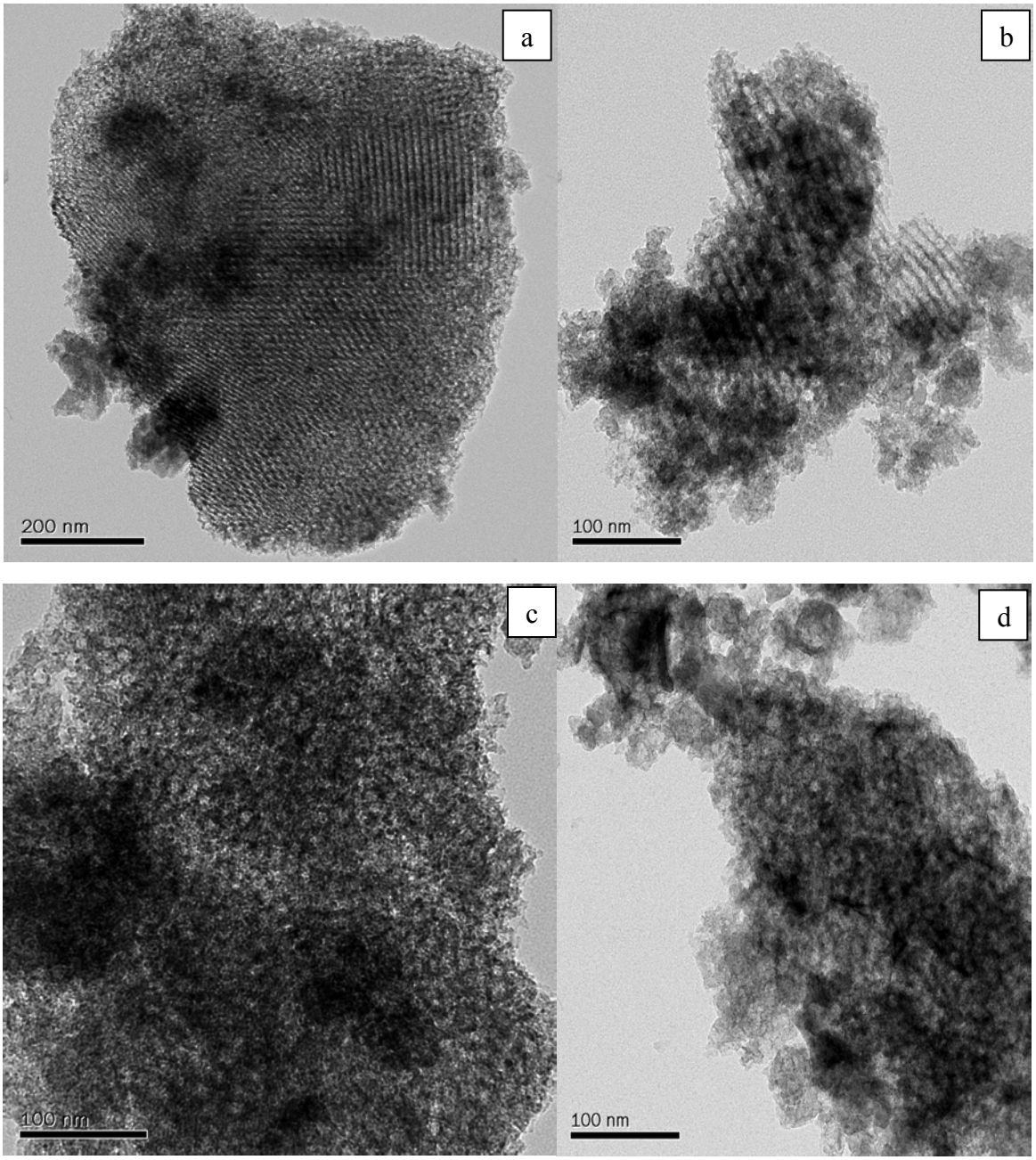

Figure 5.7. Transmission electron microscopy images of NiMo/SBA-15 (a); NiMo/Zr-SBA-15 (Mo 12) (b); NiMo/Zr-SBA-15 (Mo 17) (c); NiMo/Zr-SBA-15 (Mo 22) (d) catalysts.

5.2.4 Pyridine Adsorbed Fourier Transform Infrared Spectroscopy (Py-IR)

The acid properties on catalysts samples were examined by the FTIR spectroscopy of pyridine adsorption. Figure 5.8 shows the FTIR spectrum of pyridine adsorbed on the catalysts samples. All catalyst samples show the characteristic band at 1450 cm^{-1} (strong), 1580 cm^{-1}(weak), 1609 cm^{-1}(weak), which correspond to the pyridine adsorbed on lewis acid sites (Chen et al., 2006; Nava et al., 2007). Also, a band appeared at 1540 cm^{-1}, indicating creation of the Brønsted acid sites in all NiMo/Zr-SBA-15 samples. In addition, for all NiMo/Zr-SBA-15 samples, bands at 1490 cm^{-1} are associated with pyridine adsorbed on both Lewis and Brønsted acid sites (Chen et al., 2006). In pure NiMo/SBA-15 support, the bands corresponding to the only Lewis acid sites at 1450 cm^{-1}, 1624 cm^{-1} and 1580 cm^{-1} are observed. However, no band is observed at 1540 cm^{-1} and 1490 cm^{-1}, which corresponding to the Brønsted acidity. Hence, it can be concluded that the Brønsted acid sites were generated due to presence of zirconia in SBA-15 support. Furthermore, it is observed that the Brønsted acidity increases with the Mo loading. On the other hand, Lewis acidity is found to decrease upon increasing the Mo loading. Hence, highest Brønsted acidity is observed for the NiMo/Zr-SBA-15 (Mo 22) catalyst.

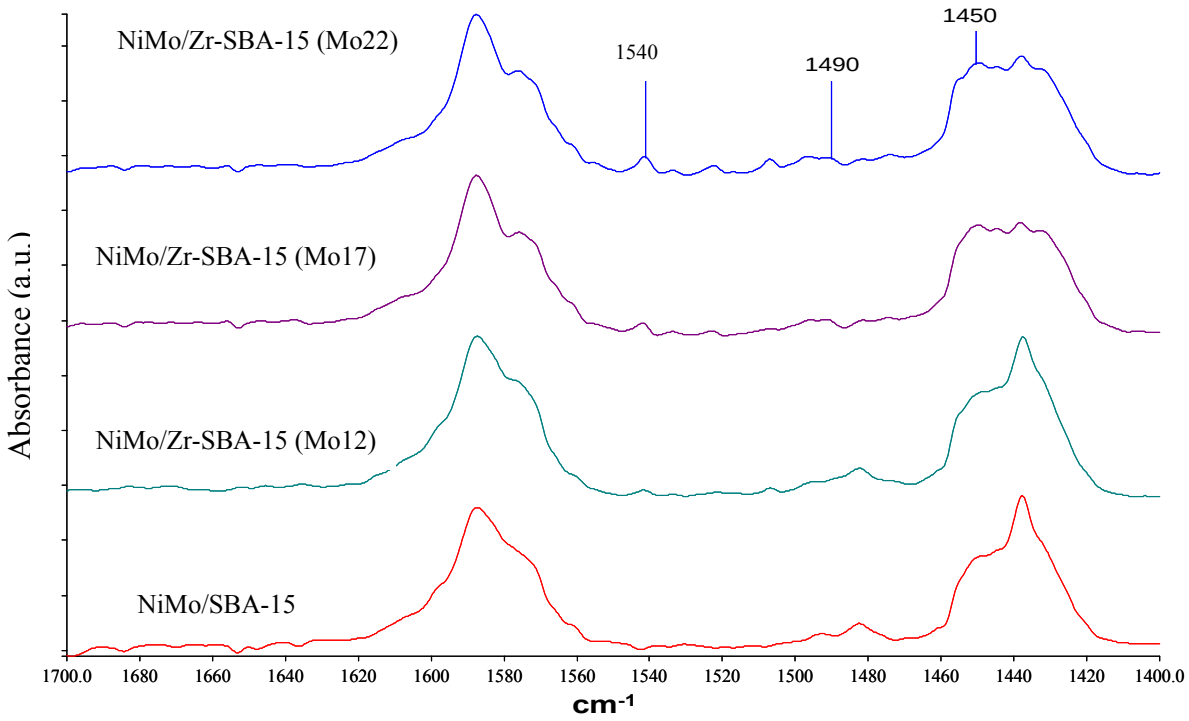

Figure 5.8. FT-IR spectra of pyridine adsorbed species on NiMo/SBA-15 and NiMo/Zr-SBA-15 catalysts with varying metal loading.

5.2.5 Powder X-ray Diffraction (XRD)

To determine the presence of any crystalline phase present in the NiMo/SBA-15 and NiMo/Zr-SBA-15 catalysts, powder XRD analysis was performed. In Figure 5.9 powder XRD pattern for NiMo catalyst supported on SBA-15 and Zr-SBA-15 support is shown. Diffraction due to the crystalline MoO_3 phase (JCPDS card 35-609 and JCPDS card 05-0508) (Gutiérrez et al., 2006a; Gutiérrez et al., 2009; Li et al., 2006) is observed for the NiMo catalysts supported on pure SBA-15 (sharp signal). However, XRD reflections of crystalline MoO_3 phase disappear for the NiMo catalyst supported on Zr-SBA-15 support. Disappearance of XRD reflection for these catalysts indicates better dispersion of nickel and molybdenum oxide due to increase in zirconia loading on pure SBA-15 support. NiMo/Zr-SBA-15 catalyst with Mo loading from 12 to 17 wt% (Ni loading 2.4 to 3.4 wt %) shows excellent dispersion of MoO_3 species, which imply that the addition of Mo and Ni significantly improve the MoO_3 dispersion. However, at higher Mo loading (22 wt %) reflection due to crystalline MoO_3 phase become pronounced, implying that the agglomeration of MoO_3 species occurs at higher metal loading.

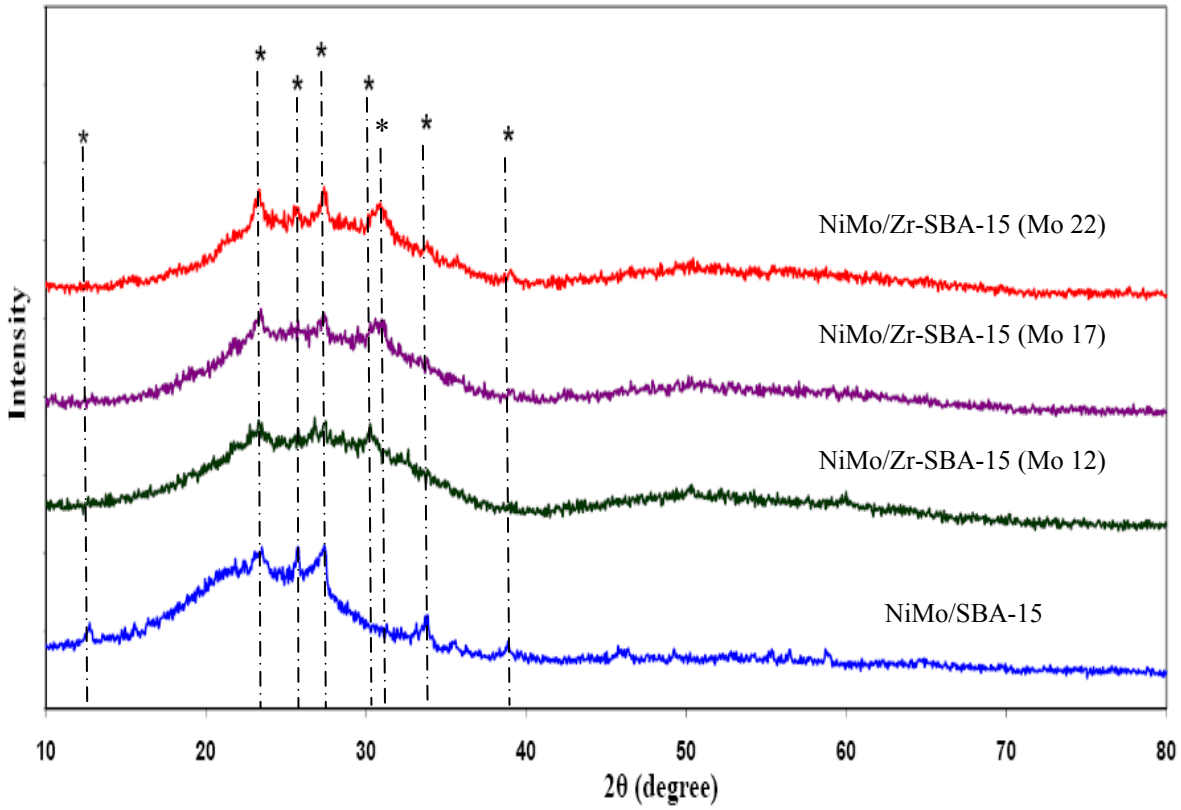

Figure 5.9. Powder X-ray diffraction pattern of NiMo/SBA-15 and NiMo/Zr-SBA-15 catalysts with varying metal loading. . * represents MoO_3 peaks (JCPDS card 35-609 and JCPDS card 05-0508).

5.2.6 Raman Spectroscopy

To investigate the nature of molybdenum oxide phases present on the NiMo catalyst supported on SBA-15 and Zr-SBA-15 supports Raman spectroscopy was employed. The Raman spectra for NiMo/SBA-15 and NiMo/Zr-SBA-15 catalyst with varying metal loading are shown in Figure 5.10. All spectra exhibit Raman bands at 285.5, 335.5, 377, 663, 816.5, 945 and 991 cm^{-1}. The band at 285.5, 335.5, 663, 816.5 and 991 cm^{-1} can be attributed to the crystalline MoO_3 particles (Ferdous et al., 2007; Sigurdson et al., 2008). From figure it is observed that intensity of these bands decreased with the incorporation of metal in NiMo catalyst. However, at higher metal loading (Mo loading of 22 wt %) the intensity of MoO_3 crystalline phase becomes sharper, implying progressive increase in the MoO_3 agglomeration with the increasing metal loading in line with the XRD observation.

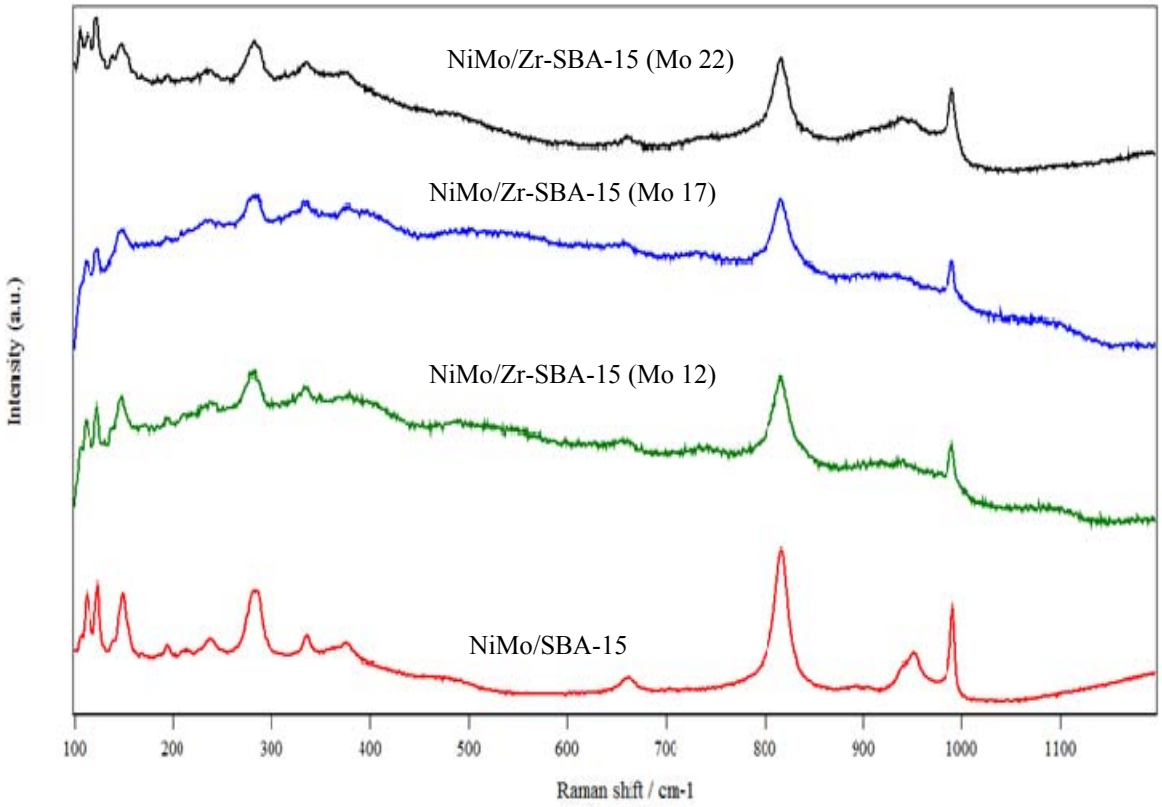

Figure 5.10. Raman spectra comparison for NiMo/SBA-15 and NiMo/Zr-SBA-15 catalysts with varying metal loading.

5.2.7 UV-DRS Spectroscopy

UV-DRS spectra of NiMo catalysts were recorded in order to obtain information about the coordination and aggregation state of Mo oxidic species. DRS spectra corresponding to Mo species is shown in Figure 5.11. The absorption due to O^{2-} to Mo^{6+} transition for molybdenum is observed in the range of 270-350 nm. The absorption band due to isolated molybdate (tetrahedral) is observed in 270-280, whereas, the absorption band due to octahedral polymolybdate is observed in 300-330 nm (Gutierrez et al., 2006). From the DRS spectra of NiMo catalysts it is evident that the mixture of Mo^{6+} of tetrahedral and octahedral species is present in all catalysts samples. The peaks intensity of spectra increases with the increasing of Mo loading. This indicates that as the Mo loading increases, there is an increase of agglomeration of polymolybdate species.

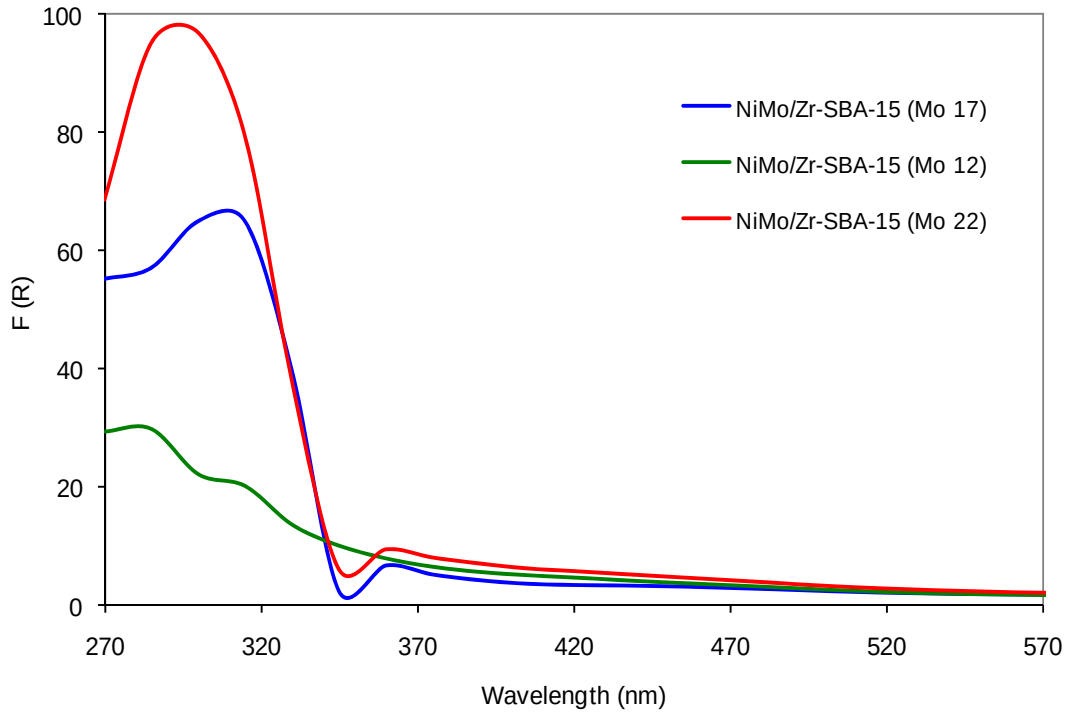

Figure 5.11. UV-DRS comparison for NiMo/Zr-SBA-15 catalysts with varying metal loading.

5.2.8 High Resolution Transmission Electron Microscopy (HRTEM)

HRTEM study is effective for getting information about the dispersion of the activated catalysts (Gutiérrez et al., 2007). Figure 5.12 represents the obtained HRTEM micrograph of sulfided NiMo/SBA-15 and NiMo/Zr-SBA-15 catalysts with varying Mo loading. In the sulfide catalyst typical fringes due to MoS_2 crystallites with 6.1 Å interplanar distances are observed. The number of stacking layers in NiMo sulfide catalyst supported on pure SBA-15 support is observed as 2-8 layers MoS_2 particles with length 40 – 90 Å, which provides inhomogeneous distribution of slab over the SBA-15 support (Gutiérrez et al., 2006a). On the other hand, for the NiMo/Zr-SBA-15 catalyst with Mo loading of 12 wt% and 17 wt%, the smaller size MoS_2 slabs are homogeneously distributed over the Zr-SBA-15 supports. However, an increase in MoO_3 loading results in worse dispersion of active phase due to increase in MoS_2 length and layers. Among all

catalysts, NiMo/Zr-SBA-15 (Mo 17) catalyst with MoS_2 length 20-40 Å and stacking layers of 2-4 shows excellent dispersion of active phase.

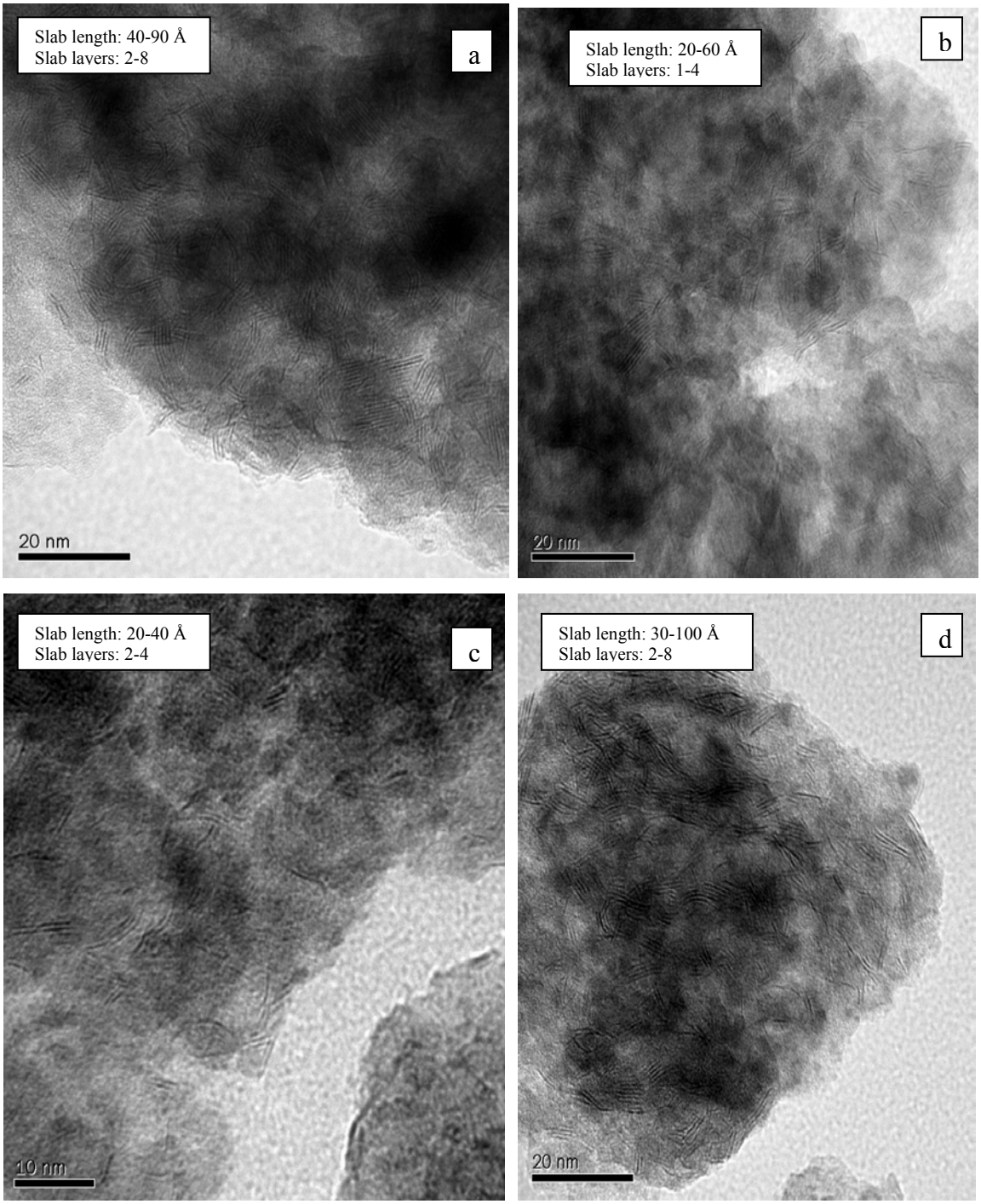

Fig 5.12. HRTEM micrograph of sulfided NiMo/SBA-15 (a), NiMo/Zr-SBA-15 (Mo 12) (b); NiMo/Zr-SBA-15 (Mo17) (c) and NiMo/Zr-SBA-15 (Mo 22) (d) catalysts

5.3 Catalytic Activity Performance Based on HDS and HDN

In the phase II, the performance of all catalysts was evaluated based on HDS and HDN activity exhibited during hydrotreatment of heavy gas oil (HGO) derived from Athabasca bitumen. All Zr-SBA-15 supported NiMo catalysts exhibited higher activity compared to the NiMo catalyst supported on SBA-15 support, implying that the metal loading improves the dispersion of Mo over support (Figure 5.13). For Zr-SBA-15 supported NiMo catalysts, increase in HDS and HDN activities were observed when the Mo loading was increased from 12 wt% to 17 wt% (Mo/Ni mass ratio of 5). This can be attributed to the better textural characteristics, better dispersion of active metal and higher acidity of NiMo/Zr-SBA-15 catalysts. However, a further increase in Mo loading up to 22 wt% led to a decrease in the HDS and HDN activity. This shows that the 17 wt% is the optimum Mo loading on Zr-SBA-15 support, which gives the highest catalytic activity. This trend may be attributed to the variation of dispersion of Mo active species over the support material. The Mo species may be well-dispersed on the support material up to 17 wt% of loading. The agglomeration of Mo species occurs at the higher metal loading, which causes the reduction in catalytic activities. The hydrotreating activity comparison of best catalyst, NiMo/Zr-SBA-15 (Mo 17) was compared with the commercial catalyst on weight basis (i.e. 2 gm catalyst) (Figure 5.14) and volume basis (i.e. 5 ml catalyst) (Figure 5.15). On weight basis, the optimum catalyst showed higher activity compared to that of the commercial catalyst. However, on volume basis, the commercial catalyst exhibited higher activity.

Also, the simulated distillation comparison of feed and product obtained by hydrotreating of HGO over optimum catalyst is shown in Figure 5.16. From the figure it is evident that the production of lighter cut is obtained due to mild cracking of the HGO. However, from the overall distribution of heavier cut of feed and heavy material, it is clear that the significant hydrocracking has not occurred during the hydrotreating of HGO by NiMo/Zr-SBA-15 (Mo 17) catalyst.

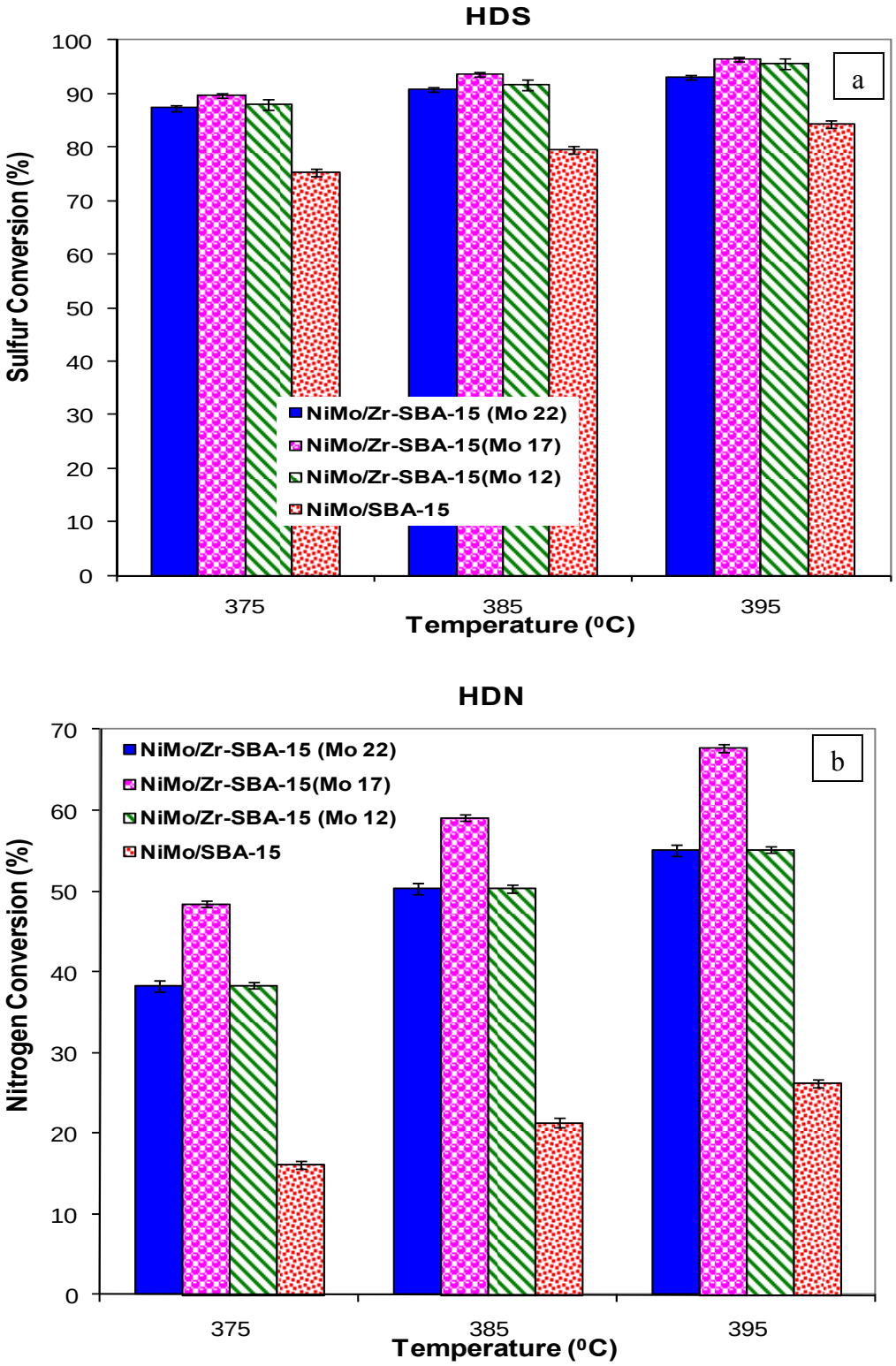

Figure 5.13. The hydrodesulfurization and hydrodenitrogenation activity (volume basis) study of NiMo/SBA-15 and NiMo/Zr-SBA-15 catalysts with varying metal loading, T = 375/385/395 °C, P=8.9MPa, LHSV = 1 h^{-1}, H_2/HC ratio 600 Nm^3/m^3. HDS (a); HDN (b)

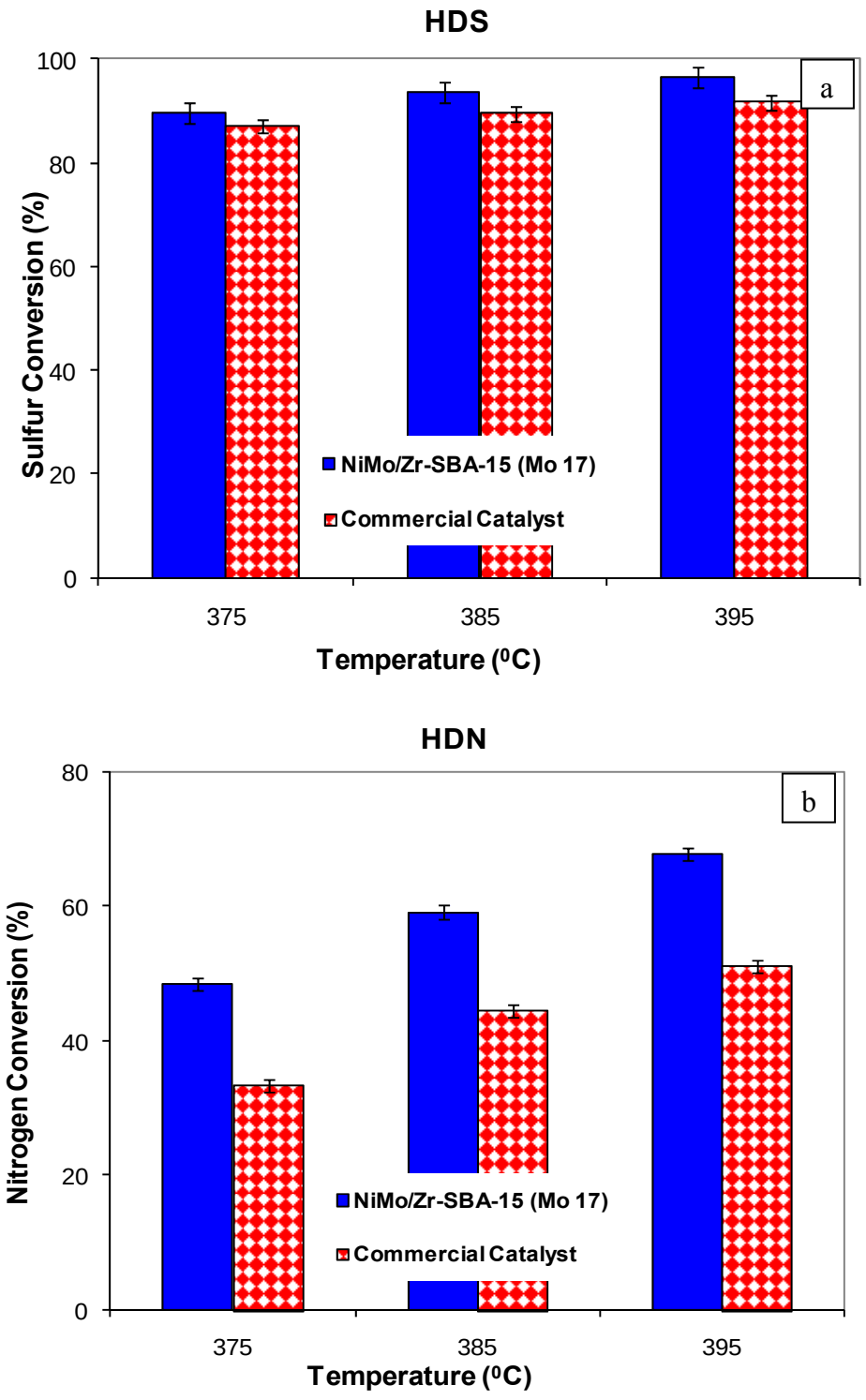

Figure 5.14. Hydrotreating activity (weight basis) comparison of NiMo/Zr-SBA-15 (Mo 17) and commercial catalysts; T = 375/385/395 °C, P=8.9 MPa, LHSV = 1 h^{-1}, H_2/HC ratio 600 Nm^3/m^3. HDS (a); HDN (b).

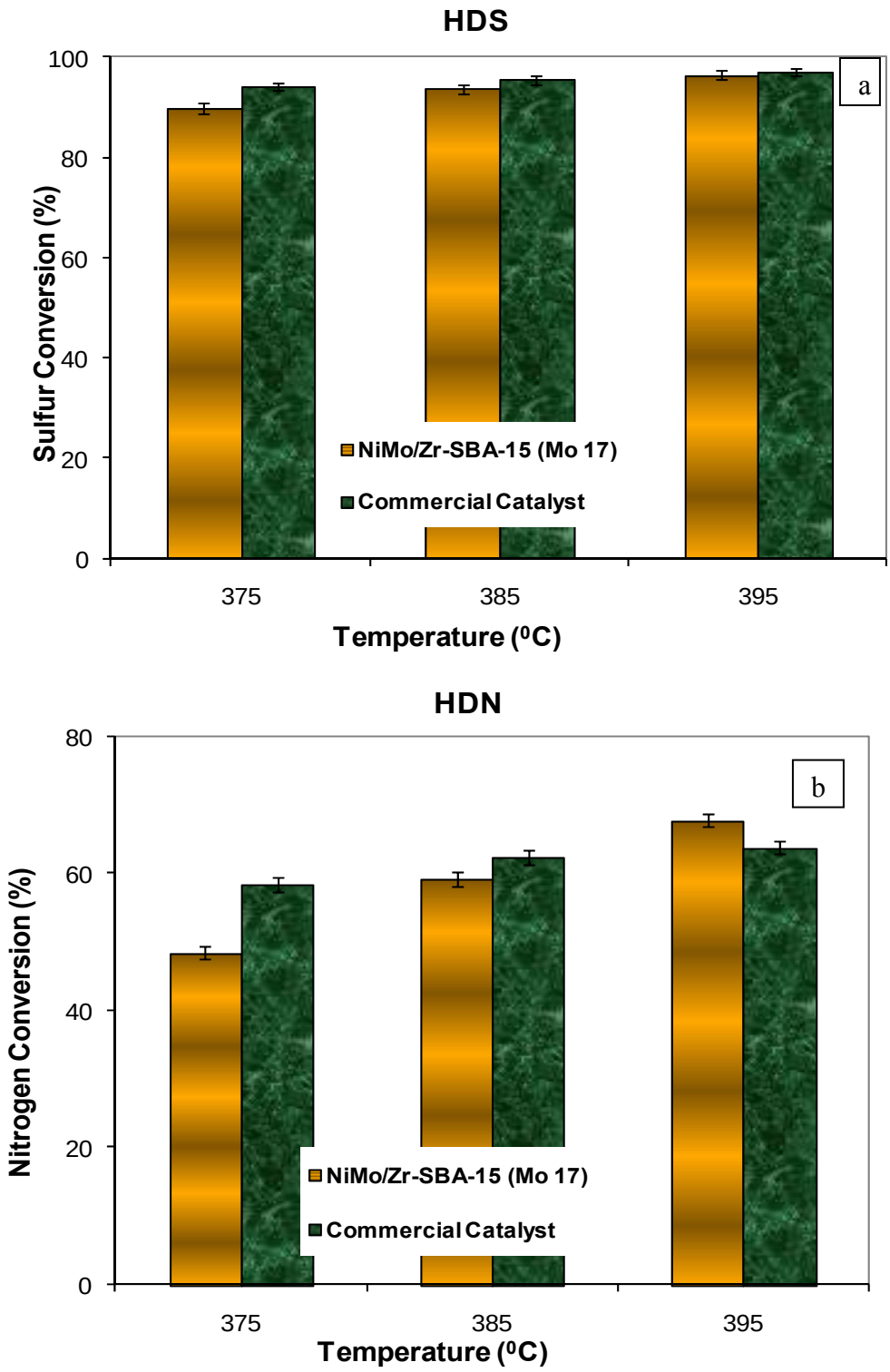

Figure 5.15. Hydrotreating activity (volume basis) comparison of NiMo/Zr-SBA-15 (Mo 17) and commercial catalysts; T = 375/385/395 °C, P=8.9 MPa, LHSV = 1 h^{-1}, H_2/HC ratio 600 Nm^3/m^3. HDS (a); HDN (b).

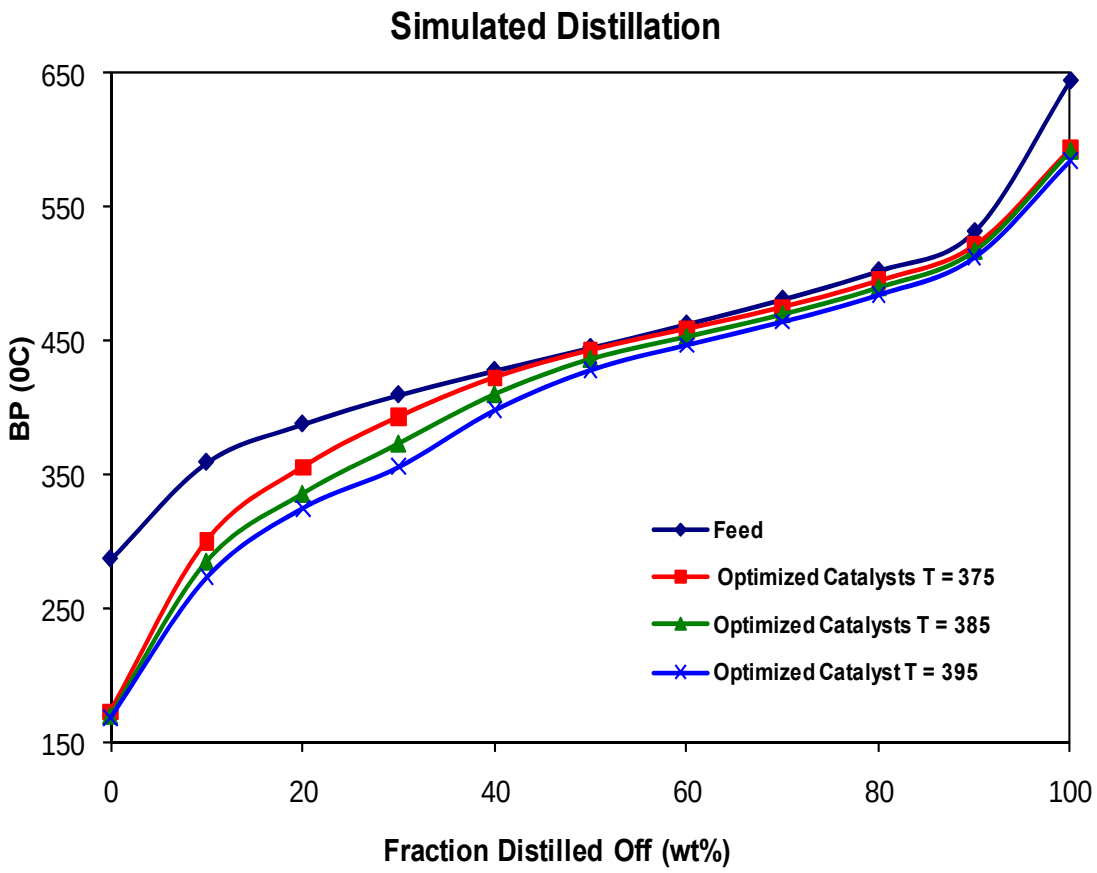

Figure 5.16. The simulated distillation of HGO feed and the product obtained by hydrotreating of HGO over optimized NiMo/Zr-SBA-15 (Mo 17) catalyst.

CHAPTER 6
KINETIC STUDY OF HDS AND HDN

This chapter describes the effect of reaction condition and kinetic study of HDS and HDN reaction over the optimized catalyst. Kinetic expression for the HDS and HDN over optimized NiMo/Zr-SBA-15 catalyst is expressed based on Power law model and Langmuir –Hinshelwood model. Also, this chapter illustrates the catalyst stability study performed on best catalyst. Furthermore, characterization of spent catalyst is explained in this section.

6.1 Effect of Reaction Condition on HDS/HDN over Optimized Catalyst

6.1.1 Effect of Temperature

The effect of temperature on the HDS and HDN activity for NiMo/Zr-SBA-15 catalyst was studied in the range of 375 to 395 °C while keeping pressure at 8.9 MPa, gas/oil ratio at 600 Nm^3/m^3 and varying LHSV value from 0.5 to 2.0 hr^{-1}. The results on the effect of temperature on HDS reaction are shown in Figure 6.1a. It is seen from the figure that as the temperature is increased, the percent of sulfur conversion increases. The sulfur conversion is higher at lower temperature range (375-385 °C) as compared to that at higher temperature (385-395 °C). The reaction temperature affects both the direct desulfurization (DDS) and hydrogenation (HYD) routes significantly during desulfurization of refractory compounds, such as 4,6-DMDBT. At lower temperature 4,6-DMDBT is easily transformed into hydrogenated product, which results into higher activity at lower temperature rather than very high temperature (Xu et al., 2004). In the present study, the sulfur conversion increases from 94.6% to 97.0% at LHSV 0.5 hr^{-1},

89.3 to 92.3 at LHSV 1.0 hr^{-1} and 83.3% to 89.2% at LHSV 1.5 hr^{-1} with increase in temperature from 375 to 385 °C. Similar trend is observed at different LHSV values for an increasing temperature from 385 to 395 °C. Therefore, a maximum sulfur conversion of 97.8 wt% can be achieved at temperature 395 °C, LHSV 0.5 hr^{-1}, pressure 8.9 MPa, and H_2/GO ratio 600 Nm^3/m^3 for hydrodesulfurization of HGO using NiMo/Zr-SBA-15 catalyst.

The result of temperature effect on HDN reaction is shown in Figure 6.1b. As the temperature is increased, the percentage of nitrogen conversion increases similar to sulfur conversion. However, the nitrogen conversion is quite significant compared to the sulfur conversion upon temperature increase. Also, nitrogen conversion is higher in the lower range of temperature as compared to that at higher range of temperature. Nitrogen conversion increases from 62.6 to 79.3 for LHSV 0.5 hr^{-1}, 48.6 to 57.7 for LHSV 1.0 hr^{-1} and 37.0 to 47.9 89.2 for LHSV 1.5 hr^{-1} while increasing temperature from 375 to 385 °C. A similar trend is observed at different LHSV values for an increasing temperature from 385 to 395 °C. Therefore, a maximum nitrogen conversion of 91.4 wt% can be achieved at temperature 395 °C, LHSV 0.5 8.9 MPa, and H_2/GO ratio 600 Nm^3/m^3 for hydrodenitrogenation of HGO using NiMo/Zr-SBA-15 catalyst.

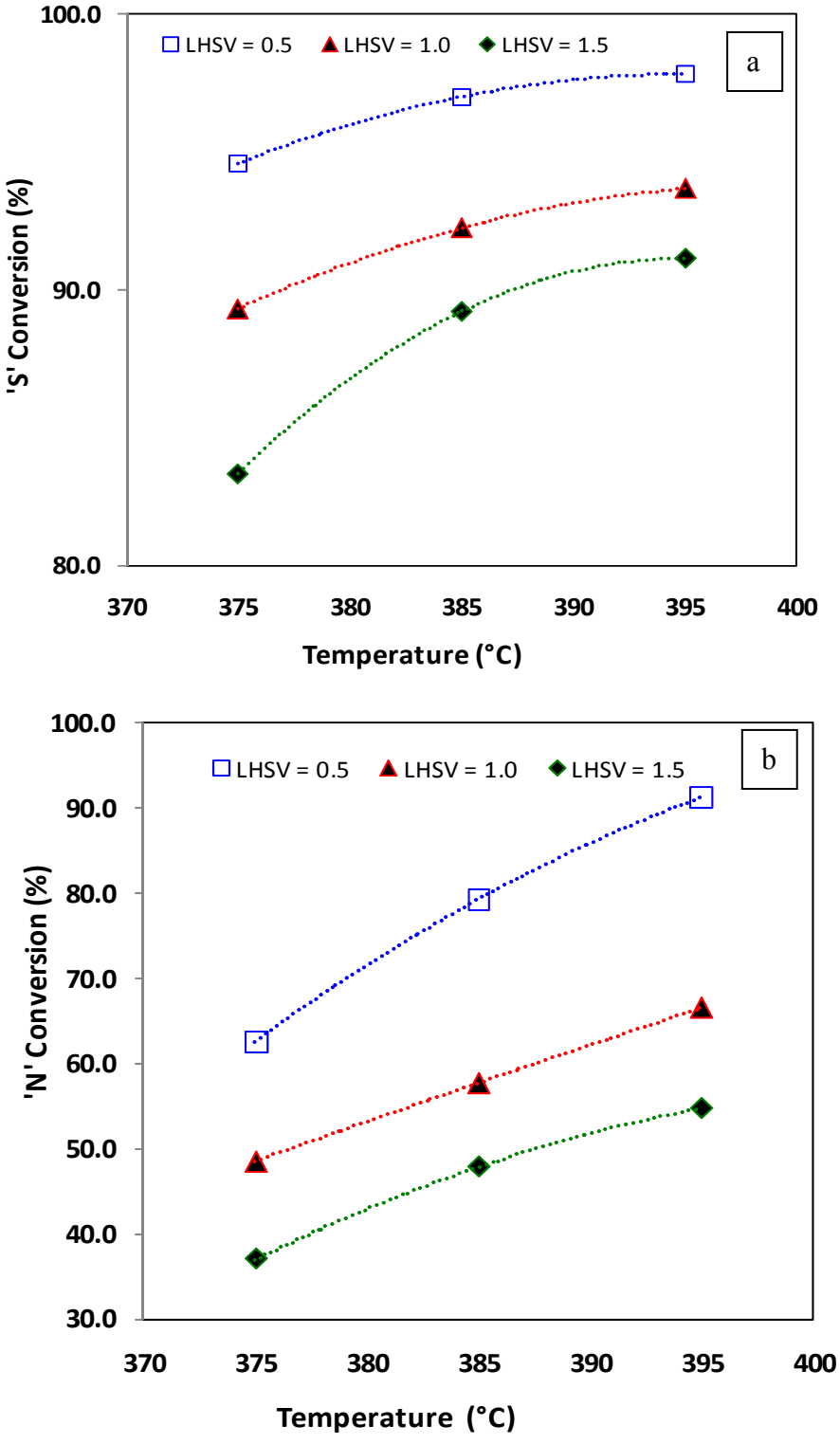

Figure 6.1: Effect of temperature on the conversion of sulfur and nitrogen present in heavy gas oil at pressure 8.9 MPa, and hydrogen/gas oil ratio 600 Nm^3/m^3; HDS (a), HDN (b).

6.1.2 Effect of LHSV

The effect of liquid hourly space velocity (LHSV) on the HDS and HDN of heavy gas oil was studied in the LHSV range from 0.5 to 1.5 h^{-1} and varying temperature from 375 °C to 395 °C, while keeping pressure at 8.9 MPa and a hydrogen/heavy gas oil volumetric ratio at 600 Nm^3/m^3. The effect of LHSV on HDS conversion is shown in Figure 6.2a. As the LHSV of heavy gas oil is decreased, the HDS conversion is increased due to increase in the contact time of the liquid with the catalyst. Also, at lower space velocity and lower temperatures allows us to achieve a high conversion of sulfur compounds where this equilibrium limitation is less pronounced. At present study highest sulfur conversion was observed at LHSV of 0.5 hr^{-1} and temperature of 395 °C. Similar observation can be made for the HDN conversion also (Figure 6.2b). Decrease of LHSV results in increase of nitrogen conversion. In this study highest nitrogen conversion of 91.4 wt% was observed at LHSV of 0.5 hr^{-1}, temperature of 395 °C, pressure 8.9 MPa, and gas/oil ratio 600 Nm^3/m^3.

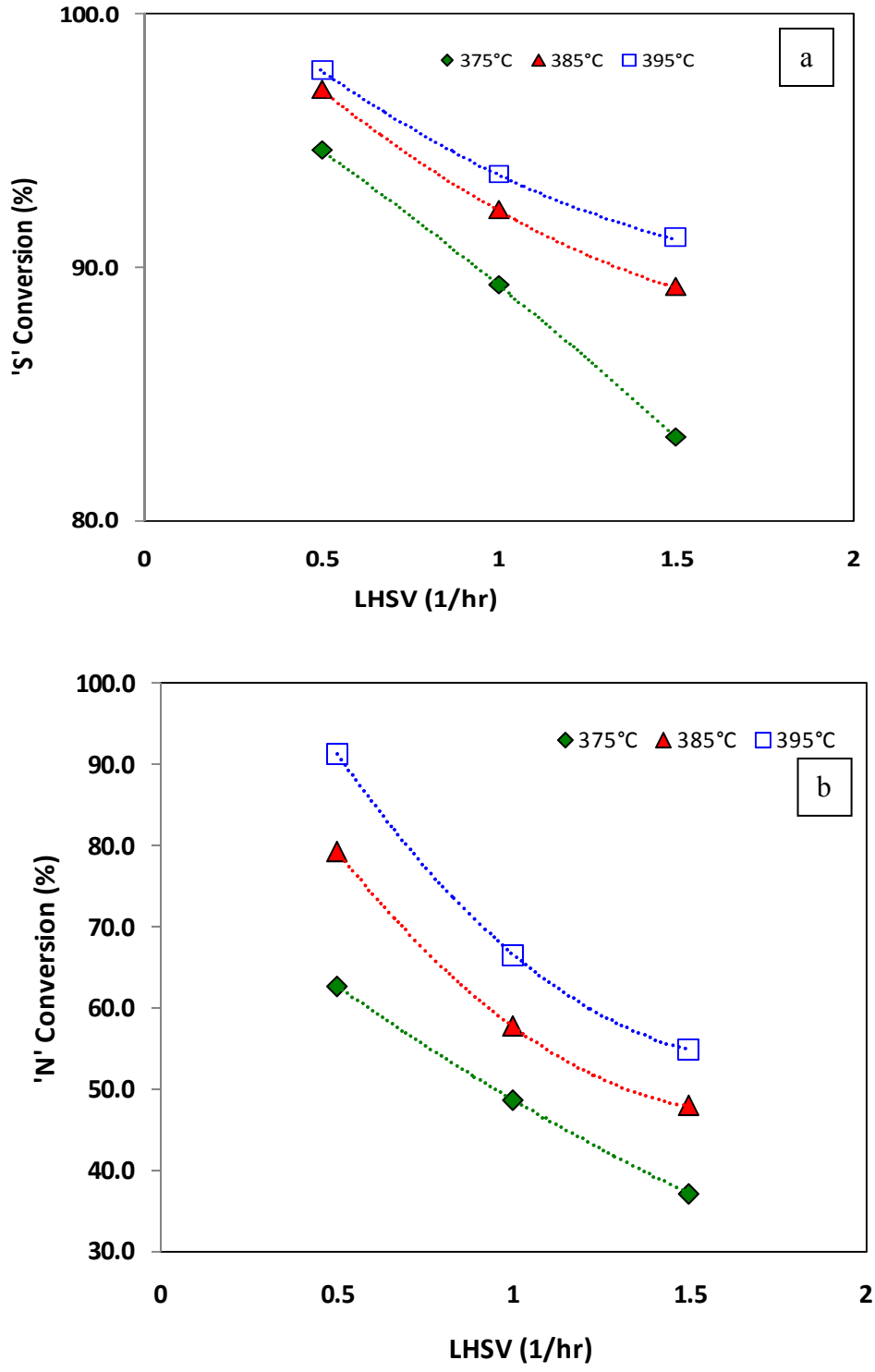

Figure 6.2: Effect of LHSV on the conversion of sulfur and nitrogen present in heavy gas oil at pressure = 8.9 MPa, and hydrogen/gas oil ratio = 600 Nm^3/m^3; HDS (a), HDN (b).

6.1.3 Effect of Pressure

The effects of reaction pressure on the HDS and HDN activities of optimized NiMo/Zr-SBA-15 catalyst were studied at three different pressure levels, namely at 7.9, 8.9 and 9.9 MPa, while keeping temperature, LHSV and gas/oil ratio at 385 °C, 1.0 h^{-1} and 600 Nm^3/m^3, respectively. The effects of pressure on HDS conversion is presented in Figure 6.3a. It can be observed from the figure that the effect of pressure on HDS of HGO was not very significant. Upon increase in pressure from 7.9 MPa to 8.9 MPa, sulfur conversion increases from 91.8 wt% to 92.3 wt% and with the increase of pressure from 8.9 MPa to 9.9 MPa, sulfur conversion increases from 92.3% to 93.2%. It can also be observed that an increase in pressure from 8.9 MPa to 9.9 MPa shows comparatively higher increase in sulfur conversions than that with the increase in pressure 7.9 to 8.9 MPa i.e. at higher pressure range the sulfur conversion is higher than that at lower pressure range. This trend is observed for the NiMo/Zr-SBA-15 catalyst because of the hydrodesulfurization of refractory molecules, such as 4,6-DMDBT, via a hydrogenation route which requires higher hydrogen pressure (Tanaka et al., 2003). Hence, increase in pressure results in increase in desulfurization of refractory molecules through hydrogenation route and thus increased catalytic activity.

Figures 6.3b represents the nitrogen conversions in the pressure range investigated. Upon the increase in pressure, nitrogen conversion is significantly higher compared to the sulfur conversion. This trend is observed due to following reasons: i) at sufficient hydrogen pressure there might be the profound effect of competitive adsorption of nitrogen compounds or ii) due to reversibility of conversion of refractory sulfur compounds such as 4,6 DMDBT at higher pressure (Topsøe et al., 1996). Upon increase of pressure from 7.9 MPa to 8.9 MPa, nitrogen conversion increases from 52.5 to 57.7 wt% and with the increase of pressure from 8.9 MPa to 9.9 MPa, nitrogen conversion

increases from 57.7 to 63.4 wt%. This might be because HDN proceeds through hydrogenation of the aromatic ring which is strongly influenced by the hydrogen partial pressure (Topsøe et al., 1996).

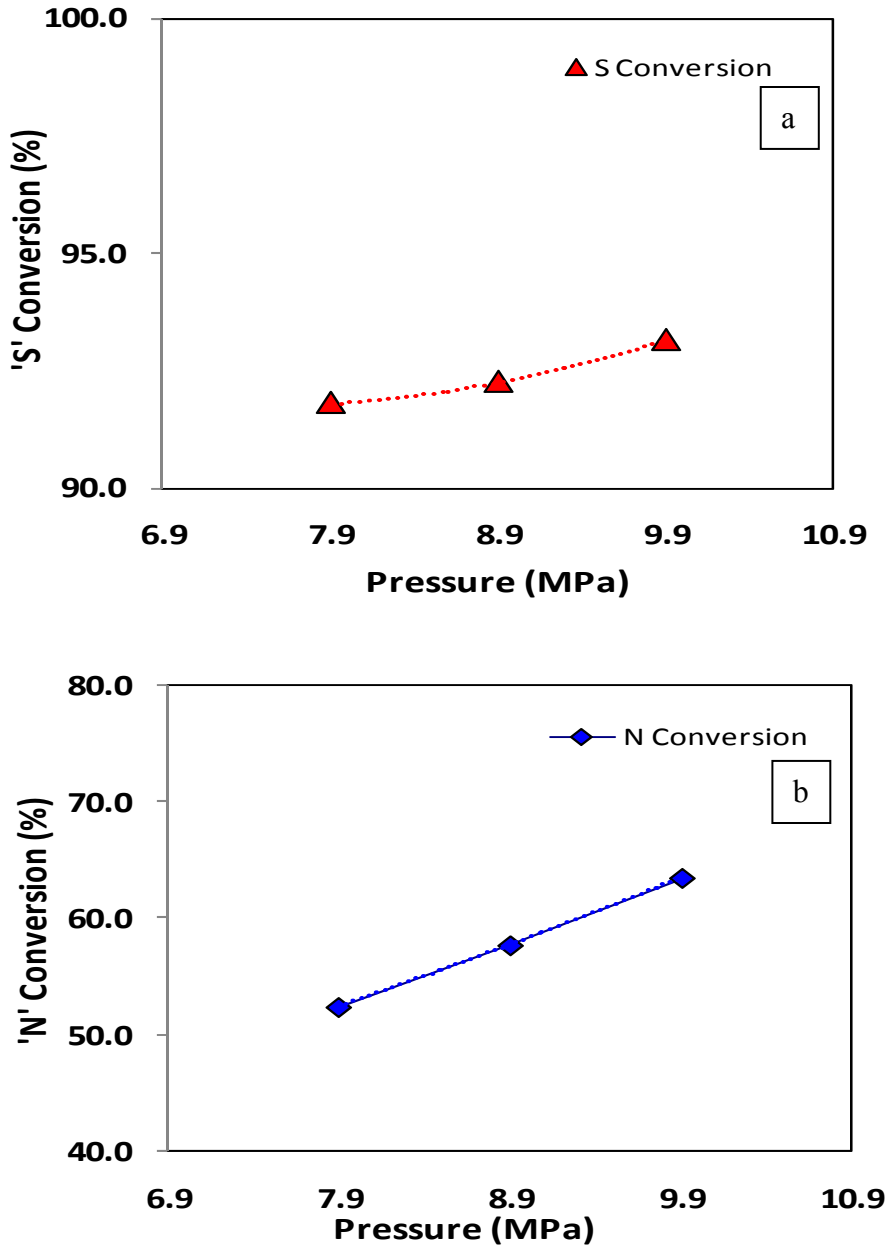

Figure 6.3: Effect of pressure on the conversion of sulfur and nitrogen present in heavy gas oil at temperature = 385 °C, LHSV = 1 hr^{-1}, and hydrogen/gas oil ratio = 600 Nm^3/m^3; HDS (a), HDN (b).

6.1.4 Effect of Hydrogen Gas/Oil Ratio

The effect of the hydrogen/heavy gas oil volumetric ratio on the conversion HDS and HDN was studied out by changing its value in the range from 400 to 800 Nm^3/m^3 while keeping temperature, pressure, and LHSV, at 385 °C, 8.9 MPa, and 1.0 h^{-1}, respectively. The effects of the gas/oil ratio on HDS and HDN are presented in Figure 6.4. It is evident from the figure that there is increase of HDS and HDN activity due to increase in hydrogen/gas oil ratio. For example, as the hydrogen/heavy gas oil ratio is increased from 400 to 600 Nm^3/m^3, the sulfur conversion increases from 90.3 to 92.3 wt% and N conversion increases from 55.5 to 57.7 wt%. For the increase in gas/oil ratio from 600 to 800 Nm^3/m^3, sulfur conversion increase from 92.3 to 93.9 wt% and nitrogen conversion increases from 57.7 to 59.5 wt%. Beyond gas/oil ratio of 800 Nm^3/m^3, both HDS and HDN conversions are not significant and the conversion becomes constant.

The effects of temperature, pressure, LHSV and H_2/GO ratio on sulfur and nitrogen conversion of HGO with optimized catalyst is shown in Table 6.1.

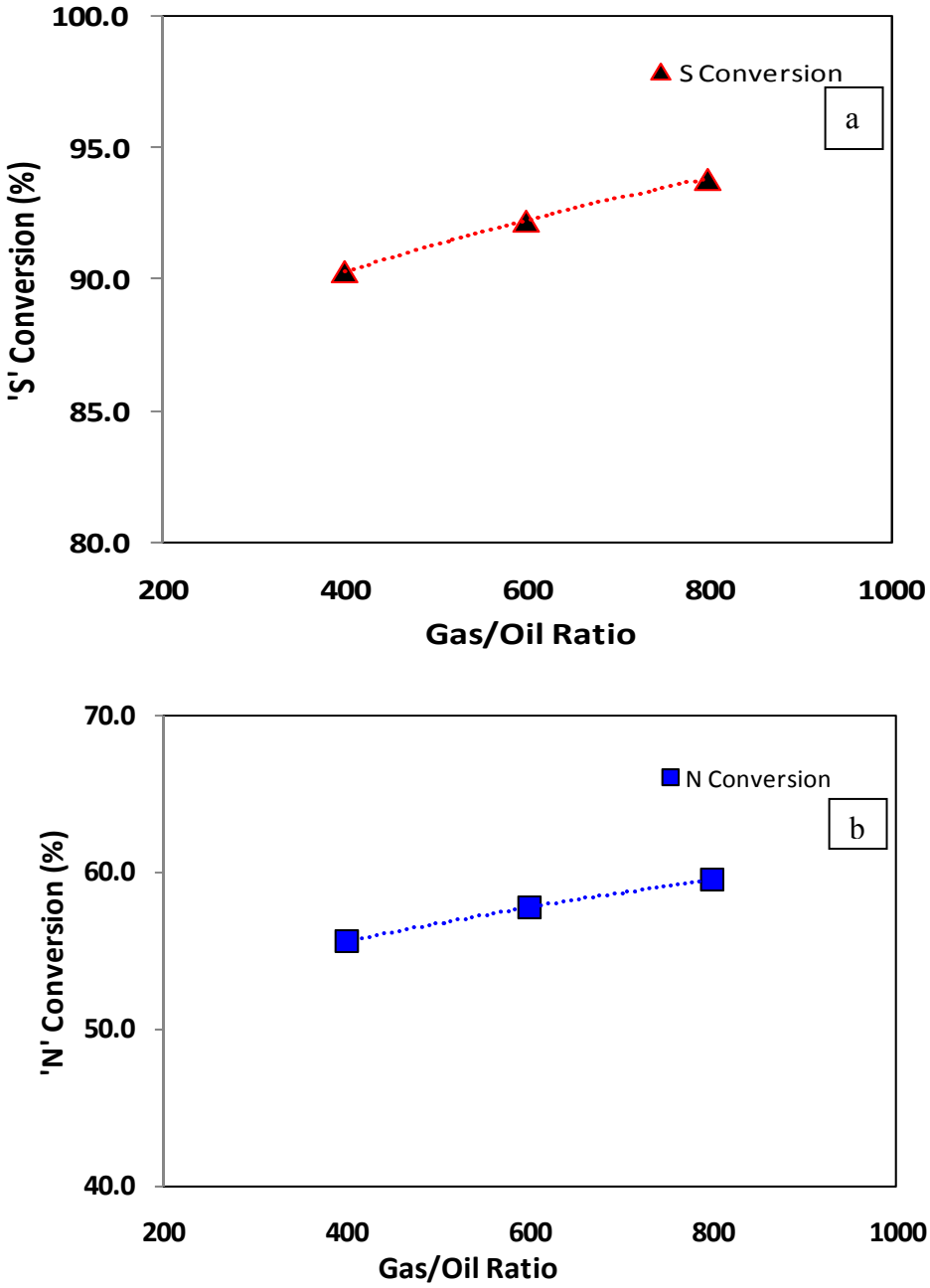

Figure 6.4: Effect of hydrogen/gas oil ratio on the conversion of sulfur and nitrogen present in heavy gas oil at temperature = 385 °C, LHSV = 1 hr^{-1}, pressure =8.9 MPa, HDS (a), HDN (b).

Table 6.1: Effect of temperature, pressure, LHSV and H_2/gas oil ratio on sulfur and nitrogen conversion for HGO with optimized catalyst.

T (°C)	P (Mpa)	LHSV (hr^{-1})	H_2/GO (Nm^3/m^3)	S Conversion wt%	N Conversion wt%
375	8.9	0.5	600	94.6	62.7
375	8.9	0.5	600	94.7	62.5
375	8.9	1	600	89.3	48.6
375	8.9	1	600	89.4	48.6
375	8.9	1.5	600	83.3	37.0
375	8.9	1.5	600	82.6	37.0
385	8.9	0.5	600	97.1	79.7
385	8.9	0.5	600	96.9	78.9
385	8.9	1	600	92.7	57.3
385	8.9	1	600	91.9	58.1
385	8.9	1.5	600	89.1	48.2
385	8.9	1.5	600	90.4	47.6
395	8.9	0.5	600	97.9	91.0
395	8.9	0.5	600	97.8	91.7
395	8.9	1	600	93.6	66.2
395	8.9	1	600	93.8	66.8

T (°C)	P (Mpa)	LHSV (hr^{-1})	H_2/GO (Nm^3/m^3)	S Conversion wt%	N Conversion wt%
395	8.9	1.5	600	90.8	55.3
395	8.9	1.5	600	91.5	54.3
385	8.9	1	800	93.9	59.7
385	8.9	1	800	93.8	59.3
385	8.9	1	400	90.0	55.3
385	8.9	1	400	90.1	55.2
385	7.9	1	600	91.7	52.9
385	7.9	1	600	91.9	52.0
385	9.9	1	600	93.8	63.0
385	9.9	1	600	92.5	63.9
370	8.9	1	600	86.7	31.0
370	8.9	1	600	89.3	43.9
370	8.9	1	600	87.5	42.5
370	8.9	1	600	87.1	42.4
370	8.9	1	600	87.7	42.8
370	8.9	1	600	86.6	41.8

6.2 Kinetic Study of HDS/HDN for the Optimum NiMo/Zr-SBA-15 Catalyst

The kinetic analysis was performed to study the effects of reaction parameters on the HDS and HDN activities over NiMo/Zr-SBA-15 (optimum with 17 wt% loading) catalyst and to investigate the effects of mass transfer limitation on the HDS and HDN reactions using micro scale trickle bed reactor. Based on these information, kinetic models were developed to predict the hydrotreating activities of the NiMo/Zr-SBA-15 catalyst exhibited during hydrotreating reaction. The following assumptions were made for the kinetic analysis:

- Trickle bed microreactor operations were considered as steady state isothermal and plug flow (Mann et al., 1988).
- The effects of H_2S and NH_3 concentrations on both the mass transfer resistance and hydrotreating activities were considered negligible (Korsten and Hoffmann, 1996).
- Axial dispersion and wall effects were neglected due to dilution of the catalyst bed with nonporous, inert particles during experimental run (Bej et al., 2000).
- Complete wetting of catalyst.

The heavy gas oil derived from Athabasca bitumen was selected as feed for kinetic study. The properties of the HGO feedstock are shown in Table 3.2. The calculation methods for molar product concentration of sulfur and nitrogen and reaction rates of HDS and HDN are presented in Appendix A. Calculation of product concentration for HDS and HDN conversion obtained from kinetic study is presented in Appendix B.

6.2.1 Evaluation of Hydrodynamic Parameters

The micro scale trickle bed reactor consists of a fixed catalyst bed in which the liquid and reacting gas hydrogen flow concurrently downward over the catalyst bed (Satterfield et al., 1969). In order to avoid deviation from ideal plug flow for the micro-scale trickle bed reactor using real feedstock over commercial size catalyst, several recommendations have been made by many authors (Bej et al., 2001a; Bej et al., 2001b; Gierman, 1988; Sie, 1999). Some of the recommendations were considered for the performing hydrotreating reaction in the trickle bed micro reactor. In order to evaluate the performance of the micro-scale reactor and hydrodynamic of the reactor, the estimation of parameters such as Péclet number, wall effect, wetting, back mixing and axial dispersion are essential (Ramírez et al., 2004). In order to investigate the plug flow behavior and evaluate the reactor performance, following hydrodynamic parameters were estimated at different operating conditions (Table 6.2).

Table 6.2: Hydrodynamic parameter evaluation for plug flow, wall effect, wetting and back-mixing.

Conditions	Undiluted	Diluted
Parameters		
Particle size (d_p), cm	0.17	0.0185
Reactor Dia. (D_b), cm	1.0	1.0
Total bed length (L), cm	6.37	21.66
L/d_p ratio	37.47	1171
D_b/d_p ratio	5.9	54.1
Deviation from plug flow	Exist	Not exist
Presence of wall effect	Present	Eliminated
Effective catalyst wetting	Not ensured	Ensured
Presence of back mixing	Present	Not present

6.2.2 Mass Transfer Resistances for the HDS and HDN

In trickle bed reactor, the conversion depends on both reaction kinetics and transport processes. For the hydrotreating reaction in trickle bed, the reaction rate is greatly influenced by various transport properties such as flow dynamics, mass transfer, and heat transfer (Ancheyta et al., 2002a). In the trickle bed reactor, where chemical reaction takes place in porous catalyst, the following mass transfer resistances are observed during transport of reacting molecules from bulk phase to the active sites of the catalyst (Bej et al., 2001a):

- from bulk gas to gas-liquid interface,
- from gas-liquid interface to bulk liquid,
- from bulk liquid to external catalyst surface
- intra-particle diffusion

Among all these resistances, resistance due to intra-particle is the predominant one (Sie and Krishna., 1998). The effects of these diffusion limitations can be significant which can affect the reported kinetic-quality data and inaccuracy in kinetic parameters estimation (Ancheyta et al., 2002b). Hence, it is imperative to evaluate the mass transfer limitation and their influence on the HDS and HDN reaction inside the trickle bed reactor. The mass transfer evaluation includes: external mass transfer resistance and internal mass transfer resistance.

External Mass Transfer Resistance for HDS and HDN:

External mass transfer resistance is observed during diffusion of hydrogen (gas phase) from gas oil (liquid phase) exterior to the catalyst external surface. External mass transfer limitation was evaluated for NiMo/Zr-SBA-15 catalyst to determine their

influence on the result on kinetic study. The external mass transfer resistance was evaluated with the Satterfield criteria (Satterfield et al., 1969). This criterion checks whether the rate of diffusion of hydrogen from bulk phase to the catalyst surface is the rate limiting step. The detailed calculation is presented in Appendix C. In order to determine whether the mass transfer is the predominant in the reaction set up, the value of the left hand side of the Satterfield criteria needs to be at least 10 times larger than the value of the right hand side (Korsten and Hoffmann, 1996). In the present study, the value of the left hand side was evaluated for both HDS and HDN reactions at all the temperature of the kinetic studies (375-395 °C).

As per the calculation, for the hydrodesulfurization, the values of LHS of Satterfield criteria were higher than the RHS value. Hence, it can be concluded that, for the HDS reaction mass transfer limitation exists. However, in case of hydrodenitrogenation reaction, at lower conversion (low temperature and higher LHSV) level, LHS values of Satterfield criteria were lower than the RHS value. This implies that the mass transfer limitation for the HDN reaction is negligible at lower conversion level. However, at higher conversion level (higher temperature and lower LHSV), most of the data satisfied the Satterfield criteria, implying that at higher conversion level mass transfer limitation exits. Furthermore, it is observed that the hydrogen consumption for HDS reaction is higher than that for HDN reaction. This trend is attributed to the presence of the high concentration of the sulfur compounds in the HGO feedstock.

Internal Mass Transfer Resistance for HDS and HDN:

In kinetic study, the presence of the internal mass transfer causes the reduction of the catalyst effectiveness and reduces the catalytic activity of the catalyst. Hence, it is

imperative to eliminate the internal mass transfer limitations, as these lead to erroneous kinetic data. Internal mass transfer limitation, i.e. pore diffusion limitation consists of the diffusion of reactants into the catalyst pores.

For the catalytic reaction, catalyst active sites should be accessible to reactants and reaction products should leave the catalyst pores easily. The effectiveness factor ***(η)*** is defined as the ratio of actual reaction rate with pore diffusion limitation and rate of reaction with surface conditions in which same sites are accessible without any diffusion limitations (Fogler, 2006). The value of catalyst effectiveness factor is valid only for isothermal condition. On the other hand, thermal conductivity limitation results in temperature gradient within the catalyst pellet (Froment G.F. and Bischoff K.B., 1990). Hence, for the calculation of internal mass transfer resistance, it is imperative to evaluate isothermality of the cross-section of the catalyst pellet. Isothermality of the catalyst pellet can be checked by two methods: A) calculating the highest temperature rise between the catalyst pellet core and surface of the pellet (Fogler, 2006) and B) Anderson's criteria (Anderson, 1963). The details of internal mass transfer analysis are presented in Appendix D.

β is defined as the ratio of maximum temperature difference that exists in the catalyst pellet core and catalyst surface and catalyst surface temperature [$\Delta T_{max} = (T_{max} - T_S)/T_S$]. β is calculated in order to estimate the temperature rise in the catalyst pellet due to the reaction. As per the calculation the value of β is 0.000003. Hence, it can be assumed that the catalyst pellet is isothermal. In order to confirm this assumption, another method, the Anderson criteria was adopted. Anderson criterion was based on the comparison between the rate of heat generation from the reaction inside the catalyst pellet

and rate of heat removal by conduction and convection. According to the calculation, the right side of the criterion was found to be far greater than the left side for both reactions; $\times 10^5$ greater in magnitude for HDS and $\times 10^7$ greater in magnitude for HDN. Hence, it can be concluded that isothermal behavior of the NiMo/Zr-SBA-15 catalyst is acceptable.

The dimensionless term, Thiele modulus ***(ϕ)*** determines whether the internal diffusion limits the overall rate of reaction or the surface reaction limits the reaction rates (Fogler, 2006). Thiele modulus is defined as ratio of intrinsic reaction rate in the absence of mass transfer limitation to the rate of diffusion through the pellet (Hill and Hill, 1977). For the calculation of effectiveness factor the value of Thiele modulus is essential, which requires the intrinsic reaction rate. However, it is difficult to determine the intrinsic reaction rate in the presence of the external mass transfer resistance. The modulus ***(ϕ)*** and effectiveness factor ***(η)*** were evaluated for HDS and HDN at the both inlet and outlet of the reactor. The results are shown in Table D.2 and Table D.3.

The values of Φ for HDS reactions were in the range of 0.791 to 2.42 at the reactor inlet and 13.09 to 37.26 at the reactor outlet. From the trend it can be observed that Φ increases over the length of the reactor from inlet to outlet. The ***η*** values estimated in the range of 0.851 to 0.948 at the reactor inlet and 0.207 to 0.455 at the reactor outlet. Furthermore, lower η values were observed at reactor outlet especially at higher temperature and lower LHSV. This implies that diffusion limitation in the catalyst pellets is quite significant at lower sulfur concentration.

The values of Φ for HDN reactions were in the range of 0.60 to 1.3 at the reactor inlet and 0.9 to 8.9 at the reactor outlet. It is observed that that Φ increases over the length of the reactor from inlet to outlet. The ***η*** values estimated in the range of 0.91 to

1.00 at the reactor inlet and 0.56 to 0.94 at the reactor outlet. In most of the cases, the value of η estimated are higher than 0.9, implying that the most of the HDN reactions are not significantly affected by internal mass transfer diffusion. However, at higher HDN conversion level (at higher temperature and lower LHSV) internal mass transfer limitations for the HDN cannot be neglected.

From the mass transfer studies, it can be concluded that the reaction rate equation for HDS reaction is extrinsic (i.e. both external and internal mass transfer limitations are present), whereas the reaction rate equation for HDN is intrinsic in most cases (i.e. no significant external and internal mass transfer limitations are present).

6.2.3 Hydrodesulfurization and Hydrodenitrogenation Rate kinetics

The following assumptions are considered to develop the rate models:

- The HDS and HDN reactions are irreversible under the operating condition (Girgis and Gates, 1991)
- The rate equations follow the Power law and Langmuir-Hinshelwood model
- The effect of hydrocracking reactions on HDS and HDN is negligible

Power law and Langmuir-Hinshelwood models were used to express the kinetic parameters that satisfactorily describe the experimental data and predict the performance of hydrotreating reactor.

6.2.4 Power Law Model

The removal of sulfur and nitrogen compounds from heavy gas oil can be described by simple Power law model. The rate expressions for HDS and HDN were fitted using non-linear regression analysis. The value of activation energy (E) and pre-exponential

constant (A) for HDS and HDN was calculated using linear regression. POLYMATH^{TM} software was employed to perform the regression analysis. The values of the determined parameters of Power law for HDS and HDN reactions are presented in Table 6.3.

The value of reaction order, n, depends on the boiling range of the feedstock and types of sulfur and nitrogen compounds present in the feed. In terms of Power law models, heavy gas oil can have HDS reaction order ranging from 1.0 to 2.5, while HDN reaction order ranges from 1.0 to 2.0 (Ferdous et al., 2006b; Mapiour et al., 2010a). The reaction order found from power law modeling for the hydrotreating activity study of NiMo/Zr-SBA-15 catalyst on HGO [reaction order for HDS – 1.8 and reaction order for HDN – 1.3] appears to be in good agreement with the reported values in the literature (Table 2.16).

The values of activation energies for the HDS and HDN conversion calculated from power law models are 115 kJ/mol and 121 kJ/mol, respectively. These values are comparable to the previous reported values (Table 2.16). Higher activation energy determined for the HDN reaction compared to the HDS reaction, implies the difficultly of removal of nitrogen compounds present in the heavy gas oil by NiMo/Zr-SBA-15 catalyst compared to that of removal of sulfur compounds. Similar trend is reported for the hydrotreatment of Athabasca bitumen derived heavy gas oil using NiMo/zeolite-alumina-silica catalyst (Diaz-Real et al., 1993; Mann et al., 1988). The value of coefficient of determination (R^2), obtained from Power law is reasonably high, implying the higher level of accuracy in the Power law model. Furthermore, simple calculation method makes power law model convenient for determining the performance of NiMo/Zr-SBA-15 catalyst activity towards the hydrotreating of heavy gas oil.

Table 6.3: Values derived from Power law model for the HDS and HDN of heavy gas oil over optimized catalyst.

$-r_{HDS} = k_{HDS} \cdot C_S^n$		$-r_{HDN} = k_{HDN} \cdot C_N^m$	
E_{HDS}	115.5 kJ/mol	E_{HDN}	120.7 kJ/mol
A_{HDS}	3.26×10^6 $M^{-0.8}\cdot s^{-1}$	A_{HDN}	1.78×10^6 $M^{-0.3}\cdot s^{-1}$
n	1.78	m	1.33
$(R^2)_{HDS}$	0.9815	$(R^2)_{HDN}$	0.9608

6.2.5 Langmuir-Hinshelwood Model

A Langmuir-Hinshelwood model was developed considering various types of competitive and non-competitive adsorptions. Following models were considered for the kinetic calculations:

A. Independent Langmuir Hinshelwood Model:

Assumption considered for this model is that two different reactions take place on different active sites, i.e. the each reaction is inhibited by its own compounds. The fitted parameter for this model is shown in Table 6.4. From this model it can be observed that the calculated HDS activation energy by this method is lower than the HDS activation energy obtained from power law model. Lower value of R^2 indicates that for the HDS reaction this equation is less predictive. For HDN reaction, the calculated activation energy by this method is higher than that obtained from power law model. This might be due to the consideration of inhibition in the Langmuir-Hinshelwood model. Similar trend is reported in the previous literature (Ferdous et al., 2006b). Higher value of R^2 for HDN reaction implies that independent Langmuir Hinshelwood is quite predictive for the

parameter calculation of HDN reaction. The result of the determined parameters of independent Langmuir-Hinshelwood model for HDS and HDN reactions are presented in Table 6.4.

Table 6.4: Values derived from Independent Langmuir-Hinshelwood model for the HDS and HDN of heavy gas oil over optimized catalyst.

$-r_{HDS} = \frac{k_{HDS} \cdot K_S \cdot C_S{}^n}{[1 + K_S \cdot C_S]}$		$-r_{HDN} = \frac{k_{HDN} \cdot K_N \cdot C_N{}^m}{[1 + K_N \cdot C_N]}$	
E_{HDS}	96.8 kJ/mol	E_{HDN}	173 kJ/mol
n	Pseudo first	m	Pseudo first
λ_S	43.4 kJ/mol	λ_N	54.4 kJ/mol
$(R^2)_{HDS}$	0.84	$(R^2)_{HDN}$	0.96

B. Co-dependent Langmuir-Hinshelwood Model:

This model is based on the assumption that both reactions take place on the same active sites of the catalyst. The calculated parameters for this model are presented in Table 6.5. It can be observed that the activation energy for HDN is in the range of reported value in the literature. However, very high value of calculated activation energy of HDS and lower value of R^2 obtained from this model indicate, that this model is not well fitted for the calculation of kinetic parameters. Hence, this model can be discarded for the calculation of the kinetic parameters.

Table 6.5: Values derived from Co-dependent Langmuir-Hinshelwood model for the HDS and HDN of heavy gas oil over optimized catalyst.

$-r_{HDS} = \frac{k_{HDS} \cdot K_S \cdot C_S^{\,n}}{\left[1 + K_S \cdot C_S + K_N \cdot C_N\right]}$		$-r_{HDN} = \frac{k_{HDN} \cdot K_N \cdot C_N^{\,m}}{\left[1 + K_S \cdot C_S + K_N \cdot C_N\right]}$	
E_{HDS}	26.4 kJ/mol	E_{HDN}	76.2 kJ/mol
n	Pseudo first	m	Pseudo first
λ_S	828 kJ/mol	λ_N	91.9 kJ/mol
$(R^2)_{HDS}$	0.81	$(R^2)_{HDN}$	0.93

C. Langmuir-Hinshelwood Model with H_2S Inhibition:

This model is based on considering the inhibition effect of H_2S during the HDS and HDN reaction. Inhibition effect occurs due to the adsorption of H_2S on the catalytic sites. The kinetic parameters calculated from this model are presented in the Table 6.6. This model is best among all the Langmuir-Hinshelwood model considered for the kinetic calculation. Calculated activation energies for HDS and HDN are 122 kJ/mol and 138 kJ/mol, which are higher than those obtained from power law model (115 kJ/mol and 120 kJ/mol). Higher activation energy for Langmuir-Hinshelwood model may be due to the consideration of the adsorption of sulfur, nitrogen and H_2S. Also, the inhibition effect of H_2S makes the HDS and HDN reaction difficult, which results in higher activation energies. Similar trend is reported for the hydrotreating of heavy gas oil using boron containing $NiMo/Al_2O_3$ catalyst (Ferdous et al., 2006b). Also, activation energy for HDN is higher than that for HDS. This can be attributed to the fact that the effect of H_2S inhibition, which might be higher in HDN reaction compared to the HDS reaction. This trend is also found for the power law model. Finally, relatively high values of regression

coefficient for this model imply that this model can predict the performance of the NiMo/Zr-SBA-15 catalyst with minimum error. Arrhenius plot for HDS and HDN derived from Langmuir-Hinshelwood model with H_2S inhibition are presented in Figure 6.5 and 6.6.

Table 6.6: Values derived from Langmuir-Hinshelwood model with H_2S inhibition for the HDS and HDN of heavy gas oil over optimized catalyst.

$-r_{HDS} = \frac{k_{HDS} \cdot K_S \cdot C_S^{\,n}}{\left[1 + K_S C_S + K_{H2S} P_{H2S}\right]}$		$-r_{HDN} = \frac{k_{HDN} \cdot K_N \cdot C_N^{\,m}}{\left[1 + K_N C_N + K_{H2S} P_{H2S}\right]}$	
E_{HDS}	122 kJ/mol	E_{HDN}	138 kJ/mol
n	Pseudo first	m	Pseudo first
λ_S	111.5 kJ/mol	λ_N	74.4 kJ/mol
$(R^2)_{HDS}$	0.977	$(R^2)_{HDN}$	0.982

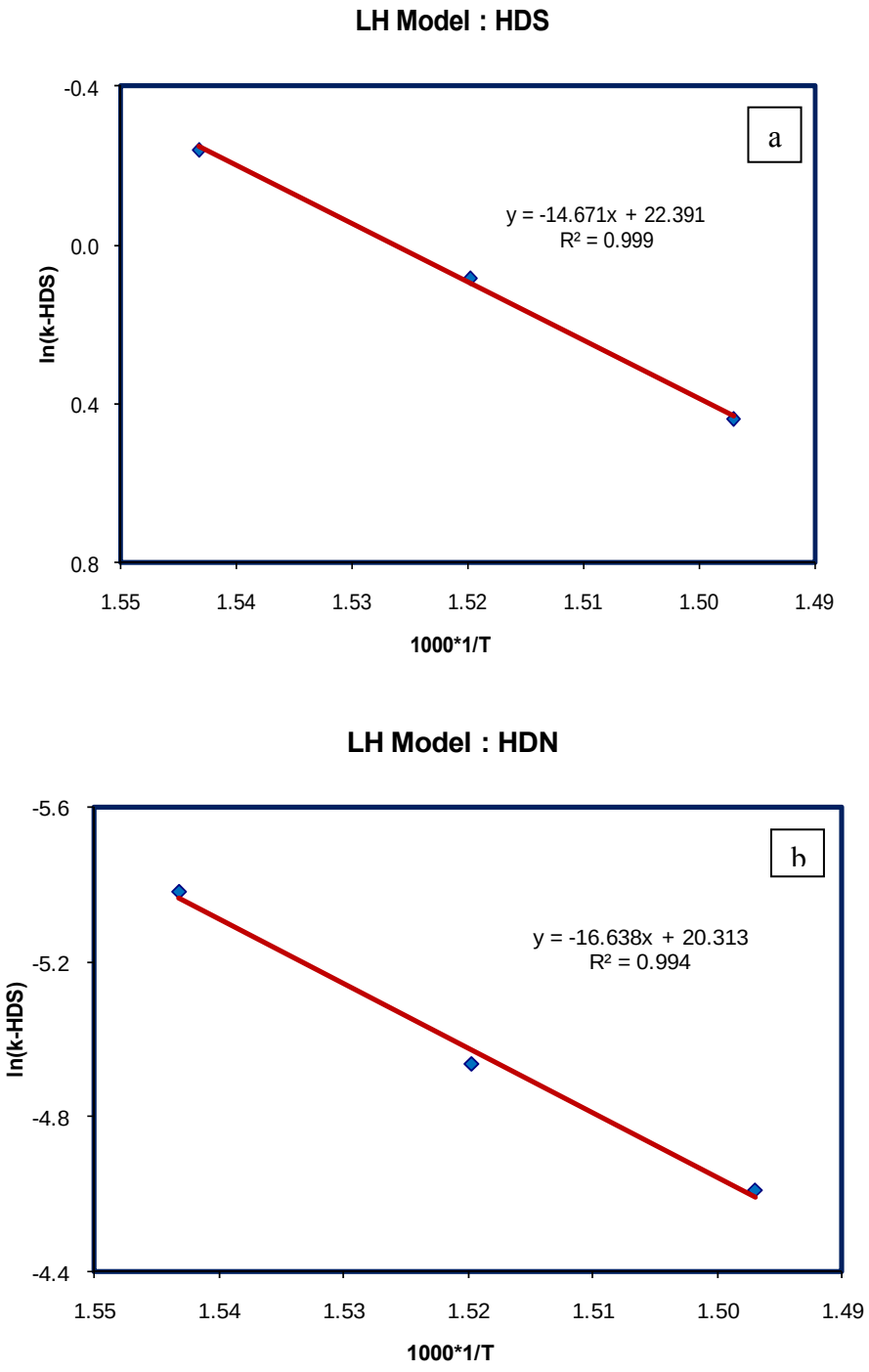

Figure 6.5: Arrhenius plot for HDS and HDN derived from Langmuir-Hinshelwood model with H_2S inhibition HDS (a), HDN (b).

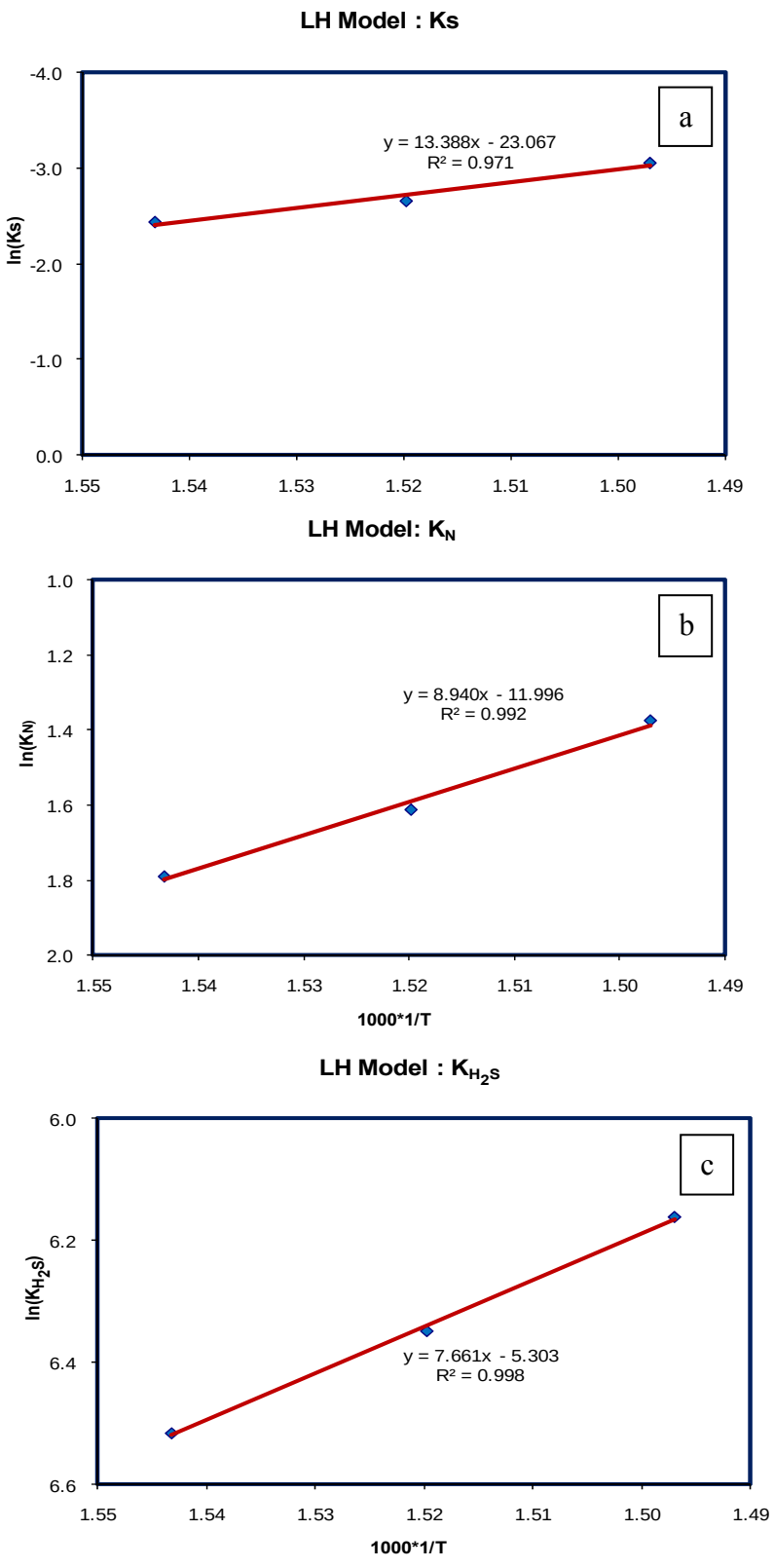

Figure 6.6: Arrhenius plot for HDS and HDN derived from Langmuir-Hinshelwood model with H_2S inhibition; sulfur (a), nitrogen (b) and H_2S (c).

6.3 Stability Study for the Optimum NiMo/Zr-SBA-15 Catalyst

In the final phase, the long term stability study with the optimum NiMo/Zr-SBA-15 catalyst was performed. The NiMo/Zr-SBA-15 (optimum), which was used for the kinetic study at different operating condition (pressure =7.9 to 9.9, temperature =375 to 385 °C, LHSV =0.5 to 1.5 hr-1, gas/oil ratio =400 to 800 Nm^3/m^3), was used for the stability study. "zero(0)"day for catalyst stability (or deactivation) study starts at the end of kinetic study (45 day), while keeping the reaction temperature at 370 °C, pressure 8.9 MPa, LHSV 1.0 hr^{-1} and gas/oil ratio 600 Nm^3/m^3. The samples were collected every 24 hours for 26 days. The HDS and HDN activity for the long term stability test is compared with the HDS and HDN activity exhibited during initial 5 days of precoking conditions (temperature at 370 °C, pressure 8.9 MPa, LHSV 1.0 hr^{-1} and gas/oil ratio 600 Nm^3/m^3). The comparison results are presented in Figure 6.7. The HDS and HDN conversion for precoking day 2^{nd}, 3^{rd} and 5^{th} days are 88.4, 87.7 and 88.4 and 48.4, 43.1 and 43.9 respectively. HDS and HDN conversion for the 20, 23^{rd} and 26^{th} days of operation are 87.9, 88.3 and 88.2 and 43.7, 44.4 and 45.5, respectively. Hence, it can be concluded that the catalyst stability remains almost constant in long term for both HDS and HDN reactions.

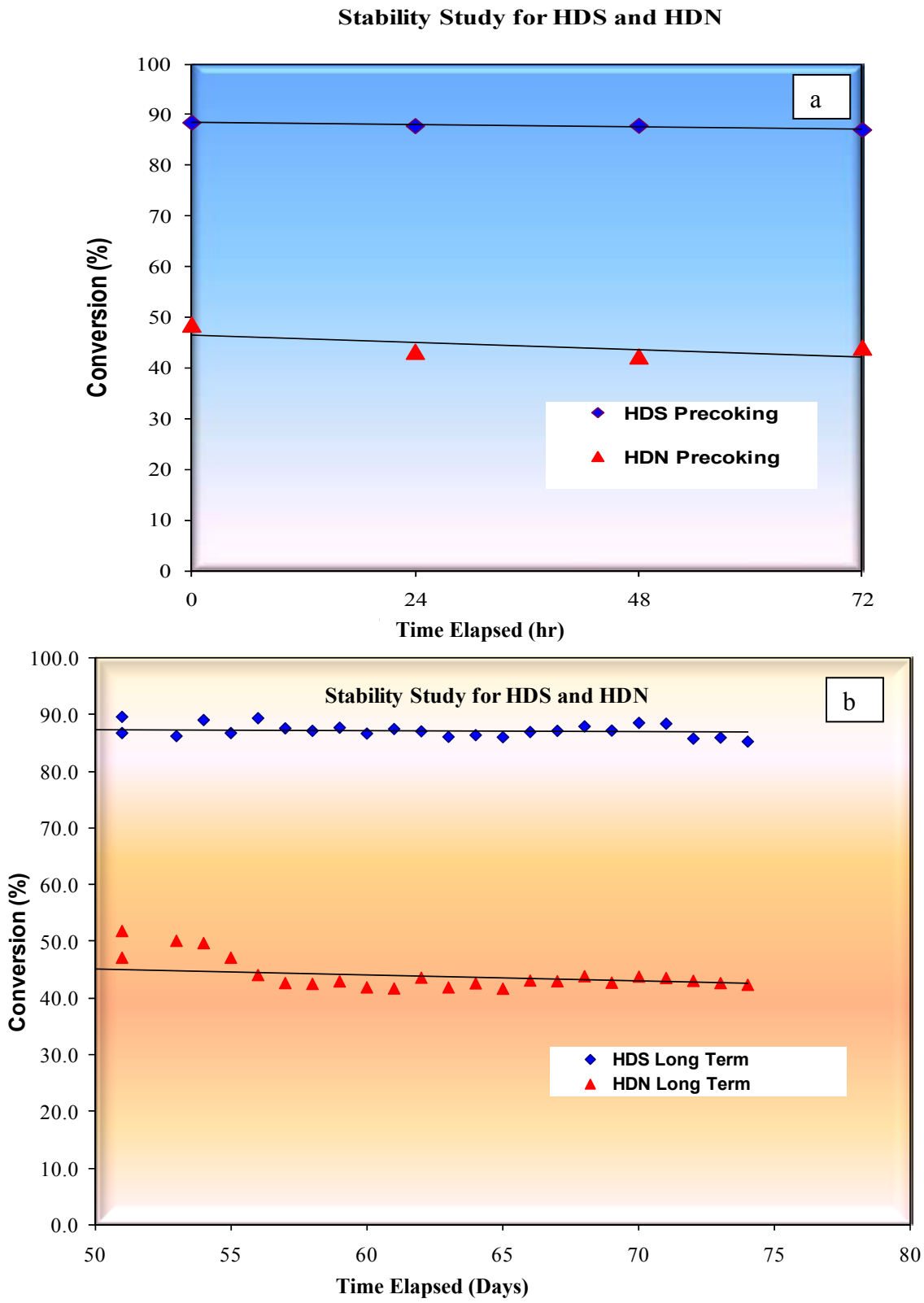

Figure 6.7: Long term stability study of optimized catalyst exhibited during hydrotreating of heavy gas oil; precooking (a), long term (b).

6.4 Characterization of Spent Catalysts

Spent catalysts were characterized with BET surface area method. Before BET analysis, the spent catalysts were treated with hexane to remove heavy gas oil and fine silicon carbide particles from the catalyst samples. Result of BET analysis for the spent catalyst is shown in the Table 6.7. It can be observed from the table that the reduction of surface area and total pore volume occur in spent catalyst. The reduction in surface area and pore volume can be attributed to the blockage of pores by carbonaceous materials or sintering of pores during the reaction.

Table 6.7: BET characterization of fresh and spent catalysts.

Catalyst	**Surface Area (m^2/g)**	**Pore Diameter (nm)**	**Pore Volume (m^3/g)**
Ph-I: Fresh NiMo/Zr-SBA-15 (Post 23)	281	10.1	0.71
Ph-I: Spent NiMo/Zr-SBA-15 (Post 23)	81	9.6	0.19
Ph-II: Fresh NiMo/Zr-SBA-15 (Mo 17)	221	10.1	0.56
Ph-II:Spent NiMo/Zr-SBA-15 (Mo 17)	76	9.0	0.17

CHAPTER 7
CONCLUSIONS AND RECOMMENDATIONS

The Main objective of this thesis was to synthesize, characterize and performance test of NiMo/Zr-SBA-15 catalyst for the hydrodesulfurization (HDS) and hydrodenitrogenation (HDN) of heavy gas oil (HGO) derived from Athabasca bitumen. In addition, the kinetic study of HDS and HDN reaction and catalyst stability study were performed for the best catalyst. A list of conclusion drawn from the thesis is presented in this section.

7.1 Conclusions

Phase - I: Hydrotreating of gas oil over NiMo/Zr-SBA-15 catalysts

SBA-15 mesoporous material was prepared and successfully modified with Zr species (Zr and ZrO_2) by both the direct and the post synthesis method. The incorporation of Zr and ZrO_2 in SBA-15 increases the surface acidity of SBA-15 support without significant change in structural ordering. Then, a series of NiMo catalysts supported on SBA-15 and Zr-SBA-15 (Direct), and Zr-SBA-15 (Post) material were prepared, characterized, and their hydrotreating activity was studied using heavy gas oil derived from Athabasca bitumen in a trickle bed reactor. From the catalytic activity test, it was found that NiMo catalysts supported on Zr-SBA-15 materials prepared by both the post synthesis method and the direct synthesis method show higher HDS and HDN activities than that of NiMo/SBA-15 catalyst. The NiMo catalyst supported on the Zr-SBA-15 (Post 23) is the best among the NiMo/Zr-SBA-15 catalyst series and this trend can be attributed to its following properties: a) excellent textural property (larger pore diameter),

b) higher zirconia loading, c) better dispersion of Mo active species, and d) higher acidity. Furthermore, the NiMo catalyst supported on the Zr-SBA-15 (Post 23) material exhibits higher catalytic activity compared to that of the commercial NiMo catalyst supported on γ-Al_2O_3 (weight basis). This can be attributed to the uniform mesoporous structure and optimum metal support interaction of the NiMo/Zr-SBA-15 (Post 23) catalyst compared to the commercial catalyst. This study reveals the potential of the NiMo/Zr-SBA-15 (Post 23) catalyst to become an efficient alternative to the conventional γ-Al_2O_3 supported commercial NiMo catalyst for the hydrotreating of heavy gas oil feedstock.

Phase-II: Metal loading optimization for NiMo/Zr-SBA-15 catalysts

In the phase II, NiMo/Zr-SBA-15 catalysts with varying metal (Mo and Ni) loading were prepare and characterized. The performance of all catalysts was evaluated based on HDS and HDN activity exhibited during hydrotreatment of heavy gas oil (HGO) derived from Athabasca bitumen. In Zr-SBA-15 supported catalysts, increase HDS and HDN activities were observed when the Mo loading was increased from 12 wt% to 17 wt% with constant Mo/Ni mass ratio of 5. This can be attributed to the better textural characteristics, better dispersion of active metal and higher acidity of NiMo/Zr-SBA-15 catalysts with increasing metal loading. However, a further increase of MoO_3 loading up to 22 wt% led to a decrease in the HDS and HDN activity. This shows that the 17 wt% is the optimum Mo loading on Zr-SBA-15 support, which gives the highest catalytic activity. This trend may be attributed to the variation of dispersion of Mo active species over the support material. The Mo species may be well-dispersed on the support material up to 17 wt% of loading. The agglomeration of Mo species occurs at the higher loading

of 22 wt%, which causes the reduction in catalytic activities. This study reveals that NiMo catalyst supported on Zr-SBA-15 support with maximum metal loading of 17 wt% Mo and 3.4 wt% Ni is the best for the hydrotreating of HGO.

Part III: Kinetic study for HDS and HDN

In the phase III, kinetic study of the optimized catalyst was performed by varying the pressure, temperature, LHSV and gas/oil ratio. Based on the data, the kinetic equation were developed using Power law and Langmuir-Hinshelwood models. As per the power law, calculated reaction orders are 1.8 and 1.3 and calculated activation energies are 115 kJ/mol and 120 kJ/mol for the HDS and HDN reaction respectively. Among the three Langmuir-Hinshelwood models, studied in this work, model with H_2S inhibition was well fitted for the calculation of kinetic parameters. As per this model, the calculated activation energies are 122 kJ/mol and 138 kJ/mol for HDS and HDN reactions respectively.

In the long term stability test, the catalyst activity remains almost constant for both HDS and HDN reactions.

7.2 Recommendations

The following recommendations are made for future work in the field of study:

- Zr-SBA-15 (Direct) support, prepared by direct synthesis method, with better textural properties and higher Zr loading needs to be prepared and performance of the better Zr-SBA-15 (Direct) supported NiMo catalyst needs to be carried out for the hydrotreatment of heavy gas oil.
- Various methods of Zr-SBA-15 support preparation by both direct and post synthesis methods are discussed in the literature review section. Some of the methods need to be

explored for the Zr-SBA-15 support preparation and performance of those supports needs to be evaluated in the hydrotreating catalyst application.

- The activity enhancement study for the NiMo catalyst supported on Zr-SBA-15 support prepared by post synthesis method needs to be explored by adding some additives such as phosphorous, boron and fluorine.
- The performance of optimized NiMo/Zr-SBA-15 catalyst needs to be done with the variety of gas oil, such as straight run light gas oil, vacuum light gas oil /heavy gas oil.
- The hydrodearomatization and hydrodemetalization study needs to done with the optimized catalyst in order to investigate the performance of this catalyst for the HDA and HDM reactions.

CHAPTER 8
LIST OF REFERENCES

Afanasiev, P., A. Thiollier, M. Breysse and J.L. Dubois, "Control of the textural properties of zirconium oxide," Topics in Catalysis. 8, 147-160 (1999).

Ahmed T., "Hydrocarbon Phase Behavior," Gulf Publishing, Houston (1989).

Amezcua, J.C., L. Lizama, C. Salcedo, I. Puente, J.M. Domínguez and T. Klimova, "NiMo catalysts supported on titania-modified SBA-16 for 4,6-dimethyldibenzothiophene hydrodesulfurization," Catalysis Today. 107-108, 578-588 (2005).

Ancheyta, J. and J.G. Speight, "Hydroprocessing of Heavy Oil and Residua," CRC Press, Taylor and Francis Group:, Boca Raton, FL (2007).

Ancheyta, J., M.J. Angeles, M.J. MacÃas, G. MarroquÃn and R. Morales, "Changes in Apparent Reaction Order and Activation Energy in the Hydrodesulfurization of Real Feedstocks," Energy & Fuels. 16, 189-193 (2002a).

Ancheyta, J., G. Marroquín, M.J. Angeles, M.J. Macías, I. Pitault, M. Forissier and R.D. Morales, "Some experimental observations of mass transfer limitations in a trickle-bed hydrotreating pilot reactor," Energy and Fuels. 16, 1059-1067 (2002b).

Anderson J. B., "Criterion for isothermal behavior of a catalyst pellet," 18, 147-148 (1963).

Babich, I.V. and J.A. Moulijn, "Science and technology of novel processes for deep desulfurization of oil refinery streams: A review," Fuel. 82, 607-631 (2003).

Bataille, F., J.L. Lemberton, G. Pérot, P. Leyrit, T. Cseri, N. Marchal and S. Kasztelan, "Sulfided Mo and CoMo supported on zeolite as hydrodesulfurization catalysts: Transformation of dibenzothiophene and 4,6-dimethyldibenzothiophene," Applied Catalysis A: General. 220, 191-205 (2001).

Bej, S.K., A.K. Dalai and J. Adjaye, "Kinetics of hydrodesulfurization of heavy gas oil derived from oil-sands bitumen," Petroleum Science and Technology. 20, 867-877 (2002).

Bej, S.K., A.K. Dalai and J. Adjaye, "Effect of hydrotreating conditions on the conversion of residual fraction and microcarbon residue present in oil sands derived heavy gas oil," Energy and Fuels. 15, 1103-1109 (2001a).

Bej, S.K., A.K. Dalai and J. Adjaye, "Comparison of hydrodenitrogenation of basic and nonbasic nitrogen compounds present in oil sands derived heavy gas oil," Energy and Fuels. 15, 377-383 (2001b).

Bej, S.K., R.P. Dabral, P.C. Gupta, K.K. Mittal, G.S. Sen, V.K. Kapoor and A.K. Dalai, "Studies on the performance of a microscale trickle bed reactor using different sizes of diluent," Energy and Fuels. 14, 701-705 (2000).

Bej, S.K., S.K. Maity and U.T. Turaga, "Search for an Efficient 4,6-DMDBT Hydrodesulfurization Catalyst: A Review of Recent Studies," Energy & Fuels. 18, 1227-1237 (2004).

Bej, S.K., A.K. Dalai and J. Adjaye, "Comparison of Hydrodenitrogenation of Basic and Nonbasic Nitrogen Compounds Present in Oil Sands Derived Heavy Gas Oil," Energy & Fuels. 15, 377-383 (2001).

Berhault, G., M. Perez De la Rosa, A. Mehta, M.J. Yácaman and R.R. Chianelli, "The single-layered morphology of supported MoS2-based catalysts-The role of the cobalt promoter and its effects in the hydrodesulfurization of dibenzothiophene," Applied Catalysis A: General. 345, 80-88 (2008).

Bhaumik, A., S. Samanta and N.K. Mal, "Highly active disordered extra large pore titanium silicate," Microporous and Mesoporous Materials. 68, 29-35 (2004).

Blin, J.L. and B.L. Su, "Tailoring pore size of ordered mesoporous silicas using one or two organic auxiliaries as expanders," Langmuir. 18, 5303-5308 (2002).

Blin, J.L., C. Otjacques, G. Herder and B. Su, "Pore size engineering of mesoporous silicas using alkanes as swelling agents," in "Studies in Surface Science and Catalysis," Abdelhamid Sayari and Mietek Jaroniec, Ed. Elsevier (2000), pp. 75-84.

Botchwey, C., A.K. Dalai and J. Adjaye, "Simulation of a two-stage micro trickle-bed hydrotreating reactor using athabasca bitumen-derived heavy gas oil over commercial NiMo/Al 2O3 catalyst: Effect of H2S on hydrodesulfurization and hydrodenitrogenation," International Journal of Chemical Reactor Engineering. 4, 1-18 (2006).

Botchwey, C., A.K. Dalai and J. Adjaye, "Kinetics of bitumen-derived gas oil upgrading using a commercial NiMo/Al2O3 catalyst," Canadian Journal of Chemical Engineering. 82, 478-487 (2004).

Breysse, M., P. Afanasiev, C. Geantet and M. Vrinat, "Overview of support effects in hydrotreating catalysts," Catalysis Today. 86, 5-16 (2003a).

Breysse, M., C. Geantet, P. Afanasiev, J. Blanchard and M. Vrinat, "Recent studies on the preparation, activation and design of active phases and supports of hydrotreating catalysts," Catalysis Today. 130, 3-13 (2008).

Broderick, D.H. and B.C. Gates, "Hydrogenolysis and Hydrogenation of Dibenzothiophene Catalyzed by Sulfided Co0-MoO3/y-AI2O3: The Reaction Kinetics," American Institute of Chemical Engineers Journal. 27, 663-673 (1981).

Burdett, J.K. and J.T. Chung, "Volcano plots, hydrodesulfurization and surface atom pair potentials," Surface Science. 236, L353-L357 (1990).

Callejas, M.A. and M.T. Martínez, "Hydroprocessing of a Maya residue. Intrinsic kinetics of sulfur-, nitrogen-, nickel-, and vanadium-removal reactions," Energy and Fuels. 13, 629-636 (1999).

Cao, L., T. Man and M. Kruk, "Synthesis of ultra-large-pore SBA-15 silica with two-dimensional hexagonal structure using triisopropylbenzene as micelle expander," Chemistry of Materials. 21, 1144-1153 (2009).

Chen, L.F., L.E. Noreña, J. Navarrete and J.A. Wang, "Improvement of surface acidity and structural regularity of Zr-modified mesoporous MCM-41," Materials Chemistry and Physics. 97, 236-242 (2006).

Chen, S.Y., J.F. Lee and S. Cheng, "Pinacol-type rearrangement catalyzed by Zr-incorporated SBA-15," Journal of Catalysis. 270, 196-205 (2010).

Chen, S.Y., L.Y. Jang and S. Cheng, "Synthesis of thermally stable zirconia-based mesoporous materials via a facile post-treatment," Journal of Physical Chemistry B. 110, 11761-11771 (2006).

Chen, S.Y., L.Y. Jang and S. Cheng, "Synthesis of Zr-incorporated SBA-15 mesoporous materials in a self-generated acidic environment," Chemistry of Materials. 16, 4174-4180 (2004).

Cheralathan, K.K., T. Hayashi and M. Ogura, "Post-synthesis coating of alumina on the mesopore walls of SBA-15 by ammonia/water vapour induced internal hydrolysis and its consequences on pore structure and acidity," Microporous and Mesoporous Materials. 116, 406-415 (2008).

Chianelli, R.R., T.A. Pecoraro, T.R. Halbert, W.-. Pan and E.I. Stiefel, "Transition metal sulfide catalysis: Relation of the synergic systems to the periodic trends in hydrodesulfurization," Journal of Catalysis. 86, 226-230 (1984).

Chorkendorff I. and Niemantsverdriet J.W., "Concept of Modern Catalysis and Kinetics," Wiley-VCH, Denmark (2003).

Chu, C.F. and K.M. Ng, "Flow in packed tubes with a small tube to particle diameter ratio," AICHE Journal. 35, 148-158 (1989).

Chuah, G.K., S. Jaenicke, S.A. Cheong and K.S. Chan, "The influence of preparation conditions on the surface area of zirconia," Applied Catalysis A: General. 145, 267-284 (1996).

Cocchetto, J.F. and C.N. Satterfield, "Chemical equilibria among quinoline and its reaction products in hydrodenitrogenation," Industrial & Engineering Chemistry Process Design and Development. 20, 49-53 (1981).

Corma, A., "From microporous to mesoporous molecular sieve materials and their use in catalysis," Chemical Reviews. 97, 2373-2419 (1997).

Daage, M. and R.R. Chianelli, "Structure-Function Relations in Molybdenum Sulfide Catalysts: The "Rim-Edge" Model," Journal of Catalysis. 149, 414-427 (1994).

Dang, Z., B.G. Anderson, Y. Amenomiya and B.A. Morrow, "Silica-supported zirconia. 1. Characterization by infrared spectroscopy, temperature-programmed desorption, and X-ray diffraction," Journal of Physical Chemistry. 99, 14437-14443 (1995).

David S.J.J. and Pujadó P. R, "Handbook of Petroleum Processing," Springer, Netherlands (2006).

De Beer, V.H.J., T.H.M. Van Sint Fiet, G.H.A.M. Van Der Steen, A.C. Zwaga and G.C.A. Schuit, "The CoO-MoO_3-γ-Al_2O_3 catalyst. V. Sulfide catalysts promoted by cobalt, nickel, and zinc," Journal of Catalysis. 35, 297-306 (1974a).

De Beer, V.H.J., T.H.M. Van Sint Fiet, G.H.A.M. Van Der Steen, A.C. Zwaga and G.C.A. Schuit, "The CoO-MoO3-γ-Al2O3 catalyst. V. Sulfide catalysts promoted by cobalt, nickel, and zinc," Journal of Catalysis. 35, 297-306 (1974b).

Delgado R. A. S., "Organometallic Modeling of the Hydrodesulfurization and Hydrodenitrogenation Reactions " Kluwer Academic, Netherland (2002).

Delmon B., "A new hypothesis explaining synergy between two phases in heterogeneous catalysis. The case of hydrodesulfurization catalysts," 88, 979-987 (1979).

Delmon, B., "New technical challenges and recent advances in hydrotreatment catalysis. A critical updating review," Catalysis Letters. 22, 1-32 (1993).

Dhar, G.M., G.M. Kumaran, M. Kumar, K.S. Rawat, L.D. Sharma, B.D. Raju and K.S.R. Rao, "Physico-chemical characterization and catalysis on SBA-15 supported molybdenum hydrotreating catalysts," Catalysis Today. 99, 309-314 (2005).

Dhar, G.M., B.N. Srinivas, M.S. Rana, M. Kumar and S.K. Maity, "Mixed oxide supported hydrodesulfurization catalysts—a review," Catalysis Today. 86, 45-60 (2003).

Diaz-Real, R.A., R.S. Mann and I.S. Sambi, "Hydrotreatment of athabasca bitumen derived gas oil over Ni-Mo, Ni-W, and Co-Mo catalysts," Industrial and Engineering Chemistry Research. 32, 1354-1358 (1993).

Ding, L., Y. Zheng, Z. Zhang, Z. Ring and J. Chen, "HDS, HDN, HDA, and hydrocracking of model compounds over Mo-Ni catalysts with various acidities," Applied Catalysis A: General. 319, 25-37 (2007).

Domínguez-Crespo, M.A., A.M. Torres-Huerta, L. Díaz-García, E.M. Arce-Estrada and E. Ramírez-Meneses, "HDS, HDN and HDA activities of nickel–molybdenum catalysts supported on alumina," Fuel Processing Technology. 89, 788-796 (2008).

Dorian, J.P., H.T. Franssen and D.R. Simbeck, "Global challenges in energy," Energy Policy. 34, 1984-1991 (2006).

D'Souza, L., A. Suchopar, K. Zhu, D. Balyozova, M. Devadas and R.M. Richards, "Preparation of thermally stable high surface area mesoporous tetragonal ZrO2 and Pt/ZrO2: An active hydrogenation catalyst," Microporous and Mesoporous Materials. 88, 22-30 (2006).

Du, Y., S. Liu, Y. Zhang, F. Nawaz, Y. Ji and F. Xiao, "Urea-assisted synthesis of hydrothermally stable Zr-SBA-15 and catalytic properties over their sulfated samples," Microporous and Mesoporous Materials. 121, 185-193 (2009).

Eijsbouts, S., "On the flexibility of the active phase in hydrotreating catalysts," Applied Catalysis A: General. 158, 53-92 (1997).

Environmental Canada, "http://www.ec.gc.ca/cleanair-airpur/caol/ogeb/fuels/reports," Oct, 2009.

Eswaramoorthi, I., V. Sundaramurthy, N. Das, A.K. Dalai and J. Adjaye, "Application of multi-walled carbon nanotubes as efficient support to NiMo hydrotreating catalyst," Applied Catalysis A: General. 339, 187-195 (2008).

Feng, P., X. Bu, G.D. Stucky and D.J. Pine, "Monolithic mesoporous silica templated by microemulsion liquid crystals [23]," Journal of the American Chemical Society. 122, 994-995 (2000).

Ferdous, D., A.K. Dalai and J. Adjaye, "Comparison of product selectivity during hydroprocessing of bitumen derived gas oil in the presence of NiMo/Al2O3 catalyst containing boron and phosphorus," Fuel. 85, 1286-1297 (2006a).

Ferdous, D., A.K. Dalai and J. Adjaye, "Hydrodenitrogenation and hydrodesulfurization of heavy gas oil using NiMo/Al2O3 catalyst containing boron: Experimental and kinetic studies," Industrial and Engineering Chemistry Research. 45, 544-552 (2006b).

Ferdous, D., N.N. Bakhshi, A.K. Dalai and J. Adjaye, "Synthesis, characterization and performance of NiMo catalysts supported on titania modified alumina for the hydroprocessing of different gas oils derived from Athabasca bitumen," Applied Catalysis B: Environmental. 72, 118-128 (2007).

Ferrer, F.J., F. Frutos, J. García-López, C. Jiménez and F. Yubero, "Electrical characteristics of mixed Zr-Si oxide thin films prepared by ion beam induced chemical vapor deposition at room temperature," Thin Solid Films. 517, 5446-5452 (2009).

Fogler H.S., "Elements of Chemical Reaction Engineering," Prentice Hall, Upper Saddle River, New Jersey (2006).

Froment G.F. and Bischoff K.B., "Chemical Reactor Analysis and Design," (1990).

Fulvio, P.F., S. Pikus and M. Jaroniec, "Tailoring properties of SBA-15 materials by controlling conditions of hydrothermal synthesis," Journal of Materials Chemistry. 15, 5049-5053 (2005).

Furimsky E., "Catalysts for Upgrading Heavy Petroleum Feeds. " Studies in Surface Science and Catalysis. 169, 1-387 (2007).

Furimsky, E. and F.E. Massoth, "Hydrodenitrogenation of petroleum," Catalysis Reviews - Science and Engineering. 47, 297-489 (2005).

Furimsky, E. and F.E. Massoth, "Deactivation of hydroprocessing catalysts," Catalysis Today. 52, 381-495 (1999).

Fuxiang, L., Y. Feng, L. Yongli, L. Ruifeng and X. Kechang, "Direct synthesis of Zr-SBA-15 mesoporous molecular sieves with high zirconium loading: Characterization and catalytic performance after sulfated," Microporous and Mesoporous Materials. 101, 250-255 (2007).

Garg, S., K. Soni, G.M. Kumaran, M. Kumar, J.K. Gupta, L.D. Sharma and G.M. Dhar, "Effect of Zr-SBA-15 support on catalytic functionalities of Mo, CoMo, NiMo hydrotreating catalysts," Catalysis Today. 130, 302-308 (2008).

Gary J.H. and Handwerk G.E., "Petroleum Refining Technology and Economics " Marcel Dekker (2001).

Gierman, H., "Design of laboratory hydrotreating reactors. Scaling Down of Trickle-flow Reactors," Applied Catalysis. 43, 277-286 (1988).

Girgis, M.J. and B.C. Gates, "Reactivities, reaction networks, and kinetics in high-pressure catalytic hydroprocessing," Industrial & Engineering Chemistry Research. 30, 2021-2058 (1991).

Gómez-Cazalilla, M., J.M. Mérida-Robles, A. Gurbani, E. Rodríguez-Castellón and A. Jiménez-López, "Characterization and acidic properties of Al-SBA-15 materials prepared by post-synthesis alumination of a low-cost ordered mesoporous silica," Journal of Solid State Chemistry. 180, 1130-1140 (2007).

Grange, P., "Catalytic hydrodesulfurization." Catalysis Reviews - Science and Engineering. 21, 135-181 (1980).

Grange, P. and X. Vanhaeren, "Hydrotreating catalysts, an old story with new challenges," Catalysis Today. 36, 375-391 (1997).

Gray M.R., "Upgrading Petroleum Residues and Heavy Oils," Marcel Dekker Inc. (1994), pp. 348.

Gutiérrez, O.Y., A. Erika, I. Puente and T. Klimova, "Application of new ZrO2-SBA-15 materials as catalytic supports: Study of intrinsic activity of Mo catalysts in deep HDS," Chemical Engineering Communications. 196, 1163-1177 (2009).

Gutiérrez, O.Y., D. Valencia, G.A. Fuentes and T. Klimova, "Mo and NiMo catalysts supported on SBA-15 modified by grafted ZrO2 species: Synthesis, characterization and evaluation in 4,6-dimethyldibenzothiophene hydrodesulfurization," Journal of Catalysis. 249, 140-153 (2007).

Gutiérrez, O.Y., G.A. Fuentes, C. Salcedo and T. Klimova, "SBA-15 supports modified by Ti and Zr grafting for NiMo hydrodesulfurization catalysts," Catalysis Today. 116, 485-497 (2006a).

Gutiérrez, O.Y., K.A. Romero, G.A. Fuentes and T. Klimova, "New NiMo catalysts supported on ZrO2-modified SBA-15 materials for 4,6-dimethyldibenzothiophene hydrodesulfurization," Studies in Surface Science and Catalysis. 162, 355-362 (2006b).

Gutiérrez, O.Y., F. Pérez, G.A. Fuentes, X. Bokhimi and T. Klimova, "Deep HDS over NiMo/Zr-SBA-15 catalysts with varying MoO3 loading," Catalysis Today. 130, 292-301 (2008).

Hagen J., "Industrial Catalysis A Practical Approach," Wiley-Vch, Germany (2006).

Hagen, A., D. Wei and G.L. Haller, "Titanium containing MCM-41 molecular sieves prepared by secondary treatment,"Studies in Surface Science and Catalysis 117, 191-200(1998).

Harris, S. and R.R. Chianelli, "Catalysis by transition metal sulfides: A theoretical and experimental study of the relation between the synergic systems and the binary transition metal sulfides," Journal of Catalysis. 98, 17-31 (1986).

Hensen, E.J.M., P.J. Kooyman, Y. Van der Meer, A.M. Van der Kraan, V.H.J. De Beer, J.A.R. Van Veen and R.A. Van Santen, "The relation between morphology and hydrotreating activity for supported MoS2 particles," Journal of Catalysis. 199, 224-235 (2001).

Hill C. G. and Hill D., "An Introduction to Chemical Engineering Kinetics and Reactor Design," John Wiley and Sons (1977).

Hinnemann, B., J.K. NØrskov and H. TopsØe, "A density functional study of the chemical differences between type I and type II MoS2-based structures in hydrotreating catalysts," Journal of Physical Chemistry B. 109, 2245-2253 (2005).

Hong, N., L. Mingfeng, G. Xiaodong, S. Yahua and L. Dadong, "New Progress of Producing Clean Fuels— Hydrogenation Catalyst and Technology Developed by RIPP," Research Institute of Petroleum Processing , SINOPEC. (2006).

Huang, W., A. Duan, Z. Zhao, G. Wan, G. Jiang, T. Dou, K.H. Chung and J. Liu, "Ti-modified alumina supports prepared by sol-gel method used for deep HDS catalysts," Catalysis Today. 131, 314-321 (2008a).

Huang, Z.-., W. Bensch, L. Kienle, S. Fuentes, G. Alonso and C. Ornelas, "SBA-15 as support for MoS2 and Co-MoS2 catalysts derived from thiomolybdate complexes in the reaction of HDS of DBT," Catalysis Letters. 122, 57-67 (2008b).

International Energy Outlook, 2., "International Energy Outlook, 2004,"Http://www. Iea. org/textbase/nppdf/free/2004/weo2004. Pdf Oct, 2009, 577(2004).

Jacobsen, C.J.H., N.Y. Topsoe, H. Topsoe, L. Kellberg and H.J. Jakobsen, "Quantitative 1H MAS NMR Studies of Structurally Different OH Surface Groups on η-Al2O3 and Mol-/η-Al2O3 Catalysts," Journal of Catalysis. 154, 65-68 (1995).

Jana, S.K., R. Nishida, K. Shindo, T. Kugita and S. Namba, "Pore size control of mesoporous molecular sieves using different organic auxiliary chemicals," Microporous and Mesoporous Materials. 68, 133-142 (2004).

Jayne, D., Y. Zhang, S. Haji and C. Erkey, "Dynamics of removal of organosulfur compounds from diesel by adsorption on carbon aerogels for fuel cell applications," International Journal of Hydrogen Energy. 30, 1287-1293 (2005).

Ji, Y., P. Afanasiev, M. Vrinat, W. Li and C. Li, "Promoting effects in hydrogenation and hydrodesulfurization reactions on the zirconia and titania supported catalysts," Applied Catalysis A: General. 257, 157-164 (2004).

Jia, M., P. Afanasiev and M. Vrinat, "The influence of preparation method on the properties of NiMo sulfide catalysts supported on ZrO2," Applied Catalysis A: General. 278, 213-221 (2005).

Jiménez, F., V. Kafarov and M. Nuñez, "Modeling of industrial reactor for hydrotreating of vacuum gas oils. Simultaneous hydrodesulfurization, hydrodenitrogenation and hydrodearomatization reactions," Chemical Engineering Journal. 134, 200-208 (2007).

Joshi, Y.V., P. Ghosh, M. Daage and W.N. Delgass, "Support effects in HDS catalysts: DFT analysis of thiolysis and hydrolysis energies of metal-support linkages," Journal of Catalysis. 257, 71-80 (2008).

Kabe T., Ishihara A. and Qian W., "Hydrodesulfurization and Hydrodenitrogenation Chemistry and Engineering," Kodansha,Wiley-VCH, Tokyo (1998), pp. 374.

Kabe, T., W. Qian and A. Ishihara, "Elucidation of hydrodesulfurization mechanism using 35S radioisotope pulse tracer methods," Catalysis Today. 39, 3-12 (1997).

Kabe, T., W.H. Qian and A. Ishihara, "Study of Hydrodesulfurization of Dibenzothiophene on Ni-Mo/Al2O3, Mo/Al2O3, and Ni/Al2O3 Catalysts by the Use of Radioisotope 35S Tracer," Journal of Catalysis. 149, 171-180 (1994).

Kabe, T., W.H. Qian, S. Ogawa and A. Ishihara, "Mechanism of Hydrodesulfurization of Dibenzothiophene on Co-Mo/Al2O3 and Co/Al2O3 Catalyst by the Use of Radioisotope 35S Tracer," Journal of Catalysis. 143, 239-248 (1993).

Kemdeo, S.M., V.S. Sapkal and G.N. Chaudhari, "TiO2-SiO2 mixed oxide supported MoO3 catalyst: Physicochemical characterization and activities in nitration of phenol," Journal of Molecular Catalysis A: Chemical. 323, 70-77 (2010).

Kim, D.J., B.C. Dunn, P. Cole, G.C. Turpin, R.D. Ernst, R.J. Pugmire and E.M. Eyring, "Ordered Mesoporous Silica Supported Cobalt Catalysts for FT Synthesis: Impregnation Method and Solvent Exchange," CFFS Annual Technical Meeting. (2004).

Klicpera, T. and M. Zdražil, "Preparation of high-activity MgO-supported Co-Mo and Ni-Mo sulfide hydrodesulfurization catalysts," Journal of Catalysis. 206, 314-320 (2002).

Klimova, T., E. Rodríguez, M. Martínez and J. Ramírez, "Synthesis and characterization of hydrotreating Mo catalysts supported on titania-modified MCM-41," Microporous and Mesoporous Materials. 44-45, 357-365 (2001).

Klimova, T., L. Peña, L. Lizama, C. Salcedo and O.Y. Gutiérrez, "Modification of activity and selectivity of NiMo/SBA-15 HDS catalysts by grafting of different metal oxides on the support surface," Industrial and Engineering Chemistry Research. 48, 1126-1133 (2009).

Knudsen, K.G., B.H. Cooper and H. Topsøe, "Catalyst and process technologies for ultra low sulfur diesel," Applied Catalysis A: General. 189, 205-215 (1999).

Korsten, H. and U. Hoffmann, "Three-Phase Reactor Model for Hydrotreating in Pilot Trickle-Bed Reactors," American Institute of Chemical Engineers Journal. 42, 1350-1360 (1996).

Kostova, N.G., A.A. Spojakina, K. Jiratova, O. Solcova, L.D. Dimitrov and L.A. Petrov, "Hexagonal mesoporous silicas with and without Zr as supports for HDS catalysts," Catalysis Today. 65, 217-223 (2001).

Krishnan, J.M. and K.R. Rajagopal, "Review of the uses and modeling of bitumen from ancient to modern times," Applied Mechanics Reviews. 56, 149-214 (2003).

Kruk, M. and L. Cao, "Pore size tailoring in large-pore SBA-15 silica synthesized in the presence of hexane," Langmuir. 23, 7247-7254 (2007).

Kushmerick, J.G., S.A. Kandel, P. Han, J.A. Johnson and P.S. Weiss, "Atomic-Scale Insights into Hydrodesulfurization," Journal of Physical Chemistry B. 104, 2980-2988 (2000).

Landau, M.V., "Deep hydrotreating of middle distillates from crude and shale oils," Catalysis Today. 36, 393-429 (1997).

Landau, M.V., L. Vradman, X. Wang and L. Titelman, "High loading TiO2 and ZrO2 nanocrystals ensembles inside the mesopores of SBA-15: Preparation, texture and stability," Microporous and Mesoporous Materials. 78, 117-129 (2005).

Lauritsen, J.V., J. Kibsgaard, G.H. Olesen, P.G. Moses, B. Hinnemann, S. Helveg, J.K. Nørskov, B.S. Clausen, H. Topsøe, E. Lægsgaard and F. Besenbacher, "Location and coordination of promoter atoms in Co- and Ni-promoted MoS2-based hydrotreating catalysts," Journal of Catalysis. 249, 220-233 (2007).

Ledoux, M.J., O. Michaux, G. Agostini and P. Panissod, "CoMo sulfide catalysts studies by metal solid NMR: The question of the existence of the chemical synergy," Journal of Catalysis. 96, 189-201 (1985).

Lee S., Speight J.G. and Loyalka S.K., "Handbook of Alternative Fuel Technologies," CRC Press, Taylor and Francis Group: Boca Raton, FL. (2007).

Lettow, J.S., Y.J. Han, P. Schmidt-Winkel, P. Yang, D. Zhao, G.D. Stucky and J.Y. Ying, "Hexagonal to mesocellular foam phase transition in polymer-templated mesoporous silicas," Langmuir. 16, 8291-8295 (2000).

Li, B., S. Inagaki, C. Miyazaki and H. Takahashi, "Preparation of highly ordered mesoporous silica materials and application as immobilized enzyme supports in organic solvent," Chemical Journal on Internet. 2, 1-9 (2000).

Li, W., F. Cheng, Z. Tao and J. Chen, "Vapor-transportation preparation and reversible lithium intercalation/deintercalation of α-MoO3 microrods," Journal of Physical Chemistry B. 110, 119-124 (2006).

Lin, C.-., H.-. Lin, C.-. Mou and S.-. Liu, "Periodic mesoporous silicas via templating of new triblock amphiphilic copolymers," Microporous and Mesoporous Materials. 91, 151-155 (2006).

Liu, K. and F.T.T. Ng, "Effect of the nitrogen heterocyclic compounds on hydrodesulfurization using in situ hydrogen and a dispersed Mo catalyst," Catalysis Today. 149, 28-34 (2010).

Liu, Y.M., Y. Cao, N. Yi, W.L. Feng, W.L. Dai, S.R. Yan, H.Y. He and K. Fan, "Vanadium oxide supported on mesoporous SBA-15 as highly selective catalysts in the oxidative dehydrogenation of propane," Journal of Catalysis. 224, 417-428 (2004).

Lu, M., A. Wang, X. Li, X. Duan, Y. Teng, Y. Wang, C. Song and Y. Hu, "Hydrodenitrogenation of quinoline catalyzed by MCM-41-supported nickel phosphides," Energy and Fuels. 21, 554-560 (2007).

Luan, Z., E.M. Maes, P.A.W. Van Der Heide, D. Zhao, R.S. Czernuszewicz and L. Kevan, "Incorporation of titanium, into mesoporous silica molecular sieve SBA-15," Chemistry of Materials. 11, 3680-3686 (1999).

Maity, S.K., M.S. Rana, S.K. Bej, J. Ancheyta-Juárez, G. Murali Dhar and T.S.R. Prasada Rao, "Studies on physico-chemical characterization and catalysis on high surface area titania supported molybdenum hydrotreating catalysts," Applied Catalysis A: General. 205, 215-225 (2001).

Maity, S.K., M.S. Rana, B.N. Srinivas, S.K. Bej, G. Murali Dhar and T.S.R. Prasada Rao, "Characterization and evaluation of ZrO2 supported hydrotreating catalysts," Journal of Molecular Catalysis A: Chemical. 153, 121-127 (2000).

Mann, R.S., I.S. Sambi and K.C. Khulbe, "Hydrofining of heavy gas oil on zeolite-alumina supported nickel-molybdenum catalyst," Industrial and Engineering Chemistry Research®. 27, 1788-1792 (1988).

Mapiour, M., V. Sundaramurthy, A.K. Dalai and J. Adjaye, "Effects of hydrogen partial pressure on hydrotreating of heavy gas oil derived from oil-sands bitumen: Experimental and kinetics," Energy and Fuels. 24, 772-784 (2010a).

Mapiour, M., V. Sundaramurthy, A.K. Dalai and J. Adjaye, "Effects of the operating variables on hydrotreating of heavy gas oil: Experimental, modeling, and kinetic studies," Fuel. 89, 2536-2543 (2010b).

Marroquín, G., J. Ancheyta and C. Esteban, "A batch reactor study to determine effectiveness factors of commercial HDS catalyst," Catalysis Today. 104, 70-75 (2005).

Matsushita, K., A. Hauser, A. Marafi, R. Koide and A. Stanislaus, "Initial coke deposition on hydrotreating catalysts. Part 1. Changes in coke properties as a function of time on stream," Fuel. 83, 1031-1038 (2004).

Mears, D.E., "Tests for transport limitations in experimental catalytic reactors," Industrial and Engineering Chemistry: Process Design and Development. 10, 541-547 (1971).

Melero, J.A., J.M. Arsuaga, P.D. Frutos, J. Iglesias, J. Sainz and S. Blázquez, "Direct synthesis of titanium-substituted mesostructured materials using non-ionic surfactants and titanocene dichloride," Microporous and Mesoporous Materials. 86, 364-373 (2005).

Mochida, I. and K.-. Choi, "An overview of hydrodesulfurization and hydrodenitrogenation," Journal of the Japan Petroleum Institute. 47, 145-163 (2004).

Montesinos-Castellanos, A. and T.A. Zepeda, "High hydrogenation performance of the mesoporous NiMo/Al(Ti, Zr)-HMS catalysts," Microporous and Mesoporous Materials. 113, 146-162 (2008).

Moses, P.G., B. Hinnemann, H. Topsøe and J.K. Nørskov, "The effect of Co-promotion on MoS2 catalysts for hydrodesulfurization of thiophene: A density functional study," Journal of Catalysis. 268, 201-208 (2009).

Moulijn, J.A., A.E. Van Diepen and F. Kapteijn, "Catalyst deactivation: Is it predictable? What to do?" Applied Catalysis A: General. 212, 3-16 (2001).

Nagarajan, R., "Solubilization of hydrocarbons and resulting aggregate shape transitions in aqueous solutions of Pluronic® (PEO-PPO-PEO) block copolymers," Colloids and Surfaces B: Biointerfaces. 16, 55-72 (1999).

Namba, S., A. Mochizuki and M. Kito, "Fine control of pore size of highly ordered MCM-41 by using template mixtures of dodecyltrimethylammonium bromide/hexadecyltrimethylammonium bromide with various molar ratios," Chemistry Letters., 569-570 (1998).

Nava, R., R.A. Ortega, G. Alonso, C. Ornelas, B. Pawelec and J.L.G. Fierro, "CoMo/Ti-SBA-15 catalysts for dibenzothiophene desulfurization," Catalysis Today. 127, 70-84 (2007).

Newalkar, B.L., J. Olanrewaju and S. Komarneni, "Microwave-hydrothermal synthesis and characterization of zirconium substituted SBA-15 mesoporous silica," Journal of Physical Chemistry B. 105, 8356-8360 (2001).

Nørskov, J.K., B.S. Clausen and H. Topsøe, "Understanding the trends in the hydrodesulfurization activity of the transition metal sulfides," Catalysis Letters. 13, 1-8 (1992).

Owusu-Boakye, A., A.K. Dalai, D. Ferdous and J. Adjaye, "Experimental and kinetics studies of aromatic hydrogenation in a two-stage hydrotreating process using NIMO/AL2O3 and NIW/AL 2O3 catalysts," Canadian Journal of Chemical Engineering. 84, 572-580 (2006).

Prins, R., M. Egorova, A. Röthlisberger, Y. Zhao, N. Sivasankar and P. Kukula, "Mechanisms of hydrodesulfurization and hydrodenitrogenation," Catalysis Today. 111, 84-93 (2006).

Probst K., Wohlfahrt K., “Empirical estimate of effective diffusion coefficients in porous systems”, Chemie Ingenieur Technik, 737-738, 51, 1979

Rahimi, P., C. Fairbridge, M. Oballa, C. Wong and A. Somogyvari, "Effect of hydrotreating on the stability of synthetic crude from western Canada," ACS Division of Fuel Chemistry, Preprints. 43, 13-15 (1998).

Ramírez, L.F., J. Escobar, E. Galván, H. Vaca, F.R. Murrieta and M.R.S. Luna, "Evaluation of diluted and undiluted trickle-bed hydrotreating reactor with different catalyst volume," Petroleum Science and Technology. 22, 157-175 (2004).

Ratnasamy, P. and S. Sivasanker, "Structural chemistry of Co-Mo-alumina catalysts." Catalysis Reviews Softcover Ed. 22, 401-429 (1980).

Rayo, P., J. Ramírez, M.S. Rana, J. Ancheyta and A. Aguilar-Elguézabal, "Effect of the incorporation of Al, Ti, and Zr on the cracking and hydrodesulfurization activity of NiMo/SBA-15 catalysts," Industrial and Engineering Chemistry Research. 48, 1242-1248 (2009).

Rayo, P., M.S. Rana, J. Ramírez, J. Ancheyta and A. Aguilar-Elguézabal, "Effect of the preparation method on the structural stability and hydrodesulfurization activity of NiMo/SBA-15 catalysts," Catalysis Today. 130, 283-291 (2008).

Richardson J. T., "Principles of Catalyst Development," Springer, New York (1989).

Rodríguez, M.A. and J. Ancheyta, "Modeling of hydrodesulfurization (HDS), hydrodenitrogenation (HDN), and the hydrogenation of aromatics (HDA) in a vacuum gas oil hydrotreater," Energy and Fuels. 18, 789-794 (2004).

Salas, P., J.A. Wang, H. Armendariz, C. Angeles-Chavez and L.F. Chen, "Effect of the Si/Zr molar ratio on the synthesis of Zr-based mesoporous molecular sieves," Materials Chemistry and Physics. 114, 139-144 (2009).

Sampieri, A., S. Pronier, J. Blanchard, M. Breysse, S. Brunet, K. Fajerwerg, C. Louis and G. Pérot, "Hydrodesulfurization of dibenzothiophene on MoS2/MCM-41 and MoS2/SBA-15 catalysts prepared by thermal spreading of MoO3," Catalysis Today. 107-108, 537-544 (2005).

Satterfield, C.N., "Heterogeneous Catalysis in Industrial Practice," McGraw-Hill, New York (1991).

Satterfield, C.N. and S.H. Yang, "Catalytic hydrodenitrogenation of quinoline in a trickle-bed reactor. Comparison with vapor phase reaction," Industrial & Engineering Chemistry Process Design and Development. 23, 11-19 (1984).

Satterfield,C.N.,Pelossof A.A., Sherwood T.K., "Mass transfer limitations in trickle bed reactor," 15, 224-226 (1969).

Sayari, A., "Catalysis by crystalline mesoporous molecular sieves," Chemistry of Materials. 8, 1840-1852 (1996).

Schmidt-Winkel, P., J. Lukens W.W., P. Yang, D.I. Margolese, J.S. Lettow, J.Y. Ying and G.D. Stucky, "Microemulsion templating of siliceous mesostructured cellular foams with well-defined ultralarge mesopores," Chemistry of Materials. 12, 686-696 (2000).

Schuit, G.C.A. and B.C. Gates, "Chemistry and engineering of catalytic hydrodesulfurization," AICHE Journal. 19, 417-438 (1973).

Schulz, H., M. Schon and N.M. Rahman, "Chapter 6 Hydrogenative Denitrogenation of Model Compounds as Related to the Refining of Liquid Fuels,"Studies in Surface Science and Catalysis 27, 201-255(1986).

Sie, S.T., "Reaction order and role of hydrogen sulfide in deep hydrodesulfurization of gas oils: Consequences for industrial reactor configuration," Fuel Processing Technology. 61, 149-171 (1999).

Sigurdson, S., V. Sundaramurthy, A.K. Dalai and J. Adjaye, "Phosphorus promoted trimetallic NiMoW/γ-Al2O3 sulfide catalysts in gas oil hydrotreating," Journal of Molecular Catalysis A: Chemical. 291, 30-37 (2008).

Song, C., "An overview of new approaches to deep desulfurization for ultra-clean gasoline, diesel fuel and jet fuel," Catalysis Today. 86, 211-263 (2003).

Song, C. and X. Ma, "New design approaches to ultra-clean diesel fuels by deep desulfurization and deep dearomatization," Applied Catalysis B: Environmental. 41, 207-238 (2003).

Soni, K., K.C. Mouli, A.K. Dalai and J. Adjaye, "Influence of frame connectivity of SBA-15 and KIT-6 supported NiMo catalysts for hydrotreating of gas oil," Catalysis Letters. 136, 116-125 (2010).

Speight J. G., "The Desulfurization of Heavy Oil and Residua " Marcel Dekker (1999).

Speight, J.G., "Upgrading heavy oils and residua: the nature of the problem."Studies in Surface Science and Catalysis, 515-527(1984).

Speight, J.G., "The Chemistry and Technology of Petroleum," CRC Press, Taylor and Francis Group:, Boca Raton, FL, (2006).

Sun, J., H. Zhang, D. Ma, Y. Chen, X. Bao, A. Klein-Hoffmann, N. Pfänder and D.S. Su, "Alkanes-assisted low temperature formation of highly ordered SBA-15 with large cylindrical mesopores," Chemical Communications., 5343-5345 (2005).

Szczodrowski, K., B. Prélot, S. Lantenois, J.-. Douillard and J. Zajac, "Effect of heteroatom doping on surface acidity and hydrophilicity of Al, Ti, Zr-doped mesoporous SBA-15," Microporous and Mesoporous Materials. 124, 84-93 (2009).

Szczodrowski, K., B. Prélot, S. Lantenois, J. Zajac, M. Lindheimer, D. Jones, A. Julbe and A. van der Lee, "Effect of synthesis conditions on the pore structure and degree of heteroatom insertion in Zr-doped SBA-15 silica-based materials prepared by classical or microwave-assisted hydrothermal treatment," Microporous and Mesoporous Materials. 110, 111-118 (2008).

Taguchi, A. and F. Schüth, "Ordered mesoporous materials in catalysis," Microporous and Mesoporous Materials. 77, 1-45 (2005).

Tanaka, Y., H. Iki, K. Hayasaka and S. Hatanaka, "A Practical Approach to 10 ppm Sulfur Diesel Production,"13th Annual Saudi-Japanse Symposium - Catalysts in Petroleum Refining and Petrochemicals, Proceedings, 90-96(2003).

Topsøe, H., "The role of Co-Mo-S type structures in hydrotreating catalysts," Applied Catalysis A: General. 322, 3-8 (2007).

Topsøe, H., B.S. Clausen and Massoth, "Hydrotreating Catalysis –Science and Technology,Vol 11," Springer, Berlin (1996).

Topsøe, H., B.S. Clausen, R. Candia, C. Wivel and S. Mørup, "In situ Mössbauer emission spectroscopy studies of unsupported and supported sulfided CoMo

hydrodesulfurization catalysts: Evidence for and nature of a CoMoS phase," Journal of Catalysis. 68, 433-452 (1981).

Topsoe, H. and B.S. Clausen, "Importance of Co-Mo-S type structures in hydrodesulfurization. " Catalysis Reviews. 26, 395-420 (1984).

Tsamatsoulis, D. and N. Papayannakos, "Investigation of intrinsic hydrodesulphurization kinetics of a VGO in a trickle bed reactor with backmixing effects," Chemical Engineering Science. 53, 3449-3458 (1998).

Van Hasselt, B.W., P.J.M. Lebens, H.P.A. Calis, F. Kapteijn, S.T. Sie, J.A. Moulijn and C.M. Van den Bleek, "A numerical comparison of alternative three-phase reactors with a conventional trickle-bed reactor. The advantages of countercurrent flow for hydrodesulfurization," Chemical Engineering Science. 54, 4791-4799 (1999).

Van Looij, F., P. Van Der Laan, W.H.J. Stork, D.J. DiCamillo and J. Swain, "Key parameters in deep hydrodesulfurization of diesel fuel," Applied Catalysis A: General. 170, 1-12 (1998).

Vissers J. P. R., Beer V. H. J., Prins R., "The Role of Co in Sulphidised CO-MO Hydrodesulphurisation Catalysts supported on Carbon and Alumina," 83, 2145-2155 (1987).

Voorhoeve, R.J.H., "Electron spin resonance study of active centers in nickel-tungsten sulfide hydrogenation catalysts," Journal of Catalysis. 23, 236-242 (1971).

Vradman, L., M.V. Landau, M. Herskowitz, V. Ezersky, M. Talianker, S. Nikitenko, Y. Koltypin and A. Gedanken, "High loading of short WS2 slabs inside SBA-15: Promotion with nickel and performance in hydrodesulfurization and hydrogenation," Journal of Catalysis. 213, 163-175 (2003).

Wan Y. and Zhao D., "On the Controllable Soft-Templating Approach to Mesoporous Silicates," 107, 2821 (2006).

Wijngaarden R.J., Kronberg A., Westerterp K.R., "Industrial Catalysis: Optimizing Catalysts and Processes," Wiley-VCH, Weinheim (1998).

Wu, S., Y. Han, Y.C. Zou, J.W. Song, L. Zhao, Y. Di, S.Z. Liu and F.S. Xiao, "Synthesis of Heteroatom Substituted SBA-15 by the "pH-Adjusting" Method," Chemistry of Materials. 16, 486-492 (2004).

Xu, Y., H. Shang, R. Zhao and C. Liu, "The studies of hydrodesulfurization of 4,6-dimethyldibenzothiophene on sulfided Mo/γ-Al2O3: The effects of reactive temperature and pressure,"ACS Division of Fuel Chemistry, Preprints 49(2004).

Yu, C.C., S. Ramanathan and S.T. Oyama, "New catalysts for hydroprocessing: Bimetallic oxynitrides MI-MII-O-N (MI, MII = Mo, W, V, Nb, Cr, Mn, and Co). Part I. Synthesis and characterization," Journal of Catalysis. 173, 1-9 (1998).

Yui, S., "Producing quality synthetic crude oil from Canadian oil sands bitumen," Journal of the Japan Petroleum Institute. 51, 1-13 (2008).

Yui, S. and T. Dodge, "Catalyst deactivation, kinetics, and product quality of mild hydrocracking of bitumen-derived heavy gas oils," Petroleum Science and Technology. 24, 351-365 (2006).

Yui, S.M. and E.C. Sanford, "Mild hydrocracking of bitumen-derived coker and hydrocracker heavy gas oils: Kinetics, product yields, and product properties," Industrial and Engineering Chemistry Research®. 28, 1278-1284 (1989).

Zhang, J., Z. Ma, J. Jiao, H. Yin, W. Yan, E.W. Hagaman, J. Yu and S. Dai, "Surface functionalization of mesoporous silica SBA-15 by liquid-phase grafting of zirconium phosphate," Microporous and Mesoporous Materials. 129, 200-209 (2010).

Zhao, D., Q. Huo, J. Feng, B.F. Chmelka and G.D. Stucky, "Nonionic triblock and star diblock copolymer and oligomeric sufactant syntheses of highly ordered, hydrothermally stable, mesoporous silica structures," Journal of the American Chemical Society. 120, 6024-6036 (1998a).

Zhao, D., J. Feng, Q. Huo, N. Melosh, G.H. Fredrickson, B.F. Chmelka and G.D. Stucky, "Triblock copolymer syntheses of mesoporous silica with periodic 50 to 300 angstrom pores," Science. 279, 548-552 (1998b).

APPENDIX A:

Calculation of Molar Product Concentrations of N/S and Reaction Rates of HDN/HDS

The sulfur and nitrogen concentrations in the feed and product gas oil liquids are found via the following equations:

$$C_S = \frac{(ppm_{wt}) \cdot \rho_L}{(10^6) \cdot M_S} = \frac{(ppm_{wt}) \cdot (0.98 \times 10^3 \frac{g}{L})}{(10^6) \cdot (32.0640 \frac{g}{mol})} \quad [A.1]$$

$$C_N = \frac{(ppm_{wt}) \cdot \rho_L}{(10^6) \cdot M_N} = \frac{(ppm_{wt}) \cdot (0.98 \times 10^3 \frac{g}{L})}{(10^6) \cdot (14.0067 \frac{g}{mol})} \quad [A.2]$$

ρ_L = Density of HGO feedstock and product (assumed equal)

$C_{S/N}$ = Sulfur/nitrogen heteroatom concentration, mol/L (M)

$M_{S/N}$ = Sulfur/nitrogen molecular weight, g/mol

The reaction rates of hydrodesulfurization and hydrodenitrogenation reactions are calculated based on the following equations:

$$\{R_{HDS}\} = \frac{([Co]_S - [C_P]_S) \cdot LHSV}{(3600 \frac{s}{h}) \cdot \rho_{CAT}} \quad [A.3]$$

$$\{R_{HDN}\} = \frac{([Co]_N - [C_P]_N) \cdot LHSV}{(3600 \frac{s}{h}) \cdot \rho_{CAT}} \quad [A.4]$$

$\{R_{HDS/HDN}\}$ = Global rate of the HDS/HDN reaction, mol/(s·kg-cat)

$[C_{O/P}]_{S/N}$ = Feedstock/product concentration of sulfur/nitrogen, mol/L

LHSV = Liquid hourly space velocity, h^{-1}

ρ_{CAT} = Catalyst pellet density (NiMo/Zr-SBA-15 catalyst)

APPENDIX B:

Calculation of product concentration for HDS and HDN conversion obtained from kinetic study:

Table B.1: Calculation of product concentration for HDS and HDN conversion obtained from kinetic study.

T (°C)	P (Mpa)	LHSV (hr^{-1})	H_2/GO Ratio (Nm^3/m^3)	$[C_P]_S$ (mol/L)	$[C_P]_N$ (mol/L)
375	8.9	0.5	600	0.0571	0.0805
375	8.9	0.5	600	0.0562	0.0809
375	8.9	1	600	0.1130	0.1109
375	8.9	1	600	0.1120	0.1109
375	8.9	1.5	600	0.1756	0.1358
375	8.9	1.5	600	0.1834	0.1357
385	8.9	0.5	600	0.0304	0.0437
385	8.9	0.5	600	0.0326	0.0454
385	8.9	1	600	0.0772	0.0920
385	8.9	1	600	0.0857	0.0904
385	8.9	1.5	600	0.1151	0.1117
385	8.9	1.5	600	0.1118	0.1130
395	8.9	0.5	600	0.0224	0.0194
395	8.9	0.5	600	0.0234	0.0178
395	8.9	1	600	0.0671	0.0729
395	8.9	1	600	0.0657	0.0715

T (°C)	P (Mpa)	LHSV (hr^{-1})	H_2/GO Ratio (Nm^3/m^3)	$[C_P]_S$ (mol/L)	$[C_P]_N$ (mol/L)
395	8.9	1.5	600	0.0970	0.0965
395	8.9	1.5	600	0.0892	0.0986
385	8.9	1	800	0.0637	0.0870
385	8.9	1	800	0.0656	0.0877
385	8.9	1	400	0.1052	0.0963
385	8.9	1	400	0.1046	0.0965
385	7.9	1	600	0.0877	0.1016
385	7.9	1	600	0.0848	0.1034
385	9.9	1	600	0.0650	0.0797
385	9.9	1	600	0.0790	0.0779
370	8.9	1	600	0.1399	0.1488
370	8.9	1	600	0.1123	0.1209
370	8.9	1	600	0.1312	0.1239
370	8.9	1	600	0.1359	0.1242
370	8.9	1	600	0.1300	0.1233
370	8.9	1	600	0.1409	0.1256

APPENDIX C:

Evaluation of External Mass Transfer Resistance for HDS and HDN Reactions:

For determining whether the rate of hydrogen diffusion into heavy gas oil was the rate determining step or not, Charles N. Satterfield (1969) (Satterfield, 1969) criteria was used. The criterion is defined as:

$$\boxed{\frac{10 d_p}{3 C_{H_2}} \left(\frac{-1}{V_C} \frac{dn}{dt} \right) > K_{OVR}} \qquad [C.1]$$

K_{OVR} = Overall mass transfer coefficient for hydrogen, cm/s

C_{H2} = Hydrogen concentration in the liquid phase at equilibrium, mol/mL

$\left(\frac{-1}{V_C} \frac{dn}{dt} \right)$ = Rate of hydrogen conversion in the reaction, mol/(s·mL)

V_c = Volume of loaded catalyst = 5.0 mL

d_P = Average diameter of the catalyst particles = 0.17 cm

The validation of the Satterfield criterion would determine that the mass transfer was dominant in the overall reaction.

Evaluation of the overall mass transfer coefficient (k_{OVR}):

The overall mass transfer coefficient was found by the following equation:

$$\boxed{\frac{1}{k_{OVR}} = \frac{1}{k_L} + \frac{1}{k_S}} \qquad [C.2]$$

The variables are defined as:

k_L = Liquid film side hydrogen –gas oil mass transfer coefficient, cm/s

k_S = Solid side hydrogen –gas oil mass transfer coefficient, cm/s

Calculation of the gas/liquid mass transfer coefficient (k_L):

The gas/liquid mass transfer coefficient was estimated using a correlation by Goto and Smith (1975):

$$\frac{k_L \cdot a_L}{D_L} = \alpha_1 \cdot \left(\frac{L_A \cdot a_L}{\mu_L}\right)^{\alpha_2} \sqrt{\frac{\mu_L}{\rho_L D_L}} \qquad [C.3]$$

The variables are:

a_L = Interfacial surface area over unit volume $\left(\frac{6(1-\varepsilon)}{D_P}\right) \approx =$ 24.7 cm^{-1}

(Assuming the interfacial surface area is equal to the catalyst pellet surface area)

ε = Bed porosity = 0.3 (Wijngaarden R.J., Kronberg A., Westerterp K.R., 1998)

L_A = Liquid mass flow over cross-sectional area, g/(s·cm2)

μ_L = Viscosity of HGO at the operating temperature, g/(s·cm)

D_L = Diffusivity of hydrogen in HGO, cm^2/s

ρ_L = Density of HGO at the operating conditions, g/mL

α_1 = Constant based on the catalyst particle properties* = 7

α_2 = Constant based on the catalyst particle properties* = 0.4

* α_1 and α_2 values found by Korsten and Hoffman (1996) for d_P = 0.17 cm.

Calculation of HGO viscosity (μ_L):

A correlation developed by Glasso (Ahmed T., 1989)was used for determining the viscosity of HGO at the operating temperatures:

$$\mu_L = 3.141 \times 10^{10} \cdot (T - 460)^{-3.444} (\log^0 API)^a \qquad [C.4]$$

$$a = 10.3133 \cdot \log(T - 460) - 36.447 \qquad [C.5]$$

The variables are defined as:

T = Operating temperature, °R

$°API = \frac{141.5}{SG} - 131.5$

SG = Specific gravity of HGO at 15.6°C = 0.98

$°API \approx 12.89$

a = -7.12 to -6.84 (for temperatures ranging from 375°C to 395°C)

μ_L = 1.99 cP to 2.4 cP (for temperatures ranging from 375°C to 395°C)

Calculation of HGO average molecular weight (M_{AVE}):

Average molecular weight of gas oil was evaluated from the Aspen software.

Calculation of diffusivity of hydrogen in gas oil (D_L):

A correlation by Wilke and Chang (1955) was used for calculating the effective diffusivity of hydrogen:

$$\frac{D_L \cdot \mu_L}{T} = (7.4 \times 10^{-8}) \sqrt{\frac{X \cdot M_{AVE}}{V_b^{0.6}}} \qquad [C.6]$$

The variables are defined as:

X = Association parameter = 1 for hydrocarbon mixtures

V_b = Hydrogen molar volume at the normal boiling point

V_b = 14.3 mL/mol (Wiljngaarden et al., 1998)

D_L = 7.64 ×10-^{5} cm^2/s to 9.56 ×10^{-5} cm^2/s

(for temperatures ranging from 375°C to 395°C)

Calculation of HGO density at reaction temperatures and pressures:

A correlation by Standing and Katz (Jiménez et al., 2007) was found for determining the density of gas oils at reactor operating conditions:

$$\rho_L = \rho_{15.6} - \Delta\rho_T + \Delta\rho_P \qquad [C.7]$$

$\Delta\rho_T$ = Temperature density correlation, lbs/ft^3

$\Delta\rho_P$ = Pressure density correlation, lbs/ft^3

$$\Delta\rho_P = [0.167 + (16.181\times10^{-0.0425\rho_{15.6}})]\cdot[\frac{P}{1000}] - 0.01\cdot[0.299 + (263\times10^{-0.603\rho_{15.6}})]\cdot[\frac{P}{1000}]^2 \qquad [C.8]$$

$$\Delta\rho_T = [0.0133 + (152.4\cdot(\rho_{15.6} + \Delta\rho_P)^{-2.45})]\cdot[T - 520] - [8.10\times10^{-6} - (0.0622\times10^{-0.764(\rho_{15.6}+\Delta\rho_P)})]\cdot[T - 520]^2 \qquad [C.9]$$

The values applied to these equations were:

P = 7.9 MPa to 9.9 MPa

T = 1160°R to 1200°R (375°C to 395°C)

From these pressure and temperature values:

$\Delta\rho_P$ = 0.235 to 0.295 lbs/ft^3

$\Delta\rho_T$ = 9.222 to 9.624 lbs/ft^3

ρ_L = 830 to kg/m^3 to 836 kg/m^3

Finally, from the previously calculated values:

k_L = 1.13 ×10^{-4} cm/s to 1.9 ×10^{-4} cm/s

Calculation of the liquid/solid mass transfer coefficient (k_S):

The liquid/solid mass transfer coefficient was estimated using a correlation by Van Krevelen and Krekels (Froment G.F. and Bischoff K.B., 1990):

$$\frac{k_S}{D_L \cdot a_S} = 1.8 \cdot \sqrt{\frac{L_A}{a_S \cdot \mu_L}} \cdot \left(\frac{\mu_L}{\rho_L \cdot D_L}\right)^{1/3} \quad [C.10]$$

The variables are defined as:

a_S = Liquid/solid interfacial surface area = a_L = 24.7 cm^{-1}

Using the previously determined terms:

k_S = 0.9733×10^{-3} cm/s to 1.949×10-^{3} cm/s

Calculation of the equilibrium concentration of hydrogen in gas oil (C_{H2}):

The equilibrium concentration of hydrogen in gas oil was calculated by applying Henry's constant with the assumption of limited solubility:

$$C_{H2} = \frac{P}{H_{H2}} \quad [C.11]$$

The variables are defined as:

H_{H2} = Henry's constant for hydrogen in HGO, MPa·m3/mol

P = Operating pressure = 7.9 MPa to 9.9 MPa

Henry's constant can be calculated using the equation below:

$$H_{H2} = \frac{v_N}{\lambda_{H2} \cdot \rho_L} \quad [C.12]$$

The variables are defined as:

v_N = Hydrogen molar volume at standard conditions = 22.4 L/mol

ρ_L = Density of HGO at the operating conditions = 830 kg/m^3 to 836 kg/m^3

λ_{H2} = Hydrogen solubility in HGO, mL/(kg·MPa)

A correlation established by (Korsten and Hoffmann, 1996)was applied to estimate the solubility of hydrogen in gas oil fractions:

$$\lambda_{H2} = z_0 + z_1 \cdot T + z_2 \cdot \frac{T}{\rho_{20}} + z_3 \cdot T^2 + z_4 \cdot \frac{1}{(\rho_{20})^2} \quad [C.13]$$

The parameters are defined as:

z_0 = -0.55973

z_1 = -0.42947×10^{-3}

z_2 = 3.07539×10^{-3}

z_3 = 1.94593×10^{-6}

z_4 = 0.83578

T = Operating temperature = 375°C to 395°C

ρ_{20} = Density of HGO at 20°C = 0.98 g/ml

For the operating conditions, the following value ranges were found:

λ_{H2} = 1.58×10^3 ml/(kg·MPa) to 1.68×10^3 ml/(kg·MPa)

H_{H2} = 1.602 MPa·m3/mol to 1.696 MPa·m3/mol

C_{H2} = 4.84×10^{-4} mol/ml to 6.12 ×10^{-4} mol/ml

Calculating the hydrogen conversion rate for HDS and HDN:

The following simplified stoichiometric equations were used for finding the rate of hydrogen conversion for both hydrodesulfurization and hydrodenitrogenation:

$$|R-S| + x_{HDS} H_2 \longrightarrow |R-H|_{[2x_{HDS}-2]} + H_2S \quad [C.14]$$

$$|R-S| + x_{HDN} H_2 \longrightarrow |R-H|_{[2x_{HDN}-2]} + NH_3 \quad [C.15]$$

The rates of nitrogen and sulfur removal for varying operating conditions applied to the hydrotreating process were determined from section and Appendix B of the report. Equations C.14 and C.15 allow for the following substitutions:

$$\boxed{\left(\frac{-1}{V_C}\cdot\frac{dn}{dt}\right)=\left(\frac{x_{HDS}\cdot r_{HDS}}{V_C}\right)} \qquad [C.16]$$

$$\boxed{\left(\frac{-1}{V_C}\cdot\frac{dn}{dt}\right)=\left(\frac{x_{HDN}\cdot r_{HDN}}{V_C}\right)} \qquad [C.17]$$

Where r_{HDS} is the molar rate of sulfur removal and r_{HDN} is the molar rate of nitrogen removal achieved from the hydrotreating catalyst (mol/s). Assuming the hydrogenation of a 5-membered thiophenic ring for sulfur removal and a 6-membered basic pyridinic ring for nitrogen removal, the following stoichiometric values were assumed for the HDS and HDN reactions of heavy gas oil:

$$\boxed{x_{HDS}=4.0} \qquad \boxed{x_{HDN}=5.0}$$

Given these assumed values for each reaction, the following value ranges were found for each side of the Satterfield inequality:

Hydrodesulfurization Reaction:

Left hand side of Satterfield's criterion = 5.79×10^{-4} cm/s to 16.26×10^{-4} cm/s

Right hand side of Satterfield's criterion = 1.015×10^{-4} cm/s to 1.732×10^{-4} cm/s

Hydrodenitrogenation Reaction:

Left hand side of Satterfield's criterion = 0.99×10^{-4} cm/s to 2.51×10^{-4} cm/s

Right hand side of Satterfield's criterion = 1.015×10^{-4} cm/s to 1.732×10^{-4} cm/s

A summary of all the operating conditions and estimated parameters contributing to these results can be found in Table C.1 on the following page.

Table C.1 : Summary of the external mass transfer resistances study performed for a trickle bed hydrotreating reactor loaded with NiMo/Zr-SBA-15 catalyst

Parameter	Symbol	Units	Value	Range
Pressure	P	Mpa	8.9	7.9-9.9
Temperature	T	^0C	385	375-395
Av boling point of HGO	T_B	^0C	436	-
Liquid hourly space velosity	LHSV	hr^{-1}	1	0.5-1.5
Feed flow rate	L	g/hr	4.9	2.45-7.35
Catalyst particle size	d_P	cm	0.17	-
Bed porosity (Wijngaarden et al 1998)	ε	-	0.3	-
Interfacial surface area per unit volume	α_L	cm^{-1}	24.7	
Liquid mass flow per unit area	L_A	$x\ 10^{-3}$ g/(cm^2.s)	1.73	0.87-2.60
HGO density @ operating condition	ρ_L	kg/m^3	832.59	830-836
HGO density @ 15^0C	ρ_{15}	kg/m^3	980	-
HGO density @ 20^0C	ρ_{20}	kg/m^3	980	-
Pressure density correlation	$\Delta\rho_P$	lbs/ft^3	0.2649	0.235-0.295
Temperature density correlation	$\Delta\rho_T$	lbs/ft^3	9.467	9.222-9.624
HGO specific gravity @60^0F	SG	-	0.98	-
API density rating	^0API	-	12.89	-
Constant in viscosity correlation	α	-	-6.950	(-)7.12 - (-)6.84
HGO average molecular weight	M_{AVE}	kg/mol	361.4	-
HGO viscosity @ operating temp	μ_L	cP	2.144	1.993-2.400
Henry's constant	H_{H2}	$x10^{-2}$ Mpa-m^3/gmol	1.639	1.602-1.696
H_2 molecular volume, std condition	v_N	cc/mol	22400	-
Concentration of H_2 in HGO	C_{H2}	$x\ 10^{-4}$ mol/cc	5.47	4.84-6.12
Solubility of H2 in HGO (Hoffman et al,	λ_{H2}	$x\ 10^3$ cc/kg	1.64	1.58-1.68
Bulk diffusivity of H_2	D_L	$x\ 10^{-5}$ cm^2/s	8.75	7.64-9.56
Particle properties constant (Korsten &	α_1	-	7	-
Particle properties constant (Korsten &	α_2	-	0.4	-
Liquid side: H_2/HGO mass transfer	k_L	$x\ 10^{-4}$ cm/s	1.56	1.13-1.9
Solid side: H_2/HGO mass transfer	k_S	$x10^{-3}$ cm/s	14.81	0.973-1.949
Overall mass transfer cofficient	k_{OVR}	$x\ 10^{-4}$ cm/s	1.41	1.015-1.732
Rate of H_2 consumption for HDS reaction	$(x_{HDS}.r_{HDS})/V_C$	$x\ 10^{-7}$ mol.H_2/(s.cc)	10.83	5.5-16.05
Rate of H_2 consumption for HDN	$(x_{HDN}.r_{HDN})/V_C$	$x\ 10^{-7}$ mol.H_2/(s.cc)	1.72	0.927-2.448
Satterfield's criterian for HDS, LHS	S_{HDS}	$x\ 10^{-4}$	11.22	5.79-16.26
Satterfield's criterian for HDN, LHS	S_{HDN}	$x\ 10^{-4}$	1.78	0.99-2.51

APPENDIX D:
Evaluation of the Internal Mass Transfer Resistances for the HDS and HDN Reactions

The preliminary calculations performed as part of this evaluation was to see if isothermality could be assumed within the catalyst pellets. The determination of each pellet's degree of isothermality was performed in two ways: by finding both the highest potential temperature rise between the core and the surface of the pellet (Fogler, 2006), as well as by confirming Anderson's criterion (Anderson, 1963) .

Maximum temperature rise (ΔT_{MAX}):

$$\beta = \frac{\Delta T_{MAX}}{T_S} = \frac{\Delta H_{R,i} \cdot D_i \cdot [C_i]_S}{k_t \cdot T_S} \qquad [D.1]$$

The variables are defined as:

$\Delta H_{R,i}$ = Heat of HDS/HDN reaction, kJ/mol

$[C_i]_S$ = Catalyst surface concentration of sulfur/nitrogen species, mol/ml

k_t = Thermal conductivity of the NiMo/Zr-SBA-15 catalyst pellet.

kt = 1.0225 W/(cm·K) (assuming a pure catalyst pellet)

T_S = Pellet surface temperature (reaction temperatures)

Calculation of the HDS/HDN heats of reaction:

The hydrodesulfurization heat of reaction for heavy gas oil from Athabasca bitumen was approximated by using the heat of reaction range for most thiophene molecules; 63 to 66 kJ/mol of hydrogen consumed (Speight, 2006). The hydrodenitrogenation heat of reaction for HGO from Athabasca bitumen was approximated by using the heat of reaction range for most quinoline molecules; 65 to 68 kJ/mol of hydrogen consumed (Cocchetto and Satterfield, 1981). These values were converted to units of kJ/mol of sulfur/nitrogen removed by using the stoichiometric coefficients (x_{HDS} and x_{HDN}) discussed in Appendix C.

$\Delta H_{R,HDS}$ = 63 to 66 kJ/mol of H_2 consumed

$\Delta H_{R,HDS}$ = 260 kJ/mol of sulfur

$\Delta H_{R,HDN}$ = 65 to 68 kJ/mol of H_2 consumed

$\Delta H_{R,HDN}$ = 265 kJ/mol of nitrogen

Calculating the effective diffusivities of organosulfur and organonitrogen compounds in HGO ($[D_S]_E/[D_N]_E$):

The effective diffusivity of sulfur compounds was estimated by the following equation:

$$[D_i]_E = \frac{\varepsilon_P \cdot D_i}{\gamma_P} \qquad [D.2]$$

The variables are defined as:

ε_P = Porosity of the catalyst pellets

γ_P = Tortuosity of the catalyst pellets

D_i = Bulk diffusivity of organosulfur compounds, cm^2/g

A correlation by Probst and Wohlfahrt (1979) was used to find the ratio of porosity and tortuosity of pelletized catalysts:

$$\frac{\varepsilon_P}{\gamma_P} = \left[\frac{\varepsilon_P^{\,m}}{(2-\varepsilon_P)^{m+1}}\right] \qquad [D.3]$$

Values of ***m*** were found to range from 0.70 to 1.65 for porous compressed catalysts (group D). It was recommended to use an ***m*** value of 1.05 when not otherwise determined (Wijngaarden et al., 1998). Porosity values were found to range from 0.05 to 0.65 (average value was used, 0.35). Based on these conditions, the porosity/tortuosity values were found:

$$\frac{\varepsilon_P}{\gamma_P} = 0.119$$

Calculating the bulk diffusivities of organosulfur and organonitrogen compounds in HGO (D_S/D_N):

The assumption was made that the organosulfur and organonitrogen compounds held the same density, average boiling point, average molecular weight and average molar volume as the heavy gas oil feedstock. The bulk diffusivities of each species were found using the Tyn-Calus correlation (Reid et al., 1987):

$$D_i = (8.93\times10^{-8})\cdot\left(\frac{\nu_L^{0.267}}{\nu_i^{0.433}}\right)\cdot\left(\frac{T}{\mu_L}\right) = (8.93\times10^{-8})\cdot\left(\frac{T}{\mu_L\cdot\nu_i^{0.166}}\right) \quad [D.4]$$

The variables are defined as:

T = Operating temperature

μ_L = HGO viscosity at operating conditions = 1.99 cP to 2.24 cP

vi = Molar volume of sulfur/nitrogen molecules under standard conditions, mL/mol

vL = Molar volume of HGO under standard conditions, mL/mol

The molar volume of the gas oil was found by the following:

$$\nu_i = (0.285)\cdot\nu_C^{1.048} \quad [D.5]$$

$\boldsymbol{\nu_C}$= Critical specific molar volume of HGO, mL/mol

The critical specific molar volume is given by:

$$\nu_C = \nu_C^{m}\cdot M_{AVE} \quad [D.6]$$

M_{AVE} = 361 g/mol

v_C^m = Critical specific mass volume, mL/g

The critical specific mass volume of liquid was calculated using a correlation by Raizi and Daubert (Ahmed T., 1989):

$$\boxed{v_C^{\,m} = (7.5214\times10^{-3})\cdot T_b^{\,0.2896}\cdot SG^{-0.7666}} \qquad [D.7]$$

The variables are defined as:

$v_C^{\,m}$ = Critical specific mass volume, ft3/lb

T_b = Average boiling point temperature = 816.8 °F

$SG_{15.6}$ = Specific gravity at 15.6°C = 0.98

These values lead to the following results:

$v_C^{\,m}$ = 3.94 mL/g

v_C = 1423 mL/mol

v_i = 574.75 mL/mol

$Di = D_S = D_N$ = 8.332 ×10^{-6} cm2/g to 10.43 ×10^{-6} cm2/g

$[D_S]_E = [D_N]_E$ = 8.332 ×10^{-6} cm2/g to 10.43 ×10^{-6} cm2/g

The effective diffusivity values lead to isothermality ratios of:

β_{HDS} = 3.47 ×10^{-6} to 4.18×10^{-6}

β_{HDN} = 7.24×10^{-7} to 8.72 ×10^{-7}

Because the HDS and HDN reactions are occurring simultaneously, the sum of the beta values would give the overall maximum temperature change with respect to the catalyst surface temperature. This gives a highest possible ΔT_{MAX} value of 0.0034 K, which can be considered negligible.

Anderson's Criterion:

$$\boxed{\frac{|\triangle H_{R,i}|\cdot\{R_i\}\cdot d_P^{\,2}}{k_t\cdot T_S} < \frac{3\cdot T_S\cdot R}{E_i}} \qquad [D.8]$$

The variables are defined as:

$\{R_i\}$ = Global reaction rate: HDS/HDN, mol/(s·mL)

k_t = Catalyst thermal conductivity = 1.022 W/(cm·K)

R = Universal gas constant = 8.314 J/(mol·K)

E_i = Energy of activation: HDS/HDN, J/mol

The range of operating conditions tested, the values for the left and right hand side of Anderson's criterion were as follows:

Left hand side of Anderson's criterion (HDS) = 1.689×10^{-7} to 3.668×10^{-7}

Right hand side of Anderson's criterion (HDS) = 0.034 to 0.036

Left hand side of Anderson's criterion (HDN) = 4.152×10^{-9} to 9.299×10^{-9}

Right hand side of Anderson's criterion (HDN) = 0.033 to 0.0345

The results confirm that isothermal behavior can be assumed when examining the internal mass transfer resistances of the hydrotreating process. Table D.1 at the end of this appendix provides a summary of the pertinent parameters and results of the catalyst pellet isothermality study.

Calculation of Φ:

A dimensionless modulus (Φ), analogous to the Thiele modulus found without knowledge of the intrinsic reaction rate, was found for each collected sample in the kinetic study. The dimensionless modulus was used to represent an estimation of the pore diffusion resistance (Satterfield, 1991):

$$\Phi = \frac{d_P^{\,2}}{4\cdot[D]_E}\cdot\frac{\{R_i\}}{[C_i]_S} \qquad [D.9]$$

The variables are defined as:
d_P = Average diameter of the catalyst particles = 0.17 cm

$\{R_i\}$ = Global reaction rate: HDS/HDN, mol/(s·mL)

$[D_i]_E$ = Effective diffusivity of sulfur/nitrogen compounds, cm2/g

$[C_i]_S$ = Catalyst surface concentration of sulfur/nitrogen species, mol/mL

The change in the global reaction rate and the change in surface concentration of sulfur and nitrogen heteroatoms allow the dimensionless modulus to be calculated at both the inlet and outlet of the reactor. In finding the dimensionless modulus, a rough approximation of the effectiveness factor (η) could be determined by applying the following equations in unison (Satterfield, 1991):

$$\boxed{\Phi = (\varphi)^2 \cdot \eta} \qquad [D.10]$$

$$\boxed{\eta = \frac{3}{\varphi}\left[\frac{1}{\tanh(\varphi)} - \frac{1}{\varphi}\right]} \qquad [D.11]$$

Solving for the effectiveness factor using equations [D.10] and [D.11] will only provide a rough estimate of both η and φ, the true Thiele modulus. This is because equation D.10 only applies to integer-power rate equations for spherical catalyst pellets. Additionally, equation D.11 only applies to isothermal first-order reactions for spherical catalysts. Nonetheless, these equations to provide a measure of comparison between the effectiveness factors for each collected sample.

Table D.2 provides a summary of all the dimensionless modulus values for the inlet and outlet ($[\Phi_O]_S$ and $[\Phi P]_S$), as well as all the determined effectiveness factors ($[\eta_O]_S$ and $[\eta_P]_S$), for the hydrodesulfurization kinetic study.

Table D.3 provides a summary of all the dimensionless modulus values for the inlet and outlet ($[\Phi_O]_N$ and $[\Phi_P]_N$), as well as all the determined effectiveness factors ($[\eta_O]_N$ and $[\eta_P]_N$), for the hydrodenitrogenation kinetic study.

Table D.1: Summary of isothermality evaluation for NiMo/Zr-SBA-15 catalyst pellets.

Parameter	Symbol	Units	Value	Range
Pressure	P	Mpa	8.9	7.9-9.9
Temperature	T	°C	385	375-385
Av boling point of HGO	T_B	°C	436	-
Liquid hourly space velosity	LHSV	hr^{-1}	1	0.5-1.5
Feed flow rate	L	g/hr	4.9	2.45-7.35
Catalyst particle size	d_P	cm	1.7	-
HGO density @ 15 °C	ρ	kg/m3	980	-
HGO viscosity @ operating temp	μ_L	cP	2.14	1.99-2.44
Heat of HDS reaction	ΔH_{HDS}	kJ/mol	260	-
Heat of HDN reaction	ΔH_{HDN}	kJ/mol	265	-
Effective diffusivity of sulfur	$(D_E)_S$	x 10^{-6} cm^2/s	1.13	0.991-1.24
Effective diffusivity of Nitrogen	$(D_E)_N$	x 10^{-6} cm^2/s	1.13	0.991-1.25
Porosity of catalyst pellet	ε_P	-	0.35	-
Parameter m (Probst and Wohlfahrt, 1979)	m	-	1.05	-
Porosity /tortuosity ratio	ε_P/ν_L	-	0.119	-
Diffusivity of S compounds	D_S	x 10^{-6} cm^2/s	9.54	8.332-10.43
Diffusivity of N compounds	D_N	x 10^{-6} cm^2/s	9.54	8.332-10.43
Surface concentration in HGO	$C_{S,S}$	mol/l	0.772	0.0224-0.1834
Surface concentration in HGO	$C_{N,S}$	mol/l	0.091	0.018-0.149
Thermal conductivity of catalyst pellet	k_T	W/cm-K	1.022	-
Activation energy of HDS	E_{HDS}	kJ/mol	115	-
Activation energy of HDN	E_{HDS}	kJ/mol	120	-
β for HDS	β_{HDS}	$x10^{-6}$	3.88	3.47-4.18
β for HDN	β_{HDN}	$x10^{-7}$	8.11	7.24-8.72
Global HDS reaction rate	$r_{hds\ global}$	mol/s.cc $x10^{-7}$	2.71	1.38-4.01
Global HDN reaction rate	$r_{hds\ global}$	mol/s.cc $x10^{-7}$	3.43	1.88-4.96
Anderson's criteria LHS (HDS)	$(A_{HDS})_{LHS}$	$x10^{-7}$	2.72	1.689-3.668
Anderson's criteria RHS (HDS)	$(A_{HDS})_{RHS}$	-	0.035	0.034-0.036
Anderson's criteria LHS (HDN)	$(A_{HDN})_{LHS}$	$x10^{-9}$	6.78	4.152-9.299
Anderson's criteria RHS (HDN)	$(A_{HDN})_{RHS}$	-	0.034	0.033-0.0345

Table D.2: Summary of the dimensionless modulus and effectiveness factors for the internal mass transfer resistance study of HGO hydrodesulfurization.

T (°C)	P (Mpa)	LHSV (hr^{-1})	G/O Ratio (Nm^3/m^3)	$\Phi_{INLET,hds}$	$\Phi_{OUTLET,\ hds}$	$\eta_{INLET,hds}$	$\eta_{OUTLET,hds}$
375	8.9	0.5	600	0.914	16.856	0.941	0.385
375	8.9	0.5	600	0.915	17.139	0.941	0.380
375	8.9	1	600	1.726	16.080	0.891	0.398
375	8.9	1	600	1.728	16.227	0.891	0.395
375	8.9	1.5	600	2.417	14.480	0.851	0.427
375	8.9	1.5	600	2.395	13.743	0.852	0.441
385	8.9	0.5	600	0.858	29.688	0.944	0.250
385	8.9	0.5	600	0.856	27.674	0.944	0.265
385	8.9	1	600	1.637	22.304	0.896	0.314
385	8.9	1	600	1.623	19.929	0.897	0.341
385	8.9	1.5	600	2.361	21.578	0.854	0.321
385	8.9	1.5	600	2.369	22.308	0.853	0.313
395	8.9	0.5	600	0.792	37.266	0.948	0.207
395	8.9	0.5	600	0.791	35.535	0.948	0.215
395	8.9	1	600	1.515	23.743	0.904	0.299
395	8.9	1	600	1.517	24.293	0.903	0.294

T (°C)	P (Mpa)	LHSV (hr^{-1})	G/O Ratio (Nm^3/m^3)	$\Phi_{INLET,hds}$	$\Phi_{OUTLET,\ hds}$	$\eta_{INLET,hds}$	$\eta_{OUTLET,hds}$
395	8.9	1.5	600	2.203	23.906	0.863	0.297
395	8.9	1.5	600	2.221	26.214	0.862	0.276
385	8.9	1	800	1.660	27.423	0.895	0.267
385	8.9	1	800	1.657	26.568	0.895	0.273
385	8.9	1	400	1.590	15.916	0.899	0.400
385	8.9	1	400	1.591	16.009	0.899	0.399
385	7.9	1	600	1.620	19.441	0.897	0.347
385	7.9	1	600	1.625	20.157	0.897	0.338
385	9.9	1	600	1.658	26.821	0.895	0.271
385	9.9	1	600	1.634	21.776	0.896	0.319
370	8.9	1	600	1.755	13.203	0.889	0.453
370	8.9	1	600	1.808	16.942	0.886	0.383
370	8.9	1	600	1.772	14.219	0.888	0.432
370	8.9	1	600	1.763	13.657	0.889	0.443
370	8.9	1	600	1.775	14.369	0.888	0.429
370	8.9	1	600	1.753	13.093	0.889	0.455

Table D.3: Summary of the dimensionless modulus and effectiveness factors for the internal mass transfer resistance study of HGO hydrodenitrogenation.

T (°C)	P (Mpa)	LHSV (hr^{-1})	G/O Ratio (Nm^3/m^3)	$\Phi_{INLET,hdn}$	$\Phi_{OUTLET,hdn}$	$\eta_{INLET,hdn}$	$\eta_{OUTLET,hdn}$
375	8.9	0.5	600	0.606	1.623	0.960	0.897
375	8.9	0.5	600	0.604	1.608	0.960	0.898
375	8.9	1	600	0.939	1.825	0.940	0.886
375	8.9	1	600	0.939	1.826	1.004	0.886
375	8.9	1.5	600	1.074	1.705	0.931	0.892
375	8.9	1.5	600	1.074	1.706	0.931	0.892
385	8.9	0.5	600	0.705	3.477	0.953	0.793
385	8.9	0.5	600	0.697	3.312	0.954	0.801
385	8.9	1	600	1.013	2.375	0.935	0.856
385	8.9	1	600	1.026	2.448	0.934	0.852
385	8.9	1.5	600	1.277	2.465	0.918	0.848
385	8.9	1.5	600	1.261	2.404	0.919	0.854
395	8.9	0.5	600	0.736	8.183	0.951	0.590
395	8.9	0.5	600	0.742	8.964	0.951	0.564
395	8.9	1	600	1.071	3.168	0.931	0.809
395	8.9	1	600	1.081	3.258	0.931	0.804

T (°C)	P (Mpa)	LHSV (hr-1)	G/O Ratio (Nm^3/m^3)	$\Phi_{INLET,hdn}$	$\Phi_{OUTLET,\ hdn}$	$\eta_{INLET,hdn}$	$\eta_{OUTLET,hdn}$
395	8.9	1.5	600	1.341	2.997	0.914	0.818
395	8.9	1.5	600	1.317	2.880	0.917	0.825
385	8.9	1	800	1.054	2.613	0.932	0.839
385	8.9	1	800	1.048	2.576	0.933	0.845
385	8.9	1	400	0.978	2.188	0.937	0.864
385	8.9	1	400	0.976	2.179	0.937	0.864
385	7.9	1	600	0.934	1.983	0.939	0.877
385	7.9	1	600	0.919	1.916	0.940	0.881
385	9.9	1	600	1.114	3.011	0.929	0.817
385	9.9	1	600	1.129	3.124	0.928	0.811
370	8.9	1	600	0.627	0.908	0.958	0.941
370	8.9	1	600	0.889	1.586	0.942	0.899
370	8.9	1	600	0.861	1.497	0.944	0.904
370	8.9	1	600	0.858	1.488	0.944	0.905
370	8.9	1	600	0.867	1.515	0.943	0.903
370	8.9	1	600	0.845	1.451	0.945	0.907

APPENDIX E:
Permissions to Use Figures from Literatures

1. Permission to use Figure 2.2

pib255

From: Yui, Sok [Yui.Sok@syncrude.com]
Sent: Friday, April 29, 2011 8:03 AM
To: pib255
Subject: RE: Permission to use figure
Attachments: Yui OGJ 121707 - Syncrude upgrader revamp.pdf

Dear Piyali,

Regarding your inquiry to use Fig. 1 in the J of JPI for your MSc thesis, the figure appears in an open literature; therefore, no problems as far as you properly refer to the literature. It is nice to know that somebody is interested in my paper.

For your information, I am sending you my earlier O&GJ paper that is referred to as ref. no. 6 in the JPI paper. You will learn how the new UE-1 project contributes to produce the quality SCO from oil sands bitumen.

Thank you for showing your interest in my paper and good luck for your endeavor.

Sok Yui
Syncrude Canada Ltd.
Edmonton Research and Development Centre
9421 - 17 Avenue, Edmonton, Alberta T6N 1H4

Tel: (780) 970 - 6872

From: pib255 [mailto:pib255@mail.usask.ca]
Sent: Thursday, April 28, 2011 6:15 PM
To: Yui, Sok
Subject: Permission to use figure

Respected Sir,

I'm a graduate research student from University of Saskatchewan. My research topic is "Catalytic Performances of NiMo/Zr-SBA-15 Catalysts for the Hydrotreating of Bitumen Derived Heavy Gas Oil". Currently, I'm in the process of writing my thesis and I wish to use Figure 1 (A simplified Syncrude's Upgrading Process) of your journal " Producing Quality Synthetic Crude Oil from Canadian Oil Sands Bitumen" which was published in *Journal of the Japan Petroleum Institute, 51, (1), 1-13 (**2008**)*. I have made similar figure in excel sheet to use for my thesis upon your kind permission. I would be grateful to you if you give me permission for using the Figure 1 for my thesis which needs to be submitted as part of my MSc thesis defense from University of Saskatchewan, Canada.

Sincerely,

Piyali Biswas
Graduate Student
Department of Chemical Engineering
University of Saskatchewan
College of Engineering

2. Permission to use Figure 2.4

pib255

From: Chunshan Song [csong@psu.edu]
Sent: Wednesday, April 27, 2011 6:51 PM
To: pib255
Subject: RE: Permission to use figure
Attachments: CatTod2003 DeS Review.pdf

Dear Piyali Biswas

Please use the Figure and cite the attached journal reference, which is a review paper based on the conference paper you asked for.

The attached review paper is more comprehensive and more complete.

You have my permission to use the Fig 1 and Fig 17 to show the reactivities of sulfur compounds in hydrotreating.

Good luck on your study.

Chunshan Song, PhD
Director, EMS Energy Institute
Distinguished Professor of Fuel Science and Chemical Engineering
Departments of Energy & Mineral Engineering, and Chemical Engineering
Associate Director, Penn State Institutes of Energy and the Environment
The Pennsylvania State University
C211 CUL, University Park
PA 16802-2323, USA

From: pib255 [mailto:pib255@mail.usask.ca]
Sent: Wednesday, April 27, 2011 7:07 PM
To: csong@psu.edu
Subject: Permission to use figure

Dear Sir,

I'm a graduate research student from University of Saskatchewan. My research topic is "Catalytic Performances of NiMo/Zr-SBA-15 Catalysts for the Hydrotreating of Bitumen Derived Heavy Gas Oil". Currently, I'm in the process of writing my thesis and I wish to use the Figure 1 (Reactivity of various organic sulfur compounds in hydrodesulfurization versus their ring sizes and positions of alkyl substitutions on the ring) of your journal "New Approaches to Deep Desulfurization for Ultra-Clean Gasoline and Diesel Fuels: An Overview" which was published in *Fuel Chemistry Division Preprints* ***2002****, 47(2),* 438. I have made similar figure in excel sheet to use for my thesis upon your kind permission. I would be grateful to you if you give me permission for using the Figure 1 for my thesis which needs to be submitted as part of my MSc thesis defense from University of Saskatchewan, Canada.

Sincerely,

Piyali Biswas
Graduate Student
Department of Chemical Engineering
University of Saskatchewan

3. Permission to use Figure 2.12 and 2.13

ELSEVIER LICENSE
TERMS AND CONDITIONS

Apr 28, 2011

This is a License Agreement between Piyali Biswas ("You") and Elsevier ("Elsevier") provided by Copyright Clearance Center ("CCC"). The license consists of your order details, the terms and conditions provided by Elsevier, and the payment terms and conditions.

All payments must be made in full to CCC. For payment instructions, please see information listed at the bottom of this form.

Supplier	Elsevier Limited The Boulevard,Langford Lane Kidlington,Oxford,OX5 1GB,UK
Registered Company Number	1982084
Customer name	Piyali Biswas
Customer address	Department of Chemical Engineering Saskatoon, SK S7N 5A9
License number	2657920175931
License date	Apr 28, 2011
Licensed content publisher	Elsevier
Licensed content publication	Catalysis Today
Licensed content title	Effect of the nitrogen heterocyclic compounds on hydrodesulfurization using *in situ* hydrogen and a dispersed Mo catalyst
Licensed content author	Kun Liu, Flora T.T. Ng
Licensed content date	15 January 2010
Licensed content volume number	149
Licensed content issue number	1-2
Number of pages	7
Start Page	28
End Page	34
Type of Use	reuse in a thesis/dissertation
Portion	figures/tables/illustrations
Number of figures/tables /illustrations	2
Format	both print and electronic
Are you the author of this Elsevier article?	No
Will you be translating?	No
Order reference number	Fig 2.12 and 2.13
Title of your thesis/dissertation	Catalytic Performances of NiMo/Zr-SBA-15 Catalysts for the Hydrotreating of Bitumen Derived Heavy Gas Oil
Expected completion date	May 2011
Estimated size (number of pages)	230
Elsevier VAT number	GB 494 6272 12
Permissions price	0.00 USD
VAT/Local Sales Tax	0.0 USD / 0.0 GBP
Total	0.00 USD

4. Permission to use Figure 2.14

AMERICAN CHEMICAL SOCIETY LICENSE
TERMS AND CONDITIONS

Apr 27, 2011

This is a License Agreement between Piyali Biswas ("You") and American Chemical Society ("American Chemical Society") provided by Copyright Clearance Center ("CCC"). The license consists of your order details, the terms and conditions provided by American Chemical Society, and the payment terms and conditions.

All payments must be made in full to CCC. For payment instructions, please see information listed at the bottom of this form.

License Number	2657350651029
License Date	Apr 27, 2011
Licensed content publisher	American Chemical Society
Licensed content publication	Energy & Fuels
Licensed content title	Hydrodenitrogenation of Quinoline Catalyzed by MCM-41-Supported Nickel Phosphides
Licensed content author	Mohong Lu et al.
Licensed content date	Mar 1, 2007
Volume number	21
Issue number	2
Type of Use	Thesis/Dissertation
Requestor type	Not specified
Format	Print
Portion	Table/Figure/Micrograph
Number of Table/Figure /Micrographs	1
Author of this ACS article	No
Order reference number	Figure 2.14
Title of the thesis / dissertation	Catalytic Performances of NiMo/Zr-SBA-15 Catalysts for the Hydrotreating of Bitumen Derived Heavy Gas Oil
Expected completion date	May 2011
Estimated size(pages)	230
Billing Type	Invoice
Billing Address	Department of Chemical Engineering 57 campus drive Saskatoon, SK S7N 5A9 Canada
Customer reference info	
Total	0.00 USD

5. Permission to use Figure 2.19

ELSEVIER LICENSE
TERMS AND CONDITIONS

Apr 27, 2011

This is a License Agreement between Piyali Biswas ("You") and Elsevier ("Elsevier") provided by Copyright Clearance Center ("CCC"). The license consists of your order details, the terms and conditions provided by Elsevier, and the payment terms and conditions.

All payments must be made in full to CCC. For payment instructions, please see information listed at the bottom of this form.

Supplier	Elsevier Limited The Boulevard,Langford Lane Kidlington,Oxford,OX5 1GB,UK
Registered Company Number	1982084
Customer name	Piyali Biswas
Customer address	Department of Chemical Engineering Saskatoon, SK S7N 5A9
License number	2657340332966
License date	Apr 27, 2011
Licensed content publisher	Elsevier
Licensed content publication	Journal of Catalysis
Licensed content title	Location and coordination of promoter atoms in Co- and Ni-promoted MoS_2-based hydrotreating catalysts
Licensed content author	Jeppe V. Lauritsen, Jakob Kibsgaard, Georg H. Olesen, Poul G. Moses, Berit Hinnemann, Stig Helveg, Jens K. Nørskov, Bjerne S. Clausen, Henrik Topsøe, Erik Lægsgaard, Flemming Besenbacher
Licensed content date	25 July 2007
Licensed content volume number	249
Licensed content issue number	2
Number of pages	14
Start Page	220
End Page	233
Type of Use	reuse in a thesis/dissertation
Intended publisher of new work	other
Portion	figures/tables/illustrations
Number of figures/tables /illustrations	1
Format	print
Are you the author of this Elsevier article?	No
Will you be translating?	No
Order reference number	Figure 2.19
Title of your thesis/dissertation	Catalytic Performances of NiMo/Zr-SBA-15 Catalysts for the Hydrotreating of Bitumen Derived Heavy Gas Oil
Expected completion date	May 2011
Estimated size (number of pages)	230
Elsevier VAT number	GB 494 6272 12
Permissions price	0.00 USD
VAT/Local Sales Tax	0.0 USD / 0.0 GBP
Total	0.00 USD

6. Permission to use Figure 2.20

ELSEVIER LICENSE
TERMS AND CONDITIONS

Apr 27, 2011

This is a License Agreement between Piyali Biswas ("You") and Elsevier ("Elsevier") provided by Copyright Clearance Center ("CCC"). The license consists of your order details, the terms and conditions provided by Elsevier, and the payment terms and conditions.

All payments must be made in full to CCC. For payment instructions, please see information listed at the bottom of this form.

Supplier	Elsevier Limited The Boulevard,Langford Lane Kidlington,Oxford,OX5 1GB,UK
Registered Company Number	1982084
Customer name	Piyali Biswas
Customer address	Department of Chemical Engineering Saskatoon, SK S7N 5A9
License number	2657350024154
License date	Apr 27, 2011
Licensed content publisher	Elsevier
Licensed content publication	Applied Catalysis A: General
Licensed content title	The single-layered morphology of supported MoS_2-based catalysts—The role of the cobalt promoter and its effects in the hydrodesulfurization of dibenzothiophene
Licensed content author	Gilles Berhault, Myriam Perez De la Rosa, Apurva Mehta, Miguel José Yácaman, Russell R. Chianelli
Licensed content date	31 July 2008
Licensed content volume number	345
Licensed content issue number	1
Number of pages	9
Start Page	80
End Page	88
Type of Use	reuse in a thesis/dissertation
Intended publisher of new work	other
Portion	figures/tables/illustrations
Number of figures/tables /illustrations	1
Format	print
Are you the author of this Elsevier article?	No
Will you be translating?	No
Order reference number	Figure 220
Title of your thesis/dissertation	Catalytic Performances of NiMo/Zr-SBA-15 Catalysts for the Hydrotreating of Bitumen Derived Heavy Gas Oil
Expected completion date	May 2011
Estimated size (number of pages)	230
Elsevier VAT number	GB 494 6272 12
Permissions price	0.00 USD
VAT/Local Sales Tax	0.0 USD / 0.0 GBP
Total	0.00 USD

7. Permission to use Figure 2.23

ELSEVIER LICENSE
TERMS AND CONDITIONS

Apr 27, 2011

This is a License Agreement between Piyali Biswas ("You") and Elsevier ("Elsevier") provided by Copyright Clearance Center ("CCC"). The license consists of your order details, the terms and conditions provided by Elsevier, and the payment terms and conditions.

All payments must be made in full to CCC. For payment instructions, please see information listed at the bottom of this form.

Supplier	Elsevier Limited The Boulevard,Langford Lane Kidlington,Oxford,OX5 1GB,UK
Registered Company Number	1982084
Customer name	Piyali Biswas
Customer address	Department of Chemical Engineering Saskatoon, SK S7N 5A9
License number	2657341028341
License date	Apr 27, 2011
Licensed content publisher	Elsevier
Licensed content publication	Catalysis Today
Licensed content title	Asphaltene characterization as function of time on-stream during hydroprocessing of Maya crude
Licensed content author	J. Ancheyta, G. Centeno, F. Trejo, J.G. Speight
Licensed content date	30 November 2005
Licensed content volume number	109
Licensed content issue number	1-4
Number of pages	5
Start Page	162
End Page	166
Type of Use	reuse in a thesis/dissertation
Intended publisher of new work	other
Portion	figures/tables/illustrations
Number of figures/tables /illustrations	1
Format	print
Are you the author of this Elsevier article?	No
Will you be translating?	No
Order reference number	
Title of your thesis/dissertation	Catalytic Performances of NiMo/Zr-SBA-15 Catalysts for the Hydrotreating of Bitumen Derived Heavy Gas Oil
Expected completion date	May 2011
Estimated size (number of pages)	230
Elsevier VAT number	GB 494 6272 12
Permissions price	0.00 USD
VAT/Local Sales Tax	0.0 USD / 0.0 GBP
Total	0.00 USD

8. Permission to use Figure 2.24 and 2.25

ELSEVIER LICENSE
TERMS AND CONDITIONS

Apr 27, 2011

This is a License Agreement between Piyali Biswas ("You") and Elsevier ("Elsevier") provided by Copyright Clearance Center ("CCC"). The license consists of your order details, the terms and conditions provided by Elsevier, and the payment terms and conditions.

All payments must be made in full to CCC. For payment instructions, please see information listed at the bottom of this form.

Supplier	Elsevier Limited The Boulevard,Langford Lane Kidlington,Oxford,OX5 1GB,UK
Registered Company Number	1982084
Customer name	Piyali Biswas
Customer address	Department of Chemical Engineering Saskatoon, SK S7N 5A9
License number	2657351290248
License date	Apr 27, 2011
Licensed content publisher	Elsevier
Licensed content publication	Applied Catalysis A: General
Licensed content title	Catalyst deactivation: is it predictable?: What to do?
Licensed content author	J. A. Moulijn, A. E. van Diepen, F. Kapteijn
Licensed content date	30 April 2001
Licensed content volume number	212
Licensed content issue number	1-2
Number of pages	14
Start Page	3
End Page	16
Type of Use	reuse in a thesis/dissertation
Intended publisher of new work	other
Portion	figures/tables/illustrations
Number of figures/tables /illustrations	2
Format	print
Are you the author of this Elsevier article?	No
Will you be translating?	No
Order reference number	Figure 2.24 and 2.25
Title of your thesis/dissertation	Catalytic Performances of NiMo/Zr-SBA-15 Catalysts for the Hydrotreating of Bitumen Derived Heavy Gas Oil
Expected completion date	May 2011
Estimated size (number of pages)	230
Elsevier VAT number	GB 494 6272 12
Permissions price	0.00 USD
VAT/Local Sales Tax	0.0 USD / 0.0 GBP
Total	0.00 USD

9. Permission to use Figure 2.30

ELSEVIER LICENSE
TERMS AND CONDITIONS

May 08, 2011

This is a License Agreement between Piyali Biswas ("You") and Elsevier ("Elsevier") provided by Copyright Clearance Center ("CCC"). The license consists of your order details, the terms and conditions provided by Elsevier, and the payment terms and conditions.

All payments must be made in full to CCC. For payment instructions, please see information listed at the bottom of this form.

Supplier	Elsevier Limited The Boulevard,Langford Lane Kidlington,Oxford,OX5 1GB,UK
Registered Company Number	1982084
Customer name	Piyali Biswas
Customer address	Department of Chemical Engineering Saskatoon, SK S7N 5A9
License number	2664511272634
License date	May 08, 2011
Licensed content publisher	Elsevier
Licensed content publication	Microporous and Mesoporous Materials
Licensed content title	Surface functionalization of mesoporous silica SBA-15 by liquid-phase grafting of zirconium phosphate
Licensed content author	Jianan Zhang, Zhen Ma, Jian Jiao, Hongfeng Yin, Wenfu Yan, Edward W. Hagaman, Jihong Yu, Sheng Dai
Licensed content date	1 April 2010
Licensed content volume number	129
Licensed content issue number	1-2
Number of pages	10
Start Page	200
End Page	209
Type of Use	reuse in a thesis/dissertation
Portion	figures/tables/illustrations
Number of figures/tables /illustrations	1
Format	both print and electronic
Are you the author of this Elsevier article?	No
Will you be translating?	No
Order reference number	Figure 2.30
Title of your thesis/dissertation	Catalytic Performances of NiMo/Zr-SBA-15 Catalysts for the Hydrotreating of Bitumen Derived Heavy Gas Oil
Expected completion date	May 2011
Estimated size (number of pages)	230
Elsevier VAT number	GB 494 6272 12
Permissions price	0.00 USD
VAT/Local Sales Tax	0.0 USD / 0.0 GBP
Total	0.00 USD